

https://dspace.org/

The use of modified amplification factors in assessing in-plane instability of unbraced frame structures

Joseph, Stephen Brendon

2010-04-08T12:35:15Z
http://hdl.handle.net/10539/7949

Downloaded from a DSpace repository. https://dspace.org/

THE USE OF MODIFIED AMPLIFICATION FACTORS IN ASSESSING IN–PLANE INSTABILITY OF UNBRACED FRAME STRUCTURES

Stephen Brendon Joseph

A research report submitted to the Faculty of Engineering, University of the Witwatersrand, Johannesburg, in partial fulfilment of the requirements for the degree of Master of Science in Engineering.

Johannesburg, 2009

DECLARATION

I declare that this research report is my own, unaided work. It is being submitted for the Degree of Master of Science in the University of the Witwatersrand, Johannesburg. It has not been submitted before for any degree or examination in any other University.



14th day of October (year) 2009

ABSTRACT

Kemp's (1999) amplification factor method is tested in its ability to model the nonlinear in-plane behaviour of several unbraced rectangular steel portal frames. The evaluation is by means of comparison to results obtained from physical tests and advanced finite element analyses of the portals. The failure load calculations are favourable, but the load-"amplification factor" (load-*X*) relationships differ substantially between test methods. These differences are ascribed to Kemp's bilinear representation of the load-*X* relationship, the tendency of his amplification factor to underestimate loss of elastic flexural rigidity, and the assumption of a single amplification factor for an entire structure. Modifications are proposed to the limits of the bilinear load-*X* graph, and to the failure criterion of Kemp's method. These modifications maintain the simplicity and accuracy of the failure load prediction, improve the modelling of the load-*X* relationship, and provide a means of recognising upper and lower bound collapse loads.

ACKNOWLEDGEMENTS

I would like to express my gratitude towards my supervisor, Professor Alan Kemp, for his generous assistance and support throughout my research. Professor Kemp has been at hand to share his considerable knowledge of structures, and has patiently helped me apply it to all aspects of this project. His advice has been invaluable, and I appreciate it greatly.

Ernest Roelofse and the staff of the Heavy Structures Laboratory in the Department of Civil and Environmental Engineering were instrumental in the laboratory-testing phase of my project. I am grateful for their help in the fabrication of the test frames and the preparation of the testing equipment.

I thank the University of the Witwatersrand for making available the materials and equipment necessary for the testing and analysis of the frames.

DECLARATION 2

ABSTRACT 3

ACKNOWLEDGEMENTS 4

LIST OF FIGURES 8

LIST OF TABLES 11

LIST OF SYMBOLS 12

1 INTRODUCTION 15

1.1 Nonlinear Structural Analysis 15

1.2 Objectives and Reasons for Research 18

1.3 Sequence of Project Completion 19

1.4 Scope and Limitations 20

1.5 Organisation of Report 21

2 LITERATURE SURVEY 23

2.1 Geometric and Material Nonlinearity 23
2.1.1 Differential equation of moment equilibrium for P-δ effect 24
2.1.2 Storey magnifier method for P-Δ effect 27
2.1.3 The Newmark method 30
2.1.4 The finite element method 31

2.2 Instability 34
2.2.1 Elastic critical load of pin-ended column from first principles 35
2.2.2 Stability functions and practical effective length factors 36

2.3 Kennedy et al's Amplification Factor 40

2.4 Kemp's Modification for Nonrectangular Structures 44

2.5 Kemp's Treatment of Material Nonlinearity 49

3 LABORATORY TESTING 54

3.1 Coupon Tests 54
3.1.1 Test procedure 54
3.1.2 Section and material properties 55

3.2 Frame Tests 59

3.2.1 Selection of frames 59
3.2.2 Equipment and testing 61
3.2.3 Failure loads and modes 64
3.2.4 Load versus deflection and incremental amplification factor 66
3.2.5 Laboratory error 71

3.3 Comparisons with ABAQUS Tests 71

4 BILINEAR AMPLIFICATION FACTOR METHOD 78

4.1 Calculating (X_i, λ_i) 78

4.2 Calculating (X_p, λ_p) and λ_f 82

4.3 Bilinear Method Results 86

5 REASSESSMENT OF KEMP'S AMPLIFICATION FACTOR THEORY 98

5.1 Developing a Second Order Sway Equilibrium Equation 98

5.2 Validity of the Inelastic Amplification Factor 100

5.3 Application of the Amplification Factor and Failure Criterion 103

5.4 Usefulness of Test Frame Results 112
5.4.1 Section shape 113
5.4.2 Member slenderness 116
5.4.3 Support and joint behaviour 121
5.4.4 Overall impact of scale effects 121

5.5 Modifications to Kemp's Amplification Factor Theory 122

6 CONCLUSIONS AND RECOMMENDATIONS 133

6.1 Failure Load Prediction 133

6.2 Load-X Curve Approximation 135

6.3 Appraisal of Kemp's Theory 136

6.4 Recommendations 138

APPENDIX A LABORATORY COUPON TEST DATA 142

APPENDIX B TEST FRAME PHOTOGRAPHS 147

APPENDIX B TEST FRAME PHOTOGRAPHS 148

APPENDIX B TEST FRAME PHOTOGRAPHS 149

APPENDIX C LABORATORY FRAME TEST DATA 150

APPENDIX D ABAQUS FRAME TEST DATA 154

REFERENCES 160

LIST OF FIGURES

Figure		Page
2.1	The two kinds of P-delta effects	23
2.2	Simply supported beam with associated bending moments	25
2.3	The storey magnifier method	28
2.4	Member discretization by the Newmark method and equivalent nodal loads	30
2.5	Pin-ended strut under axial load	35
2.6	SANS 10162-1:2004 Nomograph for effective lengths of columns in continuous frames	38
2.7	Load versus central lateral deflection for idealized pin-ended columns	39
2.8	Load versus characteristic deflection for various analysis methods	40
2.9	First order forces and deflections of typical members in sway frames	41
2.10	Application of Kemp's amplification factor method to a pitched roof portal	48
2.11	Scholz (1981) test frame with load-Δ and load-X graphs	50
2.12	Moment-curvature graphs for a typical W-shape section	52
3.1	Typical coupon for tensile testing	55
3.2	Coupon 1a stress-strain graph	56
3.3	Cross-sectional stress and strain distributions for a mild steel section in flexure	57
3.4	Moment-curvature graphs of the test frame section	59
3.5	Geometries and loading configurations of the test frames	60
3.6	Typical test frame set-up	62
3.7	Deflected shapes and apparent hinge positions of the laboratory-tested frames	63
3.8	Probable failure mechanisms and resulting loads from plastic analysis	65
3.9	W-Δ graph of laboratory-tested span variant frames	67
3.10	W-Δ graph of laboratory-tested loading length variant frames	67
3.11	W-Δ graph of laboratory-tested sway-ratio variant frames	68
3.12	W-X graph of laboratory-tested span variant frames	69
3.13	W-X graph of laboratory-tested loading length variant frames	69
3.14	W-X graph of laboratory-tested sway-ratio variant frames	70
3.15	Deflected shapes, moments and loads at failure of the ABAQUS-tested frames	72
3.16	W-Δ graph of ABAQUS-tested span variant frames	73
3.17	W-Δ graph of ABAQUS-tested loading length variant frames	74
3.18	W-Δ graph of ABAQUS-tested sway-ratio variant frames	74
3.19	W-X graph of ABAQUS-tested span variant frames	75
3.20	W-X graph of ABAQUS-tested loading length variant frames	75
3.21	W-X graph of ABAQUS-tested sway-ratio variant frames	76
3.22	W-Δ graph of both column tops of ABAQUS-tested frames	77
4.1	Pure sway mode for the calculation of X for the test frames	78
4.2	Sign convention and free-body diagrams for calculating λ_i and X_i	79
4.3	Virtual work method for calculating Δ_{Ip}	83
4.4	Bilinear W-X graph of kempsp1 frame	89

Figure		Page
4.5	Bilinear *W-X* graph of 0.6span frame	89
4.6	Bilinear *W-X* graph of 0.8span frame	90
4.7	Bilinear *W-X* graph of 1.2span frame	90
4.8	Bilinear *W-X* graph of 1.4span frame	91
4.9	Bilinear *W-X* graph of 0.8ll frame	91
4.10	Bilinear *W-X* graph of 0.6ll frame	92
4.11	Bilinear *W-X* graph of 0.4ll frame	92
4.12	Bilinear *W-X* graph of 0.33sway frame	93
4.13	Bilinear *W-Δ* graph of kempsp1 frame	93
4.14	Bilinear *W-Δ* graph of 0.6span frame	94
4.15	Bilinear *W-Δ* graph of 0.8span frame	94
4.16	Bilinear *W-Δ* graph of 1.2span frame	95
4.17	Bilinear *W-Δ* graph of 1.4span frame	95
4.18	Bilinear *W-Δ* graph of 0.8ll frame	96
4.19	Bilinear *W-Δ* graph of 0.6ll frame	96
4.20	Bilinear *W-Δ* graph of 0.4ll frame	97
4.21	Bilinear *W-Δ* graph of 0.33sway frame	97
5.1	*W-Δ* graph of 0.6rigidspan frame	101
5.2	*W-Δ* graph of 0.6span frame	101
5.3	First order *W-Δ* graph of 0.6span frame	102
5.4	Bilinear *W-X* graph of 0.6ll frame	103
5.5	Partial elastic *W-Δ* graph of 0.6span frame	104
5.6	Calculation of the modified amplification factors $U_2^{(t)}$ and $U_2^{(g)}$	105
5.7	Derivation of the modified failure criterion	108
5.8	*W-X* graph of kempsp1 frame with modified failure criterion	110
5.9	*W-X* graph of 0.6rigidspan frame with modified failure criterion	110
5.10	*W-X* graph of 0.6span frame with modified failure criterion	111
5.11	*W-X* graph of 1.2span frame with modified failure criterion	111
5.12	Moment-curvature graphs of a typical I-section and solid rectangular section	113
5.13	Inelastic deflection of a simply supported beam	114
5.14	Test frame sections and properties	117
5.15	*W-X* graph of kempsp1(a) frame with modified failure criterion	118
5.16	*W-X* graph of kempsp1(b) frame with modified failure criterion	119
5.17	*W-X* graph of kempsp1(c) frame with modified failure criterion	119
5.18	*W-X* graph of kempsp1 frame with proposed failure criterion	126
5.19	*W-X* graph of 0.6rigidspan frame with proposed failure criterion	126
5.20	*W-X* graph of 0.6span frame with proposed failure criterion	127
5.21	*W-X* graph of 0.8span frame with proposed failure criterion	127
5.22	*W-X* graph of 1.2span frame with proposed failure criterion	128
5.23	*W-X* graph of 1.4span frame with proposed failure criterion	128
5.24	*W-X* graph of 0.8ll frame with proposed failure criterion	129
5.25	*W-X* graph of 0.6ll frame with proposed failure criterion	129
5.26	*W-X* graph of 0.4ll span frame with proposed failure criterion	130
5.27	*W-X* graph of 0.33sway frame with proposed failure criterion	130
5.28	*W-X* graph of kempsp1(a) frame with proposed failure criterion	131
5.29	*W-X* graph of kempsp1(b) frame with proposed failure criterion	131

Figure		**Page**
5.30	*W-X* graph of kempsp1(c) frame with proposed failure criterion	132
A-F1	Coupon 1b stress-strain graph	142
A-F2	Coupon 2a stress-strain graph	143
A-F3	Coupon 2b stress-strain graph	144
A-F4	Coupon 3a stress-strain graph	145
A-F5	Coupon 3b stress-strain graph	146
B-F1	Laboratory testing of the 0.6span frame	147
B-F2	Laboratory testing of the 1.2span frame	148
B-F3	Laboratory testing of the 0.6ll frame	149

LIST OF TABLES

Table		Page
2.1	First order analysis data for pitched-roof portal frame in Fig. [2.10]	49
3.1	Tensile test data of coupon 1a	56
3.2	Summary of section properties	58
3.3	Frame failure loads from plastic analysis, laboratory testing, and second order inelastic ABAQUS tests	64
4.1	Frame failure from laboratory testing, second order inelastic ABAQUS tests and bilinear amplification factor method	86
5.1	Reduced flexural rigidities *EI''* required to force correct failure load predictions from Kemp's method	120
A-T1	Tensile test data of coupon 1b	142
A-T2	Tensile test data of coupon 2a	143
A-T3	Tensile test data of coupon 2b	144
A-T4	Tensile test data of coupon 3a	145
A-T5	Tensile test data of coupon 3b	146
C-T1	Laboratory test of kempsp1 frame	150
C-T2	Laboratory test of 0.6span frame	150
C-T3	Laboratory test of 0.8span frame	151
C-T4	Laboratory test of 1.2span frame	151
C-T5	Laboratory test of 1.4span frame	152
C-T6	Laboratory test of 0.6ll frame	152
C-T7	Laboratory test of 0.4ll frame	153
C-T8	Laboratory test of 0.33sway frame	153
D-T1	ABAQUS test of kempsp1 frame	154
D-T2	ABAQUS test of 0.6span frame	154
D-T3	ABAQUS test of 0.8span frame	155
D-T4	ABAQUS test of 1.2span frame	155
D-T5	ABAQUS test of 1.4span frame	156
D-T6	ABAQUS test of 0.8ll frame	156
D-T7	ABAQUS test of 0.6ll frame	157
D-T8	ABAQUS test of 0.4ll frame	157
D-T9	ABAQUS test of 0.33sway frame	158
D-T10	ABAQUS test of 0.6rigidspan frame	158
D-T11	ABAQUS test of kempsp1(a) frame	158
D-T12	ABAQUS test of kempsp1(b) frame	159
D-T13	ABAQUS test of kempsp1(c) frame	159

LIST OF SYMBOLS

Loads, Stresses and Energy

C	compressive force
H	horizontal force
M	bending moment
M_p	fully plastic bending moment
M'_p	reduced plastic bending moment
M^*_x	virtual bending moment at point x
P	longitudinal axial force in the member
P_{crit}	elastic critical load
P_e	Euler buckling load
P_y	cross-sectional yield load
r_i	nodal force
$\boldsymbol{r}$	nodal force vector
$\boldsymbol{U}$	strain energy
V	average shear force in the member length associated with moment gradient OR horizontal shear force applied to a column top
$\boldsymbol{V}$	work done by nodal forces
W	total vertical load applied to a test frame
$\boldsymbol{\Pi}$	total stationary potential energy
σ	axial stress
σ_{res}	residual stress
σ_y	axial yield stress

Geometry and Material Parameters

A	area
a	distance from the centre of a column top to the nearest outer vertical load on a test frame
a_0, a_1	constants in the element displacement function for displacement u
b	distance from the centre of a column top to the nearest inner vertical load on a test frame OR breadth of a section
b_o, b_1, b_2, b_3	constants in the element displacement function for displacement v
d	depth of a section
d_i	nodal displacement
$\boldsymbol{d}$	nodal displacement vector
E	Young's modulus
E_s	Young's modulus in the zone of uniform plastic elongation
EI'	reduced flexural rigidity
f	shape factor
h	storey height
I	second moment of area

L	member length
u	axial displacement relative to the element or member local axes
V_e	volume of an element
v	transverse displacement relative to the element or member local axes
x	distance measured along the member or element's longitudinal axis
y_y	distance from the neutral axis to the first longitudinal fibre at yield stress
Δ	sway displacement of the member ends relative to each other
δ	transverse displacements of the member relative to its chord
ε	axial strain
ε_s	axial strain at the initiation of strain hardening
ε_y	axial strain at yield
θ	member end rotation
Φ	curvature
ϕ^*	virtual member end rotation
∂^*	virtual displacement of a load in its line of action

Factors and Constants

K	effective length factor
$\boldsymbol{k}$	element stiffness matrix
S_f	storey sway stiffness
U_1	amplification factor for P-δ effects
U_2	amplification factor for P-Δ effects
X	incremental amplification factor
η	a constant used to position the proposed failure line in the load-X space
λ	load factor
φ_i	stability function

Subscripts

1,2,3…n	arising from the nth iteration of second order effects
c	column OR collapse of the test frame in the laboratory
f	at failure of the sway frame
g	gravitational load effect OR girder
I	first order analysis
II	second order analysis
i	pertaining to load "i" OR at the formation of the first fully plastic section in the sway frame
k	at station k
max	maximum
p	at first order plastic collapse in the critical failure mechanism

s	at first order collapse in the pure sway mode
t	translational load effect
ult	ultimate load
’	pertaining to the effects of loads with unknown deflections equal to zero (in a slope deflection analysis)
’’	pertaining to the effects of member end deflections with member loads equal to zero (in a slope deflection analysis) OR double differentiation with respect to *x*

1 INTRODUCTION

1.1 Nonlinear Structural Analysis

During undergraduate studies, civil engineering students devote considerable time to learning the principals of first order elastic structural analysis. 'First order' implies that the changes in structural geometry caused by loading are ignored when establishing equations of moment and force equilibrium. 'Elastic' analysis means that there is a constant proportionality between the stress and strain of the structural material. The result of these two assumptions is that the analysis predicts 'linear' behaviour of the structure with load being proportional to stresses and deflections at all times. Since students are most familiar and comfortable with these analytical methods, they often become the methods of choice later on in the design office. First order elastic analysis provides acceptable levels of accuracy where small loads or very stiff structures ensure small deflections and elastic stresses. The assumptions of elasticity and unchanging geometry are very useful for serviceability checks as they greatly reduce the complexity of the analysis.

When designing to ultimate limit states criteria, however, the designer needs to calculate loads at which the structure loses stability. At these high levels of load, two forms of nonlinear behaviour become significant, namely 'geometric' and 'material' nonlinearity. Geometric nonlinearity arises from loads acting on the deformed shape of the structure, and material nonlinearity from a nonlinear stress-strain relationship of the load-bearing material. In the case of structural steel, the onset of significant material nonlinearity is dramatic due to the abrupt change in Young's modulus after the yield stress has been exceeded. At this point the loss in stiffness of the structure allows deflections to increase at a greater rate with respect to load, and hence geometric nonlinearity also becomes increasingly severe. The combined result of these nonlinear behaviours significantly increases the complexity of an accurate analysis of the structure. In reinforced concrete, nonlinear behaviour is even more difficult to predict due to the shape of the stress-strain curve of concrete, the weakness of concrete in tension, and the composite nature of the section. Regardless of the type of structural material, in the presence of compressive axial force, the effects of these nonlinearities are always destabilising and increase with load. They reduce the effective stiffness of the structure, and the actual stresses and deflections at a given load are larger than would be expected from an elastic analysis. Most importantly, the nonlinear behaviour results in actual collapse occurring at lower loads and often in different collapse mechanisms than predicted by first order elastic analyses. The more flexible the structure, the more severe will be the miscalculation of ultimate load capacity.

When a designer wishes to account for both forms of nonlinearity he needs to perform a second order inelastic analysis. He has the choice of using either a rigorously theoretical or simplified analytical method. The theoretical methods are typically difficult to understand and require substantial time spent building virtual models and interpreting output data. Finite element analysis is an example of a theoretical method that has become readily available in various affordable software applications.

A large proportion of engineers who use finite element analysis admit to being unsure if not ignorant of the theory behind the calculations. Such ignorance affects their ability to produce results that are consistently meaningful and reliable. This is true even for the so-called simplified analytical methods, such as the inelastic member model and the end spring model. Even these methods are relatively complex and laborious, and need to be performed using a computer. Consequently, designers find it simpler to allow for a single cause of nonlinear behaviour by using the simplified methods taught at undergraduate level.

Material nonlinearity can be accounted for by performing a conventional first order stiffness or flexibility analysis of a structure, and allowing plastic 'moment hinges' to form at the required sections. These moment hinges are usually of zero length and allow rotation to occur at the hinge while providing constant moment resistance equal to the plastic moment M_p of the section. Alternatively, the designer may use rigid-bodied plastic analysis, assuming rigid members and placing moment hinges at the locations where the moments are anticipated to equal the section's plastic moment. Using the principle of virtual work, the sway equilibrium equations can then be defined, and the first order collapse loads, or necessary section strengths determined. When geometric nonlinearity is accounted for alone, the analysis type is second order elastic. This can be performed by incorporating the stability or Berry functions in the stiffness or flexibility matrices respectively. If these matrices are very difficult to define or assemble, then the designer may choose to consider the stability of each member as if it were acting in isolation to the rest of the structure. This is done using the effective length method, which calculates the buckling load of a compression member using a modification of the Euler buckling expression. The modification is that the actual length of the member is multiplied by an effective length factor that compensates for the end conditions to provide an equivalent length of pin-ended member. Engineers commonly use this method, and the effective length factor can be determined from first principles, or referenced from tables provided in codes of practice and design handbooks.

A method that is user-friendly and popular, and that forms the subject of this research, is the amplification factor method. An amplification factor is an expression composed of variables that can be calculated from a first order analysis or measured directly from the geometry of the unloaded structure. When the amplification factor is multiplied by the relevant first order stress or deflection, the product approximates the actual total effect, and thereby accounts for geometric nonlinearity. The particular method that is investigated in this project was proposed by Kemp (1999) as an extension to the existing 'storey magnifier' method. The storey magnifier method exists in both the South African and Canadian steel design codes as an optional means of accounting for sway deflections in unbraced frames. As described in these codes, the method can only be used for rectangular frames having equal length columns and elastic stresses at all locations. In clause 8.7 of SANS 10162-1:2004, the amplification factor U_2 is defined as:

$$U_2 = \frac{1}{1 - \dfrac{\Sigma C_{ult} \Delta_{1\,ult}}{\Sigma V_{ult} h}} \tag{1.1}$$

where C = Compressive force in the member
Δ = Relative first order sway displacement of the storey
V = End shear force in the column
h = Storey height
subscript *ult* represents the conditions at ultimate load
subscript *I* represents first order analysis

The above terms of force and displacement are to be determined from a first order elastic analysis, and are calculated at ultimate load to aid the stability check of the structure. The resulting amplification factor only applies to those moments that cause end sway deflections in the members. These are called the translational moments M_t, and arise only from horizontally applied loads in the ideal rectangular frame. Moments caused by vertical loads acting through beams are named gravitational moments M_g, and are not considered to cause end sways in perfectly vertical columns. If the vertical loads act directly above the columns, there are ideally no gravitational moments. In reality, the columns of all structures possess an initial out of plumbness that causes further sway deflections under the action of gravitational load. The moments caused by the gravitational loads acting through these initial deflections may be regarded as part of the translational load effect. The South African code takes account of these eccentricities by adding a notional horizontal load at the column tops. This notional load equals 0.5% of the ultimate gravity load of the storey under consideration, and thereby approximates an initial out of plumbness of 0.5% of the storey height. The total moments at any location within the structure are expressed as follows:

$$M_{ult} = M_{ult\,g} + U_2 M_{ult\,t} \tag{1.2}$$

where M = Moment
subscript *g* represents gravitational loads
subscript *t* represents translational loads

The storey magnifier method requires proportionality between translational load and sway deflection. A prerequisite is therefore to ensure that material nonlinearity is avoided by dealing only with elastic stress conditions. Additionally, it is required that the sway mode of the structure allows this proportionality while maintaining compatibility of deflections at the joints. The pure sway mode of a rectangular frame allows the sway deflections of the columns to increase equally for a given increase in load, regardless of the extent of sway. Since the columns sway the same amount and the beam undergoes zero rotation, compatibility of deflections is always maintained at the joints. In a pitched-roof portal, however, the sway mode may cause sway deflections of the members to increase at varying rates relative to each other. These rates change depending on the extent of the sway, and thus proportionality between load and sway deflection might not be observed if compatibility is to be maintained. For this reason, the storey magnifier method is not applicable to nonrectangular frames. When using it to find the amplification factor at the ultimate load, one deals with loads that cause inelastic stress levels. Using the results from a first order analysis at ultimate load introduces inaccuracies into the calculation of U_2. The effect is to underestimate the amplification, as inelastic stresses are accompanied by loss of stiffness, greater deflections and hence increased second order effect. The magnitude

of the inaccuracy is dependent on the flexibility of the structure, which is minimised in practical structures by limits on member slenderness and allowable deflections.

Kemp (1999) proposed a modification of the storey magnifier method that extended its applicability to any shape of frame. Through his use of virtual work and sway equilibriums, Kemp's amplification theory was derived so as to be applicable to both elastic and inelastic behaviour. This allowed him to develop an amplification factor that would take account of geometric and material nonlinearity for any given load or shape of frame. As will be shown in the literature survey, Kemp wrote his amplification factor U_2 in terms of an 'incremental amplification' factor X. He found that the relationship between X and load λ could be simplified to a bilinear graph constructed between three easily definable limits. He then used this load-X graph in conjunction with his own empirical failure criterion to develop a means of calculating the inelastic instability load. These failure loads compared favourably with results of independently performed finite element analyses and laboratory tests of frames of various critical shapes. This project is an investigation of Kemp's amplification factor theory and his method of calculating collapse loads. In this report are included a review of his theory, an assessment of its predictions for a variety of idealised test frames, identifications of reasons for inaccuracies and suggestions for improvements to his theory.

1.2 Objectives and Reasons for Research

Kemp's theory provides the designer with a relatively simple and attractive means of performing two important checks on a structure, namely the calculations of deflections at serviceability loads, and the assessment of ultimate load capacity. The facilitation of the latter of these two criteria is the most important advancement, as the nonlinear behaviour of structures at serviceability loads is usually of small consequence. Kemp's method of calculating the ultimate strength makes use of empirical approximations to his observations of various structures under load. These empiricisms include the shape of the bilinear curve, the expression he uses for the reduced flexural rigidity of members with plastic hinges, and the assumption that unbraced slender frames will always fail in pure modes of sway. By its nature, empirical theory is usually limited to cases for which rigorous testing has proven its results to be consistently accurate. Since Kemp's theory proposes to be applicable to a broad range of structures and levels of load, and addresses the very important issue of ultimate strength, it is necessary for much testing of the theory to be done before it can be safely used in practice. The objectives of this research project are as follows:

- To establish how the accuracy of Kemp's method of failure load prediction is affected by changes in column to beam span ratios, as well as the positions of gravitational loads on the beams. Both the original storey amplifier method and Kemp's amplification theory imply that the amplification factor is unaffected by the positions of gravitational loads on the beams of rectangular frames. Varying the positions of these loads can be used to test this theory. As the loads gather near the centre of the beam, the predicted first order

inelastic failure mechanism shifts from a sway to a member mechanism. Thus Kemps prediction that the frames will fail in sway is also tested.

- To determine how accurately the bilinear relationship approximates the actual load-*X* relationship of a frame. Any rationalisation of a complex curve into two straight lines will result in inevitable errors of approximation. Kemp's bilinear approximation of the load-*X* curve is tested for rectangular frames of various proportions and load configurations.

- To perform a parametric study of the variables used in the amplification factor theory so as to enable suggestions of possible improvements to the theory. The assumptions made in developing the bilinear curve are adjusted and the results are discussed.

1.3 Sequence of Project Completion

This project was approached and completed in the following sequence of events:

1. A literature survey was conducted which broadly investigated modes of instability in structures, as well as various empirical and theoretical methods that have been developed to account for them. The literature survey included a detailed study of the derivation of Kemp's amplification factor theory, and its application to structures.

2. A selection of rectangular mildsteel portal frames were designed and submitted to the engineering workshop in the Heavy Structures Laboratory for fabrication. During the manufacture of these frames, coupons of the steel were prepared and tested in tension in the Heavy Structures Laboratory. The results of the load-extension recordings taken from these tests enabled the determination of the material characteristics necessary for the bilinear method and the finite element analyses. These results included the Young's modulus of the steel, the yield stresses, and the strain at which strain hardening took place. The cross-sectional geometry was used in conjunction with these properties to develop moment-curvature relationships and plastic moment capacities.

3. The completed frames were set up on the testing bed and incrementally loaded until collapse. Measurements of load and deflections were taken at each load increment to allow the construction of various curves pertinent to the amplification theory.

4. These tests were then simulated with a finite element model analysis through the use of ABAQUS. The results of the laboratory tests and the ABAQUS analysis were compared and found to be in agreement with each other. Thus they served as a benchmark against which the results of Kemp's analysis could be compared.

5. The bilinear method was applied to all the tested frames.

6. The bilinear method results were compared to those of the laboratory tests and ABAQUS analyses. The effects of the variables and assumptions of the bilinear theory were identified and were altered to try to improve the accuracy of the theory. Certain empirical improvements were suggested, and regions requiring further research were highlighted.

1.4 Scope and Limitations

The frames tested in this research project were all rectangular in shape, and thus the test results could not be used to verify the applicability of the theory to nonrectangular frames. Nonetheless, the theory of the amplification factor concerning nonrectangular frames is investigated and discussed in this report. An advantage that arose from the use of rectangular frames was that Kemp's expression for U_2 reduced to that of the storey magnifier method. This meant that the ability of his theory to model inelasticity could be tested in isolation from its ability to cope with nonrectangular structures. Consequently there were fewer possible causes of error to consider when assessing the accuracy of the load-amplification factor relationship and the collapse load prediction.

Eight frames were tested in total, each having the same column height of 400mm and varying in span and load positions. Each frame was loaded with four equal vertical point loads placed symmetrically about the midpoint of the beam, and one horizontal sway-inducing load at the top of the columns. The loading was monotonic, meaning that a constant ratio was maintained between the vertical and horizontal loads at all times. This loading regime was chosen due to an expectation that the second order load-deflection behaviour of the frames would be sensitive to the ratio of vertical to horizontal loads. This sensitivity was potentially a factor that could influence the accuracy of Kemp's theory for different loading scenarios. Since only eight frames were tested in the laboratory, it was considered sensible to eliminate this cause of variation by using monotonic loading.

The frames tested were substantially more slender than would be allowed by most steel codes. The stiffest of the frames had column slenderness ratios about the minor axis of over 300, while SANS 10162-1:2004 allows a maximum of 200 in compression members. The slenderness of the frames allowed larger sway deflections, and thus the deflections could be measured with greater accuracy in the laboratory than if stiff columns had been used. Unfortunately, these large deflections were accompanied by membrane forces that potentially altered the anticipated behaviour of the frames. The effects of these forces are discussed in detail in section 5.4 where it is concluded that only one of the test frames was appreciably weakened by tensile forces within its beam. A further consequence of the large slenderness ratios was that the column axial loads were very low at failure. Kemp (1999) noted that more research was required to increase the accuracy of his theory when axial loads exceeded 60% of the yield loads. However, for the frames tested in this project, the elastic critical collapse loads were less than 10%, and the loads at actual failure less than 3% of the yield loads.

During laboratory testing, it was decided that deflections would be recorded when the deflection under the current load was increasing by not more than one graduation, or 0.01mm, every thirty seconds. This was done to limit the time intervals between successive load increments near the collapse loads of the frames. It became evident in the tests that significant creep took place only after the formation of the first plastic hinge. At this point, the sway stiffness of the typical frame had reduced dramatically and it was obvious from the deflections and curvatures that the structure was beyond its safe working load. Most practical structures are not designed to withstand such high levels of load for prolonged periods of time. Consequently the effects that long-term creep would have had on the nonlinear behaviour of the test frames were ignored.

The same solid rectangular section was used for the beams and columns of all the frames. Initially, it was thought that the unconventional moment-curvature relationship of the section might diminish the relevance of the test results. The moment-curvature relationship affects the load-deflection behaviour of a member, and therefore the structure to which it belongs. The definition of the load-X graph requires accurate calculations of first order inelastic sway deflections at collapse of the frame. For this purpose, Kemp derived an empirical equation to account for the reduction in flexural rigidity of a member with plastic hinges. This equation, which is described further in section 2.5, was developed for application to conventional structural sections with corresponding moment-curvature relationships. Section 5.4 investigates the consequences of having used a solid rectangular section for the test frames. It is shown that Kemp's empirical means of accounting for the spread of plasticity allowed accurate calculations of deflection despite the section's unconventional moment-curvature relationship.

The test frames were not designed to be representative of any particular practical structure. Apart from the excessive member slenderness ratios and the use of solid rectangular sections, various other simplifications may have affected the accuracy of the results. These simplifications, discussed further in chapter 5, included full fixity of the supports, fully rigid welded joints, idealised loading configurations and the disregarding of residual stress effects. The lack of scalability of the test results rendered them unsuitable for the fine-tuning of empirical aspects of Kemp's method with respect to full size structures. Consequently, the proposed modifications are based on a theoretical appraisal of the method such that they retain their validity for the general case of unbraced sway frame. The modifications also include an empirical means of adjustment to allow for varying forms of instability. This modification in particular may require further investigation and development for the application to full size structures.

1.5 Organisation of Report

The following chapter of the report is the literature survey, and comprises two main parts. The first section begins with an explanation of the two types of second order effects, methods of allowing for them in member analysis, and how they relate to member instability. One of the two methods discussed is the storey magnifier method, and its derivation is given herein. This method is essentially identical to that

described by Kennedy et al (1990), but differs in the way that the derivation approaches the final expression. Following this, various techniques of calculating instability loads of members or structures are highlighted. These include the use of differential equations of moment equilibrium, effective length factors, instability functions for slope-deflection methods, and a brief explanation of the finite element method. The second part of the literature survey relates to Kemp's modifications of the storey magnifier method. Although already derived in the first part, Kennedy et al's explanation of the storey magnifier method is given as it better suits Kemp's approach to the derivation of his amplification factor. Thereafter, Kemp's modifications are discussed in detail.

Chapter 3 documents the laboratory-testing component of the research. It describes the tensile tests of the coupons and the associated calculations for determining the necessary material and section properties. The choice of test frames is explained, and the various frames and their loading configurations are given. Following this is a description of the testing equipment and the sequence of operations of the actual tests. The test results are discussed with consideration given to the collapse loads, positions of hinges and failure mechanisms, and shapes of the load versus deflection curves. The possible causes of laboratory testing error and their probable impact on the results are given, and the section is ended with a comparison between the laboratory and ABAQUS analysis results.

In chapter 4, a step-by-step procedure is given for constructing the bilinear load-X curve, and for calculating the collapse load as per Kemp's method. This procedure was applied to each test frame using a Microsoft Excel spreadsheet for the analyses. The predictions of Kemp's theory are presented and compared to the laboratory and ABAQUS results. These comparisons help to identify areas of Kemp's method that require refinement.

Chapter 5 begins with a reassessment of the theory behind Kemp's method. The reassessment identifies the assumptions and simplifications that are believed to have resulted in the errors described in the previous section. Following the discussions of Kemp's assumptions, alternative techniques are suggested where possible. These suggestions are substantiated by the results observed in the previous sections of the report, as well as by new analyses of different structures. The usefulness of the test results is discussed with regards to the physical properties of the test frames. The chapter is ended with proposals of modifications to Kemp's method that have been found to improve its accuracy, maintain its simplicity, and allow for the modelling of various types of instability.

The conclusions are summarised in chapter 6, and recommendations are given for the modification of the existing amplification factor method. Thereafter are the references and appendices of the report.

2 LITERATURE SURVEY

2.1 Geometric and Material Nonlinearity

When beam-columns are subjected to loads, the resulting bending moments can be said to comprise of two components, namely first order and second order bending moments. First order moments are those moments that are either applied directly to the member, or that arise from the transverse loads acting on the member length. Second order moments result from axial forces acting through the lateral displacements of the member. These second order moments are also known as P-delta moments, and are further divided into two subcategories, the P-δ and P-Δ moments. P-δ moments are due to the lateral displacements of the member relative to its chord, and P-Δ moments due to the lateral displacements of the member ends relative to each other. Fig. [2.1] illustrates the lateral deflections that govern the two types of P-delta effects. In members carrying compression, the effects of axial loads acting through lateral displacements will always be to increase the bending moments and deflections. The effective flexural rigidity of a beam-column will thus be reduced by P-delta effects, as will be the ultimate load carrying capacity, especially so if the member is slender.

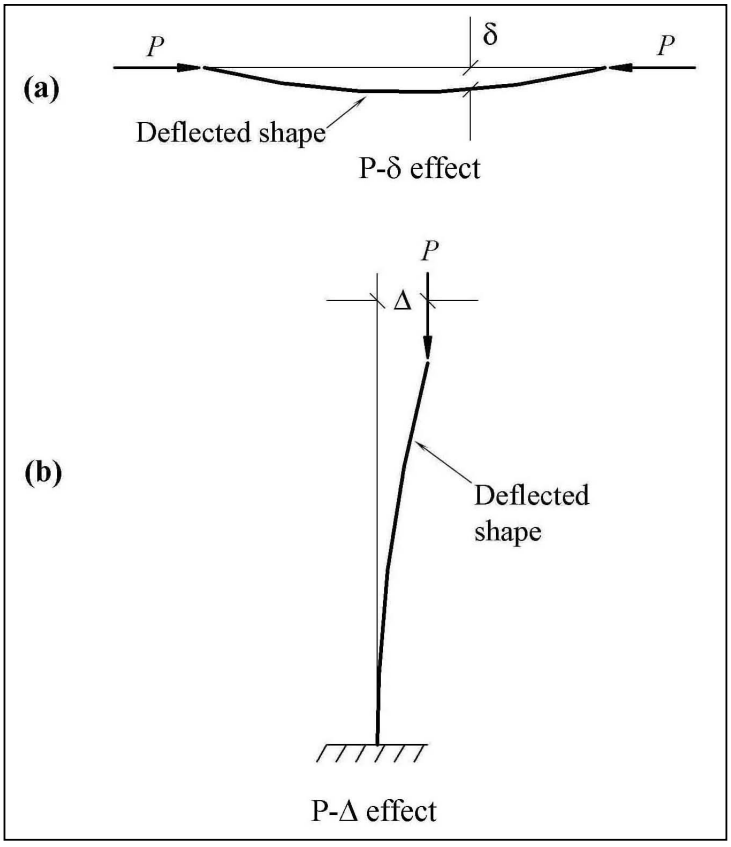


Fig. [2.1] The two kinds of P-delta effects

The behaviour of a beam-column can be defined by its load-deflection curve, and the procedure of establishing this relationship between load and deflection usually consists of two steps:

Step 1: Cross-sectional analysis

The cross-sectional analysis involves defining the moment-curvature-thrust or M-Φ-P relationship at a chosen level of axial load. In order to do so, it is necessary to know the stress-strain characteristics of the material, as well as the geometry of the section. For a rectangular cross-section with an idealised elastic-perfectly-plastic stress-strain curve, simple bending theory can be applied to easily establish a closed-form solution to the M-Φ-P relationship. For a general cross-sectional shape undergoing bi-axial bending and exhibiting nonlinear stress-strain behaviour, it becomes very difficult or even impossible to obtain a closed-form relationship. Under such circumstances, the analytical technique normally becomes an iterative computer-based method. The cross-section is divided into smaller rational shapes or layers and the contributions of each to the overall section forces are considered separately while enforcing conditions of equilibrium and compatibility. For most members, it is not necessary in the cross-sectional analysis to include the effects of axial deformations, as these are usually an order of magnitude smaller than flexural deformations.

Step 2: Member analysis

Should the simplicity of the member, its loading and support configuration permit, a closed-form solution to the member analysis may be found using bending theory alone. Below are two examples of such closed-form solutions, the first accounting for P-δ effects using a differential equation of moment equilibrium, and the second accounting for P-Δ effects using the storey magnifier method.

2.1.1 Differential equation of moment equilibrium for P-δ effect

The simply supported beam-column of Fig. [2.2a] is considered below as per Chen (1991). This member is subjected to a compressive force P, as well as end moments and transverse loads such that the maximum moment occurs at or near midspan. The total transverse deflection δ at any point is composed of the corresponding first order deflection δ_I and the second order deflection δ_{II}.

$$\delta = \delta_I + \delta_{II} \tag{2.1}$$

where δ = Transverse deflection
subscript I represents first order
subscript II represents second order

Assuming the deflection of the beam is in the shape of a half sine wave, with maximum deflection δ_{max} at the centre of the beam, the secondary moment at any point x measured along the member's longitudinal axis may be calculated as:

$$M_{II} = P\delta_{\max} \sin\frac{\pi x}{L} \tag{2.2}$$

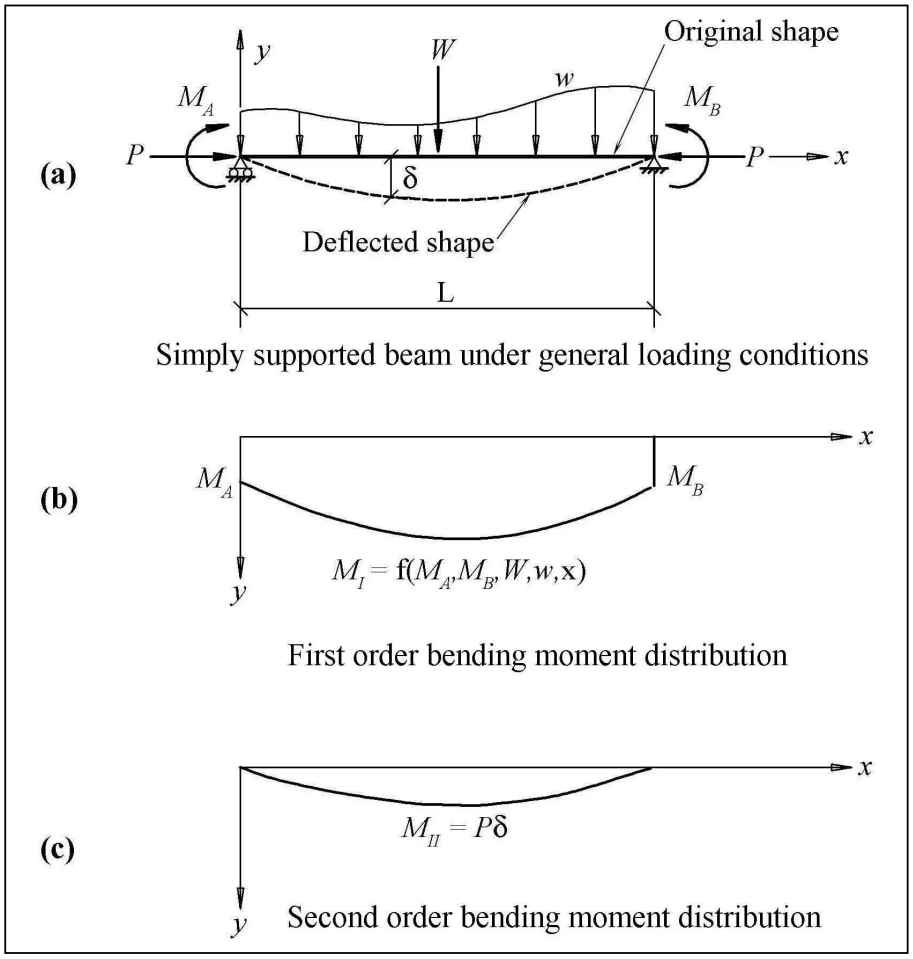


Fig. [2.2] Simply supported beam with associated bending moments

For elastic behaviour, we can also say that M_{II} can be expressed as:

$$M_{II} = -EI\delta_{II}'' \tag{2.3}$$

where superscript '' represents double differentiation with regard to x

By equating the right hand sides of equations (2.2) and (2.3) and solving for δ, we obtain:

$$\begin{aligned}\delta_{II} &= \frac{P\delta_{\max}}{EI}\left(\frac{L}{\pi}\right)^2 \sin\frac{\pi x}{L} \\ &= \delta_{\max}\frac{P}{P_e}\sin\frac{\pi x}{L}\end{aligned} \tag{2.4}$$

where P_e = Euler buckling load of the strut

At midspan, the second order deflection $\delta_{II\,max}$ can be calculated from Eqn. (2.4).

$$\delta_{II\,\max} = \delta_{\max} \frac{P}{P_e} \tag{2.5}$$

Substituting Eqn. (2.5) into Eqn. (2.1) and solving for δ_{max}:

$$\delta_{\max} = \left(\frac{1}{1 - P / P_e} \right) \delta_{I\,\max} \tag{2.6}$$

Given that

$$M_{\max} = M_{I\,\max} + P\delta_{\max} \tag{2.7}$$

we may write

$$M_{\max} = \left(\frac{1 + \psi P / P_e}{1 - P / P_e} \right) M_{I\,\max} \tag{2.8}$$

where

$$\psi = \frac{\delta_{I\,\max} P_e}{M_{I\,\max}} - 1 \tag{2.9}$$

Defining C_m as follows:

$$C_m = 1 + \psi P / P_e \tag{2.10}$$

then

$$\begin{aligned} M_{\max} &= \left(\frac{C_m}{1 - P / P_e} \right) M_{I\,\max} \\ &= U_1 M_{I\,\max} \end{aligned} \tag{2.11}$$

where

$$U_1 = \frac{C_m}{1 - P / P_e} \tag{2.12}$$

U_1 is the amplification factor to allow for P-δ effects. Its value tends to unity as P tends to zero, in accordance with the loss of P-δ effects as axial compression reduces. Note that the above definition of ψ will only give suitable results when used on a beam-column similar to the one shown in Fig. [2.2a], and when the maximum moment in the beam occurs at or near the beam's midpoint. For other conditions, ψ will need to be redefined. Essa and Kennedy (2000) have shown that in unbraced sway frames the P-δ effects on stability appear to be negligible, and that the P-Δ effects dominate.

2.1.2 Storey magnifier method for *P-Δ* effect

When lateral forces act on an unbraced rectangular frame as in Fig. [2.3a], sway deflections will occur in the columns. These deflections caused as a direct result of the applied translational loads are first order deflections. Axial loads acting through the eccentricities caused by the sway deflections will cause the frame to drift further in sway until equilibrium has been established. The additional sway deflections caused by the gravity loads are second order deflections. A simplified method of accounting for these second order moments and deflections is given by the storey magnifier method described by Rosenblueth (1965). It applies to rectangular frames in which it is assumed that each storey behaves independently of the other. This method is identical to the one described by Kennedy et al (1990), yet the derivation of the amplification factor is more elegant.

The *P-Δ* effect is approximated by a fictitious lateral load of magnitude $\Sigma P\Delta/h$ acting at the top of the column, as shown in Fig. [2.3a]. Δ is the total sway deflection on the column and is the sum of the first order sway deflection Δ_I and the second order sway deflection Δ_{II}.

$$\Delta = \Delta_I + \Delta_{II} \tag{2.13}$$

If the storey sway stiffness S_f is defined as the ratio of translational load to sway translation, then

$$S_f = \frac{horizontal\ \ force}{lateral\ \ displacement} = \frac{\Sigma H}{\Delta_I} = \frac{\Sigma H + \Sigma P\Delta / h}{\Delta} \tag{2.14}$$

Solving for Δ yields

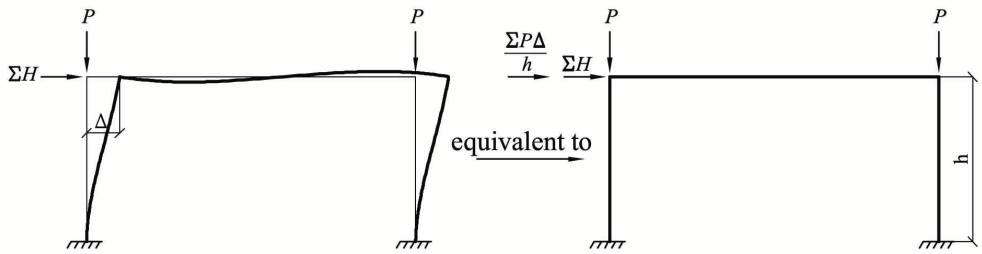
$$\Delta = \left(\frac{1}{1 - \Sigma P\Delta_I / \Sigma Hh} \right) \Delta_I = U_2 \Delta_I \tag{2.15}$$

Thus the total sway deflection can be determined by multiplying the first order deflection by an amplification factor U_2. If the storey translational moments M_t are directly proportional to the sway deflections, then

$$M_t = \left(\frac{1}{1 - \Sigma P\Delta_I / \Sigma Hh} \right) M_{It} = U_2 M_{It} \tag{2.16}$$

This method was derived to be applicable to the elastic behaviour of rectangular frames with columns of equal length. It works well for frames with stiff beams so that points of inflection occur within all the columns of each storey. It appears that the storey magnifier method can easily be adjusted for frames with vertical compression members of differing lengths. Such a structure is illustrated in Fig. [2.3b] together with the modified expressions for amplification. In the new expression for storey sway stiffness, each column is considered separately when calculating the fictitious lateral loads arising from second order effects.

(a) Rectangular frame with equal length columns



Unbraced sway frame under load Fictitious shear replacing P-Δ effect

$$S_f = \frac{horizontal\ \ force}{lateral\ \ displaceme\ nt} = \frac{\Sigma H}{\Delta_I} = \frac{\Sigma H + \Sigma P\Delta / h}{\Delta} \qquad (2.1-14)$$

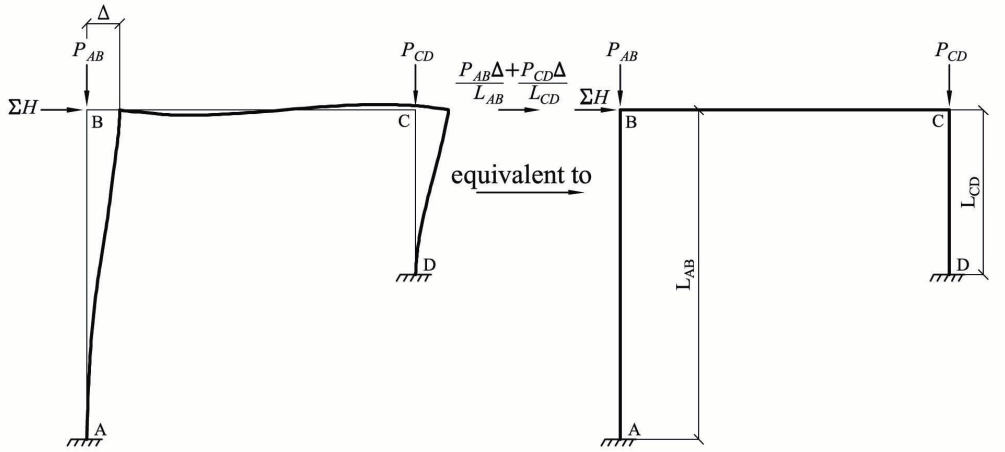
Solving for Δ yields :

$$\Delta = \left(\frac{1}{1-\Sigma P\Delta_I / \Sigma Hh}\right)\Delta_I = U_2\Delta_I \qquad (2.1-15)$$

Similarly the total translati onal moments are found as follows :

$$M_t = \left(\frac{1}{1-\Sigma P\Delta_I / \Sigma Hh}\right)M_{I\,t} = U_2 M_{I\,t} \qquad (2.1-16)$$

(b) Rectangular frame with unequal length columns



Unbraced sway frame under load Fictitious shear replacing P-Δ effect

$$S_f = \frac{horizontal\ \ force}{lateral\ displacement} = \frac{\Sigma H}{\Delta_I} = \frac{\Sigma H + P_{AB}\Delta / L_{AB} + P_{CD}\Delta / L_{CD}}{\Delta} \qquad (2.1-14a)$$

Solving for Δ yields :

$$\Delta = \left(\frac{1}{1-(P_{AB}L_{CD} + P_{CD}L_{AB})\Delta_I /(L_{AB}L_{CD}\Sigma H)}\right)\Delta_I = U_2\Delta_I \qquad (2.1-15a)$$

Similarly the total translational moments are found as follows :

$$M_t = \left(\frac{1}{1-(P_{AB}L_{CD} + P_{CD}L_{AB})\Delta_I /(L_{AB}L_{CD}\Sigma H)}\right)M_{I\,t} = U_2 M_{I\,t} \qquad (2.1-16a)$$

Fig. [2.3] The storey magnifier method

These fictitious loads are summed with the applied lateral load before dividing by the total sway deflection to define the sway stiffness.

$$S_f = \frac{horizontal\ \ force}{lateral\ displacement} = \frac{\Sigma H}{\Delta_I} = \frac{\Sigma H + P_{AB}\Delta / L_{AB} + P_{CD}\Delta / L_{CD}}{\Delta} \tag{2.14a}$$

Once again, solving for Δ isolates the new amplification factor.

$$\Delta = \left(\frac{1}{1 - (P_{AB}L_{CD} + P_{CD}L_{AB})\Delta_I / (L_{AB}L_{CD}\Sigma H)} \right) \Delta_I = U_2 \Delta_I \tag{2.15a}$$

The amplification factor in Eqn. (2.15a) reduces to the equivalent factor in Eqn. (2.15) if column lengths L_{AB} and L_{CD} are equal. The storey magnifier method is applicable to the frames of figures [2.3a] and [2.3b] for the following reasons:

- The stresses in the frames are elastic at all locations. Elastic behaviour allows for a proportional relationship between sway load and deflection, as is required by the storey sway stiffness expression.

- It is assumed that the geometries of the frames are such that the first order sway deflections of the columns arise from the applied horizontal loads only. This assumption simplifies the expression for the storey sway stiffness by forcing sway deflection to be a function of a single load. Consequently the second order overturning moments can be resolved into a fictitious horizontal load that contributes to the sway of the structure in a predictable manner.

- The compression members sway by a uniform amount in the same direction. This is ensured by the stiff horizontal beam that joins the column tops. Since all the columns sway together, the fictitious sway loads are aligned and can be summed together. In this way, one may consider the total sway load, as well as the total resistance to sway of all the members.

Various complications of the storey magnifier method arise with the introduction of inclined members. These members are prone to sway by different amounts and in different directions to each other. Such sway deflections may arise regardless of the direction of the applied load, and the deflections will have varying sensitivities to loads and second order effects. In general, it cannot be said that a single sway deflection will be representative of an entire structure's response to second order effects. Nor can the fictitious sway loads from the individual members be summed, as they will be acting in different directions. Each load may have a unique relationship to the second order sway deflection. Clearly it is no longer a simple task to define a sway stiffness expression that accounts for total load and total stiffness. In many practical scenarios, the storey magnifier method falls short in its ability to account for geometric nonlinearity. Writing a differential equation of moment equilibrium for a frame will also be unfeasible due to the difficulty involved in doing so. Fortunately, designers are able to take advantage of the power that computers have to iteratively analyse a problem. The Newmark method is an example of an iterative analysis that combines bending theory with repetitive estimation and correction. It is described below as per Chen (1991).

2.1.3 The Newmark method

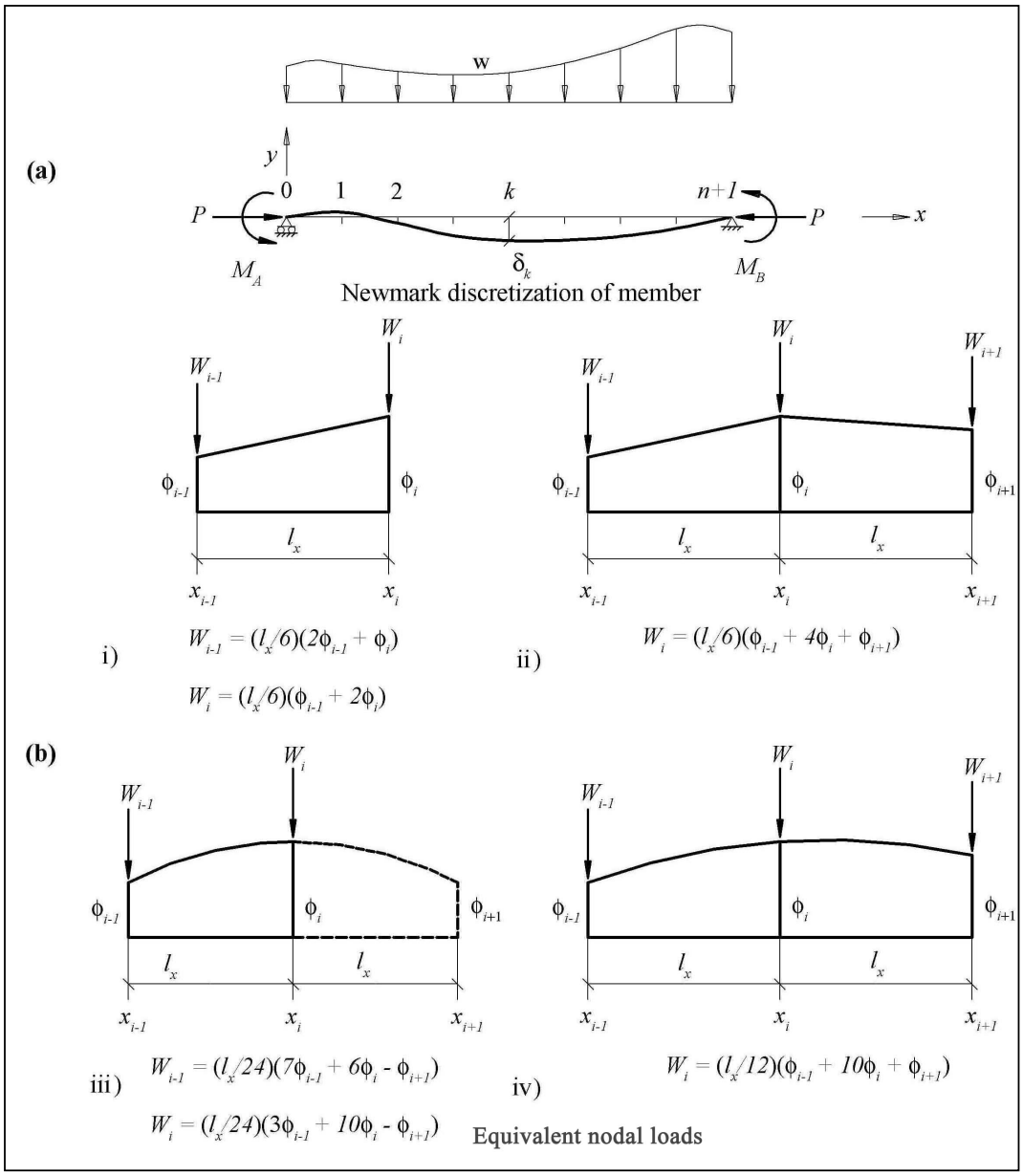


Fig. [2.4] Member discretization by the Newmark method and equivalent nodal loads

The procedure of the Newmark method is applied to beam-columns as follows:

1. The member is divided into n segments by (n +1) stations. This can be seen in Fig. [2.4a].

2. A value of deflection is assumed at every station under the given loads where δ_k represents the deflection at station k.

3. The moment is determined at all stations by summing the respective first order moments (applied to member ends or due to transverse loads) and second order moments (the product of the axial load and lateral displacements).

4. The curvature at each station is calculated using the M-Φ-P relationship.

5. A curvature distribution between the nodes is assumed, and the equivalent nodal loads are calculated. These nodal loads are applied to the member as conjugate beam loads in order to calculate slope and deflection at the stations. Examples of typical curvature distributions and equivalent nodal loads are given in Fig. [2.4b].

6. If the differences between the deflections calculated in step 5 and those of step 2 are acceptably small, load is added and the procedure repeated until the peak of the load deflection curve is reached. If the differences are too large, the deflections from step 5 become the deflections of step 2, and steps 3 to 5 are repeated until convergence occurs.

The finite element method is an advanced form of structural analysis capable of allowing for nonlinearities arising from changes in the conditions of structural geometry, material properties, boundaries, or any combination thereof. It currently provides the most comprehensive approach to the analysis of structures and thus provided a suitable benchmark with which to compare the accuracy of a proposed new method. Below is a brief explanation of the theory of finite element analysis.

2.1.4 The finite element method

In essence, the finite element method creates a stiffness matrix for a structure for the calculation of deflections during the loading process. This matrix is composed of the assembled stiffness matrices of the elements that are used to model the structure. As load changes, the structure stiffness matrix is updated to reflect the current structural geometry, stress conditions and possible changes at supports. If an iterative form of solution algorithm is chosen for the analysis, then by the end of each load step, the programme will ensure that the differences between the internal and external force vectors of the structure and load system are within specified tolerances.

In preparation for the finite element method, the designer chooses a suitable type of element that is capable of being used to model the relevant structural responses. An element is representative of a small length of member, and so various element types exist for the modelling of beams, plates, shells and so on. Each element possesses nodes that represent the locations where they are joined to other elements, and hence where forces are transferred between, and to, elements. In the case of the portal frames that were modelled using ABAQUS, the elements were of the double noded, two-dimensional beam variety throughout. Material and section properties are assigned to the element to enable the calculation of stresses and strains. Each member of the structure is modelled by choosing the positions of the nodes within its length. Assembling the elements thus is known as ‘meshing’ the model, and the resulting ‘mesh’ plays an important role in determining the accuracy with which the programme can analyse response.

The object of discretising members into a number of elements is that bending theory can be applied to each element. In so doing, the behaviour of a member can be more accurately approximated than if one were to do so knowing only the member's end stresses and deflections. Thus it follows that a finer mesh (i.e. smaller elements but more of them) will produce more accurate results, albeit requiring more computing time. Meshes may be constructed so as to be finer, where required for reasons of output accuracy or for achieving three-dimensional shapes, or coarser, to reduce computing time, in different parts of the structure. Meshing is also such as to provide nodes in the positions where supports and joints occur, and where loads are applied.

Displacement functions are chosen that relate the displacements at any point within an element to that point's position within the element. Since the displacement functions dictate the deflected shape of the element, it is prudent for the user to have some knowledge of the load-deflection behaviour of the structure being analysed. Examples of such functions for two-dimensional beams are

$$u = a_0 + a_1 x \tag{2.17}$$

$$v = b_0 + b_1 x + b_2 x^2 + b_3 x^3 \tag{2.18}$$

where u = Axial displacement relative to the element local axes
v = Transverse displacement relative to the element local axes
x = Distance along the length of the element

Each element's boundary conditions are used to determine its unique values of the coefficients a_i and b_i. Since the boundary conditions are actually the nodal displacements, the transverse and axial displacements of the elements can be expressed in terms of the respective nodal displacements.

There are various methods that can be used to derive the stiffness matric of an element. One such method is to use the principle of conservation of potential energy, as described by Chen (1991). The total stationary potential energy $\boldsymbol{\Pi}$ of the element is composed of the strain energy $\boldsymbol{U}$, and the work done by nodal forces $\boldsymbol{V}$.

$$\mathbf{\Pi} = \mathbf{U} + \mathbf{V} \tag{2.19}$$

where $\boldsymbol{\Pi}$ = Total stationary potential energy
$\boldsymbol{U}$ = Strain energy
$\boldsymbol{V}$ = Work done by nodal forces

The strain energy is defined in the general case as

$$\mathbf{U} = \int_{Ve}\int_{\varepsilon} \sigma \, \mathrm{d}\varepsilon \, \mathrm{d}V_e = \int_{0}^{L}\int_{A}\int_{\varepsilon} (\sigma \, \mathrm{d}\varepsilon) \, \mathrm{d}A \, \mathrm{d}x \tag{2.20}$$

where σ = Axial stress
ε = Axial strain
V_e = Volume of the element

A = Area of the element
L = Length of the element

Strain can be expressed as a differential of the displacement functions (2.17) and (2.18), and stress can easily be related to strain in terms of Hooke's law. Consequently, Eqn. (2.20) can be written as a function of nodal displacements.

The work done by nodal forces is written as

$$\mathbf{V} = -\sum_{i=1}^{n} r_i \, d_i = -\mathbf{d}^T \, \mathbf{r} \tag{2.21}$$

where r_i = Nodal force
d_i = Nodal displacement
$\boldsymbol{r}, \boldsymbol{d}$ = Vectors of nodal forces and displacements respectively

Equilibrium is achieved when the first variation of the total potential energy equals zero.

$$\delta\mathbf{\Pi} = \delta(\mathbf{U} + \mathbf{V}) = \delta\mathbf{U} + \delta\mathbf{V} = 0 \tag{2.22}$$

Substituting the equations for $\boldsymbol{U}$ and $\boldsymbol{V}$, written in terms of the nodal force and displacement vectors, into Eqn. (2.21), the solution is

$$(\mathbf{k}\,\mathbf{d} - \mathbf{r})\delta\mathbf{d} = 0 \tag{2.23}$$

The non-trivial solution to this expression is

$$\mathbf{r} = \mathbf{k}\,\mathbf{d} \tag{2.24}$$

where $\boldsymbol{k}$ = Stiffness matrix for the element

The structure stiffness matrix assembled from the element stiffness matrices accurately describes how the structure responds to load under the conditions for which that stiffness matrix is derived. If the behaviour of the structure is nonlinear, the addition of load will necessitate successive recalculations of the structure stiffness matrix such that the predicted load-deflection curve remains on the equilibrium path. In order to overcome the problem of excessive computation time, there exist several solution algorithms that solve within user-defined tolerances for various types of nonlinear behaviour. The simplest type is non-iterative and solves the problem of nonlinearity by adopting small load increments. At the end of the application of each load increment, the stiffness matrix is recalculated using the new deflections and forces, but without ensuring that the load-deflection curve is on the equilibrium path. This method is known as the 'simple incremental method'. The more advanced methods measure the unbalanced force vector (i.e. the difference between the external and internal force vectors) after each iteration, and reapply it to the structure with a new calculation of stiffness matrix and deflection. Only when the unbalanced force vector is acceptably small, is the next load or deflection increment applied

2.2 Instability

The culmination of most analyses of compression members is the calculation of a load at which the member fails. Instability of a compression member occurs when an addition of load reduces the stiffness of the member, or specific regions thereof, to zero, resulting in progressive deflection and failure. Considering the in-plane behaviour of a column and ignoring the possibility of local buckling, instability may occur in one of three basic ways:

1. **Yielding of the cross-section**: This occurs when the axial force P_y equals the product of the cross-sectional area and the yield stress of the material. This type of failure is unlikely as the slenderness ratios of most practical columns are such that considerably smaller loads will induce failure in flexure. Yielding of the cross-section is a type of inelastic instability, but it is usually not associated with P-delta effects and sway failures of frames.

2. **Elastic instability**: At the elastic instability load P_{cr}, a column carries the hypothetical maximum axial load prior to failure in flexure. It is calculated while assuming a linear elastic stress-strain relationship in the member. P_{cr} is independent of the magnitude of stress in the material and consequently is not affected by yield stress. Should P_{cr} be exceeded, P-delta effects will cause instability of the entire compression member, as opposed to failures of specific zones that are subjected to high stresses. Elastic instability is also independent of the magnitude of transverse loads, except in the capacity of these loads to alter axial loads in the compression members.

3. **Inelastic instability**: The initial imperfections in the fabrication of the members, as well as the asymmetry of the loading or of the structure itself, cause amplification of sway-related deflections and stresses. Before the elastic instability load is reached, the stresses in the section at certain points in the structure become entirely plastic. These plastic sections create a mechanism that allows the structure to fail in flexure.

While the elastic critical load is one that cannot be reached for a real structure, it is a useful point to begin in understanding instability. In solving for P_{cr}, the designer performs a second order elastic analysis, thereby allowing for geometric nonlinear behaviour. In frames that permit sway, it is often the P-delta effects that govern the mode of failure of the frame. Since the yielding of the structural material will only weaken the structure, the inclusion of material nonlinearity in the calculation of instability can be seen as a development of the concept of the elastic critical load.

Below are described three means of determining the elastic critical load. The first example is a derivation of P_{cr} from first principles for a geometrically perfect pin-ended column. The second example is the use of stability functions that can be substituted into the stiffness matrix and is therefore more readily and conveniently applied to structures consisting of more than one member. The last example is the use of effective length factors that have been predefined for the common end conditions of a column.

2.2.1 Elastic critical load of pin-ended column from first principles

The simplest elastic critical load that can be solved for is the load that causes a geometrically perfect pin-ended column to achieve a state of neutral equilibrium under perfectly axial loading. At this load, the *P*-δ effect is sufficient to maintain transverse deflections within the member after transverse loading and/or applied end moments have been removed. On the load-deflection graph, this is known as the bifurcation point, and the magnitude of the transverse deflection at this load is arbitrary. Unstable equilibrium occurs when the critical load is exceeded, and is characterised by collapse of the member.

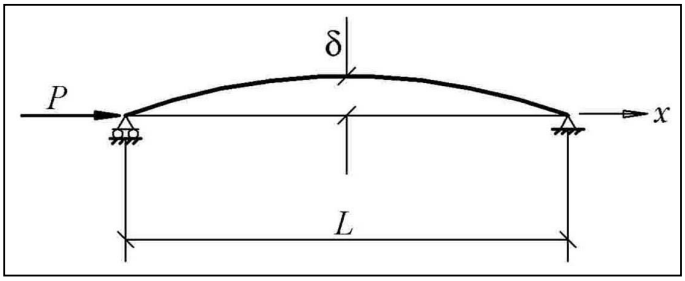


Fig. [2.5] Pin-ended strut under axial load

The elastic critical load of a column can be solved for by first defining the differential equation of moment equilibrium for the member. The differential equation, when solved, produces a solution whose unknowns consist of constants of integration, and the axial force required to maintain the member in a non-straight configuration. Applying the known boundary conditions of the member allows the value of load to be found. Below is an example of this technique used to find the Euler buckling load of a pinned-pinned column shown in Fig. [2.5]. The differential equation can be shown to be

$$EI\frac{\mathrm{d}^4\delta}{\mathrm{d}x^4}+P\frac{\mathrm{d}^2\delta}{\mathrm{d}x^2}=0 \tag{2.25}$$

The general solution to Eqn. (2.25) is

$$\delta = A\sin kx + B\cos kx + Cx + D \tag{2.26}$$

where $k=\sqrt{P/(EI)}$ (2.27)

Recognising that the boundary conditions of curvature and deflection at both supports are equal to zero, the following system of linear equations can be constructed:

$$\begin{bmatrix} 0 & 1 & 0 & 1 \\ 0 & -k^2 & 0 & 0 \\ \sin kL & \cos kL & L & 1 \\ -k^2\sin kL & -k^2\cos kL & 0 & 0 \end{bmatrix}\begin{pmatrix} A \\ B \\ C \\ D \end{pmatrix}=\begin{pmatrix} 0 \\ 0 \\ 0 \\ 0 \end{pmatrix} \tag{2.28}$$

Using vector notation, Eqn. (2.28) can be simplified to

$$\mathbf{CX} = \mathbf{0} \tag{2.29}$$

For a non-trivial solution the determinant of $\boldsymbol{C}$ must equal zero, hence after simplification

$$k^4 L \sin kL = 0 \tag{2.30}$$

k will not equal zero, so

$$kL = n\pi \quad n = 1, 2, 3, ... \tag{2.31}$$

Substituting Eqn. (2.27) into Eqn. (2.31) for P_{cr}

$$P_{cr} = \frac{n^2 \pi^2 EI}{L^2} \tag{2.32}$$

Instability will occur for the lowest value of P, thus when n equals unity,

$$\begin{aligned} P_{cr} &= \frac{\pi^2 EI}{L^2} \\ &= P_e \end{aligned} \tag{2.34}$$

By selecting a value of n, substituting k into the equation for deflection, and solving for the boundary conditions, it will be seen that all the constants except A will be equal to zero. The value of A cannot be solved for, indicating that the deflected shape of the column is that of a sine wave, but the amplitude thereof is arbitrary.

By solving in a similar manner for columns of different support conditions, expressions can be derived for the critical loads and written as

$$\begin{aligned} P_{cr} &= \frac{\pi^2 EI}{K^2 L^2} \\ &= \frac{P_e}{K^2} \end{aligned} \tag{2.35}$$

where K = Effective length factor

The value of the elastic critical load will not actually be reduced by initial curvatures of the members, provided it is assumed that the stresses remain elastic in the cross-section.

2.2.2 Stability functions and practical effective length factors

When the slope-deflection equations are derived for a member taking into consideration the effect of an axial load, the result is that ‘stability functions’ are

introduced to the member stiffness matrix. The member stiffness equations for a two-dimensional beam-column ignoring axial deflections and torsion are restated as

$$\begin{pmatrix} V_A \\ M_A \\ V_B \\ M_B \end{pmatrix} = \frac{EI}{L} \begin{bmatrix} \varphi_1 / L^2 & \varphi_2 / L & -\varphi_1 / L^2 & \varphi_2 / L \\ \varphi_2 / L & \varphi_4 & -\varphi_2 / L & \varphi_3 \\ -\varphi_1 / L^2 & -\varphi_2 / L & \varphi_1 / L^2 & -\varphi_2 / L \\ \varphi_2 / L & \varphi_3 & -\varphi_2 / L & \varphi_4 \end{bmatrix} \begin{pmatrix} v_A \\ \theta_A \\ v_B \\ \theta_B \end{pmatrix} \tag{2.36}$$

where φ_1, φ_2, φ_3 and φ_4 are stability functions

The stability functions are expressed as functions of the ratio of axial load to the Euler buckling load of the strut. These functions are usually printed in tables to save the designer the trouble of recalculation as axial loads change. Since stability functions are derived while assuming conditions of linear elastic behaviour of the material, they can conveniently be used to find the elastic critical load of a structure. Once the structure's stiffness matrix has been assembled, the user solves for the value of load that renders the determinant of the matrix equal to zero. At this load, the stiffness matrix is impossible to invert, and the structure is elastically unstable. Were the stability functions to be omitted, or calculated for conditions of zero axial loads in the struts, the stiffness matrix would always dictate geometrically linear behaviour with unique values of deflections for each load.

Depending on the analysis methods available to the designer, and the complexity of the structure at hand, it may not be feasible to define the stiffness matrix of the entire frame. Under such circumstances, the designer may wish to consider each member of the frame as if it were acting in isolation, but take into account the restraining effects that adjacent members may have on it. The magnitude of the restraining forces are usually proportional in some way to the respective degrees of freedom of the member ends, but can be prohibitively difficult to quantify for practical structures. For the convenience of the designer, many design handbooks provide simple methods of evaluating the effective length of columns with various common end conditions. With the effective length factor known, the designer can simply apply it in Eqn. (2.35) to find the elastic critical load, or as required by a relevant clause of the design code. In SANS 10162-1:2004 the instability load is considered for the condition in which sway deflections are prevented. The provided means of calculating the effective length factor is through the use of the nomograph that has been reproduced in Fig. [2.6]. The value of G is determined for the top of the column and the bottom, and the straight line joining the two points intersects the middle line at the correct value of effective length factor K. G is defined as follows:

$$G = \frac{\Sigma I_c / L_c}{\Sigma I_g / L_g} \tag{2.37}$$

where I_c = Second moment of area of a column section
L_c = Unsupported length of a column
I_g = Second moment of area of a girder section
L_g = Unsupported length of a girder

Σ applies to all members rigidly connected to the relevant joint and lying in the plane in which instability is being considered

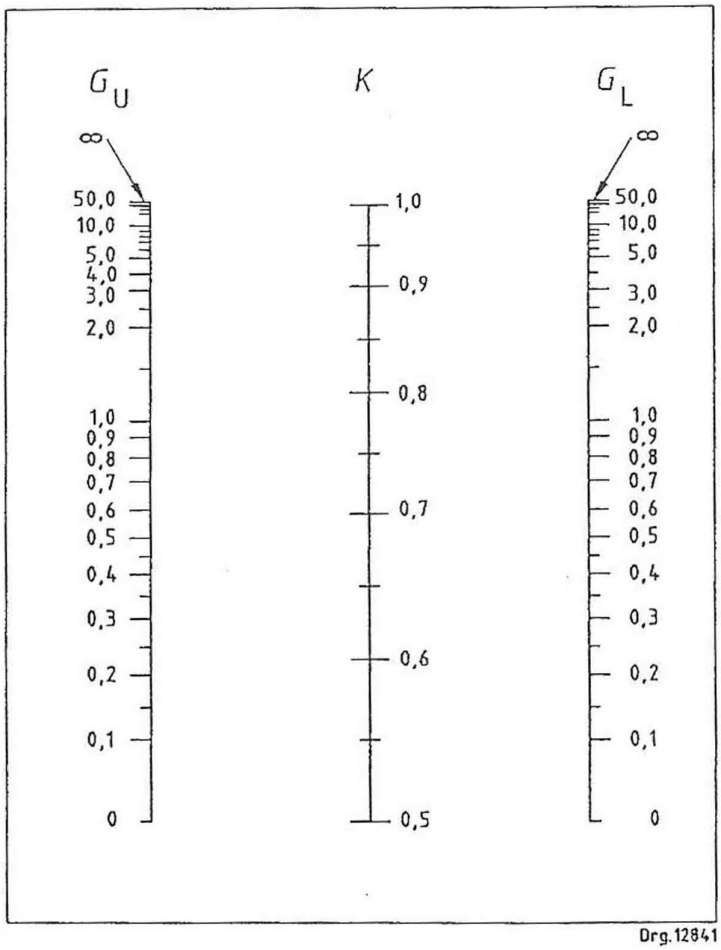


Fig. [2.6] SANS 10162-1:2004 Nomograph for effective lengths of columns in continuous frames

When considering the effects of material nonlinearity on the instability of a structure, the complexity of the calculation increases greatly. The relationship of stress to strain can no longer be represented by a simple linear equation, and thus the equations of equilibrium and compatibility within a structure may change continuously as regions thereof achieve plasticity. A true description of the behaviour of a structure as it approaches actual inelastic instability necessitates the iterative approach of calculations to account for its ever-changing response to load. Where geometric nonlinearity can be ignored, simple first order plastic analysis may provide sufficiently accurate estimations of critical loads. In unbraced frames permitting modes of sway failure, however, the design should account for both forms of nonlinear behaviour acting together. Material inelasticity will affect each structure differently depending on the structural material, the configuration of the structure and position and type of loads acting upon it. Nevertheless, it can be said that the yielding of structural material will have the effect of reducing the stiffness and thereby decreasing its load carrying capacity. Although strain hardening may occur if

deflections are sufficient, material inelasticity will usually cause a structure to fail at a load that is less than the elastic critical load P_{cr}.

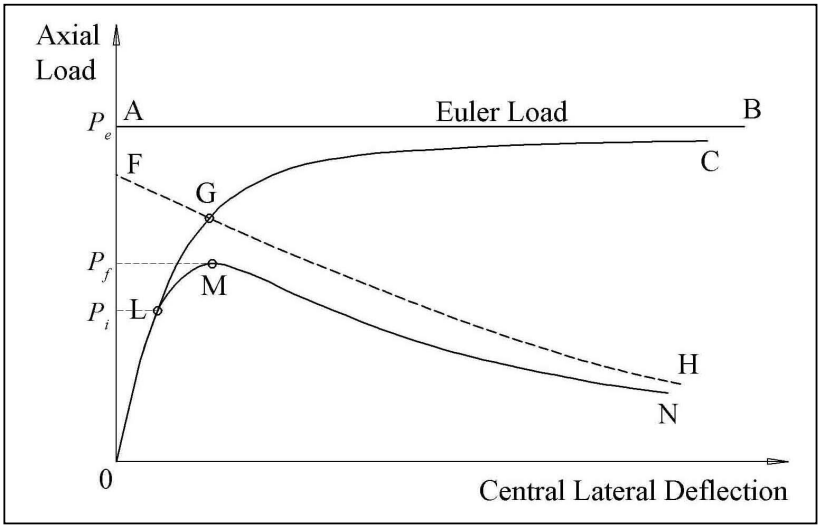


Fig. [2.7] Load versus central lateral deflection for idealised pin-ended columns

The various possible forms of instability are summarised for a pinned column in the graph of Fig. [2.7]. This graph, showing axial load versus central lateral deflection, is a reproduction from *Structural Analysis* by Coates, Coutie and Kong (1997). Line OAB represents the load-deflection curve of a perfectly straight strut whose crush load P_y is higher than the Euler load P_e. If P_y is lower than P_e, the curve will follow the path OFGH. An initially non-straight strut with an effectively infinite yield stress will trace OGC, being asymptotic to P_e. This curve reveals how nonlinearity in structural response is caused by changing geometry of the structure. Note that the nonlinearity becomes progressively worse as the elastic critical load is approached. This fact can be verified by observing that the vector of deflections of a strut tends to infinity as the determinant of the stiffness matrix tends to zero. A real strut will follow curve OGC to point L whereupon yielding of the cross-section begins. Here it can be seen that yielding of the material increases the non-linear response of a real strut. At point M the maximum load carrying capacity P_f is reached and a fully plastic section occurs prior to collapse.

Figure [2.8] is a reproduction of Chen's (1991) generalised graph of loads versus characteristic deformations of a plane frame. Each curve in the graph results from a different type of analysis. Depending upon which forms of nonlinear behaviour are accounted for, the analogies between the curves of Fig. [2.8] and the idealised curves of Fig. [2.7] are clear. The analysis methods used in this project are as follows:

1. **First-order elastic analysis**: To determine the 'limit of elastic behaviour' for Kemp's bilinear load-X relationship.

2. **Second-order elastic analysis**: To determine the elastic critical loads of the frames.

3. **Simple first-order plastic analysis**: To establish the collapse loads of the critical plastic mechanisms and thereby define the 'limit of plastic behaviour'

of Kemp's bilinear λ-X relationship. This analysis was also used to calculate the pure sway collapse loads of the frames.

4. **Advanced first-order plastic analysis**: A finite element analysis for the calculation of first order deflections. These deflections were used to define a proper λ-X graph.

5. **Second-order spread-of-plasticity analysis**: A finite element analysis for comparison of results and evaluation of Kemp's theory.

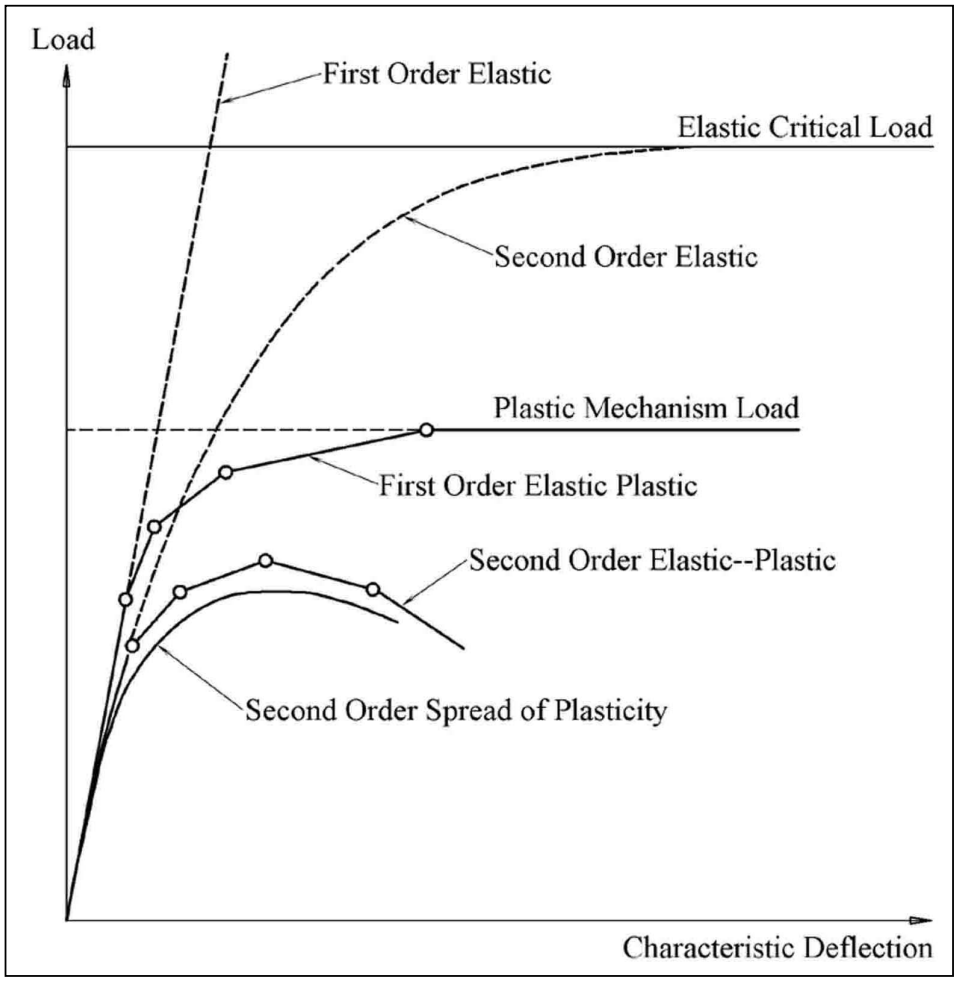
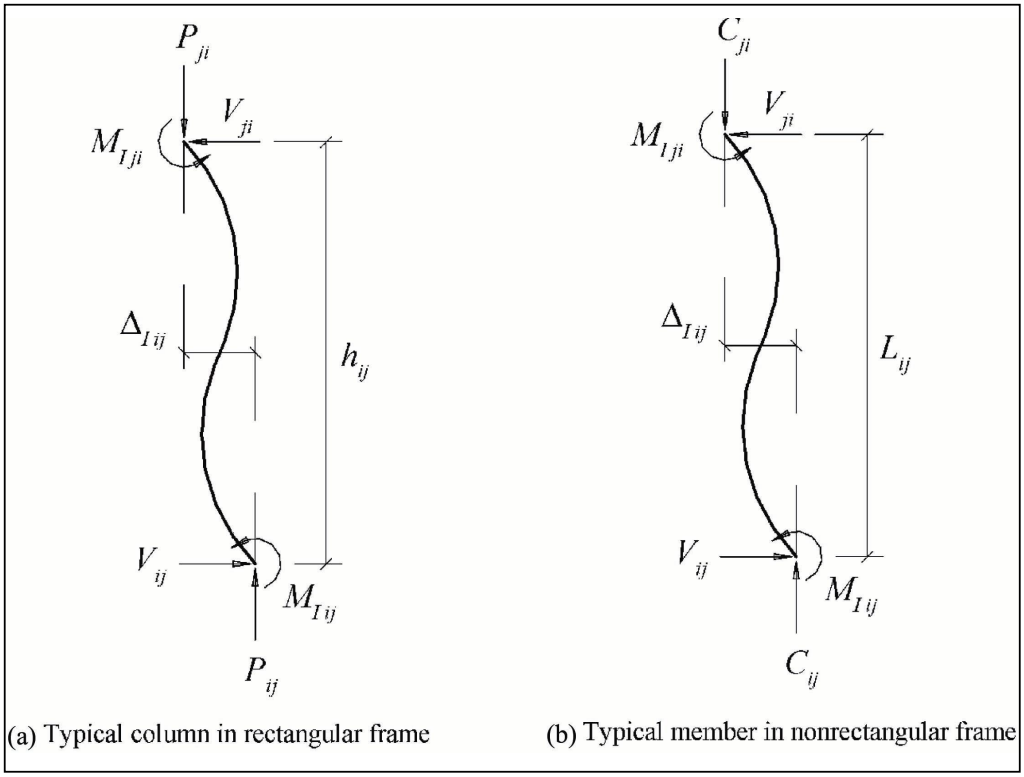


Fig. [2.8] Load versus characteristic deflection for various analysis methods

2.3 Kennedy et al's Amplification Factor

Kennedy et al (1990) give a review of the rationale of the interaction equations for beam-column design as stated in the 1989 version of the Canadian steel design standard. In the member strength interactions of this code, as in SANS 10162-1:2004, an amplification factor for P-Δ effects in unbraced rectangular sway frames may be used in lieu of a second order analysis. This amplification factor U_2 is identical to the

amplification factor as calculated for the story magnifier method in section 2.1.2 of this report. Kennedy et al, however, derive U_2 in the manner described below.



(a) Typical column in rectangular frame (b) Typical member in nonrectangular frame

Fig. [2.9] First order forces and deflections of typical members in sway frames

Figure [2.9a] illustrates a typical column of a rectangular sway frame under the effects of gravitational and sway loads. The forces and deflections shown in this figure are calculated from a first order elastic analysis. From consideration of first order moment equilibrium for the all the columns we have the following relationship

$$\Sigma(M_{I\,ij} + M_{I\,ji}) = -\Sigma V_{ij} h_{ij} \tag{2.38}$$

where subscript I represents first order analysis
subscripts ij and ji represent member end conditions

Bending moments, shear forces, and the associated rotations and sway deflections are positive anticlockwise. The moment summation on the left hand side of Eqn. (2.38) comprises both translational and gravitational column end moments. Since the columns are assumed to be perfectly vertical prior to loading, the gravitational loads do not contribute to the first order sway of the frame. The moments in the columns from the gravitational loads sum to zero, thus the summation of the total first order moments is equivalent to summation of the first order translational moments.

$$\Sigma(M_{I\,ij} + M_{I\,ji}) = \Sigma(M_{I\,t\,ij} + M_{I\,t\,ji}) \tag{2.39}$$

where subscript t represents translational effects

The second order moment may be dealt with in increments by considering the action of the axial loads P_{ij} in the columns acting through the first order sway deflections Δ_{Iij}. For elastic stress conditions, the first iteration of the second order translational moments can be written as follows:

$$\begin{aligned}\Sigma(M_{1t\,ij} + M_{1t\,ji}) &= -\Sigma P_{ij}\Delta_{I\,ij} = -\Sigma P\Delta_I \\ &= -h\left(\frac{\Sigma P\Delta_I}{h}\right)\end{aligned} \tag{2.40}$$

where subscript *1* represents the first iteration of second order effect

The subscripts *ij* are dropped on the right hand side of Eqn. (2.40) as the column heights and sway deflections of all the columns are identical. It can be seen that the axial loads acting through the first order sway deflection Δ_I are likened to the effect of an artificial horizontal load of magnitude $\Sigma P\Delta_I/h$ acting at the column tops. This artificial shear produces a further increment of sway deflection Δ_1, which by proportion is

$$\Delta_1 = \left(\frac{\Sigma P\Delta_I}{\Sigma Vh}\right)\Delta_I \tag{2.41}$$

The effect of the vertical loads acting through the new increment of sway deflection Δ_1 is considered in the same manner as above, and produces the second iteration of second order translational moments.

$$\begin{aligned}\Sigma(M_{2t\,ij} + M_{2t\,ji}) &= -h\left(\frac{\Sigma P\Delta_1}{h}\right) \\ &= -h\left(\frac{\Sigma P\Delta_I}{h}\right)\left(\frac{\Sigma P\Delta_I}{\Sigma Vh}\right) \qquad \text{(by Eqn. (2.41))} \\ &= -\Sigma(M_{1t\,ij} + M_{1t\,ji})\left(\frac{\Sigma P\Delta_I}{\Sigma Vh}\right) \qquad \text{(by Eqn. (2.40))}\end{aligned} \tag{2.42}$$

Thus a further artificial shear of $(\Sigma P\Delta_1/h)(\Sigma P\Delta_1/\Sigma Vh)$ is considered, producing yet another incremental deflection Δ_2. This process of calculating successive deflections and artificial shears results in infinite sums for both total moment and total deflection. Each sum is a geometric series in which the successive terms vary by a ratio of $(\Sigma P\Delta_1/\Sigma Vh)$. For sway deflection, the sum is expressed as per Eqn. (2.43).

$$\begin{aligned}\Delta &= \Delta_I + \Delta_1 + \Delta_2 + \ldots + \Delta_n \\ &= \Delta_I\left[1 + \frac{\Sigma P\Delta_I}{\Sigma Vh} + \ldots + \left(\frac{\Sigma P\Delta_I}{\Sigma Vh}\right)^n\right] \\ &= \Delta_I\left[1 + X + \ldots + X^n\right]\end{aligned} \tag{2.43}$$

where the incremental amplification factor X is expressed as

$$X = \frac{\Sigma P \Delta_I}{\Sigma V h} \tag{2.44}$$

Since the value of this ratio is always less than one, the limit of Eqn. (2.43) is written

$$\Delta \rightarrow \frac{\Delta_I}{1 - X} = U_2 \Delta_I \tag{2.45}$$

where the amplification factor U_2 is expressed as

$$U_2 = \frac{1}{1 - X} \tag{2.46}$$

The incremental translational moments may be summed in a similar manner to the deflections to obtain the total translational moments.

$$\begin{aligned} \Sigma(M_{t\,ij} + M_{t\,ji}) &= U_2 \Sigma(M_{I\,t\,ij} + M_{I\,t\,ji}) \\ &= -U_2 \Sigma V h \end{aligned} \tag{2.47}$$

Since the sum of gravitational column end moments equals zero, Eqn. (2.47) can be rewritten in terms of total end moments.

$$\Sigma(M_{ij} + M_{ji}) = -U_2 \Sigma V h \tag{2.48}$$

Alternatively, this equation can be expressed as follows:

$$\begin{aligned} \Sigma(M_{ij} + M_{ji}) &= -\Sigma V h - U_2 \Sigma P \Delta_I \\ &= -\Sigma V h - \Sigma P \Delta \end{aligned} \tag{2.49}$$

The amplification factor has been derived to express second order effects as proportions of first order translational moments and deflections. Assuming that the unloaded columns are perfectly vertical, the gravitational loads do not contribute to first order sway. For this reason, gravitational moments are not amplified. As mentioned previously in this report, first order translational moments will arise from gravity loads acting on out-of-plumb columns. These moments can be accounted for by applying notional horizontal loads at the column tops. In the case of the South African steel code, the notional load equals 0.5% of the ultimate gravity load of the storey under consideration, and thereby approximates an initial out-of-plumbness of 0.5% of the storey height. The notional load effects are treated as part of the first order translational load effects. To calculate the total moment at any column end, the amplified first order translational moment is added to the unamplified gravitational moment, as per Eqn. (2.50). The first order translational moments are calculated with the structure bearing translational loads only. The axial force and shear force terms in the amplification factor are calculated with all loads in place.

$$M = U_2 M_{It} + M_g \tag{2.50}$$

It is clear that this amplification factor is dependant upon the linear relationship between translational loads and sway deflection. In order that this linearity is maintained, Kennedy et al stipulate the following conditions:

1. The frame must have horizontal beams, and vertical columns of equal lengths. The sway mode of such a structure will ensure that all columns sway by an equal amount, and are affected equally by *P-Δ* effects regardless of each column's axial load or end shear. This maintains compatibility at the joints at every iteration of the derivation, and allows the same amplification factor to be applied to any of the columns. The rectangular frame also allows the distinction to be made between loads that cause first order sway deflections of the columns, and loads that cause compression in the columns.

2. The stresses in the members must remain elastic such that proportionality may be used to calculate successive increments of sway deflection (as per Eqn. (2.41)). If the storey sway stiffness S_f changes during the consideration of second order effects, the sum of incremental deflections will no longer be the geometric series described by Eqn. (2.43). This will invalidate the expression for U_2 in terms of X. For an elastic frame subjected to monotonic loading (i.e. translational loads increase in proportion to gravitational loads), X will vary linearly with load. As addition of load causes the spread of plasticity the storey sway stiffness will reduce accordingly. If the *P-Δ* effects at a given load do not significantly alter the storey sway stiffness S_f then the expressions for X and U_2 will still apply. The amplification factor will be applicable to sway deflection, but not to moment as sections will approach their maximum moment capacities and minimum flexural rigidities. As instability is approached, however, the structure becomes increasingly sensitive to *P-Δ* effects. Every iteration of second order effects will reduce the sway stiffness, thereby causing loss of proportionality between load and deflection. This will render the expression for U_2 in terms of X progressively less reliable as the collapse load is approached.

2.4 Kemp's Modification for Nonrectangular Structures

This approach uses the sway equilibrium equation as an alternative means of calculating the incremental amplification factor. The formulation of a sway equilibrium equation requires the identification of the relevant independent mode of sway for the frame. For a given sway mode, a structure is conceived with pinned joints placed at the locations where the mode requires plastic hinge rotations. The members of the structure are allowed to rotate rigidly at the pins (i.e. the members themselves remain straight) by an arbitrary amount and thereby to create a set of compatible virtual deflections. The system of loads on the actual structure, as well as the internal force system determined from a first order analysis is 'placed' on the structure in its displaced configuration. This sets up systems of internal and external virtual work. Since the members of the virtual displacement system are rigid, the

virtual work of bending moments and forces within the member lengths equals zero. The only actual internal forces to be considered in the sway equilibrium equation are member end moments. The internal work is summed over all the members, and the external work is summed over all the applied loads. The summations of internal and external virtual work are equated to give the sway equilibrium equation (2.51)

$$-\Sigma(M_{I\,ij} + M_{I\,ji})\phi^*_{ij} = \Sigma P_i \partial^*_i \tag{2.51}$$

where ϕ^* = Virtual member end rotation
∂^* = Virtual displacement of load P in the line of action of the load

Bending moments, shears and rotations are positive anticlockwise. Internal work done by a bending moment is positive when the moment acts in the opposite direction, and hence resists, the rotation at its pin. External work is positive when the load moves in the direction in which it acts. Once member loads have been resolved into equivalent joint loads, the average shear force over a member length may be determined from considerations of moment equilibrium to be

$$V_{ij} = -\frac{M_{I\,ij} + M_{I\,ji}}{L_{ij}} \tag{2.52}$$

where V = Average shear force in member length associated with moment gradient

Average shear force equals the actual member end shear force when there are no transverse loads acting within the member's length. Using the relationships described by equations (2.51) and (2.52), it can be seen that

$$\Sigma V_{ij} L_{ij} \phi^*_{ij} = -\Sigma(M_{I\,ij} + M_{I\,ji})\phi^*_{ij} \tag{2.53}$$

Fig. [2.9b] represents a typical member in a sway frame of any shape. From Eqn. (2.38) we have the following relationship:

$$M_{I\,ij} + M_{I\,ji} = -V_{ij} L_{ij} \tag{2.54}$$

Ignoring the distinction between translational and gravitational moments, the equilibrium of the sum of the first order end moments and the first iteration of the second order end moments may be written as

$$M_{I+1\,ij} + M_{I+1\,ji} = -V_{ij} L_{ij} - C_{ij} \Delta_{I\,ij} \tag{2.55}$$

where C = Axial force in member
subscript $I+1$ represents the sum of the first order analysis and the first iteration of second order analysis

The moments M_I can now be expressed in terms of M_{I+1} using the above two formulae.

$$M_{I\,ij} + M_{I\,ji} = M_{I+1\,ij} + M_{I+1\,ji} + C_{ij}\Delta_{I\,ij} \tag{2.56}$$

Since the principal of virtual work is valid only for first order analysis, Eqn. (2.56) can be used to demonstrate how second order effects can be accounted for in the virtual work equation Eqn. (2.53).

$$\Sigma V_{ij} L_{ij} \phi^*_{ij} = -\Sigma(M_{I+1\,ij} + M_{I+1\,ji})\phi^*_{ij} - \Sigma C_{ij}\Delta_{I\,ij}\phi^*_{ij} \tag{2.57}$$

As in the storey amplifier method, the axial loads acting through the first order sway deflections induce second order moments, which in turn increase the sway deflections and thereby set up a system of incrementally increasing second order moments and sway deflections. Previously, the factor by which successive calculations of deflections and moments differed was expressed as a ratio of the sum of the first iteration of second order moments $\Sigma P\Delta_I$ to the sum of the first order translational moments ΣVh. This ratio was enabled by virtue of the linear behaviour of a rectangular frame, and cannot be applied to the nonrectangular frame. Kemp's approach calculates a ratio X based on virtual work expressions of the first iteration of P-Δ effects and the first order moments thus

$$\begin{aligned} X &= \frac{-\Sigma(M_{I+1\,ij} + M_{I+1\,ji})\phi^*_{ij} - (-\Sigma(M_{I\,ij} + M_{I\,ji})\phi^*_{ij})}{\Sigma V_{ij} L_{ij} \phi^*_{ij}} \\ &= \frac{\Sigma C_{ij}\Delta_{I\,ij}\phi^*_{ij}}{\Sigma V_{ij} L_{ij} \phi^*_{ij}} \qquad \text{(by Eqn. (2.56))} \\ &= \frac{\Sigma C_{ij}\Delta_{I\,ij}\phi^*_{ij}}{\Sigma P_i \partial^*_i} \qquad \text{(by Eqn. (2.51))} \end{aligned} \tag{2.58}$$

After the nth iteration of second order effect, Eqn. (2.57) appears as follows

$$\begin{aligned} \Sigma V_{ij} L_{ij} \phi^*_{ij} = &-\Sigma(M_{I+1+2+\ldots+n\,ij} + M_{I+1+2+\ldots+n\,ji})\phi^*_{ij} \\ &-(\Sigma C_{ij}\Delta_{I\,ij}\phi^*_{ij})(1 + X + X^2 + X^3 + \ldots + X^n) \end{aligned} \tag{2.59}$$

As n tends to infinity, the limit of this sum tends to

$$\begin{aligned} \Sigma V_{ij} L_{ij} \phi^*_{ij} &\to -\Sigma(M_{ij} + M_{ji})\phi^*_{ij} - (\Sigma C_{ij}\Delta_{I\,ij}\phi^*_{ij})(1 + X + X^2 + X^3 + \ldots + X^n) \\ &= -\Sigma(M_{ij} + M_{ji})\phi^*_{ij} - \frac{\Sigma C_{ij}\Delta_{I\,ij}\phi^*_{ij}}{1 - X} \qquad \text{for } X \le 1 \\ &= -\Sigma(M_{ij} + M_{ji})\phi^*_{ij} - U_2 \Sigma C_{ij}\Delta_{I\,ij}\phi^*_{ij} \end{aligned} \tag{2.60}$$

where the expression for U_2 in terms of X remains as follows

$$U_2 = \frac{1}{1 - X} \tag{2.61}$$

Since the virtual sway rotations ϕ^*_{ij} of the sway mode of a rectangular frame are equal for all columns, ϕ^* will cancel out of the expression for X. This results in the same expression for X as calculated by the storey amplifier method, and hence the storey amplifier method becomes a special case of the sway equilibrium approach.

The three main advantages of the sway equilibrium approach are stated by Kemp (1990) as follows:

1. It can be applied to any arrangement of members. It is important to note that in structures with more than one mode of sway, the amplification factor must be determined for the independent mode of sway most likely to occur at failure.

2. There is no need for the distinction between loads that cause first order sway deflections of the columns, and loads that cause compression in the columns. The relative contribution of any type of load is accounted for by the relevant sway mechanism used for the calculation of X.

3. The principle of virtual work is applicable to any type of first order elastic or inelastic analysis. The sway equilibrium approach should therefore not be limited to elastic analyses only.

An example of the derivation of the amplification factor is given for the structure shown in Fig. [2.10a]. It is the left hand half of a symmetrical pitched-roof portal frame and is subjected to a uniformly distributed vertical load. The independent sway mode considered for the sway equilibrium equation is shown in Fig. (2.10b). Hinges are introduced at B and C, and joint C is moved downwards an arbitrary amount of one meter to induce the set of compatible virtual sway deflections. The results of a first order analysis of the structure are displayed in Table [2.1]. The average shears V_{ij} have been calculated as per Eqn. (2.52). The value of X is calculated using Eqn. (2.58).

$$X = \frac{\Sigma C_{ij}\Delta_{I\,ij}\phi^*_{ij}}{\Sigma P_i \partial^*_i}$$

$$= \frac{C_{AB}\Delta_{I\,AB}\phi^*_{AB} + C_{BC}\Delta_{I\,BC}\phi^*_{BC}}{(5.67\lambda)(15)\partial^*_{BC\,ave}}$$

$$= \frac{(85.0)(0.0235)(0.0333) + (61.6)(-0.12)(-0.0667)}{(5.67)(15)(0.5)} \qquad \text{(for } \lambda = 1\text{)}$$

$$= 0.013$$

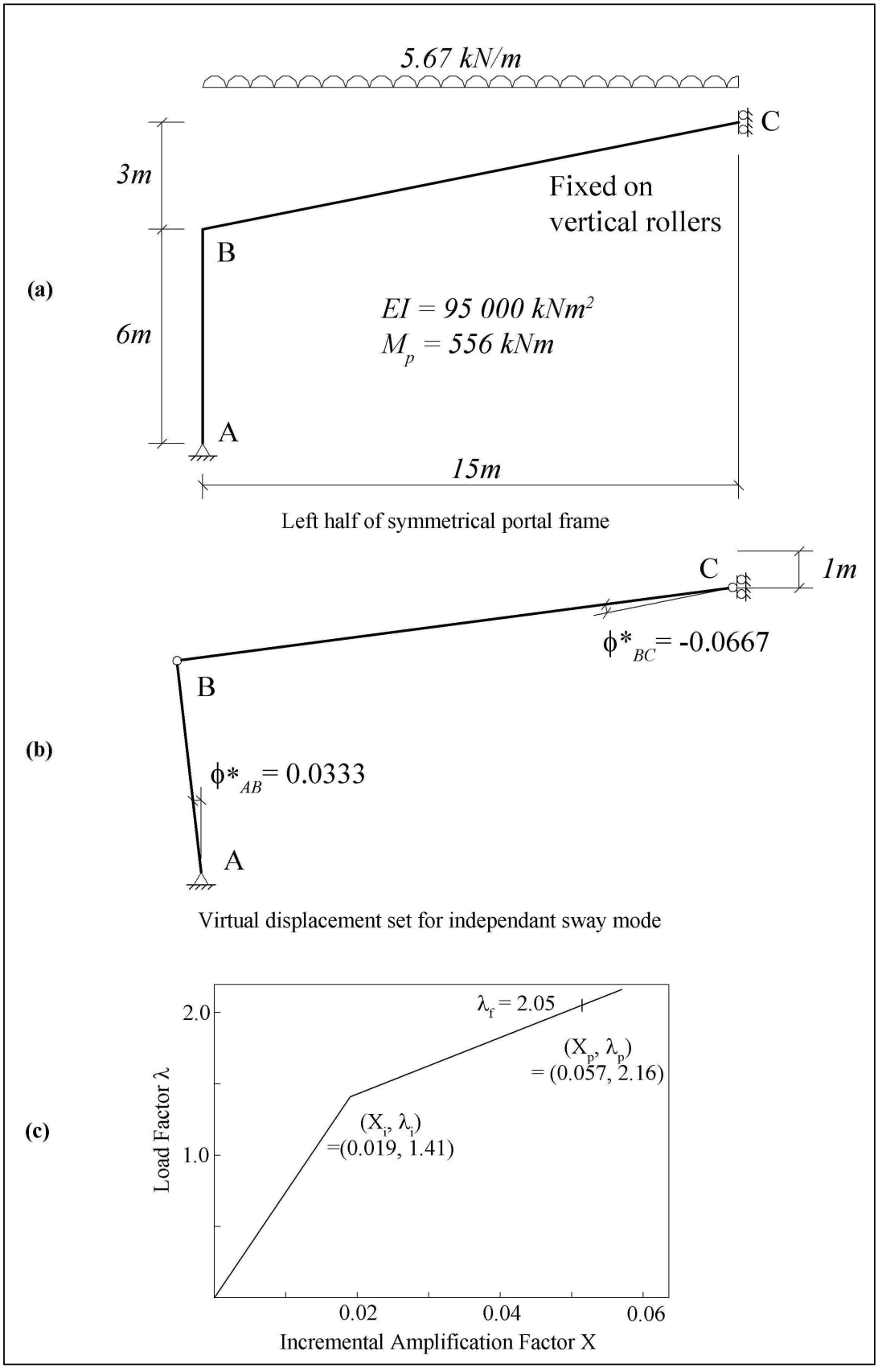


Fig. [2.10] Application of Kemp's amplification factor method to a pitched roof portal

Note that the distance $\partial^*_{ij\,ave}$ represents the average virtual distance through which the uniformly distributed load on member *ij* moves. The amplification factor is calculated according to Eqn. (2.61).

$$U_2 = \frac{1}{1-X}$$
$$= \frac{1}{1-0.013}$$
$$= 1.013$$

Load factor λ	Member	Length L (m)	Axial force C (kN)	Shear force V (kN)	Sway deflection Δ (m)	Virtual rotation ϕ^* (rad)	X
λ_n = 1	AB	6	85	54.2	0.0235	0.0333	
	BC	15.3	61.6	-31.1	-0.12	-0.0667	0.013
λ_i = 1.41	AB	6	120	76.3	0.0331	0.0333	
	BC	15.3	86.7	-43.8	-0.169	-0.0667	0.019
λ_p = 2.16	AB	6	183.5	92.7	0.121	0.0333	
	BC	15.3	108.9	-71.8	-0.615	-0.0667	0.057

Table [2.1] First order analysis data for pitched-roof portal frame in Fig. [2.10]

2.5 Kemp's Treatment of Material Nonlinearity

The application of the virtual work amplification factor is a means of accounting for geometric nonlinearity. Theoretically, material nonlinearity is implicitly accounted for by calculating the amplification factor using a first order inelastic analysis. It is possible to accurately define the nonlinear load-*X* relationship for a given structure by performing first order inelastic analyses at sufficiently small load intervals. The act of doing so, however, negates the object of using the simplified method of amplification factors. Kemp (1990) uses the example of the frame tested by Scholz (1981) to explain his proposed simplification of the true load-*X* curve. Scholz's frame is illustrated in Fig. [2.11]. Under monotonic loading, the first order sway deflection Δ_I of the frame, as calculated from an elastic-plastic analysis, varies linearly with load λ until the formation of the first plastic hinge. At this point, the slope of the load-Δ_I curve reduces with the loss of sway stiffness of the frame. The reduction of slope occurs with the formation of each new hinge until a mechanism allows the frame to collapse. The nonlinear load-*X* curve has a similar shape to the nonlinear load-Δ_I curve. Kemp approximates it with a linear distribution between the limits of elastic behaviour (X_i, λ_i) and first order plastic collapse in the critical combined collapse mechanism (X_p, λ_p). This bilinear curve is shown in Fig. [2.11c].

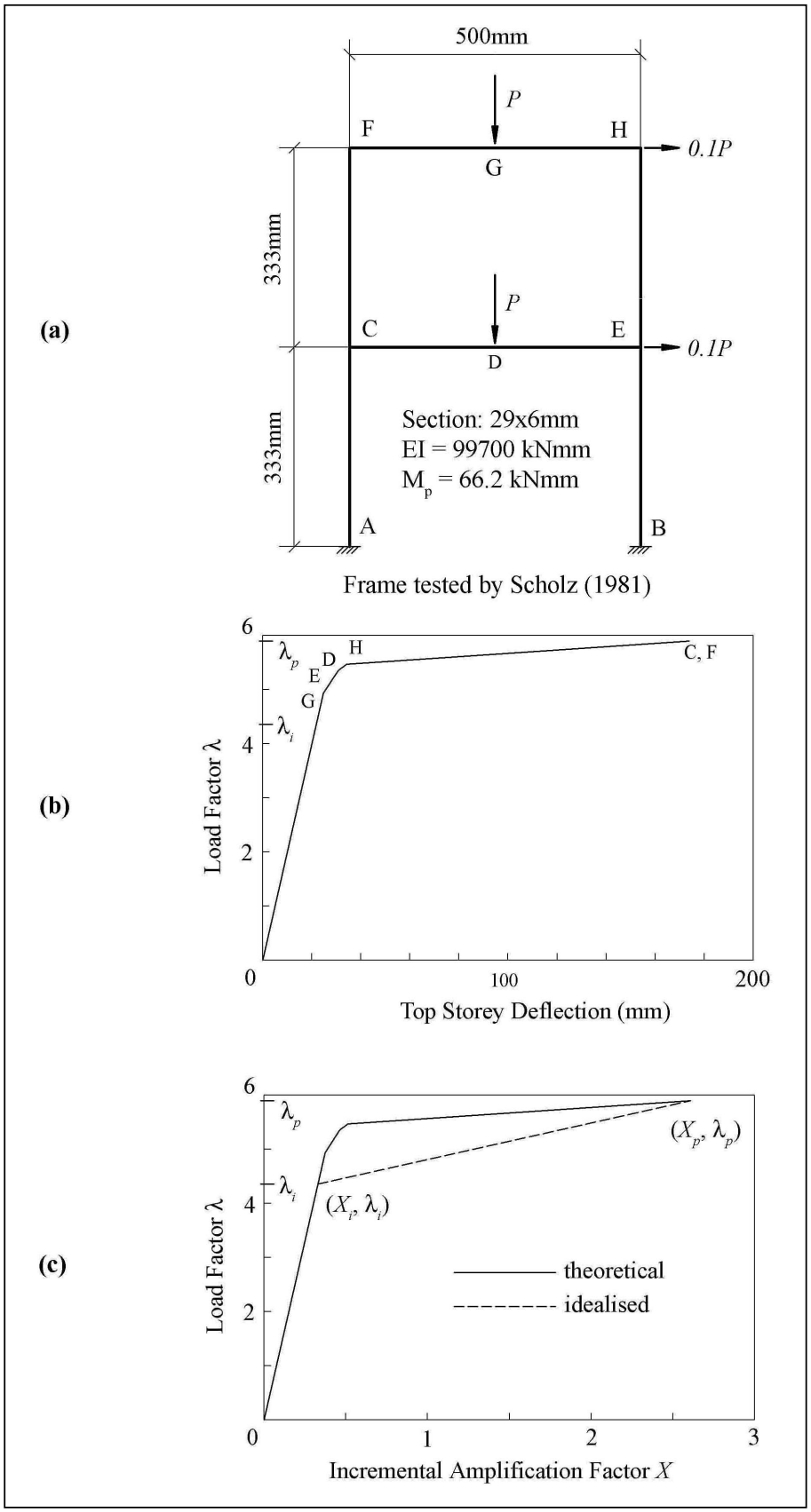


Fig. [2.11] Scholz (1981) test frame with load-Δ and load-*X* graphs

The value of X can be found for any load between zero and λ_p by using the following formulae:

$$0 < \lambda < \lambda_i \quad : \quad X = X_i \left(\frac{\lambda}{\lambda_i} \right) \tag{2.62}$$

$$\lambda_i < \lambda < \lambda_p \quad : \quad X = X_i + \left(\frac{(X_p - X_i)(\lambda - \lambda_i)}{\lambda_p - \lambda_i} \right) \tag{2.63}$$

If gravitational loads remain constant, then X remains equal to X_i until load λ_i is reached. Thereafter, Eqn. (2.63) will again apply.

Currently the limit of elastic behaviour for a steel section is represented by the satisfaction of the interaction equation Eqn. (2.64). The calculation of U_2 for this equation requires a first order elastic analysis of the frame, and the identification of the prevailing independent mode of sway.

$$\frac{C}{C_y} + \frac{U_2 M_I}{M_p} + \frac{0.5\sigma_{res}}{\sigma_y} = 1.0 \tag{2.64}$$

where σ = Axial stress in a longitudinal fibre
0.5 = Weighting factor for residual stress in steel sections
subscript *res* represents residual stress effects from rolling of the section

The calculation of the limit (X_p, λ_p) is performed using conventional plastic analysis. It must include the effects of the reduced plastic moment M'_p, as well as the reduced flexural rigidity EI'. The reduced plastic moment M'_p is calculated by ignoring equal areas closest to the centroid that are capable of resisting the axial force when at yield stress. The axial force used when calculating M'_p is the estimated axial force at failure of the frame. As yielding occurs under the combined action of axial force, bending moment and residual stress, the flexural rigidity of a typical W-shape will reduce as shown by the solid line in the graph of Fig. [2.12]. Kemp (2000) proposes a bilinear simplification for the moment-curvature graph, shown by the dashed line in the same figure. The bilinear approximation is such that a member subjected to a bending moment that varies linearly from zero to M'_p will rotate by the same amount at a maximum curvature of $15M_p/EI$. The reduced flexural rigidity given by the slope of the 'elastic' portion of the bilinear graph is determined from the following empirical equation:

$$\frac{EI'}{EI} = \frac{1}{f} - \frac{1.1C}{C_y} \tag{2.65}$$

where f = Shape factor of the section

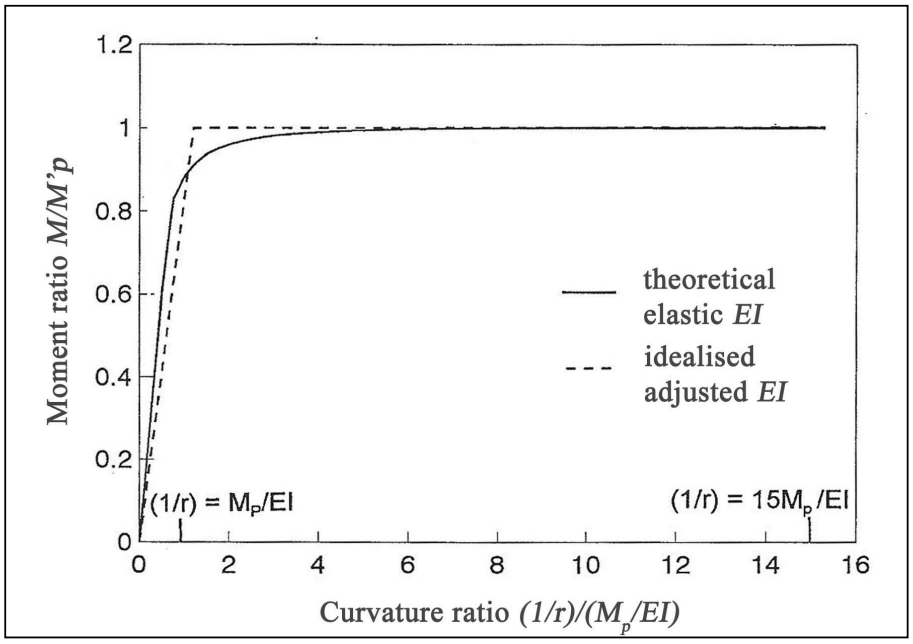


Fig. [2.12] Moment-curvature graphs for a typical W-shape section

This assumed elastic-perfectly-plastic flexural behaviour is used to model the spread of plasticity in members in which plastic hinges form during the formation of the critical sway collapse mechanism. There are various difficulties involved in calculating the limit (X_p, λ_p). The designer must be able to identify the critical combined collapse mechanism and calculate the first order inelastic sway deflections in this mode prior to collapse. The calculation of the deflections involves the use of virtual work, and requires a careful distribution of virtual force so as to avoid the inclusion of unknown plastic hinge rotations. For this reason, it is important that the designer knows the sequence in which the hinges form. If the critical collapse mechanism is a partial mechanism, the virtual work will also require the calculation of various indeterminate moments owing to the structure's static indeterminacy. Kemp (1989, 1990b, 1997, 1999) has developed a general flexibility-based method of elastic and inelastic analysis that addresses these issues. Section 4.2 of this report describes the determination of the critical combined collapse mechanisms and associated sway deflections for the test frames.

Calculation of the inelastic instability load λ_f is based upon the assumption that the *P-Δ* effects result in an independent mode of sway becoming the actual collapse mode. This independent mode of sway should be the same mode used in the calculation of the limits of the bilinear load-*X* graph. In calculating λ_f, the first order collapse load λ_s for the chosen sway mode is first calculated using first order plastic analysis. When the product of the load and its corresponding amplification factor taken from the load-*X* graph equals λ_s, then inelastic instability is said to have occurred.

$$U_2 \lambda_f = \lambda_s \tag{2.66}$$

For the portal frame in Fig. [2.10a], $\lambda_s = \lambda_p = 2.16$ and Eqn. (2.66) yields a failure load at $\lambda_f = 2.05$. This load equals the failure load determined for this frame by a flexibility based, second order elastic-plastic analysis. The load-X graph illustrating the position of the failure load is shown in Fig. [2.10c].

3 LABORATORY TESTING

Laboratory testing took place in the Hillman Heavy Structures Laboratory during the year 2001. The objective of the tests was to capture data such that the following information could be established:

1. **Section and material properties:** These properties, determined from the results of tensile tests, were required for bilinear method calculations as well as for finite element analysis.

2. **Failure loads:** These observed loads provided a means of direct comparison to the predictions of instability made by the bilinear theory.

3. **Hinge positions:** The hinge positions helped to indicate the failure modes of the frames, and thereby tested the assumption that the unbraced sway frames would fail in modes of pure sway.

4. **The load-deflection curves:** The observed deflections were reduced to first order deflections, thus enabling the construction of the actual load-X relationships of the frames. The load-Δ curves were also useful in identifying the loads at which inelastic behaviour commenced.

3.1 Coupon Tests

3.1.1 Test procedure

Laboratory work commenced with the tensile tests of the steel section used to produce the frames. This section was a 25mm X 5mm mild steel flat, supplied in 6m lengths from the laboratory stock. Each frame was built from a single length of flat so as to minimise the variation of material properties between its members. Two coupons were prepared for testing purposes from each of the three supplied lengths. The coupons were milled to nominal cross-sections of 15mm X 5mm over parallel lengths of 350mm. Each cross-section was measured at three locations along its length such that its average cross-sectional area could be calculated. A strain gauge was fitted to measure extension over a gauge length of 203mm, following which the coupon was prepared for testing in the hydraulic Macklow-Smith testing machine. An illustration of a typical coupon is given in Fig. [3.1]. Within the elastic range of stresses, load was increased in 2kN increments with readings of deflection taken at each increment. When the deflection readings indicated that the stress-strain behaviour was becoming nonlinear, the testing machine was set to strain the specimen at a constant rate and readings of load were recorded for every 1mm increase in extension of the gauge length. This process was continued until sufficient strain-hardening had taken place to allow the calculation of steel stiffness E_s in the zone of uniform plastic elongation.

The tests enabled the calculation of engineering stresses and strains only, as no measurements were taken of cross-sectional dimensions during loading.

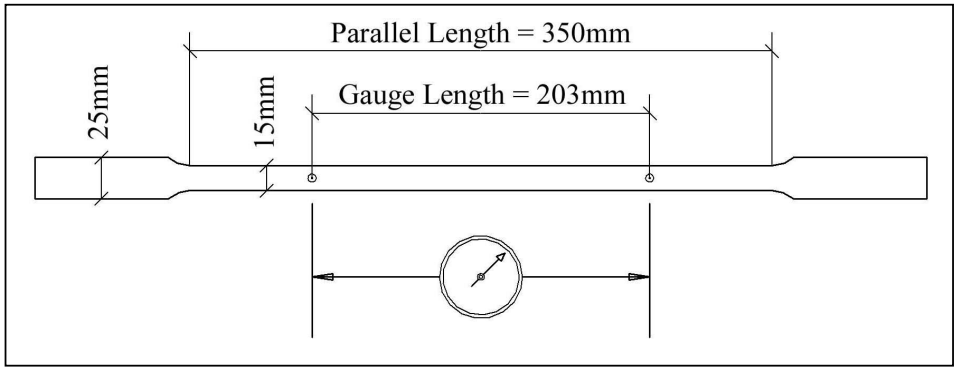


Fig. [3.1] Typical coupon for tensile testing

3.1.2 Section and material properties

The test results of coupon 1a, as recorded in Table [3.1], were typical of the coupon tests and are used here to describe the treatment of the data. The stress-strain graph of this test is illustrated in Fig. [3.2]. It shows clearly defined zones of elastic deformation, non-uniform plastic elongation (during which Lüders bands propagated across the coupon), and uniform plastic elongation as strain hardening took place. The data logging intervals were too coarse to allow the calculation of the upper yield stress, however yielding appeared to occur at a strain of 0.0018 with a lower yield stress of 315MPa. Young's modulus E was determined graphically from an enlarged portion of the stress-strain graph and was found to be 207GPa. Strain-hardening appeared to initiate at a strain of 0.025, increasing the stiffness of the plastically strained steel E_s to 2.35GPa.

Simple bending theory shows that for a partly yielded solid rectangular section in uniaxial flexure, bending moment is related to the distribution of cross-sectional axial stresses as follows:

$$M = \sigma_y b\left(\frac{d^2}{4} - \frac{y_y^2}{3}\right) \tag{3.1}$$

where b = Breadth of section
d = Depth of section
y_y = Distance from neutral axis to first longitudinal fibre at yield stress

The above formula assumes that the stress-strain relationship is elastic-plastic, and that the section carries no axial load. A diagram of such a section is given in Fig. [3.3]. When y_y equals zero, the section is completely plastic, and the moment is the fully plastic moment M_p.

$$M_p = \frac{\sigma_y b d^2}{4} \tag{3.2}$$

COUPON 1a				L (mm)	A (mm^2)	C (kN)	ΔL (mm)	σ (MPa)	ε	E (GPa)	σ_y (MPa)
				203	76.41	0	0	0	0	207	315
						2	0.03	26.176	0.000148		
	Width (mm)	Thickness (mm)	A (mm^2)			4	0.055	52.352	0.000271		
End 1	15.1	5.07	76.557			6	0.08	78.528	0.000394		
						8	0.105	104.704	0.000517		
	Width (mm)	Thickness (mm)	A (mm^2)			10	0.13	130.880	0.000640		
Middle	15.12	5.04	76.2048			12	0.155	157.056	0.000764		
						14	0.18	183.232	0.000887		
	Width (mm)	Thickness (mm)	A (mm^2)			16	0.21	209.408	0.001034		
End 2	15.08	5.07	76.4556			18	0.235	235.584	0.001158		
						20	0.26	261.760	0.001281		
						22	0.285	287.936	0.001404		
						24	0.32	314.112	0.001576		
						24.84	0.555	325.106	0.002734		
						25.01	1.055	327.331	0.005197		
						25.2	1.555	329.818	0.007660		
						24.8	2.055	324.583	0.010123		
						25.39	2.555	332.305	0.012586		
						24.75	3.055	323.928	0.015049		
						24.9	3.555	325.891	0.017512		
						25.3	4.055	331.127	0.019975		
						24.85	4.555	325.237	0.022438		
						24.3	5.055	318.039	0.024901		
						24.87	5.555	325.499	0.027365		
						26.1	6.055	341.597	0.029828		
						26.93	6.555	352.460	0.032291		
						27.47	7.055	359.528	0.034754		
						27.97	7.555	366.072	0.037217		
						28.41	8.055	371.830	0.039680		
						28.82	8.555	377.196	0.042143		
						29.21	9.055	382.301	0.044606		
						29.55	9.555	386.751	0.047069		

Where:

L = Gauge lengh
A = Cross-sectional area
C = Tensile load
ΔL = Extension
σ = Axial stress
ε = Axial strain
E = Young's modulus
σ_y = Yield stress

Table [3.1] Tensile test data of Coupon 1a

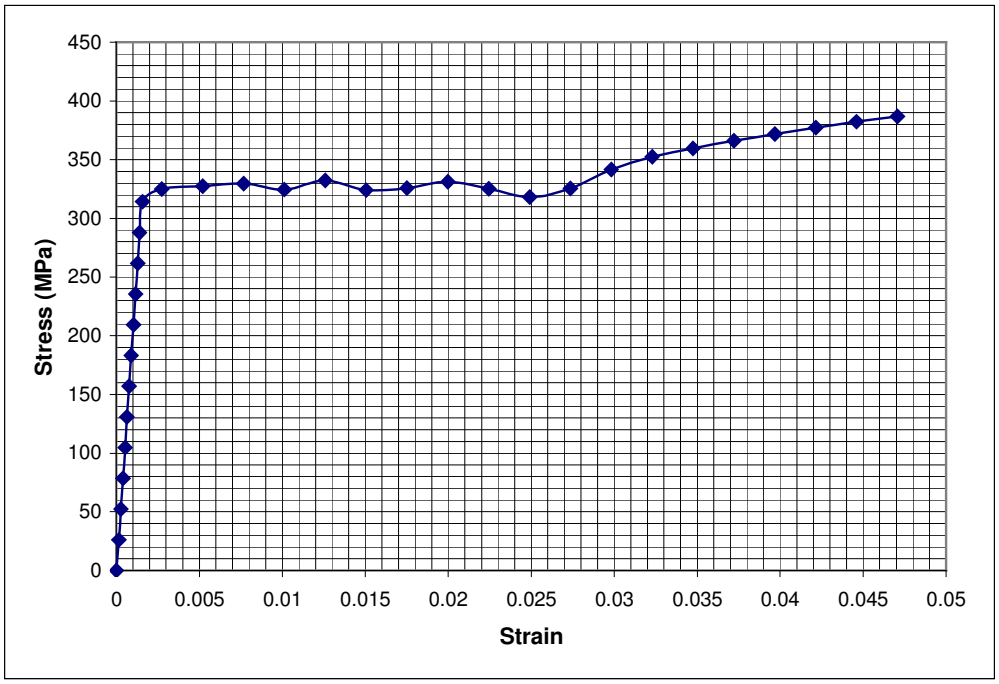


Fig. [3.2] Coupon 1a stress-strain graph

Equation (3.2) is the solution of the classical stress block approach, returning a value of 50.4Nm for coupon 1a. In the presence of axial load, the contribution to M_p of the yielded cross-sectional area closest to the neutral axis that is capable of resisting the axial load is usually ignored. The highest column load recorded during the laboratory testing of the frames was 0.65kN. This axial load could be resisted by a 25mm wide by 0.084mm deep portion of the section at yield stress. When placed symmetrically about the neutral axis, this portion of the section would contribute less than 0.03% of the full M_p. For this reason, the effects of axial load on M_p were ignored in the bilinear method calculations.

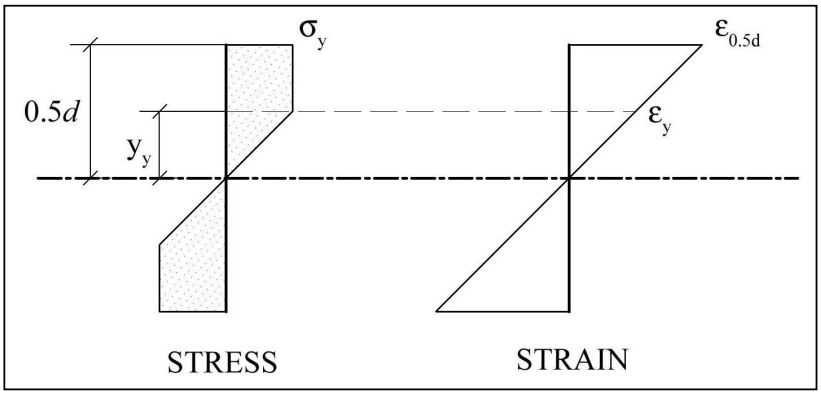


Fig. [3.3] Cross-sectional stress and strain distributions for a mild steel section in flexure

The effects of strain-hardening on flexure were considered by calculating the proportion of M_p attained before strain-hardening began at the outer fibres of the section. When strain-hardening begins at these outer fibres, by proportion of the cross-sectional strain diagram we have the following relationship:

$$\frac{\varepsilon_y}{y_y} = \frac{\varepsilon_s}{0.5d}$$
$$\rightarrow \frac{y_y}{0.5d} = \frac{\varepsilon_y}{\varepsilon_s} \qquad (3.3)$$

where ε = Strain
Subscript *y* represents the condition of yielding
Subscript *s* represents the condition of strain hardening

Dividing Eqn. (3.1) by Eqn. (3.2), we get the ratio of the moment for the partially yielded section to that of the fully plastic moment:

$$\frac{M}{M_p} = 1 - \frac{1}{3}\left(\frac{y_y}{0.5d}\right)^2$$
$$= 1 - \frac{1}{3}\left(\frac{\varepsilon_y}{\varepsilon_s}\right)^2 \qquad \text{(by Eqn. (3.3))} \qquad (3.4)$$

Substituting in the values for ε_y and ε_s as taken from the coupon stress-strain graph, one finds that had the member flexed sufficiently for strain hardening to take place, the section would already have achieved 99.8% of its full plastic moment.

SECTION PROPERTIES SUMMARY		d (mm)	E (GPa)	σ_y (MPa)	M_p (Nm)
Section 1	Coupon 1a	5.06	207.0	315	50.4
	Coupon 1b	5.00	216.7	320	50.0
Section 2	Coupon 2a	4.98	216.5	320	49.6
	Coupon 2b	5.15	207.1	315	52.2
Section 3	Coupon 3a	5.04	207.2	318	50.5
	Coupon 3b	5.07	218.0	315	50.6
Average Section		**5.05**	**212.08**	**317.17**	**50.6**

Table [3.2] Summary of section properties

The test data and stress-strain curves for the remainder of the coupons follow in Appendix A. These results are summarised in Table [3.2]. From the distribution of section properties across the coupons, it seemed reasonable to average the properties across the three original lengths of flat bar. The section properties of the 'average section' were used to define the input for the finite element analysis, as well as for the bilinear amplification factor method. The yield stresses listed in Table [3.2] were determined by a subjective interpretation of the coupon stress-strain curves. Subsequent calculations using the offset method and a plastic strain of 0.2 percent produced an average yield stress of 320.83MPa. This value was only 1.16 percent greater than the 317.17MPa used in the member and frame analyses. Errors of greater magnitude are routinely expected in the testing process due to the combined effects of strain rate variations, grip and coupon misalignment, measurement error and the natural variation of material properties. Moreover, larger errors were inherent to the testing process of the frames themselves. For these reasons it was deemed unnecessary to reanalyse the frames and members with a yield stress of 320.83MPa.

The finite element analysis of the frames required the input of the moment-curvature relationship of the section. For elastic flexure, this relationship was defined by the fundamental bending formula of Eqn. (3.6) below.

$$M = \frac{EI}{R} = EI\Phi \qquad \left(for\ M \le \frac{\sigma_y I}{0.5d}\right) \tag{3.6}$$

For the conditions of inelastic flexure, Eqn. (3.1) can be modified to give moment in terms of curvature:

$$M = M_p - \varepsilon_y^2 \sigma_y b\left(\frac{1}{3\Phi^2}\right) \qquad \left(for\ M \ge \frac{\sigma_y I}{0.5d}\right) \tag{3.7}$$

The curve given by the two formulae above is presented in Fig. [3.4], along with the simplified quad-linear representation that was used as input for the ABAQUS model.

Although the graph ends at the point that strain hardening would have begun, ABAQUS showed that this degree of curvature was only achieved in very localised regions near failure.

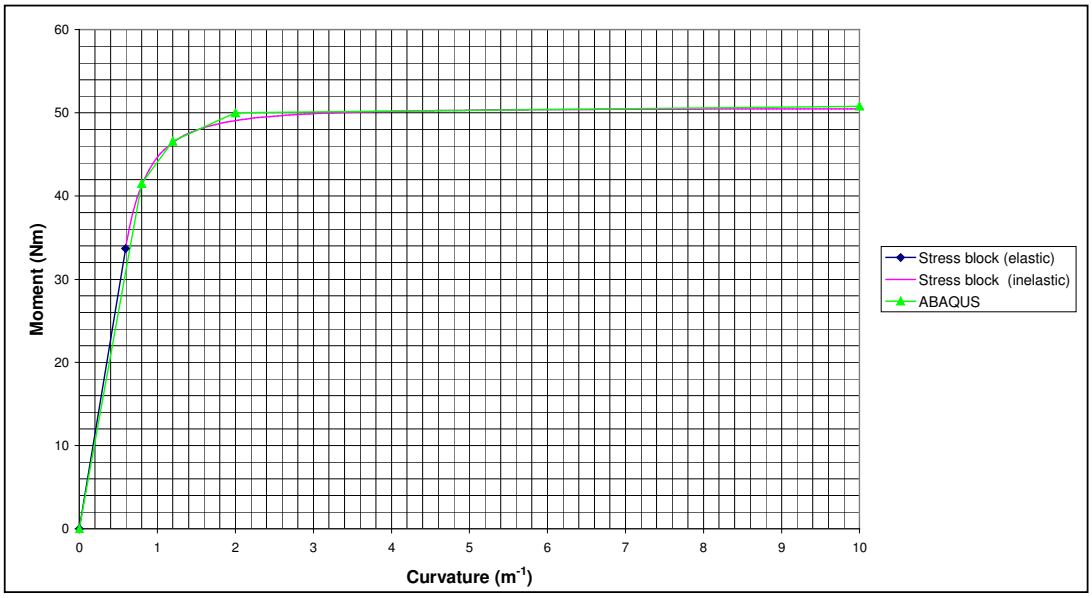


Fig. [3.4] Moment-Curvature graphs of the test frame section

3.2 Frame Tests

3.2.1 Selection of frames

The frames were based on a portal structure that had been tested previously in a postgraduate civil engineering course at the university. Each frame was of single bay and single storey construction, and was supported by fully fixed column bases. The section was orientated to force bending about the weak axis so as to exclude the effects of out-of-plane behaviour. Loading was applied monotonically, and was achieved vertically by means of four equal concentrated loads placed symmetrically about the beam's centre, and horizontally by a single concentrated load applied at a column top. Diagrams of the frames and their loading configurations are given in Fig. [3.5]. The distance between the outermost vertical loads was labelled the 'loading length', and the ratio of total horizontal load to total vertical load the 'sway ratio'. The frame named 'kempsp1' was identical to the postgraduate course portal, with a height of 400mm, a span of 800mm and a sway ratio of 20%. The remaining frames were variations of the kempsp1 frame.

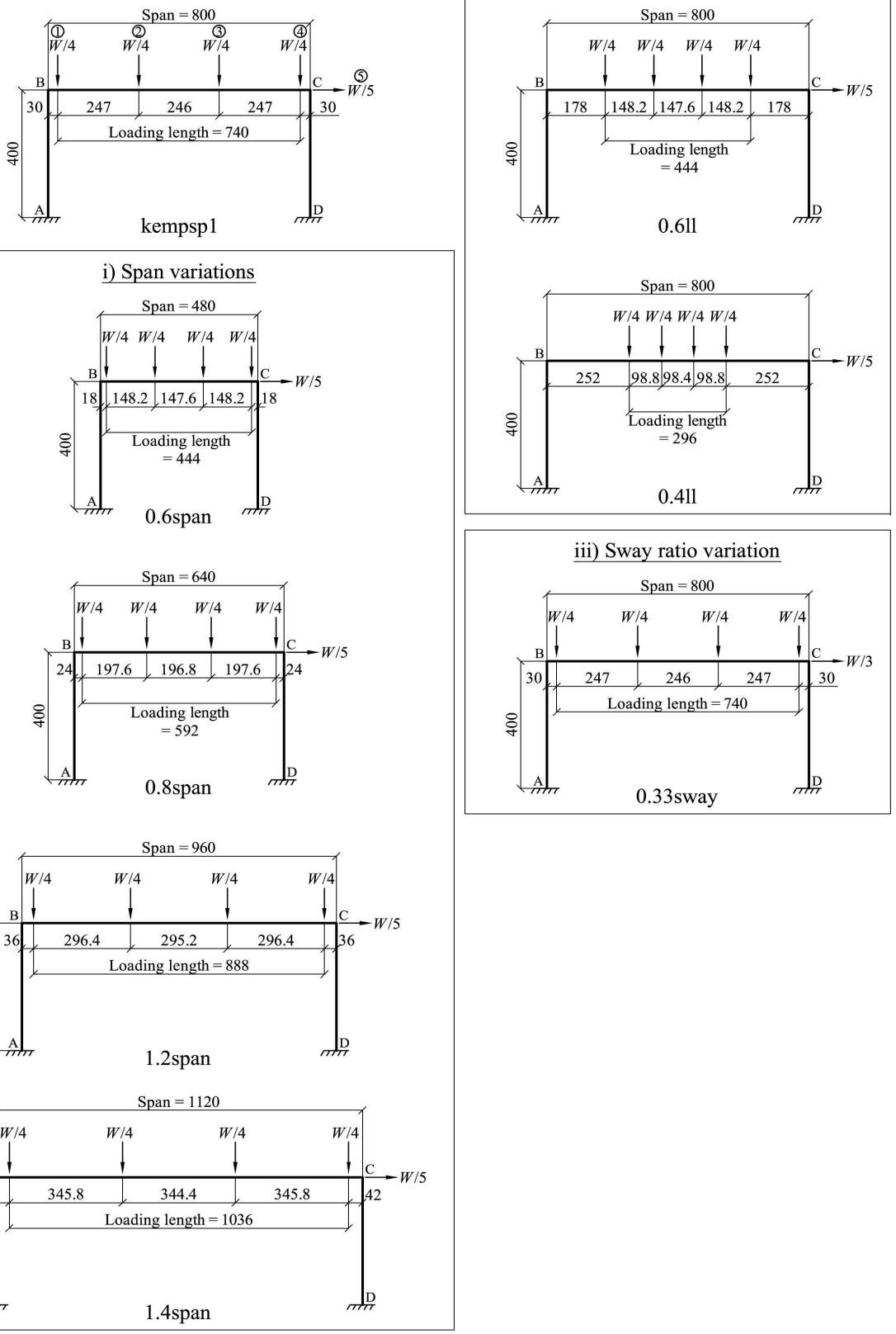


Fig. [3.5] Geometries and loading configurations of the test frames

i) **Span variations:** The '0.6span', '0.8span', '1.2span' and '1.4span' frames varied from 60% to 140% of the span of the kempsp1 frame. These frames also had a sway ratio of 20%, but the respective loading lengths increased or decreased proportionately to the spans. The column heights, as with all the frames, remained unchanged at 400mm.

ii) **Loading length variations:** The '0.6ll' and '0.4ll' frames had similar geometries and sway ratios to the kempsp1 frame, but with loading lengths of 60% and 40% respectively of the kempsp1 loading length.

iii) **Sway ratio variation:** The '0.33sway' frame had the same geometry and loading length as the kempsp1, but with a sway ratio of 33.33%. This frame was initially to be tested as a '0.8ll', but it was decided that the '0.6ll' and '0.4ll' frames would test the effect of loading length variations sufficiently.

The choice of rectangular frames and concentrated gravity loads had various associated benefits. It greatly simplified the processes of fabrication, laboratory testing, the interpretation of test results, and general structural analysis. The single pure sway mode of the frames required only the column top deflections and corresponding loads to define the load-X relationship. Measuring sway for inclined members would have been significantly more complicated and would have introduced further possibility of laboratory error. The slender members used in the frames allowed for very pronounced deflected shapes. This aided accurate measurement of sway deflections and thereby ensured high quality data for the construction of the load-X graphs. Since only two welds were necessary in each frame, the locations at which section properties varied were minimised. The application of point loads helped to indicate the positions at which hinges might form and thus made sway mode failures more predictable. Since these loads were applied by means of hanging weights, the possibility of a poorly calibrated load cell giving an incorrect reading was eliminated.

3.2.2 Equipment and testing

A typical test frame set-up is illustrated in Fig. [3.6]. Fixity of the column bases was achieved through the use of purpose made clamps. Each clamp comprised a sturdy steel block, the top of which had been slotted to receive a column. The clamps were positioned on a trestle table to suit the span of the frame, and were then fastened to the table by means of G-clamps. With the frame in place, a bolt in the side of each clamp was tightened to secure the column bases in position. Two analogue plunger-type dial indicators were mounted on the trestle table, one for measuring horizontal sway deflection at joint B, and one for vertical deflection of the centre of the beam. Recordings of deflection were taken from each gauge for the zero load condition.

Two separate load hangers were used for the application of load. The construction of the vertical load hanger was such as to divide the weight of the loading plates into four equal loads and apply them to the beam in the specified positions. Vertical load hangers, or components thereof were made for each variation of loading length.

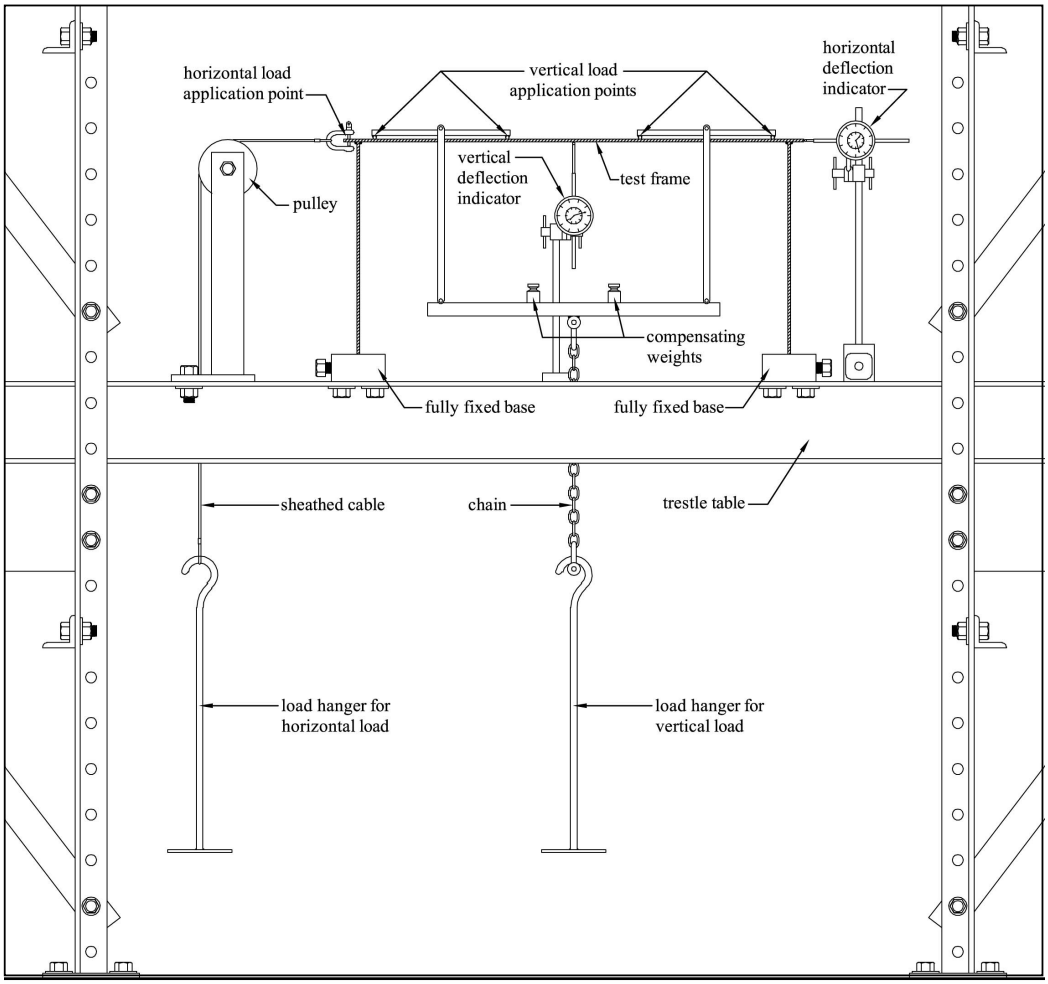


Fig. [3.6] Typical test frame set-up

The ability of the hangers to move with the structure helped ensure that the loads remained vertical at all times. The horizontal load hanger transferred the load to the column top by means of a sheathed steel cable routed over a pulley. The load hangers were weighed, and then placed on the frame. Small compensating weights were added to the hangers to maintain the correct sway ratios, and deflection readings were recorded under the corrected weight of the hangers. Appendix B includes photographs of the testing of three frames in the laboratory.

The loading plates were available in masses of 500g, 1kg, 2kg, 5kg and 10kg. Load was applied to the two hangers in the necessary proportions, and deflections recorded after each placement of load. Large load increments were used at low levels of load. When deflection readings indicated that nonlinear behaviour was beginning to take place, the load increments were decreased in size to allow the nonlinear behaviour to be followed more accurately. Load increments then became as small as the available weights allowed until failure occurred. Collapse of the frames was regarded as having occurred when the addition of load caused an increasing rate of deflection with time. The failure load W_f was taken as the load preceding that under which the frame actually collapsed. This was a conservative approach, as the actual failure load would have fallen between W_f and the collapse load W_c.

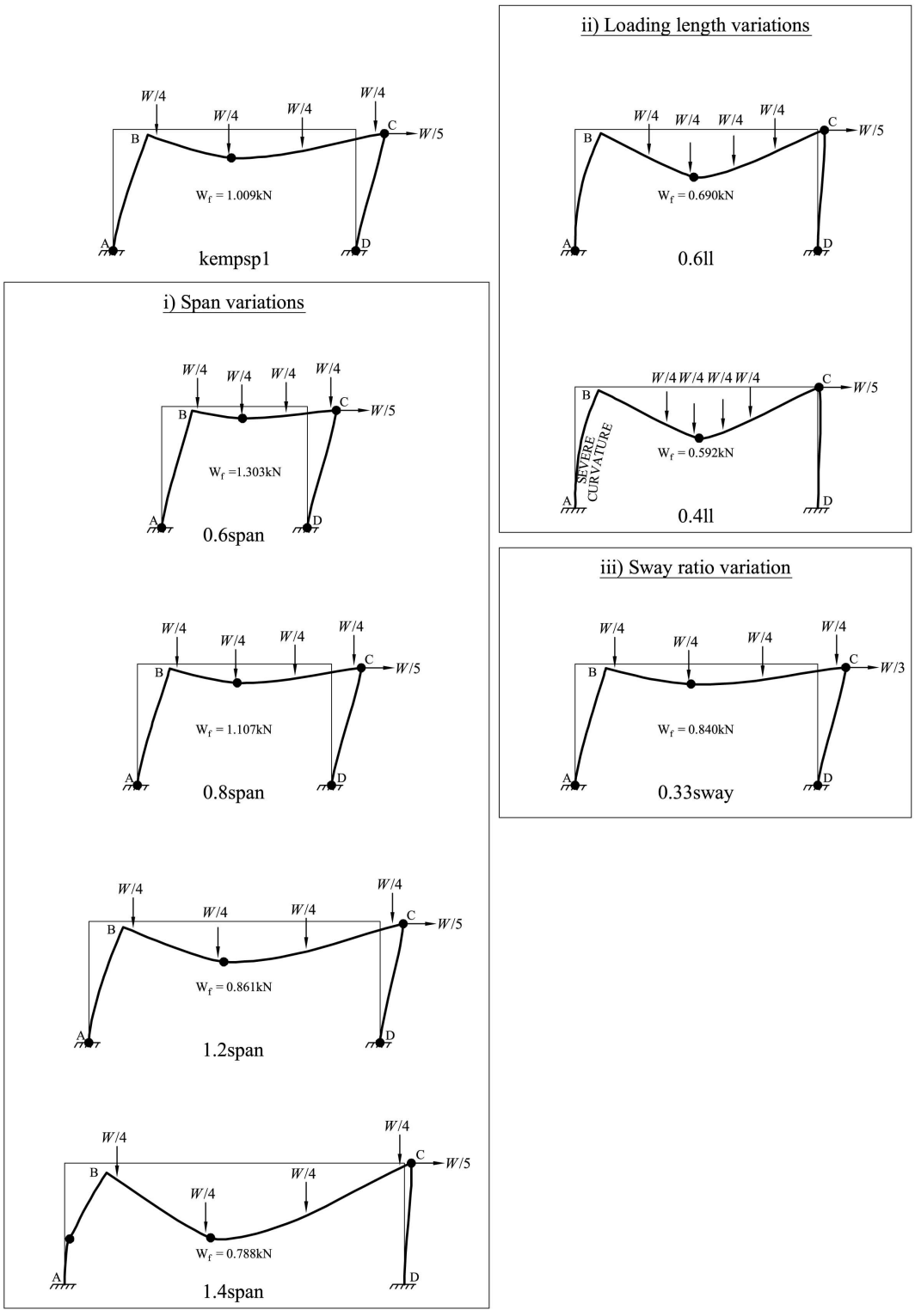


Fig. [3.7] Deflected shapes and apparent hinge positions of the laboratory-tested frames

During the elastic behaviour of the frame, the deflections caused by each addition of load were achieved within a few seconds of having placed the load. Nearing the loads at which the first hinges were anticipated, creep began to take place and the frames took longer to stop deflecting under the loads. This became progressively severe as loads increased, with frames taking up to 45 minutes per increment to reach full deflections near failure loads. Readings of deflection were recorded when the deflection under the current load was increasing by not more than one graduation, or 0.01mm, every thirty seconds.

3.2.3 Failure loads and modes

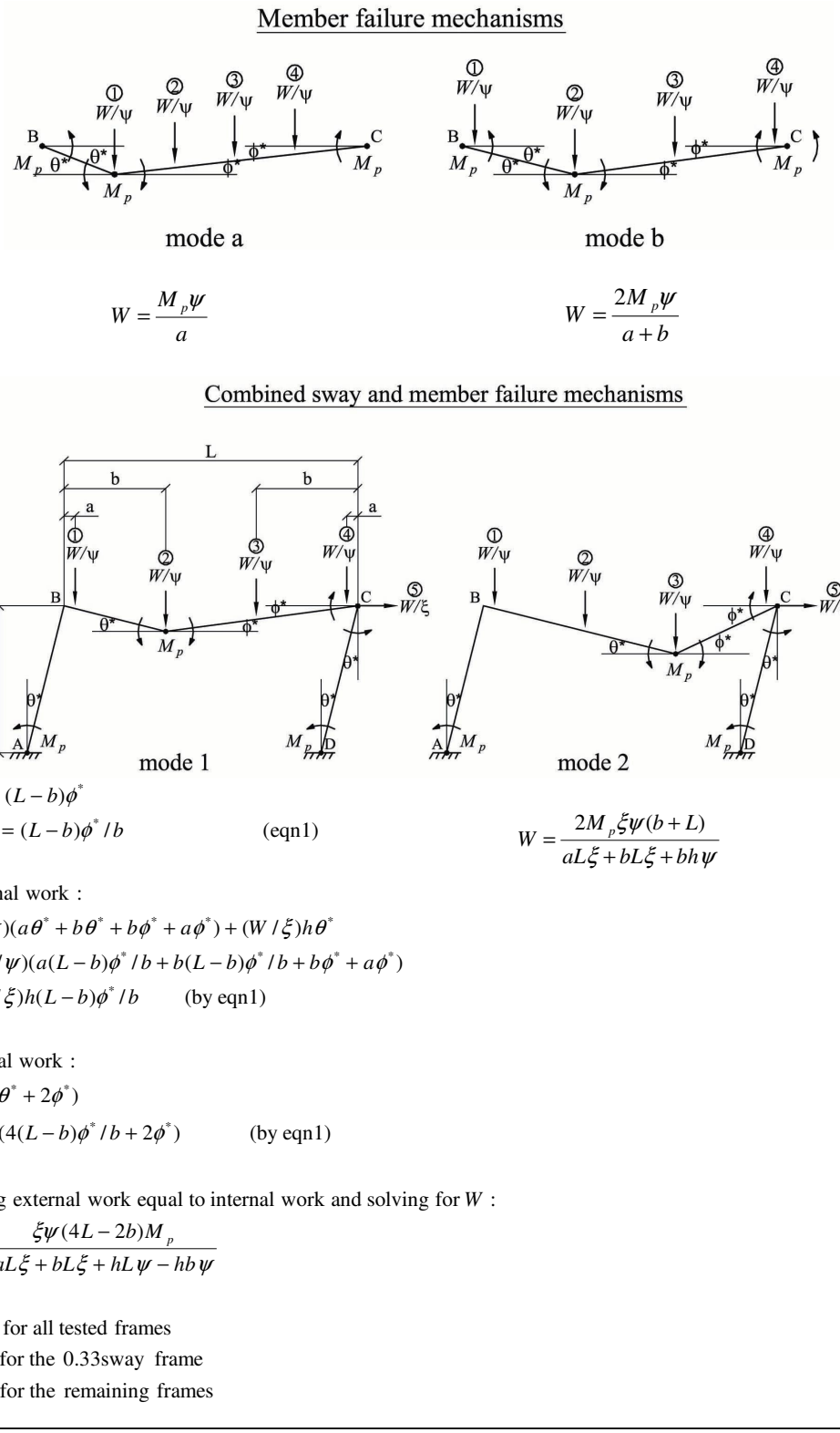
Figure [3.7] shows the recorded failure loads W_f and the approximate deflected shapes of the laboratory-tested frames. The locations of the plastic hinges after collapse are marked on the diagrams with small solid-shaded circles. These hinge locations were determined by inspection of the frames after they had been unloaded and removed from the testing rig. Hinges were characterised by localised regions of pronounced permanent curvature and were often accompanied by the fracture of mill scale. Hinges at joint C formed approximately 10mm below the actual joint in all test cases. This was probably due to the local strengthening effect of the weld fillet on the joint. None of the welds displayed obvious signs of fracture after the tests.

	PLASTIC ANALYSIS		LABORATORY TEST		ABAQUS		
	Member mech. (kN)	Combined mech. (kN)	W_f (kN)	W_c (kN)	W_{tA} (2nd order inelastic) (kN)	*Difference as % of ABAQUS results* Minimum difference	Range of difference
kempsp1	1.319 mode b	1.297 mode 1	1.009	1.033 mode 1	1.017 mode 1	0.00%	-1.57% to 0.79% (negative bias)
0.6span	2.198 mode b	1.702 mode 1	1.303	1.327 mode 1	1.284 mode 1	-1.48%	-3.35% to -1.48% (negative bias)
0.8span	1.648 mode b	1.472 mode 1	1.107	1.131 mode 1	1.135 mode 1	0.35%	0.35% to 2.47% (positive bias)
1.2span	1.099 mode b	1.137 mode 2	0.861	0.886 mode 1	0.917 mode 1	3.38%	3.38% to 6.11% (positive bias)
1.4span	0.942 mode b	1.008 mode 2	0.788	0.813	0.811 approximating mode 1	0.00%	-0.25% to 2.84% (positive bias)
0.6II	0.803 mode b	0.898 mode 2	0.69	0.715 mode 1	0.732 approximating mode 1	2.32%	2.32% to 5.74% (positive bias)
0.4II	0.672 mode b	0.784 mode 2	0.592	0.641	0.624 approximating mode 1	0.00%	-2.72% to 5.13% (positive bias)
0.33sway	1.319 mode b	1.021 mode 1	0.84	0.855 mode 1	0.832 mode 1	-0.96%	-2.76% to -0.96% (negative bias)

Table [3.3] Frame failure loads from plastic analysis, laboratory testing, and second order inelastic ABAQUS tests

First order plastic analyses were performed on those modes of member and combined member and sway collapse that were anticipated to be most likely. Figure [3.8] illustrates four such modes and the respective formula for the calculation of the collapse loads. The two possible member failure mechanisms were labelled modes ‘a’ and ‘b’, and the most critical combined mechanisms were labelled modes ‘1’ and ‘2’. An example of the derivation of such a collapse load is shown for mode 1 in the same figure. Table [3.3] summarises these first order plastic collapse loads, the

laboratory test loads and the failure loads of the second order inelastic ABAQUS analyses of all the frames.



$$W = \frac{M_p \psi}{a} \qquad W = \frac{2M_p \psi}{a+b}$$

$$b\theta^* = (L-b)\phi^*$$

$$\Rightarrow \theta^* = (L-b)\phi^*/b \qquad \text{(eqn1)}$$

$$W = \frac{2M_p \xi\psi(b+L)}{aL\xi + bL\xi + bh\psi}$$

External work :

$$(W/\psi)(a\theta^* + b\theta^* + b\phi^* + a\phi^*) + (W/\xi)h\theta^*$$

$$= (W/\psi)(a(L-b)\phi^*/b + b(L-b)\phi^*/b + b\phi^* + a\phi^*)$$

$$+ (W/\xi)h(L-b)\phi^*/b \qquad \text{(by eqn1)}$$

Internal work :

$$M_p(4\theta^* + 2\phi^*)$$

$$= M_p(4(L-b)\phi^*/b + 2\phi^*) \qquad \text{(by eqn1)}$$

Setting external work equal to internal work and solving for W :

$$W = \frac{\xi\psi(4L-2b)M_p}{aL\xi + bL\xi + hL\psi - hb\psi}$$

$\psi = 4$ for all tested frames

$\xi = 3$ for the 0.33sway frame

$\xi = 5$ for the remaining frames

Fig. [3.8] Probable failure mechanisms and resulting loads from plastic analysis

It appeared that the combined mechanism of mode 1 prevailed for all of the laboratory-tested frames except for the 1.4span and 0.4ll examples. This mode required hinges at joints A, C and D, and under load 2. The plastic analysis shows that mode 1 produced the lowest first order failure loads for the kempsp1, 0.8span, 0.6span and 0.33sway frames, and as such was the expected failure mode. For the remaining frames, due to their increased spans and/or decreased loading lengths, the first order member mechanisms became more critical than the first order combined mechanisms. In the case of the 0.6ll frame, the failure load of the critical combined mechanism was twelve percent larger than that of the critical member mechanism. In spite of this trend, the P-Δ effects were sufficient to induce sway-related failures in all of the frames. For 1.2span and 0.6ll frames the combined mechanism of mode 2 actually produced a lower first order failure load than that of mode 1. In light of this, I am unsure why the actual frames failed in mode 1.

The 1.4span frame failed with clearly defined hinges at joint C, under load 2, and approximately 150mm from joint A in member AB. This seemed an unlikely failure mode given that four hinges were required for the mechanism condition. However, ABAQUS analyses of the frame revealed that the entire length of member AB was stressed beyond the yield moment M_y at failure. The distributed loss of flexural rigidity resulted in plastic rotation throughout the length of member AB, thereby allowing the unconventional failure mode observed in the laboratory. A similar mode occurred in the 0.4ll frame, as evidenced by the permanent curvature throughout member AB after failure. In both frames, the severe deflections of the beams were accompanied by tensile forces that drew the column tops towards each other. The columns were so forced to bear their axial loads whilst in a bowed shape, resulting in excessive P-δ moments. Failure modes involving plastic flexural stresses throughout a column length would be most improbable in structures that conform to codified slenderness ratio limits.

3.2.4 Load versus deflection and incremental amplification factor

The load-Δ graphs for each frame were constructed directly from the test data and are illustrated in figures [3.9] to [3.11]. The data for the laboratory tests are tabulated in Appendix C. All curves, except that of the 1.4span frame, exhibit clearly defined regions of linear response to load prior to the development of plastic moment hinges and significant P-delta effects. The high slenderness of the 1.4span frame resulted in large deflections at low levels of load, and hence geometrically nonlinear behaviour developed before inelastic stresses. Each frame had utilised the majority of its load carrying capacity before the formation of the first hinge at joint C. While some of the curves appear to show several abrupt changes in slope, there was uncertainty as to whether these locations accurately represent the loads at which successive hinges formed. It became apparent after running the ABAQUS tests that the remaining hinges required to form a mechanism would often form simultaneously and in quick succession. In retrospect, significantly smaller load increments should have been used such that these hinges could be shown reliably on the graphs.

The span variation load-Δ graph of Fig. [3.9] shows a trend of increasing sway stiffness with decreasing span. It also shows that nonlinear behaviour began at higher loads in the stiffer frames. This trend helped to identify a possible weld failure in the

0.8span frame. The hinge at joint C in the 0.8span frame occurred at approximately the same load as it did in the less stiff kempsp1 frame. The loading length variation frames shared the same geometry and sway ratio and thus were expected to have the same initial sway stiffness. This was verified by the load-Δ curves of Fig. [3.11], which possess similar slopes until the first hinge formation in the 0.4ll frame. Unfortunately, the nonlinear behaviour of this frame was not captured since there was only one load increment separating the first hinge formation from failure. As the loading lengths decreased, the bending moments in the beams became greater, causing the spread of plasticity at lower loads.

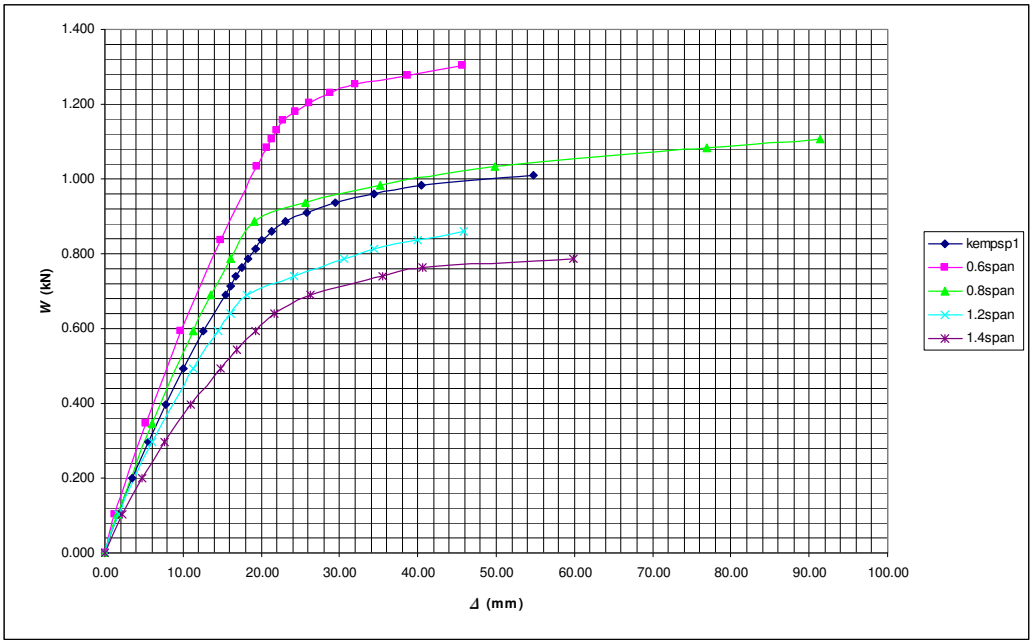


Fig. [3.9] W-Δ graph of laboratory-tested span variant frames

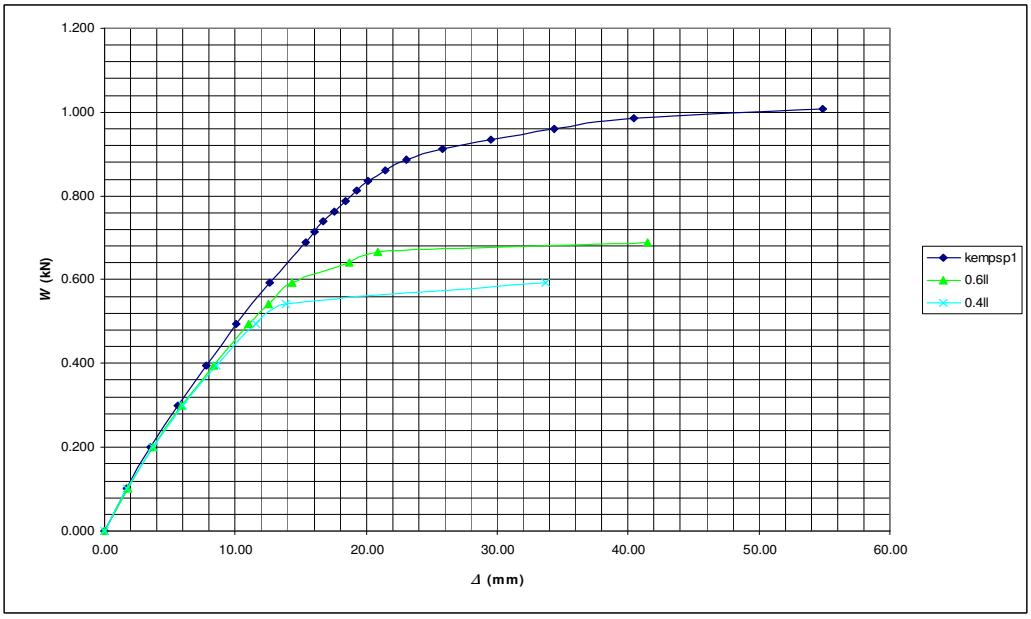


Fig. [3.10] W-Δ graph of laboratory-tested loading length variant frames

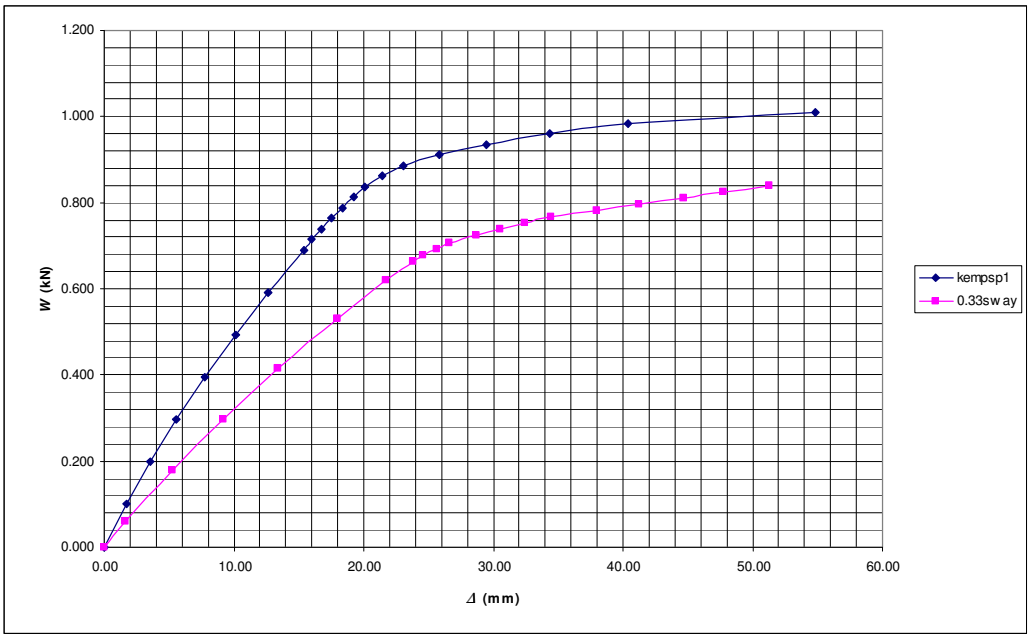


Fig. [3.11] W-Δ graph of laboratory-tested sway-ratio variant frames

In Fig. [3.11], the 0.33sway frame displays a shallower load-Δ curve than the kempsp1 frame due to its larger proportion of lateral load. The shapes of the two curves are, however, quite similar given the identical geometries, load positions and failure modes of both frames.

The load-X graphs required manipulation of the observed deflections to determine the incremental amplification factors. For a rectangular frame, the expression for X as given by Eqn. (2.58) simplifies to the following:

$$\begin{aligned} X &= \frac{\Sigma C_{ij}\Delta_{I\,ij}\phi^*_{ij}}{\Sigma V_{ij}L_{ij}\phi^*_{ij}} \\ &= \frac{\phi^*\Delta_I\Sigma C_{ij}}{\phi^* L\Sigma V_{ij}} \\ &= \frac{C\Delta_I}{VL} \end{aligned} \tag{3.8}$$

Since the sway ratio V/C and the column length L remained the same in the tests, X is effectively equal to the product of a constant and the first order deflection Δ_I. Substituting this value of X into Eqn. (2.45) gives the following relationship:

$$\begin{aligned} \Delta &= \frac{\Delta_I}{1-X} \\ &= \frac{\Delta_I}{1-(C\Delta_I/VL)} \end{aligned} \tag{3.9}$$

Eqn. (3.9) can be rearranged to express Δ_I in terms of Δ.

$$\Delta_I = \frac{\Delta}{1+(C\Delta)/(VL)} \tag{3.10}$$

This formula was used to convert the recorded deflections into first order deflections, which in turn were substituted into Eqn. (3.8) to produce the values of *X*. The load-*X* graphs are shown in figures [3.12] to [3.14]. The curves are similar in shape to the corresponding load-*Δ* curves, but the relative loss of stiffness after the formation of the first hinge is less pronounced in the load-*X* curves. This results from *X* being expressed as a function of a first order deflection, hence the weakening effects of geometric nonlinearity are excluded.

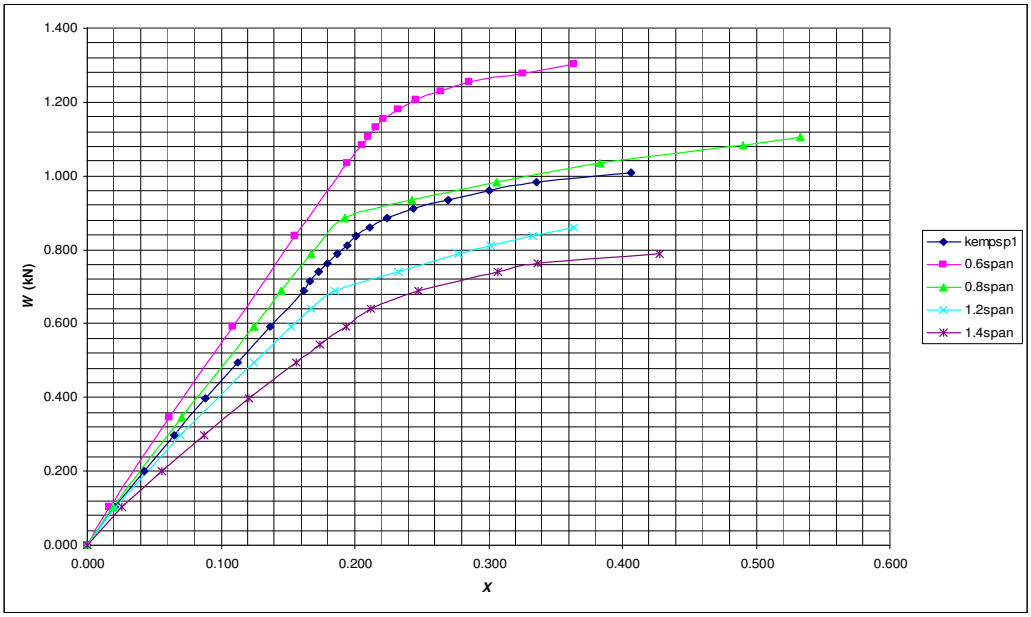


Fig. [3.12] W-X graph of laboratory-tested span variant frames

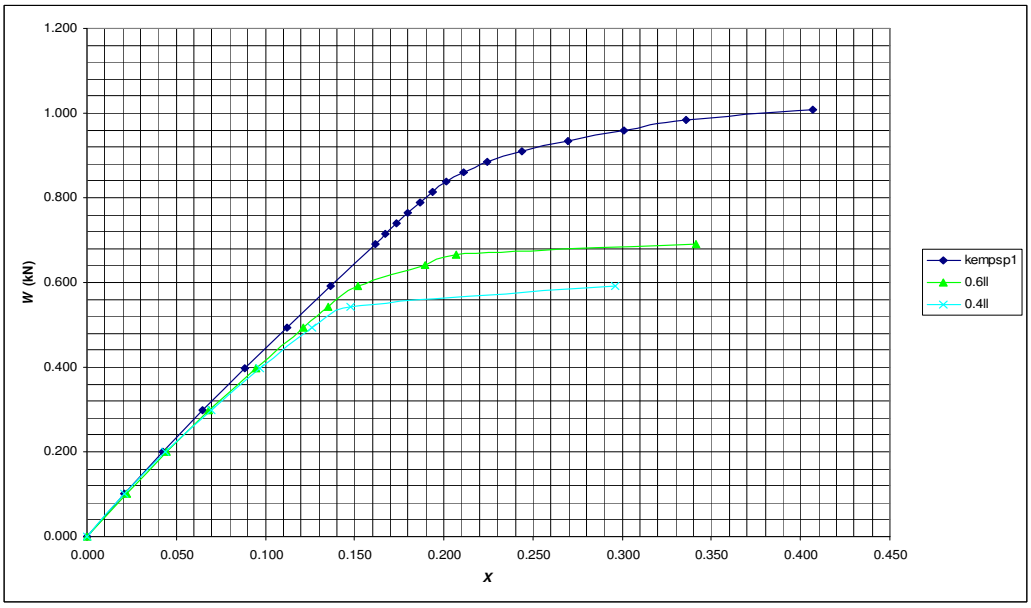


Fig. [3.13] W-X graph of laboratory-tested loading length variant frames

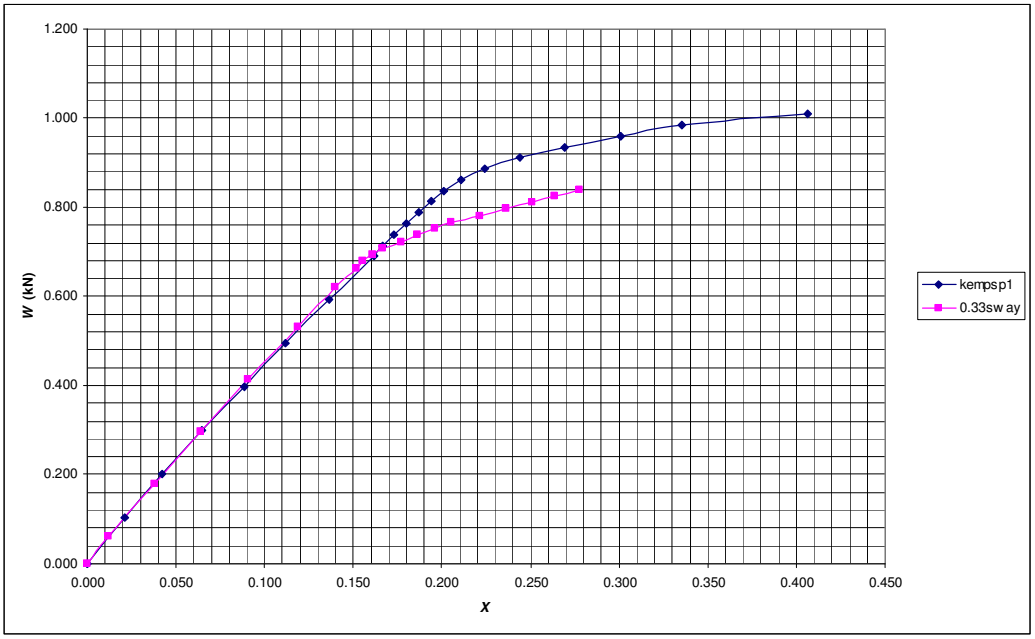


Fig. [3.14] W-X graph of laboratory-tested sway ratio variant frames

The load-*X* graph of the loading length variations shows that, in the case of the frames tested in this project, the positions of the gravitational loads on the beams certainly affected the load-*X* relationship. A further consequence of the expression for *X* is demonstrated by the sway ratio variation graphs of Fig. [3.14]. These graphs show the kempsp1 and 0.33sway frames as having the same slope in the elastic zone for the load-*X* curves, yet markedly different plastic zone slopes for the load-Δ curves. This can be explained as follows:

During elastic behaviour of the frame, the first order sway deflection is proportional to the total shear force on the frame:

$$\begin{aligned} \Delta_1 &\propto V \\ &= B_1 V \end{aligned} \tag{3.11}$$

where B_1 = Constant

Substituting Eqn. (3.11) into the expression for *X* as given by Eqn. (3.8):

$$\begin{aligned} X &= \frac{C\Delta_1}{VL} \\ &= \frac{C(B_1 V)}{VL} \\ &= B_2 C \end{aligned} \tag{3.12}$$

where $B_2 = B_1/L$

Eqn. (3.12) shows that for a given frame with set load positions, during elastic behaviour the amplification factor U_2 should be independent of the sway ratio.

3.2.5 Laboratory error

The most significant source of laboratory error was most probably the variable strengths of the welded joints. The 0.8span frame demonstrated that in spite of a weld fracture being invisible to the naked eye, it could severely compromise the stiffness of a frame. The only way to guard against the destabilising effect of a weak joint was to ensure that the weld was stronger than the parent section. This was achieved for most of the frames as the hinges formed slightly below joint C. The sizes of the weld fillets in relation to the lengths of the members were small enough that their effects on sway stiffness were ignored.

The greatest practical refinement that could have been made to the testing process would have been to use smaller increments of load. Large increments should not have introduced errors into the testing process, but the sparsely populated load-Δ graphs made the nonlinear behaviour of the frames difficult to interpolate. Fortunately, they did allow failure loads to be determined quite accurately as the smallest load increment was only 4% of the lowest failure load. Should future testing be performed on similar frames, it is recommended that vertical load increments of 500 to 600 grams be used once load-Δ data indicates that nonlinear behaviour is taking place. This should enable the researcher to identify with confidence the loads at which successive hinges form.

Further smaller sources of error included the degree of fixity of the bases, the effect of impact loads as weights were placed on the hangers, material defects and initial member curvatures, and the alignment of deflection gauges. Though the degree of restraint of the clamps on the column bases was not measured, there appeared to be a good degree of fixity in all test cases. This assumption was due to the hinges having formed immediately above the clamps, with no permanent curvature observed in the gripped lengths. Some difficulty was experienced in placing the initial larger load plates of ten kilograms or more gently on the load hangers. As the loads were set down, they struck the hanger causing impact loads and momentary spikes in deflection. Fortunately, when the structure was closer to collapse and thus more sensitive to load, the lighter load plates could be placed more carefully on the hangers to reduce this effect. Material defects were unlikely over such small lengths of section, and the tensile tests of the coupons showed that all the original lengths had similar material properties. Initial curvatures of the members were insignificant in comparison to the curvatures induced by the first few increments of load.

3.3 Comparisons with ABAQUS Tests

The failure loads of the second order inelastic ABAQUS analyses are presented in Table [3.3]. These loads were compared to the laboratory results by expressing the differences between corresponding failure loads as a percentage of the ABAQUS

loads. For each frame, a margin of error was calculated based on the fact that actual failures had occurred in the laboratory when the loads were between W_f and W_c.

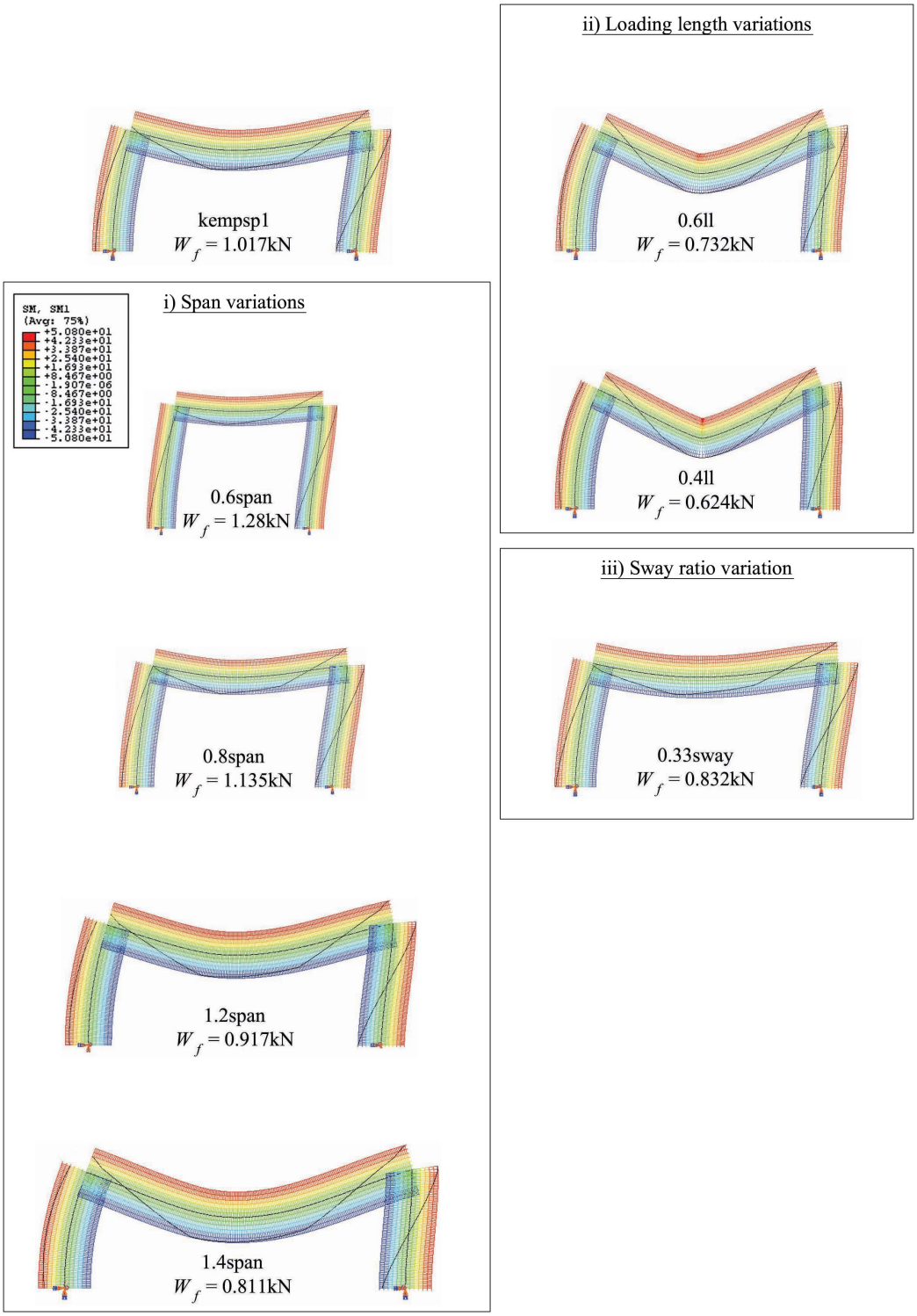


Fig. [3.15] Deflected shapes, moments and loads at failure of the ABAQUS-tested frames

Since both the laboratory testing process and the ABAQUS analyses were subject to various inherent errors, an explanation of the discrepancies between the results for each frame would likely be inconclusive. The laboratory errors have been discussed above, while the ABAQUS errors arose from idealised section properties (which themselves were derived from laboratory tests) and boundary conditions, and simplified meshes and displacement functions. The range of differences, as seen in the last column of Table [3.3], reveals in general that loads obtained from ABAQUS were slightly higher. The 1.2span frame exhibited the highest positive margin of error at +6.11%, while the 0.6span frame had the largest negative margin of –3.35%. Even the 0.8span frame, which appeared to fail at the weld, had a possible error range of only +0.35% to +2.47%. The remaining frames differed by no more than 5.74%. In the cases of the kempsp1, 1.4span and 0.4ll frames, the ABAQUS loads fell between the W_f and W_c laboratory loads.

In Fig. [3.15], the bending moment diagrams are shown superimposed on the deflected shapes of the ABAQUS frames at failure. The hinge positions, and thus the failure modes, compared favourably with those of the laboratory tests which are illustrated in Fig. [3.7]. However, in two cases ABAQUS indicated a broader distribution of plastic flexural stress than the relatively short moment hinges seen in the laboratory. For the 0.6ll frame, ABAQUS calculated that the highest degree of flexure was situated about the middle of column AB, rather than concentrated in a hinge at joint A. It also showed near-uniform flexure of column AB in the 1.4span frame, while the laboratory test revealed a definite hinge 150mm from joint A. This hinge may have been due to post failure deformation as the frames had been allowed to deform continuously to ensure that collapse had take taken place.

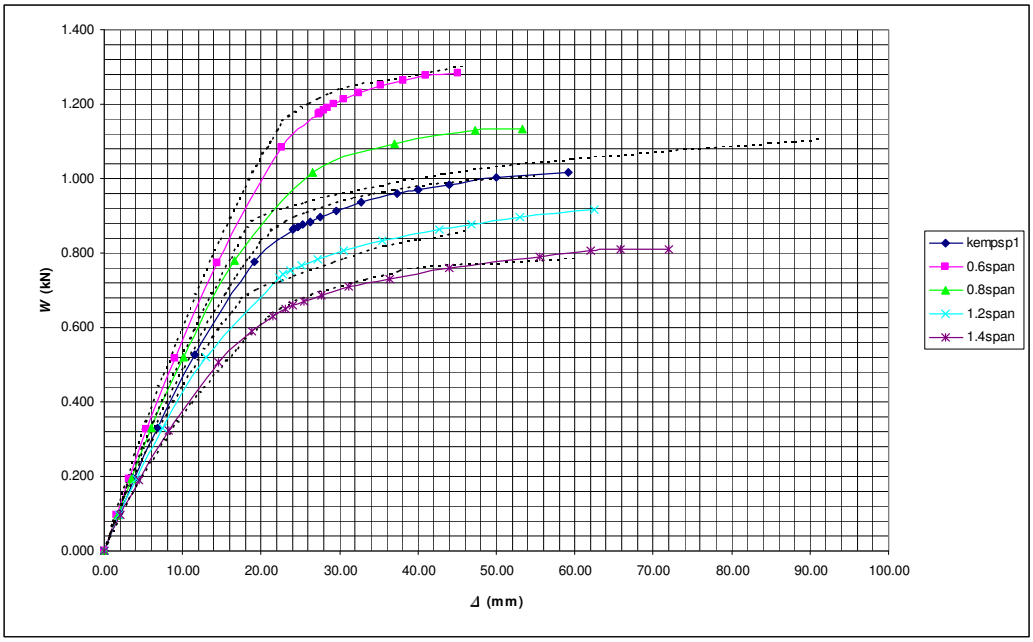


Fig. [3.16] W-Δ graph of ABAQUS-tested span variant frames

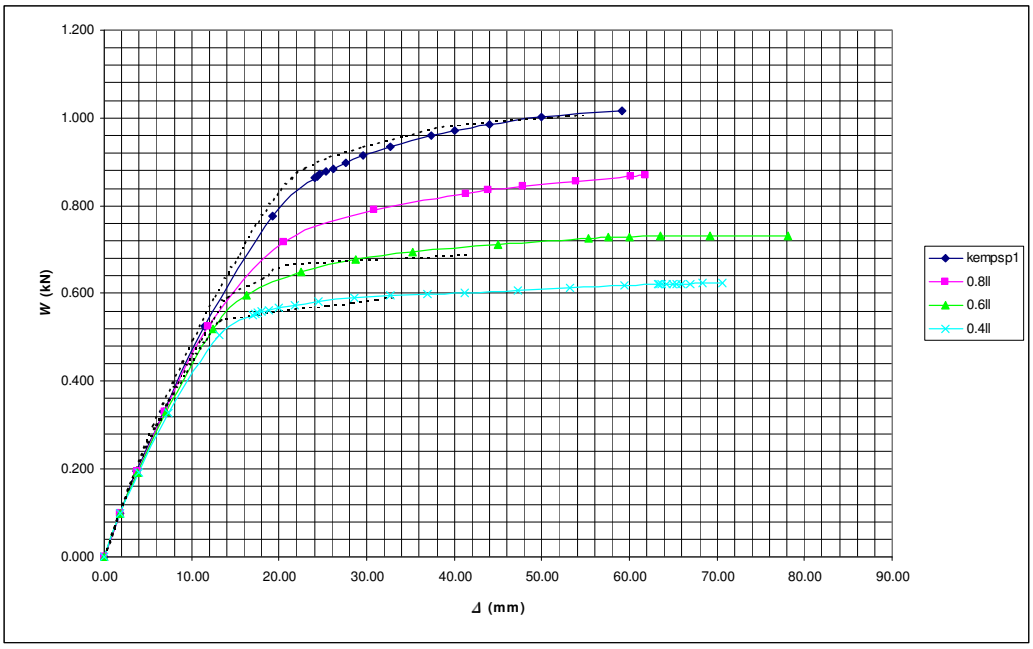


Fig. [3.17] W-Δ graph of ABAQUS-tested loading length variant frames

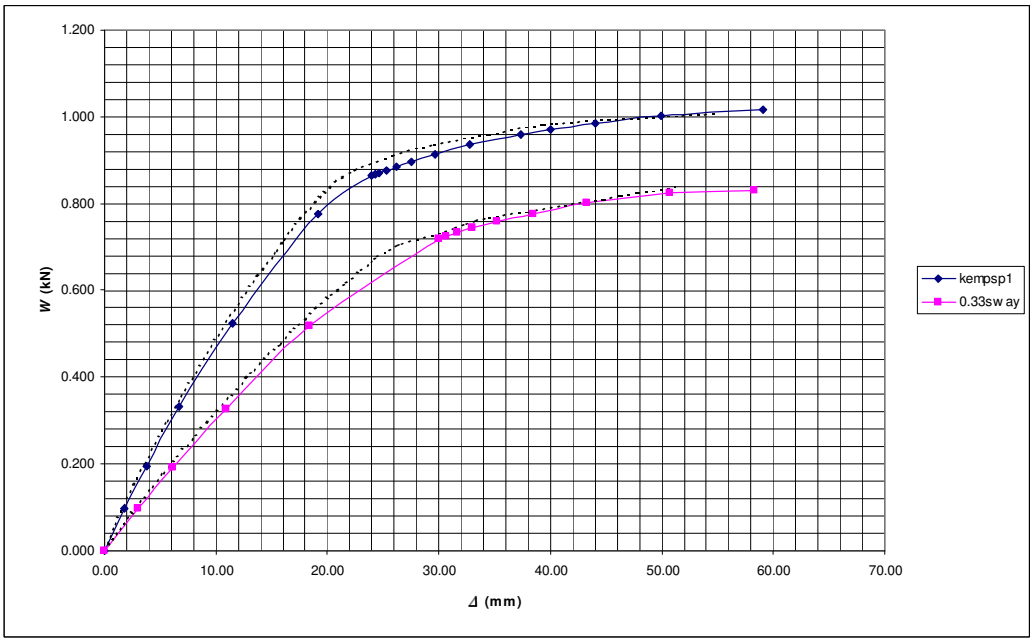


Fig. [3.18] W-Δ graph of ABAQUS-tested sway-ratio variant frames

The ABAQUS load-Δ graphs are illustrated in figures [3.16] to [3.18], and the data used to construct these curves are tabulated in Appendix D. The corresponding curves from the laboratory tests are represented in the graphs by the dotted black lines. In all three graphs, the correlation between the two sets of curves is clear. The ABAQUS models tended to underestimate slightly the elastic sway stiffness of the frames in all cases except the 1.4span frame. These curves also showed a less severe transition into nonlinear behaviour, and smoother loss of stiffness thereafter. This may have been due to the simplified moment-curvature relationship that was used to

model the ABAQUS frames, or as a result of the coarse load intervals used in the laboratory. Similar correlation is seen between the two sets of load-*X* graphs given in figures [3.19] to [3.21]. There is a pronounced difference between the ABAQUS and laboratory results for the 0.8span frame, supporting the possibility that there was a weld failure at joint C in this instance. The laboratory test curve for this frame shows that the frame continued to deflect extensively in the nonlinear zone until a collapse load was attained that was close to its ABAQUS counterpart.

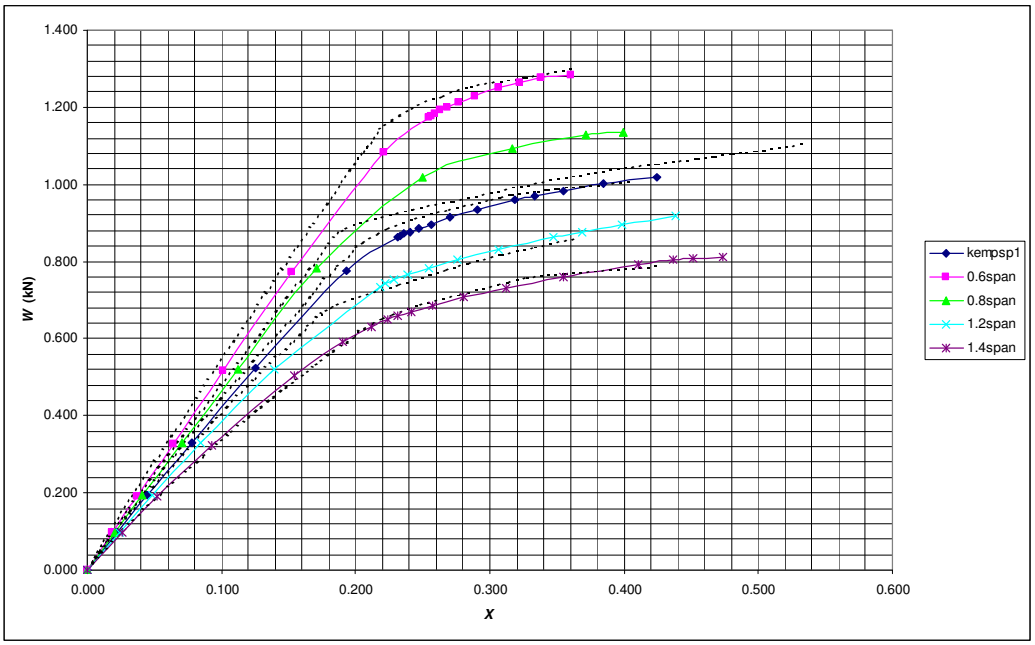


Fig. [3.19] W-X graph of ABAQUS-tested span variant frames

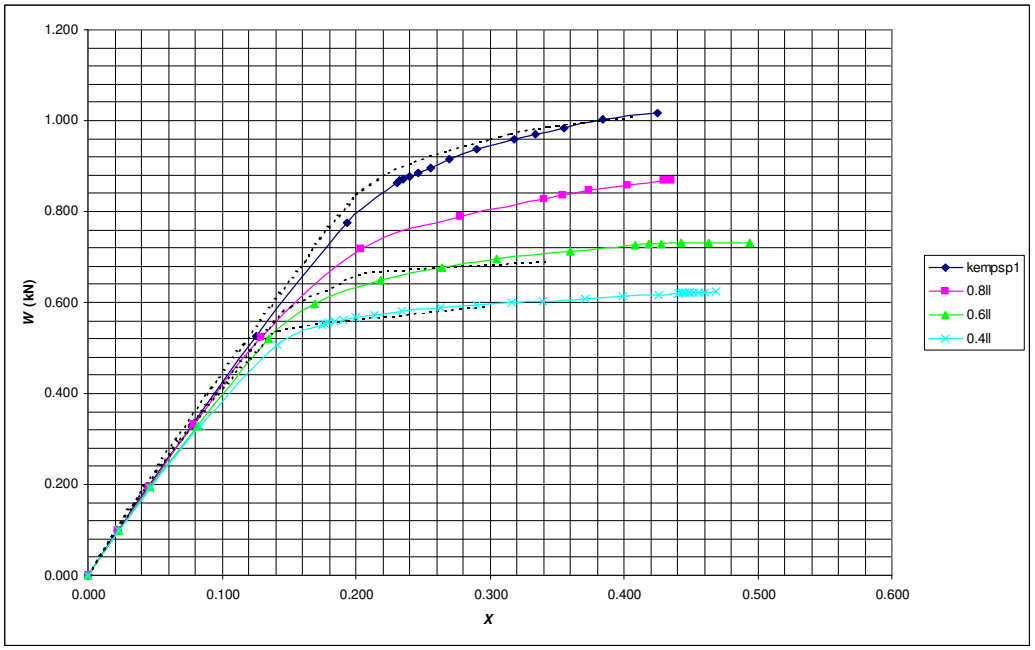


Fig. [3.20] W-X graph of ABAQUS-tested loading length variant frames

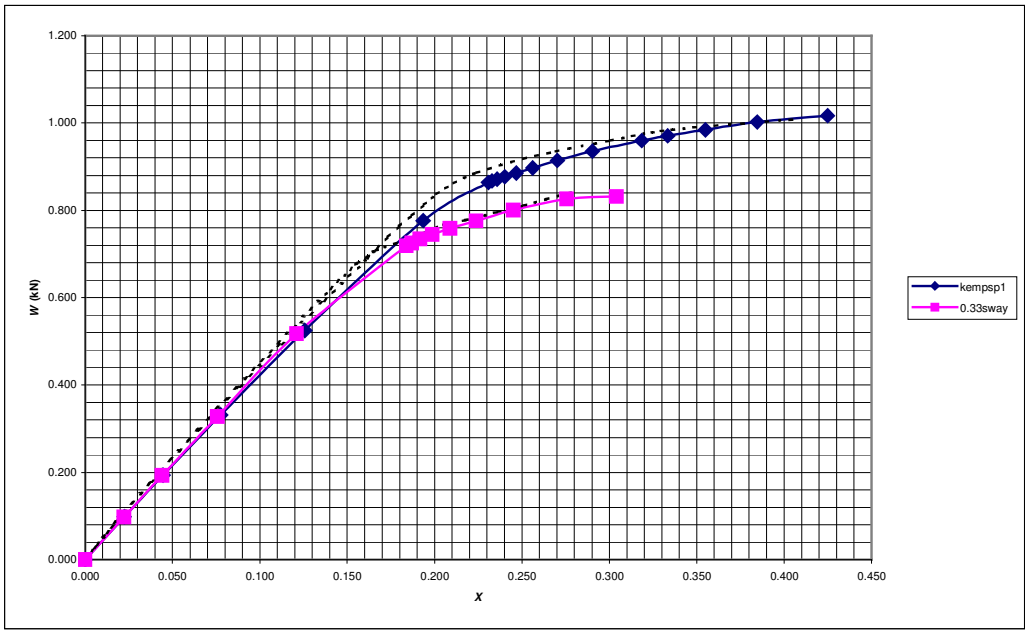


Fig. [3.21] W-X graph of ABAQUS-tested sway-ratio variant frames

During the laboratory tests, sway deflection was measured only at joint B. ABAQUS results later revealed that significant discrepancies existed between the values of horizontal deflection of the two column tops. This resulted from the sagging of the flexible beams that reduced the horizontal distances between the member ends. Illustrated in Fig. [3.22] is a load-Δ graph showing deflections of both the column tops of four selected frames. In the stiffest example, the 0.6span frame, there was little difference between the sway deflections of both columns. As the spans became longer and the beams sagged more severely, the column tops were drawn closer together. In the example of the highly flexible 1.4span frame, joint C actually began to move in the opposite direction to the applied sway load prior to failure. This trend was even more apparent in the 0.4ll frame, where the deflection of joint C at failure was reduced to less than its value at the formation of the first plastic hinge. While this behaviour did not present a problem for the purposes of comparing the laboratory and ABAQUS results, it introduced a complication into the calculation of the amplification factor. The isolation of the first order deflection Δ_I required the condition that the first order deflections of both column tops were equal. This point was shown in Eqn. (3.7) where the expression $\Sigma C_{ij}\Delta_{I\,ij}\phi_{ij}^{*}$ was rewritten as $\phi_{ij}^{*}\Delta_{I\,ij}\Sigma C_{ij}$. With equal first order deflections and only one amplification factor, it followed that the theory would erroneously predict equal second order deflections of the column tops. Clearly the amplification factor had not been derived to account for this consequence of large deflection theory. The deflection of joint B was exaggerated by the sagging of the beams, thus the load-Δ and load-X graphs based thereupon would underestimate the sway stiffnesses of the columns.

In the practical design of single bay rectangular frames with equal height columns the assumption that actual sway deflections are equal for all columns is more applicable. The 0.6span frame, which showed minor differences between the column sways from zero load to failure, had column slenderness ratios of over 320. In clause 10.4.2.1 of

SANS 10162-1:2004, it is stipulated that the maximum allowable slenderness ratio of a member in compression is 200 unless action is taken to control flexibility, sag, vibration and slack. Consequently, practical frames will be even stiffer and therefore less susceptible to differing sway deflections between columns. Furthermore, considerations of serviceability will also result in stiffer structures. In industrial type structures supporting elastic cladding, the vertical deflections are limited to span/180, as are the lateral deflections due to wind. In the 0.6span frame, both of these deflection recommendations were violated before the load had reached 22% of the frame's ultimate load capacity. Unfortunately, it was necessary to limit the sizes of the test frames due to constraints on the materials and equipment required to fabricate and test them. Since the frames were small, the members were slender such that accurate recordings could be taken of deflections.

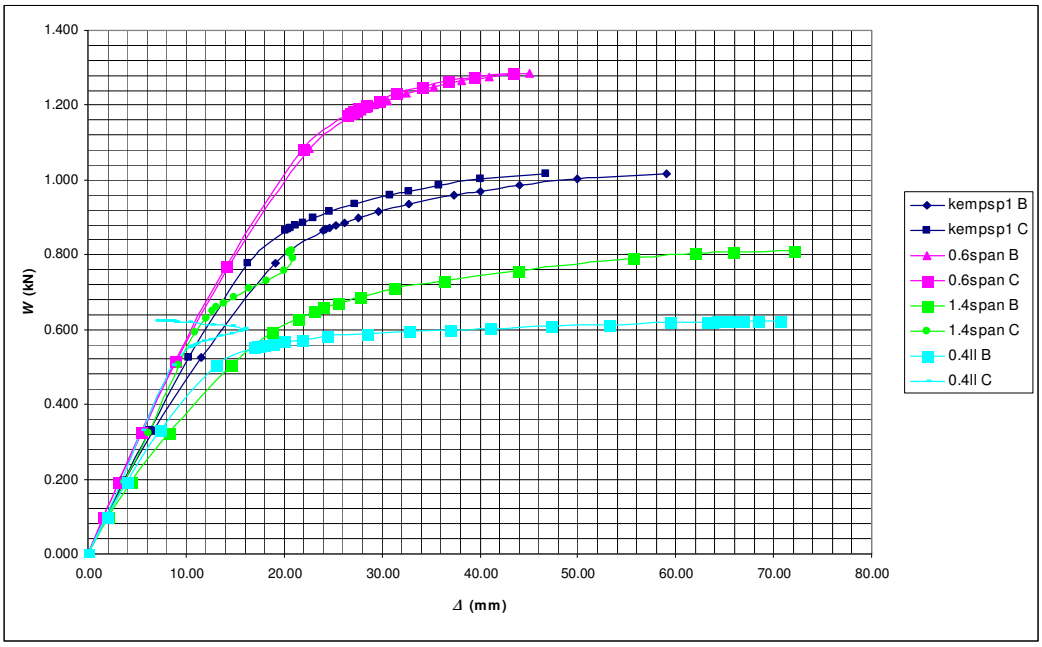


Fig. [3.22] W-Δ graph of both column tops of ABAQUS-tested frames

Given that the maximum failure loads produced by two independent methods of testing did not deviate from each other by more than 6.2%, the ABAQUS and laboratory results compared favourably. Most accepted methods of structural analysis routinely miscalculate failure loads by more than this margin. The flexible frames were highly nonlinear in their behaviour, yet ABAQUS produced very similar load-Δ graphs to the laboratory tests, and replicated the actual failure modes in all cases. This verifies that both methods were performed correctly, and that the results could be used to test and refine Kemp's amplification factor theory for at least the frames tested in this project.

4 BILINEAR AMPLIFICATION FACTOR METHOD

The pure sway collapse mode used in the calculation of the incremental amplification factor *X* for the test frames is shown in Fig. [4.1]. Once simplified by taking account of the common sway rotations and column lengths, the expression for *X* was reduced to the following:

$$\begin{aligned} X &= \frac{C\Delta_I}{VL_{AB}} \\ &= \frac{W\Delta_I}{(W/\xi)L_{AB}} \\ &= \frac{\xi\Delta_I}{L_{AB}} \end{aligned} \tag{4.1}$$

where: W/ξ is the translational load on the frame

The following two subsections explain the first order elastic and plastic analyses that were performed on the frames to define the bilinear incremental amplification factor graphs, as well as the calculation of the failure loads. In section 4.3 the predictions of the amplification theory are presented for the frames, and comparisons are made with the results of the laboratory and ABAQUS tests.

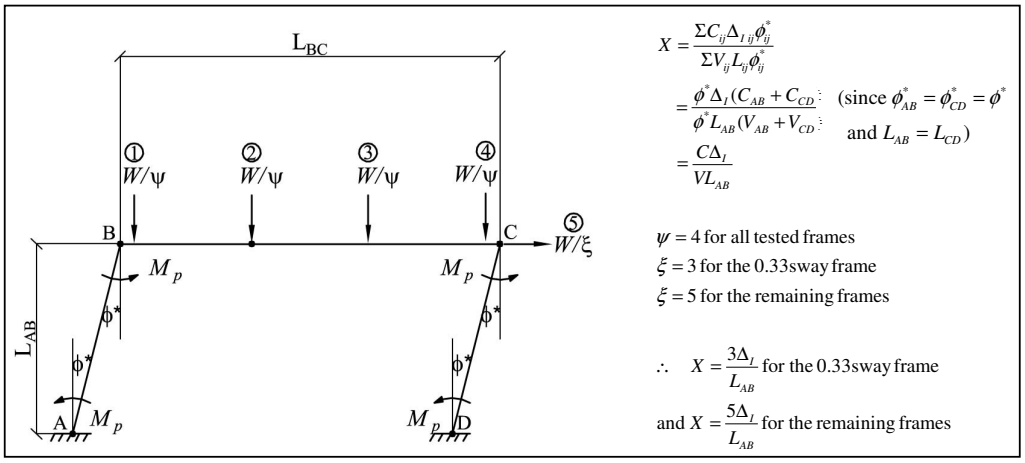


Fig. [4.1] Pure sway mode for the calculation of *X* for the test frames

4.1 Calculating (X_i, λ_i)

The point (X_i, λ_i) represents the limit of elastic behaviour of a structure. The load factor λ_i is found by using a first order elastic analysis to satisfying the interaction equation of (4.2).

$$\frac{C}{C_y} + \frac{U_2 M_I}{M_p} + \frac{0.5\sigma_{res}}{\sigma_y} = 1.0 \tag{4.2}$$

This equation approximates the load at the formation of the first fully plastic section. As joint C was consistently the location of greatest flexure during elastic behaviour, it became the subject of Eqn. (4.2) for all of the test frames. Residual stress effects were ignored in this project, hence the term $0.5\sigma_{res}/\sigma_y$ was neglected in the calculations. Each frame was analysed to produce the forces, deflections and load at which Eqn. (4.2) was satisfied at joint C. The structural analyses were performed using the member stiffness equations of the slope-deflection method. Axial distortions of the members were ignored, and the three unknowns were identified as the rotations of joints B and C, and the sway deflection of the frame. Fig. [4.2] illustrates the global and local axes, showing the positive directions for moments, rotations, and individual forces and translations.

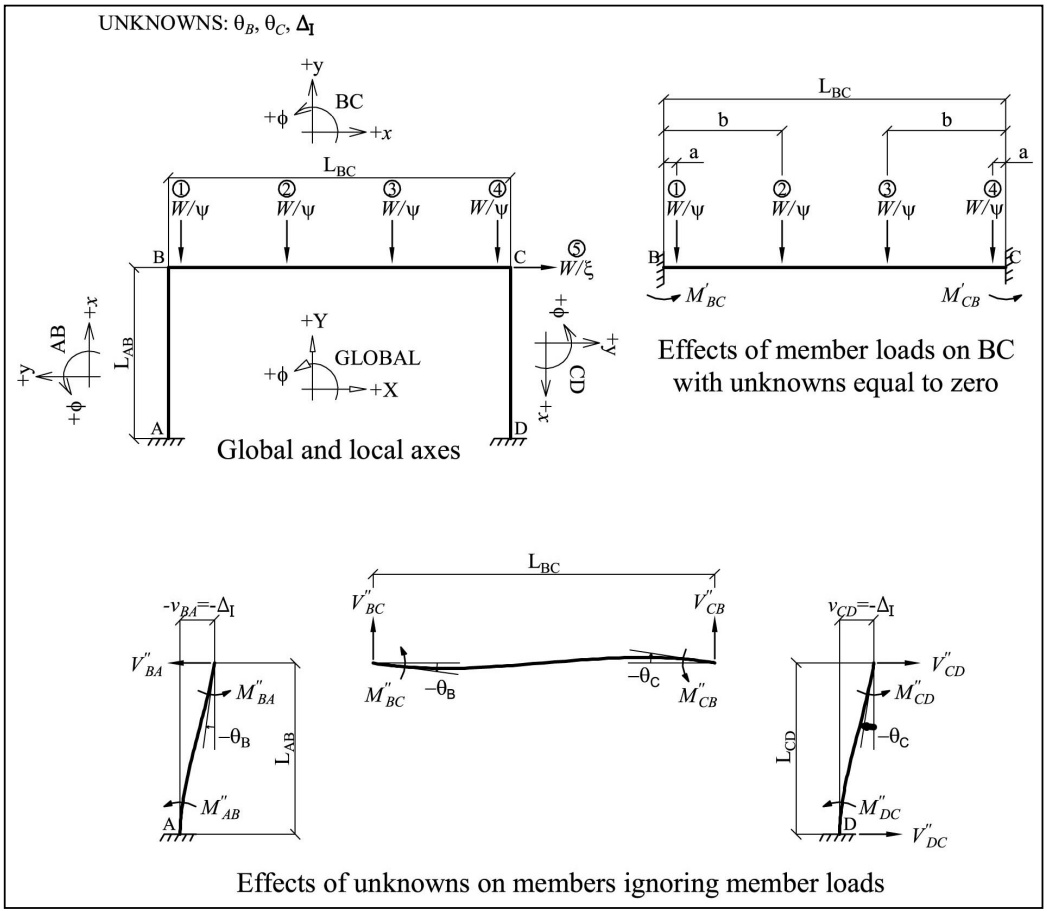


Fig. [4.2] Sign convention and free-body diagrams for calculating λ_i and X_i

The effects of the loads and the effects of the unknowns on the structure were each considered separately. These effects were then summed and conditions of force equilibrium and compatibility of deflection were used to construct a stiffness matrix for the frame. Member BC was the only member subjected to transverse loads within its length. The end moments of BC for fixed-ended conditions were calculated for each load acting in isolation, following which the principle of superposition was applied to obtain the effect of all the loads acting simultaneously (To reduce

cumbersome notation, the subscript *I* has been retained in this subsection only for first order sway deflection Δ_I.).

$$\begin{aligned} M'_{BC} &= (W/\psi L_{BC})(aL_{BC} + bL_{BC} - a^2 - b^2) \\ &= -M'_{CB} \end{aligned} \tag{4.3}$$

where: superscript ' represents the effects of loads with unknown deflections equal to zero

Thereafter, the effects of the unknown deflections were considered on the otherwise unloaded structure. The relevant member stiffness equations used for this analysis are presented in Eqn. (4.4) below.

$$\begin{pmatrix} V''_{ij} \\ M''_{ij} \\ V''_{ji} \\ M''_{ji} \end{pmatrix} = \frac{EI}{L} \begin{bmatrix} \varphi_1/L^2 & \varphi_2/L & -\varphi_1/L^2 & \varphi_2/L \\ \varphi_2/L & \varphi_4 & -\varphi_2/L & \varphi_3 \\ -\varphi_1/L^2 & -\varphi_2/L & \varphi_1/L^2 & -\varphi_2/L \\ \varphi_2/L & \varphi_3 & -\varphi_2/L & \varphi_4 \end{bmatrix} \begin{pmatrix} v_{ij} \\ \theta_i \\ v_{ji} \\ \theta_j \end{pmatrix} \tag{4.4}$$

where superscript '' represents the effects of member end deflections with member loads equal to zero

The stability functions assumed the values for zero axial loads in the members:

$$\varphi_1 = 12 \quad ; \quad \varphi_2 = 6 \quad ; \quad \varphi_3 = 2 \quad ; \quad \varphi_4 = 4$$

In member AB, the deflections of the fixed end A were equal to zero, thus the respective stiffness equations for end B reduced to:

$$V''_{BA} = (12EI/L^3_{AB})v_{BA} - (6EI/L^2_{AB})\theta_B \tag{4.5}$$

$$M''_{BA} = -(6EI/L^2_{AB})v_{BA} + (4EI/L_{AB})\theta_B \tag{4.6}$$

Similarly in member CD, the deflections of end D equalled zero, and the stiffness equations were as follows:

$$V''_{CD} = (12EI/L^3_{AB})v_{CD} + (6EI/L^2_{AB})\theta_C \tag{4.7}$$

$$M''_{CD} = (6EI/L^2_{AB})v_{CD} + (4EI/L_{AB})\theta_C \tag{4.8}$$

The sway deflections were considered positive in an anticlockwise direction. Hence the locally positive horizontal translation of joint B v_{BA} was equal to the sway Δ_I of the structure as a whole.

$$\begin{aligned} v_{BA} &= \Delta_I \\ &= -v_{CD} \end{aligned} \tag{4.9}$$

Using this relationship, the member stiffness equations of the columns were rewritten in terms of Δ_I:

$$V_{BA}^{"} = (12EI / L_{AB}^3)\Delta_I - (6EI / L_{AB}^2)\theta_B \quad (4.10)$$

$$M_{BA}^{"} = -(6EI / L_{AB}^2)\Delta_I + (4EI / L_{AB})\theta_B \quad (4.11)$$

$$V_{CD}^{"} = -(12EI / L_{AB}^3)\Delta_I + (6EI / L_{AB}^2)\theta_C \quad (4.12)$$

$$M_{CD}^{"} = -(6EI / L_{AB}^2)\Delta_I + (4EI / L_{AB})\theta_C \quad (4.13)$$

In member BC there was no sway and the only deflections to consider were the rotations of the member ends:

$$M_{BC}^{"} = (4EI / L_{BC})\theta_B + (2EI / L_{BC})\theta_C \quad (4.14)$$

$$M_{CB}^{"} = (2EI / L_{BC})\theta_B + (4EI / L_{BC})\theta_C \quad (4.15)$$

Summing the independently calculated effects of member loads and unknown rotations and deflections produced the equations for the total shears and moments on a single side of a joint.

$$V_{ij} = V_{ij}^{'} + V_{ij}^{"} \quad (4.16)$$

$$M_{ij} = M_{ij}^{'} + M_{ij}^{"} \quad (4.17)$$

Since no external moments were applied directly to the joints, the internal moments on opposite sides of a joint were equated with opposite signs. This created two equilibrium equations in three unknown deflections.

$$M_{BA} = -M_{BC} \quad (4.18)$$

$$M_{CB} = -M_{CD} \quad (4.19)$$

An additional independent equation arose from the necessity for horizontal equilibrium of the structure.

$$(W / \xi) - V_{AB} + V_{DC} = 0 \quad (4.20)$$

As there were no transverse loads acting on the columns, the end shears in each column were equal and opposite in direction. Thus Eqn. (4.20) was rewritten as:

$$(W / \xi) + V_{BA} - V_{CD} = 0 \quad (4.21)$$

The equilibrium equations of (4.18), (4.19) and (4.21) were arranged into the following matrix notation to aid the solution of the unknowns:

$$\begin{pmatrix} -M_{BC}^{'} \\ M_{BC}^{'} \\ W / \xi \end{pmatrix} = \begin{bmatrix} 4EI / L_{AB} + 4EI / L_{BC} & 2EI / L_{BC} & -6EI / L_{AB}^2 \\ 2EI / L_{BC} & 4EI / L_{BC} + 4EI / L_{AB} & -6EI / L_{AB}^2 \\ 6EI / L_{AB}^2 & 6EI / L_{AB}^2 & -24EI / L_{AB}^3 \end{bmatrix} \begin{pmatrix} \theta_B \\ \theta_C \\ \Delta_I \end{pmatrix} \quad (4.22)$$

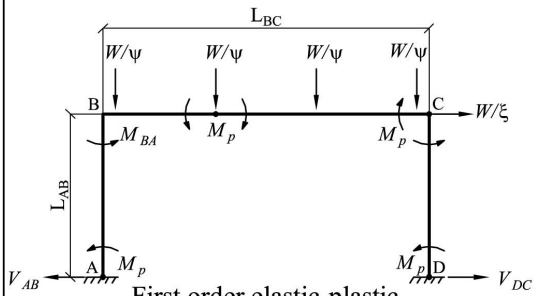
After solving for the deflection vector, the deflections were re-substituted into equations (4.10) to (4.17) to calculate total first order moments and shears at joints B and C. The calculations thus far produced the bending moment at joint C, and the terms necessary for calculating the amplification factor at a given load. The axial load in column CD, necessary for the term C/C_y in Eqn. (4.2), was calculated by recognising that it was equal to the shear force V_{CB} of member BC.

$$\begin{aligned} C_{CD} &= V_{CB} \\ &= V_{CB}^{'} + V_{CB}^{"} \\ &= W/2 - (6EI/L_{BC}^2)\theta_B - (6EI/L_{BC}^2)\theta_C \end{aligned} \tag{4.23}$$

There was now sufficient information to find a load W_i and deflection $\Delta_{I\,i}$ that would satisfy Eqn. (4.2). The value of deflection $\Delta_{I\,i}$ was substituted into Eqn. (4.1) to calculate X_i. The results of the laboratory and ABAQUS tests were graphed against load W, rather than load factor λ. Since the nominal value of total vertical load on a frame was chosen as 1kN, the magnitude of W was actually equal to and thus interchangeable with λ. For the sake of consistency, the bilinear incremental amplification factor graphs were also constructed against W.

4.2 Calculating (X_p, λ_p) and λ_f

The point (X_p, λ_p) represents the limit of plastic behaviour of a structure. This is regarded as being the critical sway collapse mechanism as determined from a first order plastic analysis. Each frame was statically indeterminate to the third degree, and had eight locations where plastic moment hinges were likely to form. These locations occurred at the supports, at joints B and C and under the vertical loads. Consequently there were five possible independent collapse mechanisms. These included four member mechanisms and the pure sway mechanism discussed above. Each member mechanism had hinges at joints B and C, and one hinge under one of the vertical loads. Two of these member modes are illustrated in Fig. [3.8], the remaining two being identical for the purposes of calculating collapse loads. Since no sway deflection of the columns occurred in the member mechanisms, the amplification factor would have equalled zero for this type of partial collapse. In the bilinear amplification method the importance of non-sway member mechanisms lies in their ability to interact with pure sway modes so as to form critical mechanisms. Complete collapse of the test frame required three hinges to render the frame statically determinate, and a fourth hinge to convert the otherwise stable structure into a mechanism. In combining a member mechanism with the pure sway mechanism, a hinge had to be eliminated at one of the critical sections so as to maintain a four-hinge scenario. The hinge was eliminated at joint B as the rotations from both the member and sway mechanisms were always in opposing directions at this location. Fig. [3.8] shows the two modes that were found to be the most critical of the combined mechanisms. The virtual work approach, as described in section 2.4, was used to solve for the collapse loads.



First order elastic-plastic moment distribution

Moments about C in member CD :

$$M_p + M_p + V_{DC} L_{AB} = 0$$

$$V_{DC} = -2M_p / L_{AB} \qquad (A)$$

By horizontal equilibriu m of the frame :

$$(W/\xi) + V_{DC} - V_{AB} = 0$$

$$V_{AB} = (W/\xi) + V_{DC}$$

$$V_{AB} = (W/\xi) - (2M_p / L_{AB}) \quad \text{(by Eqn. (A))} \qquad (B)$$

Moments about B in member AB :

$$M_p - V_{AB} L_{AB} + M_{BA} = 0$$

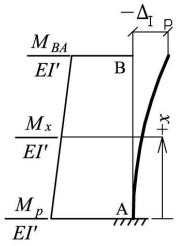
$$M_{BA} = V_{AB} L_{AB} - M_p$$

$$M_{BA} = ((W/\xi) - (2M_p / L_{AB}))L_{AB} - M_p \quad \text{(by Eqn. (B))}$$

$$M_{BA} = (WL_{AB}/\xi) - 3M_p \qquad (C)$$

Effective flexural rigidity :

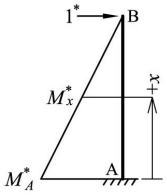
$$EI' = EI((1/f) - (1.1C/C_y)) \qquad (2.65)$$



'Actual' compatibility system

By proportion :

$$M_x / EI' = (1/EI')(M_p + (M_{BA} - M_p)(x/L_{AB})) \qquad (4.24)$$



'Virtual' equilibrium system

Moments about A :

$$M^*_A - (1^*)L_{AB} = 0$$

$$M^*_A = (1^*)L_{AB} \qquad (D)$$

By proportion :

$$M^*_x / (L_{AB} - x) = M^*_A / L_{AB}$$

$$M^*_x = M^*_A (L_{AB} - x)/L_{AB}$$

$$M^*_x = (1^*)L_{AB}(L_{AB} - x)/L_{AB} \quad \text{(by Eqn.(D))}$$

$$M^*_x = (1^*)(L_{AB} - x) \qquad (4.25)$$

VIRTUAL WORK FORMULA

External work :

$$1^*(-\Delta_{I\,p}) \qquad (4.26)$$

Internal work :

$$\int_0^{L_{AB}} M^*_x (M_x / EI')dx$$

$$\int_0^{L_{AB}} (1^*)(L_{AB} - x)(1/EI')(M_p + (M_{BA} - M_p)(x/L_{AB}))dx \quad \text{(by Eqn.'s (4.24) and (4.25))} \qquad (4.27)$$

Equating internal and external work and solving for $\Delta_{I\,p}$:

$$\Delta_{I\,p} = -L^2_{AB}(M_{BA} + 2M_p)/6EI'$$

$$\Delta_{I\,p} = -L^2_{AB}((WL_{AB}/\xi) - 3M_p + 2M_p)/6EI' \quad \text{(by Eqn.(C))}$$

$$\Delta_{I\,p} = L^2_{AB}(M_p - (WL_{AB}/\xi))/6EI' \qquad (4.28)$$

Fig. [4.3] Virtual work method for calculating $\Delta_{I\,p}$

Thus far in each virtual work calculation, an ‘actual’ equilibrium system of known moments and unknown loads was imposed on an unrelated virtual compatibility

system of rigid-bodied sways and rotations. The resulting virtual work equation was used to solve for the unknown collapse load. The virtual work principle is equally applicable when a virtual equilibrium system is imposed on an unrelated 'actual' compatibility system of unknown deflections and known curvatures. In such a case, the virtual work equation can be used to solve for the unknown deflections. This is a powerful and convenient method of calculating deflections in structures, although complications may arise when plastic moment hinges occur in the structure under consideration. The rotations that occur at the hinges account for a portion of the strain energy stored by the structure. Consequently, the plastic hinge rotations become additional unknowns that can be difficult and time consuming to determine. However, since the force and compatibility systems need not be related, it may be possible to distribute the virtual bending moments such that they do not encounter any hinges. If the virtual bending moments are zero at the hinge locations, then the internal virtual work done at the hinges equals zero, and the hinge rotations no longer need to be determined. Below is a description of this technique as it was used to calculate the sway deflections Δ_{Ip} for the test frames.

The compatibility system comprised the unknown sway deflection Δ_{Ip} and the curvature of member AB at the point of first order elastic-plastic collapse in the critical mode. The curvature at any point in AB was expressed as the quotient of the bending moment and the effective flexural rigidity *EI'* of this member. The reduced flexural rigidity was described in section 2.5 by the following empirical equation:

$$EI' = EI((1/f) - (1.1C/C_y)) \tag{2.65}$$

where: f = Shape factor of the section (=1.5 for a solid rectangular section)

The bending moment distribution in AB was relatively simple to define as the hinges had reduced the frame to a statically determinate structure. The equations of static equilibrium used to derive the moment distribution are shown in Fig. [4.3]. Below is the expression for 'actual' curvature in AB at a point distant x from A.

$$M_x / EI' = (1/EI')(M_p + (M_{BA} - M_p)(x/L_{AB})) \tag{4.24}$$

where $M_{BA} = (WL_{AB}/\xi) - 3M_p$

The equilibrium system comprised a unit virtual force acting at the location of and in line with Δ_{Ip}, and the corresponding selected distribution of virtual bending moments. Elastic-plastic analyses of the frames revealed that in each case the final hinge of the critical mechanism would form at joint A. Member AB was chosen to resist the moments as if it were a vertical cantilever from joint A. Consequently, the virtual bending moment distribution did not encounter plastic hinge rotations until collapse had been initiated. As shown in Fig. [4.3] the virtual bending moment in AB at any point distant x from A was:

$$M_x^* = (1^*)(L_{AB} - x) \tag{4.25}$$

The external work was equal to the product of the virtual force and the sway deflection.

$$\text{External work} = (1^*)(-\Delta_{I\,p}) \tag{4.26}$$

The internal work was equal to the product of the virtual moment and the 'actual' curvature integrated over the length of member AB.

$$\begin{aligned}\text{Internal work} &= \int_0^{L_{AB}} M_x^*(M_x / EI')dx \\ &= \int_0^{L_{AB}} (1^*)(L_{AB} - x)(1/EI')(M_p + (M_{BA} - M_p)(x/L_{AB}))dx\end{aligned} \tag{4.27}$$

Equating the external and internal work and solving for the deflection yielded:

$$\Delta_{I\,p} = L_{AB}^2(M_p - (WL_{AB}/\xi))/6EI' \tag{4.28}$$

This deflection was used in Eqn. (4.1) to calculate the value of X_p. Solving for the failure load W_f involved the simultaneous solution of the following two equations:

$$W_f = W_i + (X_f - X_i)(W_p - W_i)/(X_p - X_i) \tag{4.29}$$

$$U_2 W_f = W_s \tag{4.30}$$

where: subscript *f* represents failure
subscript *s* represents first order plastic collapse in the pure sway mode

Eqn. (4.29) is the relationship between load and X in the inelastic portion of the bilinear curve, while Eqn. (4.30) states that actual failure of the frame will occur when the amplified load equals the first order pure sway collapse load. The failure criterion of Eqn. (4.30) describes a straight line in the load-X space that intersects the x-axis at $X = 1$ and the y-axis at $W = W_s$. This further simplifies the process of solving for the failure load by allowing the designer to find graphically the intersection of the two graphs. Solving the graphs analytically however, it transpired that X_f was equal to the following equation:

$$X_f = \frac{X_i(\lambda_p - \lambda_s) + X_p(\lambda_s - \lambda_i)}{\lambda_s(X_p - X_i) + \lambda_p - \lambda_i} \tag{4.31}$$

The value of X_f was substituted into Eqn. (4.29) to find the failure load W_f. The load-deflection graphs were constructed by manipulating information taken from closely spaced intervals in the bilinear load-X graph. Each value of X was used in Eqn. (4.1) to calculate an appropriate value of first order deflection Δ_I, as well as in Eqn. (2.46) to find the corresponding amplification factor U_2. The amplified first order deflections were then graphed such that they could be compared to the results from the laboratory and ABAQUS tests.

4.3 Bilinear Method Results

	LABORATORY TEST $W_{f(L)}$ (kN)	ABAQUS $W_{f(A)}$ (kN)	BILINEAR AMPLIFICATION FACTOR METHOD $W_{f(K)}$ (kN)	$100*(W_{f(K)}-W_{f(A)})/W_{f(A)}$ (%)
kempsp1	1.009 mode 1	1.017 mode 1	0.966	-5.01
0.6span	1.303 mode 1	1.284 mode 1	1.285	0.08
0.8span	1.107 mode 1	1.135 mode 1	1.104	-2.73
1.2span	0.861 mode 1	0.917 mode 1	0.857	-6.54
1.4span	0.788	0.811 approximating mode 1	0.771	-4.93
0.8ll	N/A	0.869 mode 1	0.812	-6.56
0.6ll	0.69 mode 1	0.732 approximating mode 1	0.707	-3.42
0.4ll	0.592	0.624 approximating mode 1	0.632	1.28
0.33sway	0.84 mode 1	0.832 mode 1	0.873	4.93

Table [4.1] Frame failure from laboratory testing, second order inelastic ABAQUS tests and bilinear amplification factor method

The failure loads for the test frames as predicted by Kemp's bilinear method are presented in Table [4.1]. Corresponding load-X and load-Δ graphs from the three methods of analysis are shown together in figures [4.4] to [4.21] at the end of this chapter. The following observations were made in a comparison of the bilinear method to the ABAQUS and laboratory tests:

- There was an excellent degree of correlation between the failure loads of all three methods. Table [4.1] displays the differences between the bilinear method loads and the ABAQUS counterparts, expressed as percentages of the latter. Kemp's failure loads varied from within –6.5 percent to +4.9 percent of the ABAQUS loads. The test frames were flexible and were therefore highly susceptible to second order effects. Kemp's accurate failure loads thus seemed compelling evidence in favour of his theory's ability to approximate inelastic instability.

- Kemp's failure loads were progressively lower than the ABAQUS counterparts as spans increased. This trend was absent between the ABAQUS and laboratory results, and was therefore probably a consequence of Kemp's theory. It is suspected that the progressive under-estimation of strength with increasing spans resulted from the neglect of the effects of moment redistribution. The ABAQUS tests revealed that as the spans increased, the loss of stiffness and strength after the formation of the first fully plastic section became more gradual. This retention of strength was enabled by

moment redistribution as the frames became more flexible. The bilinear load-X graph does not allow for the manner in which moment redistribution affects the shape of the actual load-X curve after plastic stresses are encountered.

- Kemp's failure load for the kempsp1 frame was lower than the ABAQUS counterpart, yet the discrepancies between loads reduced as the loading lengths shortened. Given that the loading length variation frames shared similar geometries, it was unlikely that this trend was due to changes in the ability of the frames to redistribute moment. Rather, it must have resulted from the sequence of plastic hinge formation in the frames. As the loading lengths reduced, the vertical loads caused increasingly severe moments at the column tops and at the centre of the beam. Plastic moment hinges occurred in these locations in quick succession, resulting in a rapid loss of stiffness and strength after the formation of the first hinge. This caused failure to occur in the actual test frames at progressively lower loads as the loading lengths shortened.

- Kemp's failure criterion suggests that failure will occur in a pure sway mode. The laboratory and ABAQUS tests showed that actual failure occurred in combined member and sway modes. Notwithstanding the actual failure mechanisms of the test frames, Kemp's method still provided highly accurate failure loads.

- The elastic portions of the bilinear curves were only slightly steeper than the initial portions of the corresponding laboratory and ABAQUS curves. This may have resulted from inaccuracies in the calculation of Young's modulus, but was more likely a consequence of the sagging of the flexible beams. Sway deflection in the laboratory was measured on the column top whose deflection was increased by pronounced sagging of the beam. This made each frame appear less stiff than it actually was. The differences between the elastic bilinear curves and the laboratory and ABAQUS curves were more evident in the longer span frames, where more flexible beams allowed greater differences between the sway deflections of joints B and C.

- As anticipated, the frames exhibited nonlinear behaviour at loads below Kemp's λ_i. The load λ_i represented the condition of the formation of the first fully plastic section in the structure. Prior to this condition, the stiffness of the frame had been reducing due to the spread of plasticity. The loss of section stiffness, combined with the second order effects present in the flexible test frames, resulted in the divergence of the load-X curves at relatively low loads.

- First order inelastic analyses were performed on the test frames in ABAQUS. These analyses produced sway deflections at failure that compared very favourably to the deflections calculated using Kemp's virtual work method. For the frames in which sway related failure modes were critical, load-X graphs were constructed using the ABAQUS first order analysis results. These load-X graphs are shown together with the graphs from the other analysis methods in figures [4.4] to [4.12]. Since X was a linear function of Δ_I for the test frames, comparing values of X was equivalent to comparing values of Δ_I. Even though the sway deflections of the frames were very sensitive to

load near collapse, the first order ABAQUS curves and the bilinear graphs had similar loads at X_p. This indicated that the virtual work method, as well as the empirical expression for the effective flexural rigidity given in Eqn. (2.65), provided accurate results.

- The incremental amplification factor values X_f of the bilinear method at failure were substantially larger than those of the other two methods. The larger values of X_f resulted in amplification factors that ranged from 121 percent to 212 percent of the ABAQUS U_2 values. The best-matched U_2 values were of the 0.33sway frame, followed by the increasing spans of the span variation frames, and then by the decreasing loading length variations. These discrepancies implied that the amplified failure loads of the ABAQUS and laboratory tests were correspondingly lower than the respective first order pure sway collapse loads. That the bilinear method was able to achieve excellent failure load results with markedly different amplification factors was due to the interaction of a number of factors. The main contributing factors would include the failure criterion of Eqn. (4.30) and the applicability of the inelastic amplification factor U_2 as a function of X. These influences are discussed further in chapter 5.

- The load-Δ curves that were extrapolated from the bilinear load-X graphs are presented in figures [4.13] to [4.21] together with the ABAQUS and laboratory test curves. The bilinear load-X approximation had a marked effect on the relationship between load and the total sway deflections Δ. For all of the frames, the extrapolated load-Δ curves resembled bilinear graphs possessing slight curvatures that indicated nonlinear geometric effects. At loads below W_i, the amplification factor method produced deflections that underestimated the actual deflections by twenty to thirty percent. Once again, the correlation of results was more favourable for the frames with shorter spans and greater loading lengths. At loads above W_i, the validity of the load-Δ relationship was lost in all cases.

The main objective of Kemp's bilinear amplification factor theory was to provide the designer with a simplified method of calculating the instability load of an unbraced sway frame. His approach of using sway equilibrium equations to derive an incremental amplification factor, and a bilinear approximation of the load-X relationship has been shown here to predict collapse loads that rival the quality of a finite element analysis. While it is impossible to say whether these results are representative for other shapes and types of structures, it would be pointless to attempt an improvement of this accuracy for the test frames. This is partly due to the fact that a simplified semi-empirical method cannot be expected to produce high accuracy in all cases, but also because the ABAQUS and laboratory results differed by similar margins. In chapter 5, attention is focussed rather on the validity of the inelastic amplification factor and the nature of the load-X relationship. The ensuing discussions investigate whether it is possible to modify the bilinear load-X approximation such that it more closely represents the 'actual' relationship without sacrificing the accuracy of the prediction of instability.

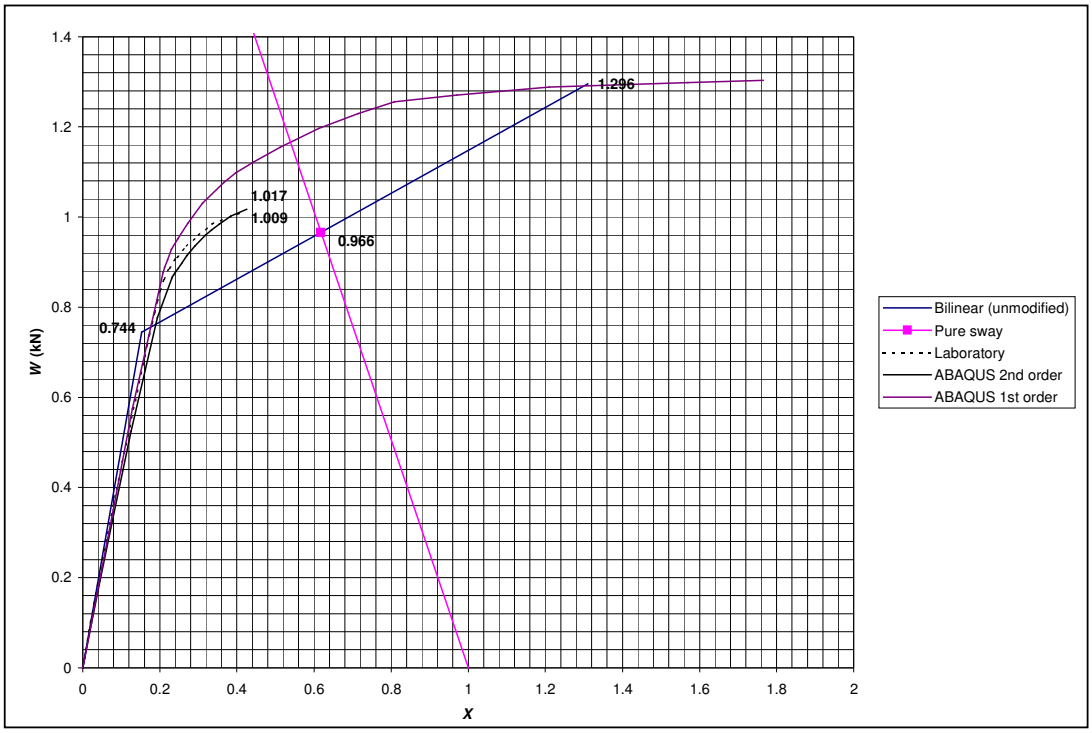


Fig. [4.4] Bilinear *W-X* graph of kempsp1 frame

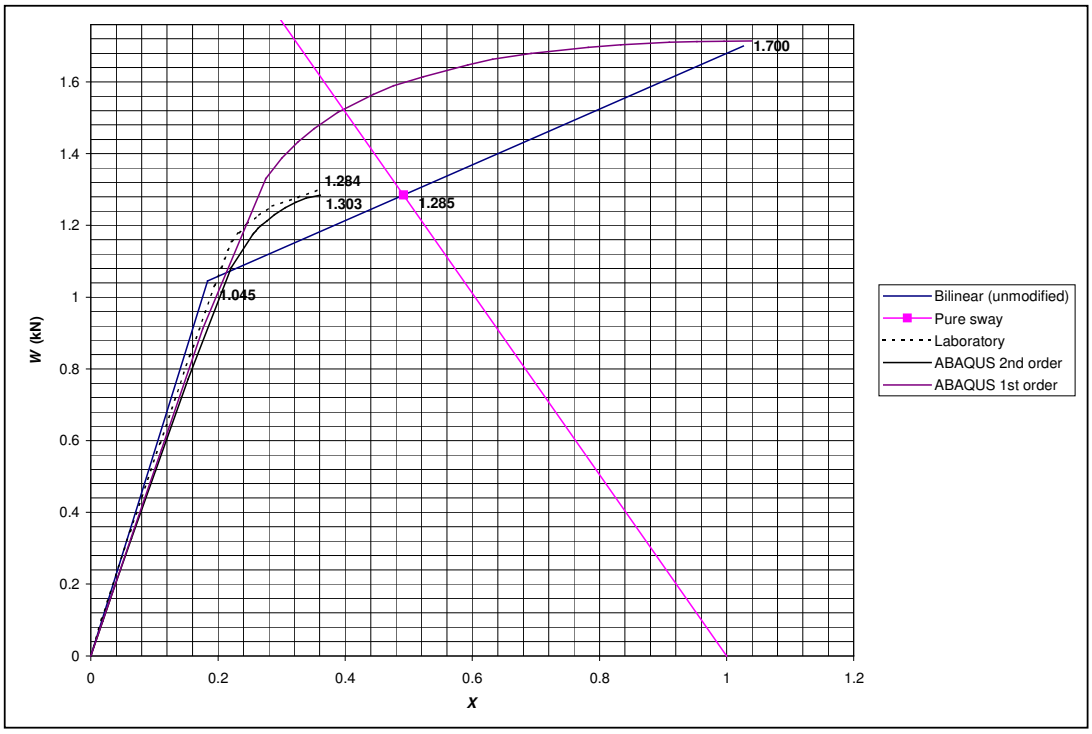


Fig. [4.5] Bilinear *W-X* graph of 0.6span frame

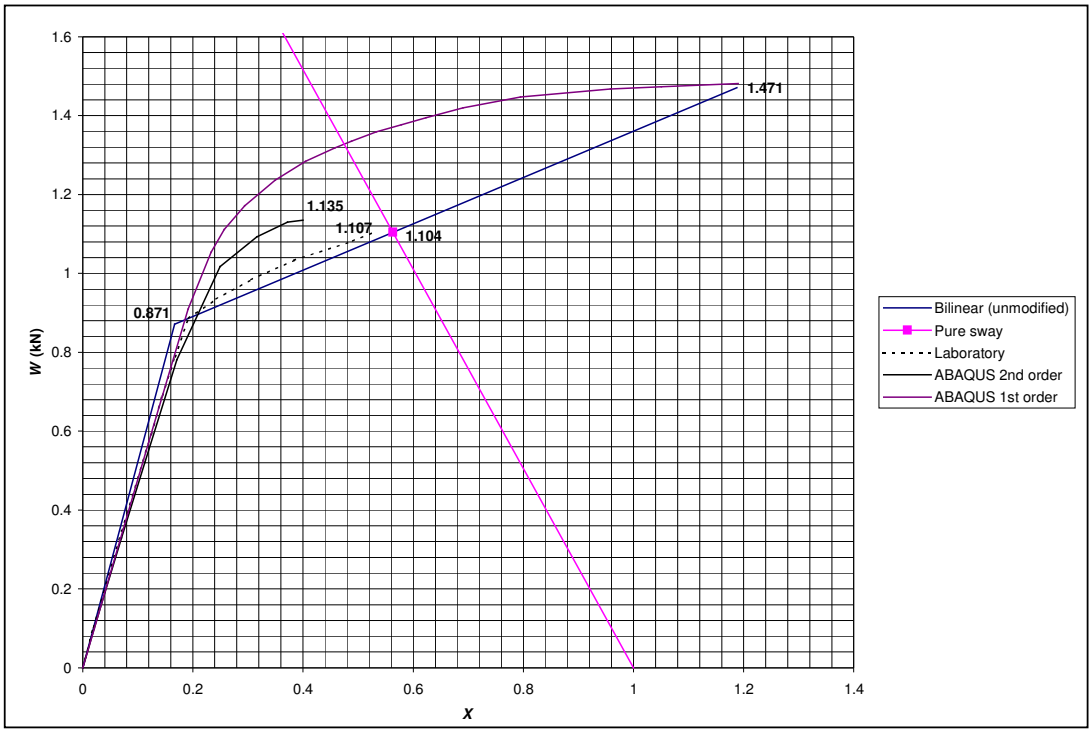


Fig. [4.6] Bilinear *W-X* graph of 0.8span frame

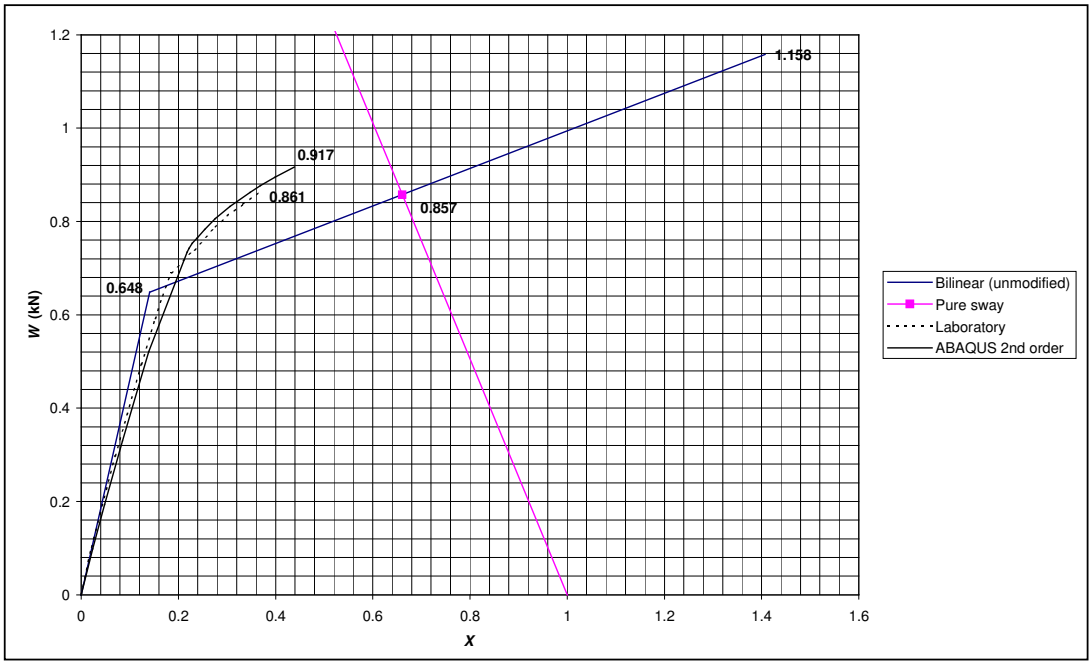


Fig. [4.7] Bilinear *W-X* graph of 1.2span frame

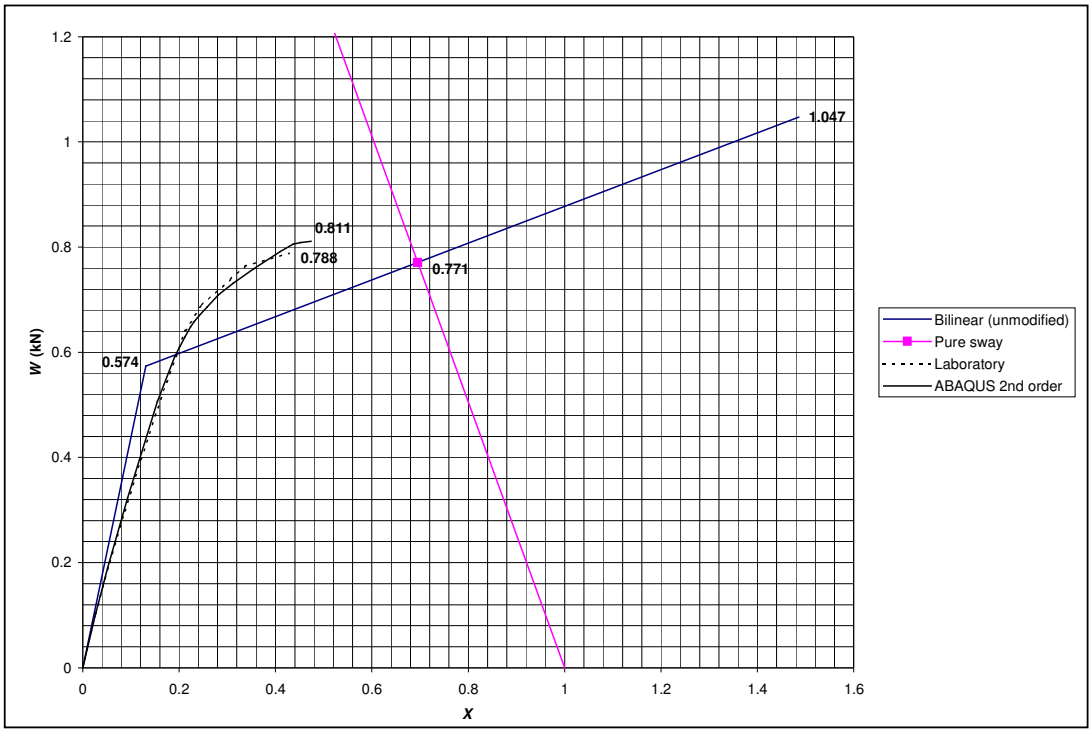


Fig. [4.8] Bilinear *W-X* graph of 1.4span frame

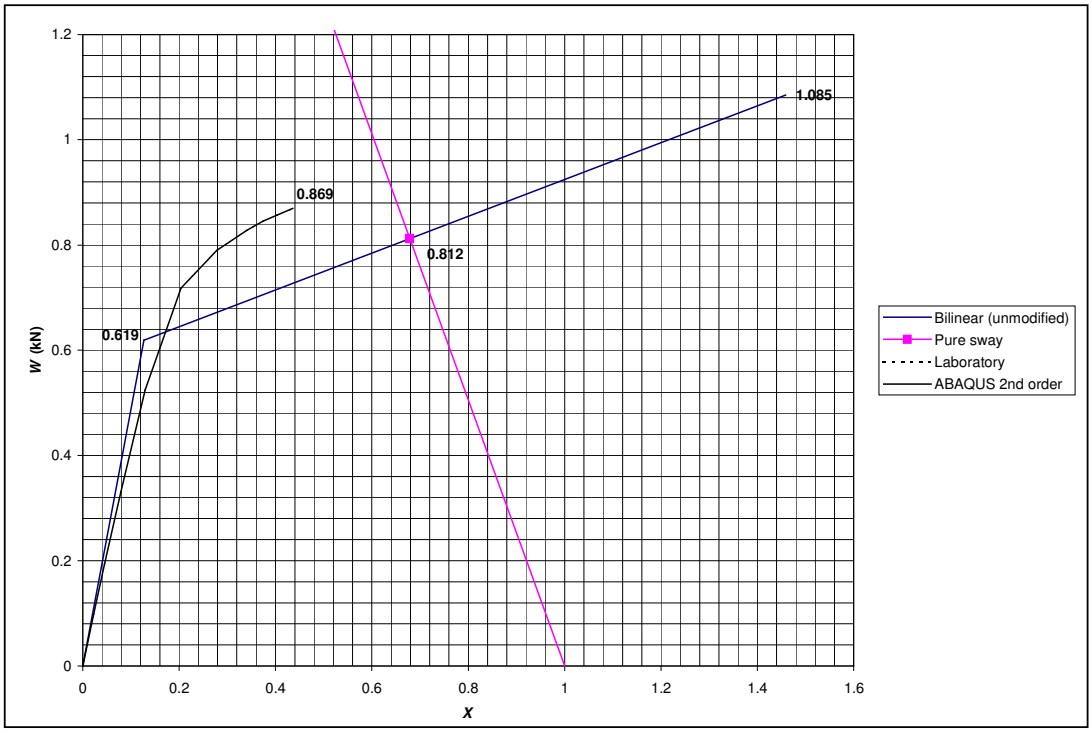


Fig. [4.9] Bilinear *W-X* graph of 0.8ll frame

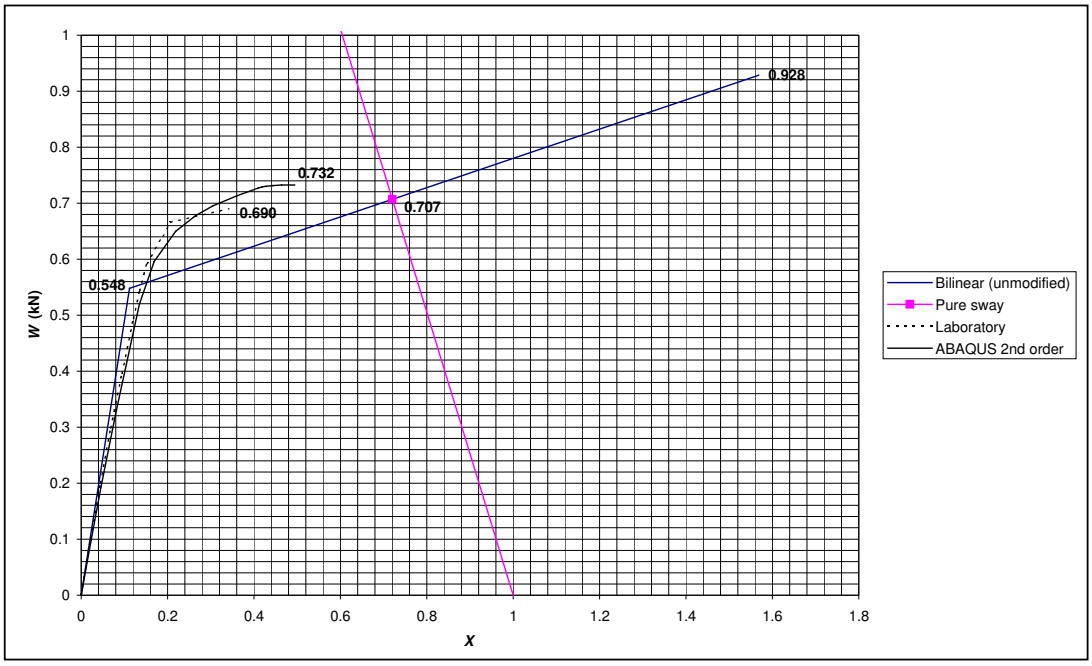


Fig. [4.10] Bilinear *W-X* graph of 0.6ll frame

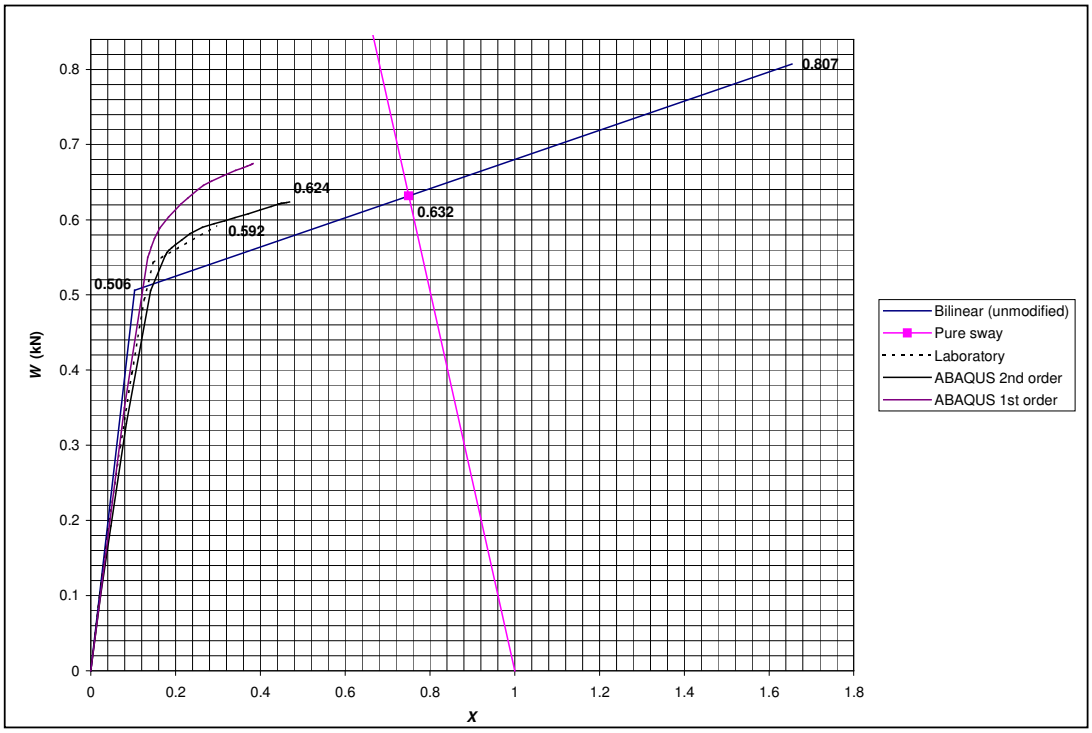


Fig. [4.11] Bilinear *W-X* graph of 0.4ll frame

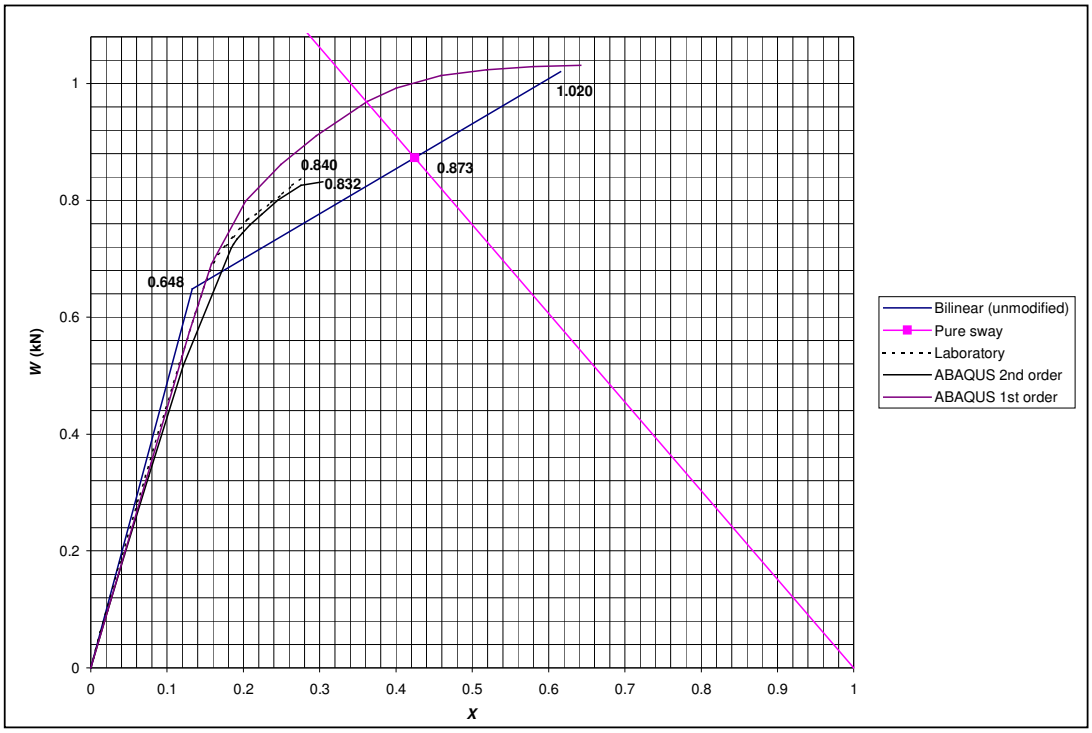


Fig. [4.12] Bilinear *W-X* graph of 0.33sway frame

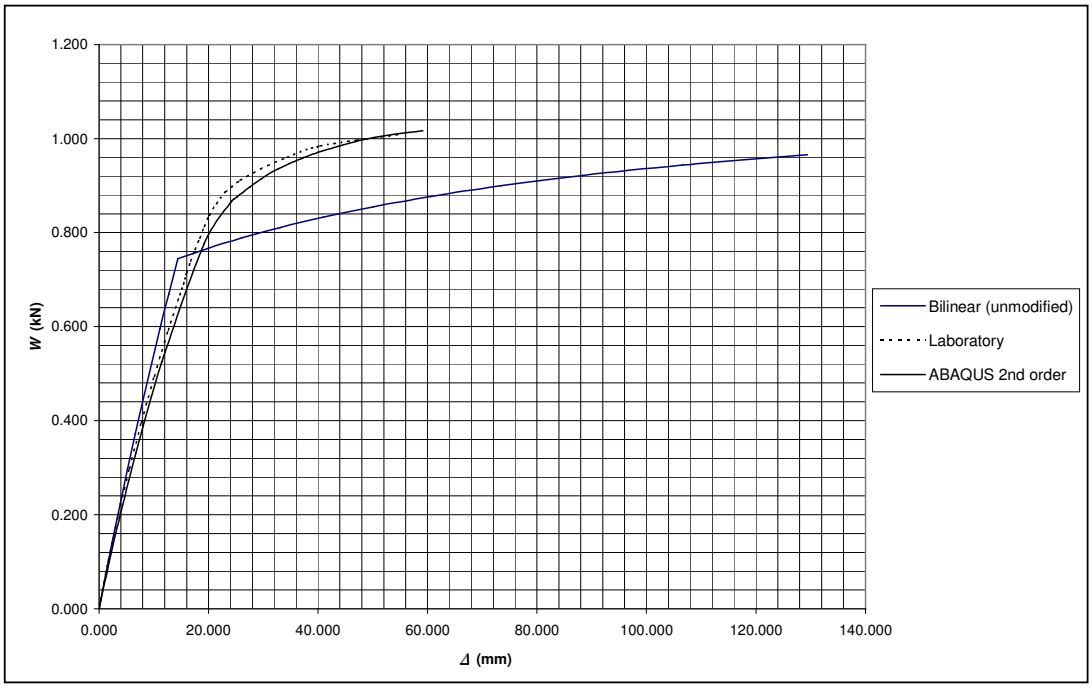


Fig. [4.13] Bilinear *W-Δ* graph of kempsp1 frame

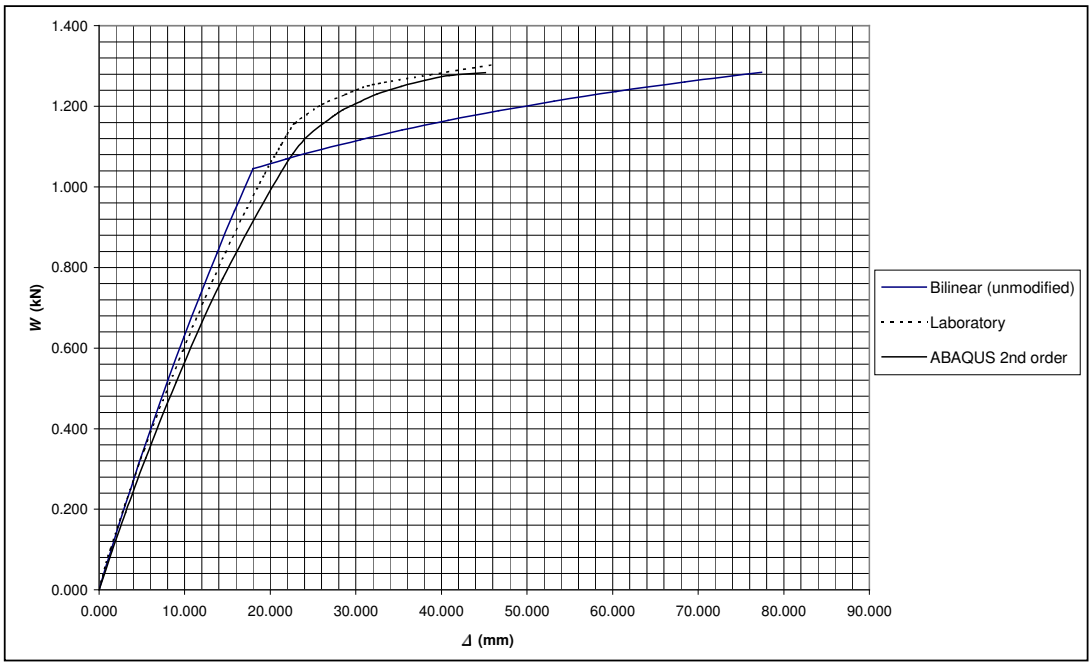


Fig. [4.14] Bilinear *W*-*Δ* graph of 0.6span frame

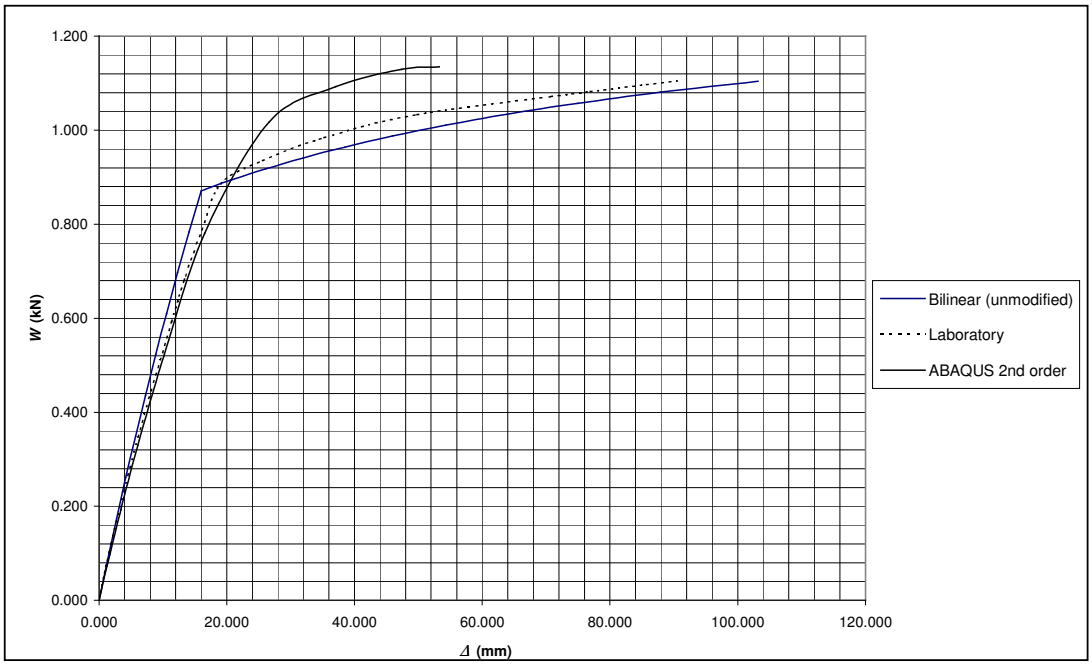


Fig. [4.15] Bilinear *W*-*Δ* graph of 0.8span frame

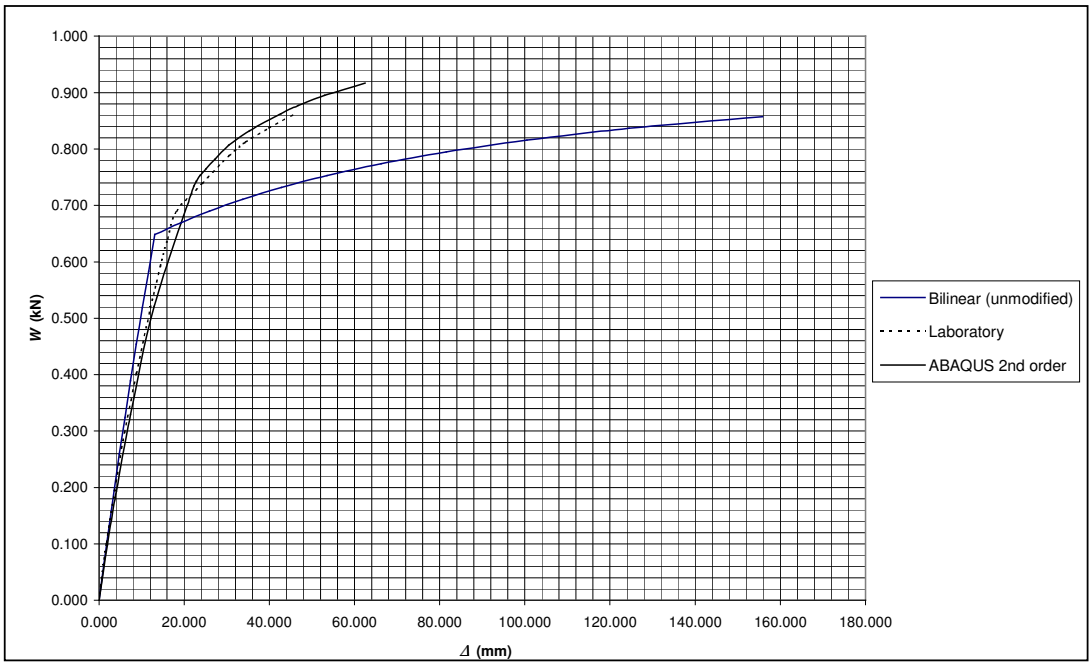


Fig. [4.16] Bilinear *W-Δ* graph of 1.2span frame

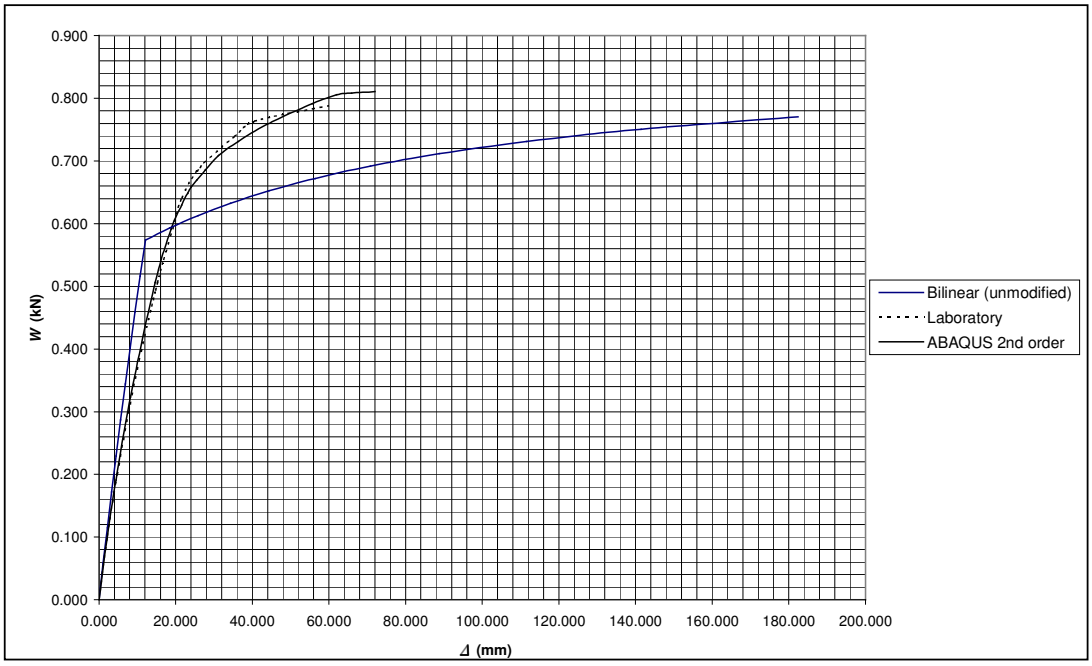


Fig. [4.17] Bilinear *W-Δ* graph of 1.4span frame

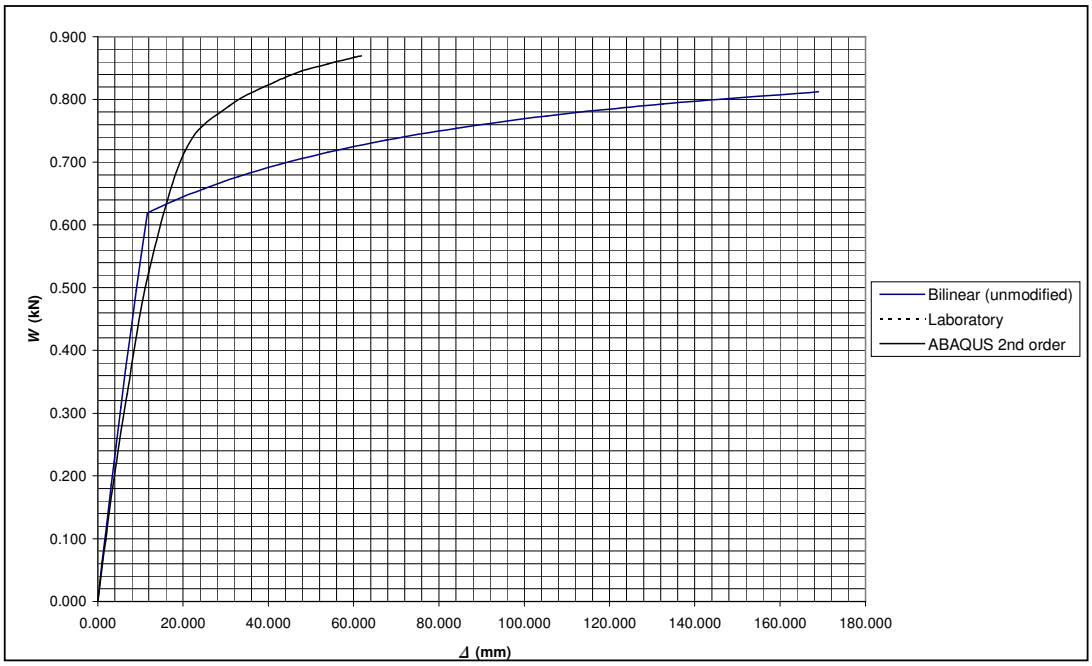


Fig. [4.18] Bilinear *W-Δ* graph of 0.8ll frame

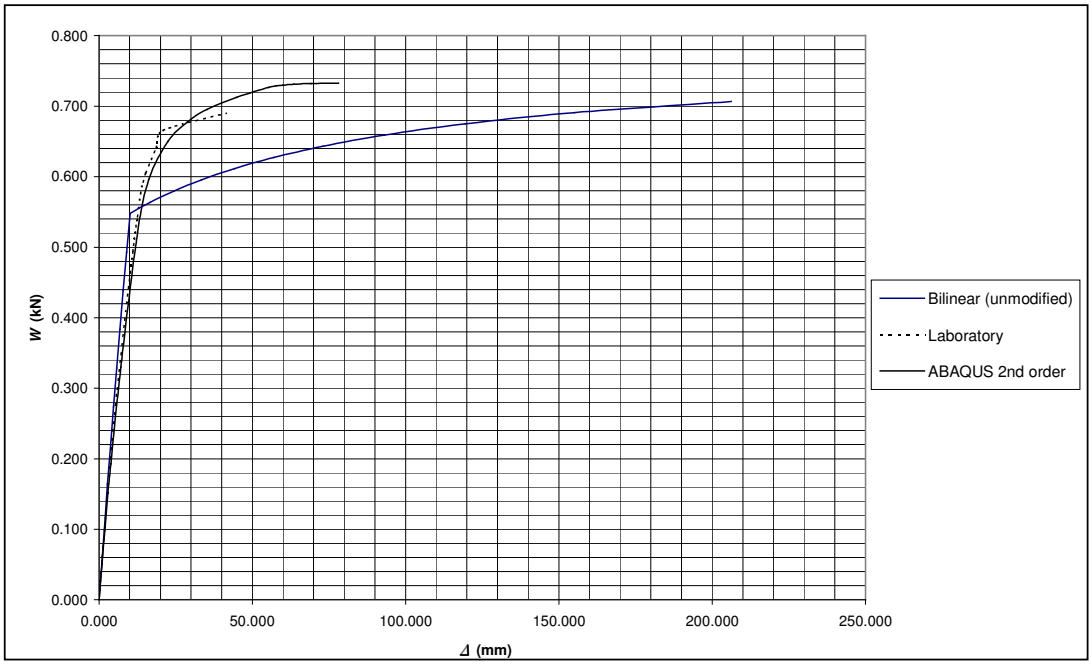


Fig. [4.19] Bilinear *W-Δ* graph of 0.6ll frame

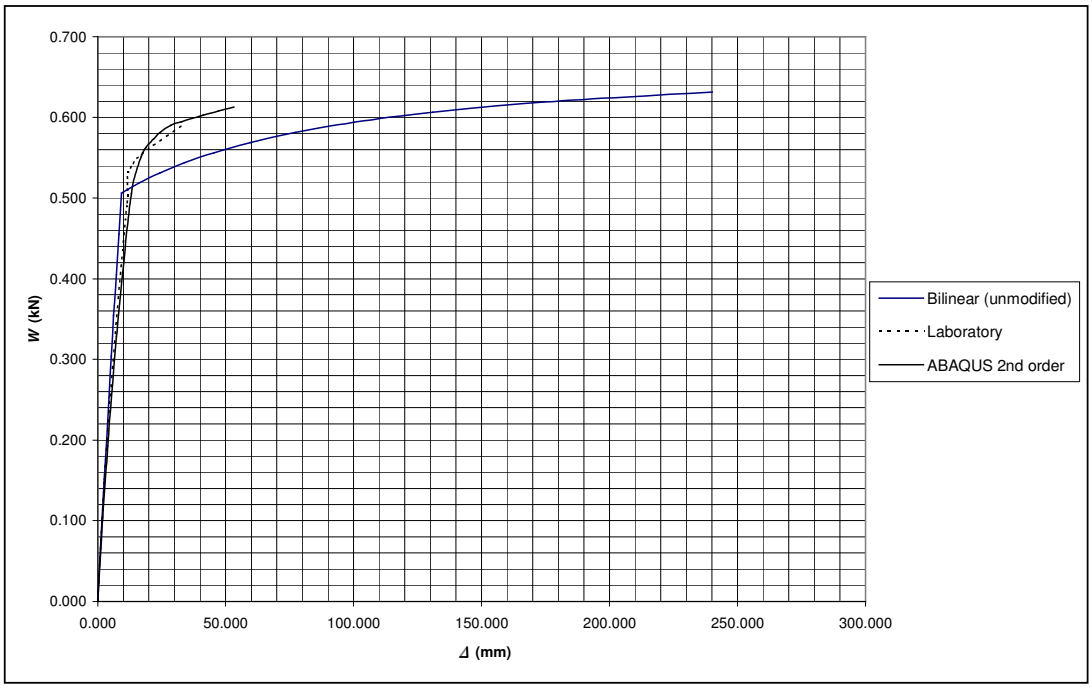


Fig. [4.20] Bilinear *W-Δ* graph of 0.4ll frame

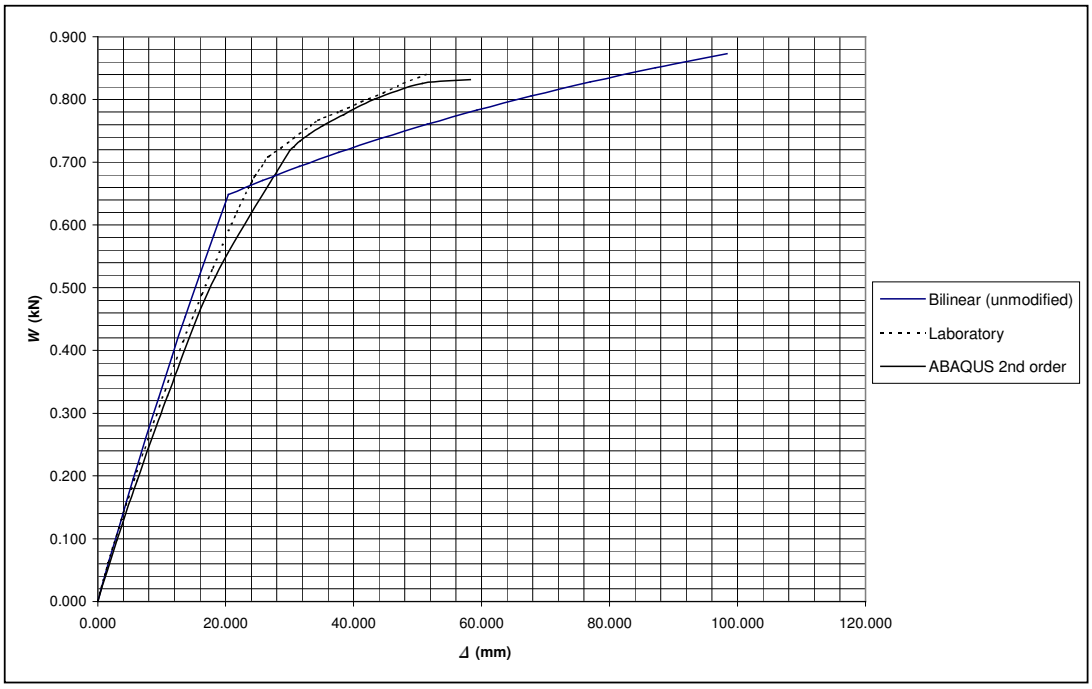


Fig. [4.21] Bilinear *W-Δ* graph of 0.33sway frame

5 REASSESSMENT OF KEMP'S AMPLIFICATION FACTOR THEORY

Kemp's method for approximating the relationship of load versus amplification factor incorporates both theoretical and empirical technique. The rigorous application of structural theory is confined to the derivation of the amplification factor, while empirical approximations are used for the load-X and moment-curvature relationships, and the failure criterion of Eqn. (4.30). The explanation of Kemp's method given in Chapter 2 is consistent with his published workings in reference 1. In this chapter, certain assumptions that Kemp used to facilitate his derivations are highlighted and discussed. Particular reference is given to those assumptions that affect the accuracy or validity of his method. It is expected that a partially empirical method will require structural theory to be contravened in order to maintain a method that is generally applicable to all sway structures. Nevertheless, a detailed look at the derivation enables informed attempts at improving the theory.

5.1 Developing a Second Order Sway Equilibrium Equation

Eqn. (2.55) was used to express the moment equilibrium of a typical member within an unbraced frame of any shape. This equilibrium equation was intended to include the first iteration of second order effects.

$$M_{I+1\,ij} + M_{I+1\,ji} = -V_{ij}L_{ij} - C_{ij}\Delta_{I\,ij} \tag{2.55}$$

In the event that a beam-column is subjected to a low compressive, or even tensile, axial force, Eqn. (2.55) will calculate that the second order moments of such a member are negligible or negative. From considerations of compatibility, however, a lightly loaded column in a rectangular frame will be forced to sway similarly to the other more heavily loaded columns. This is due to the length of the beam or floor slab that remains essentially unchanged by load. The second order effects of all the columns will be alike, thus it is apparent that Eqn. (2.55) must not be applied to members in isolation from the remaining structure. In the storey magnifier method all columns are considered simultaneously, thereby allowing the total vertical and sway loads to be taken into account in the equilibrium equations. In the analogous virtual work approach, Eqn. (2.55) may cause confusion and it should be explained that it applies only to a single-member structure.

The process of manually assessing the second order moment equilibrium of a nonrectangular structure in its entirety would be extremely complex, and highly dependent on the geometry of the given structure. Since the compression members of such a structure generally possess different lengths and load-deflection sensitivities, the equilibrium equations would be written in multiple unknowns. Incremental consideration would result in compatibility and equilibrium problems at the joints, and further complications would arise due to the spread of plasticity. Kemp needed to avoid such difficulties if he was to develop a feasible simplified method of assessing inelastic instability. By using a sway equilibrium equation, he summed the scalar

values of virtual work resulting from the first iteration of second order effects over the entire structure. In Eqn. (2.57) this value is represented by the term $\Sigma C_{ij}\Delta_{I\,ij}\phi_{ij}^{*}$.

$$\Sigma V_{ij}L_{ij}\phi_{ij}^{*} = -\Sigma(M_{I+1\,ij} + M_{I+1\,ji})\phi_{ij}^{*} - \Sigma C_{ij}\Delta_{I\,ij}\phi_{ij}^{*} \tag{2.57}$$

Kemp treated this summation of "second order virtual work" similarly to the manner in which Kennedy et al treated the first iteration of second order moments. He allowed successive iterations to increase the second order virtual work by a given proportion *X* of the previous iteration's value. In so doing, he avoided dealing with the unique incremental increases in deflections and moments at each joint. In Kennedy et al's derivation, the proportional relationship between sway moments and related displacements was used to calculate explicitly the value of *X*. The resulting incremental amplification factor was given by Eqn. (2.44).

$$X = \frac{\Sigma P\Delta_{I}}{\Sigma Vh} \tag{2.44}$$

Kennedy et al's *X* represents the ratio of the first iteration of second order moments to the total first order sway moments induced by the lateral loads on the frame. It appears that Kemp chose an analogous approach to calculating his own virtual work incremental amplification factor: Kemp's *X* represents the ratio of the first iteration of second order virtual work to the total virtual work of the frame, as shown by Eqn. (2.58).

$$\begin{aligned} X &= \frac{-\Sigma(M_{I+1\,ij} + M_{I+1\,ji})\phi_{ij}^{*} - (-\Sigma(M_{I\,ij} + M_{I\,ji})\phi_{ij}^{*})}{\Sigma V_{ij}L_{ij}\phi_{ij}^{*}} \\ &= \frac{\Sigma C_{ij}\Delta_{I\,ij}\phi_{ij}^{*}}{\Sigma V_{ij}L_{ij}\phi_{ij}^{*}} \qquad \text{(by Eqn. (2.4-6))} \\ &= \frac{\Sigma C_{ij}\Delta_{I\,ij}\phi_{ij}^{*}}{\Sigma P_{i}\partial_{i}^{*}} \qquad \text{(by Eqn. (2.4-1))} \end{aligned} \tag{2.58}$$

Although Kemp's approach seems logical, I have been unable to prove that there exists such a proportional relationship between the second order virtual works of successive iterations for an arbitrarily shaped structure. Since the virtual deflections remain unchanged, the actual second order deflections must readjust at each increment in order that the total second order virtual work can be achieved. It is thus required that these actual deflection changes occur such that the conditions of moment equilibrium, compatibility and the value of *X* are simultaneously maintained at each iteration. If so, then it is possible that the problems associated with using an incremental moment equilibrium approach are reintroduced for nonrectangular structures and inelastic stress conditions.

5.2 Validity of the Inelastic Amplification Factor

The derivation of U_2 is dependent on a proportional relationship between the load factor and the first order internal virtual work of the sway equilibrium equation. In the simple case of the test frames, this relationship translates to the proportionality between the overall load W and the first order sway deflection Δ_I. At a given load, it is the sway stiffness that defines the susceptibility of the structure to second order effects. Graphically, the sway stiffness is equal to the slope of the line joining the origin of the load-Δ_I curve to the point under consideration. This ratio between load and deflection is used in the geometric sum of Eqn. (2.60) to calculate U_2.

$$\begin{aligned}\Sigma V_{ij} L_{ij} \phi^*_{ij} &\rightarrow -\Sigma(M_{ij} + M_{ji})\phi^*_{ij} - (\Sigma C_{ij} \Delta_{I\,ij} \phi^*_{ij})(1 + X + X^2 + X^3 + \ldots + X^n) \\ &= -\Sigma(M_{ij} + M_{ji})\phi^*_{ij} - \frac{\Sigma C_{ij} \Delta_{I\,ij} \phi^*_{ij}}{1 - X} \\ &= -\Sigma(M_{ij} + M_{ji})\phi^*_{ij} - U_2 \Sigma C_{ij} \Delta_{I\,ij} \phi^*_{ij}\end{aligned} \tag{2.60}$$

Where the expression for U_2 in terms of X is as follows:

$$U_2 = \frac{1}{1 - X} \tag{2.61}$$

During loading in the elastic zone, the second order effects are calculated using the actual sway stiffness of the structure. Following the spread of plasticity however, the line joining the origin to the point under consideration cannot follow the curve of the load-Δ_I graph. The slope of this line now represents a type of 'effective' sway stiffness which averages the effect of the loss of elastic rigidity. The second order effects are calculated using the average sway stiffness in the inelastic stress state. As loads increase further the tangential and effective stiffness values diverge resulting in the progressive underestimation of second order effects. Furthermore, the geometric sum for U_2 cannot allow for the loss of stiffness due to second order strains albeit that these losses will probably become significant near failure loads only. The combined results of these two effects are shown in the load-Δ graph of Fig. [5.1] for the 0.6rigidspan frame. This frame was identical to the 0.6span frame, except for a sturdier section of 40x40mm that was used for all the members. The amplified first order deflections follow the actual total deflection curve for the elastic and the initial inelastic behaviour. As loads continue to rise, the effective stiffness used to calculate U_2 becomes progressively larger than the actual frame stiffness. This results in the underestimation of the nonlinear behaviour, indicated by the divergence of the two curves.

In the highly flexible test frames the underestimation of second order effects by Eqn. (2.61) was exacerbated by the differing column top sways, and the early onset of plasticity caused by second order effects. It was mentioned in chapter 3 that the sagging of the beams increased the deflections of the column tops on which deflections were measured in the laboratory. The large deflections of the frames resulted in second order effects that induced the loss of elastic rigidity at loads significantly lower than those predicted by first order analyses. Fig. [5.2] displays

various load-Δ graphs of the 0.6span frame. It can be seen that the first order analysis predicts the occurrence of the first plastic moment hinge at a relatively high load. This is reflected in the amplified first order deflection curve which maintains the elastic slope long after the actual frame has formed its first hinge. Being the stiffest of the test frames, the column sways of the 0.6span frame differed little from each other thus the deflection at joint B was not greatly increased by the sagging of the beam. In the 0.6rigidspan frame test, both of these effects were eliminated as the column sways differed by less than a millimetre at collapse, and the first order load-Δ_I graph showed loss of stiffness at a similar load as the second order graph.

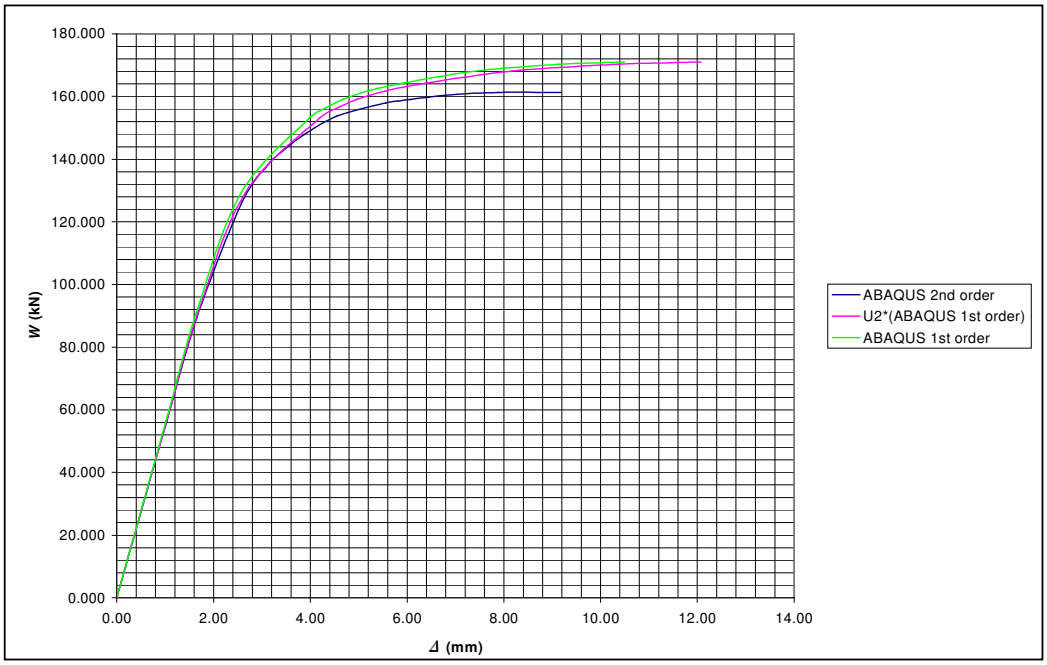


Fig. [5.1] *W*-Δ graph of 0.6rigidspan

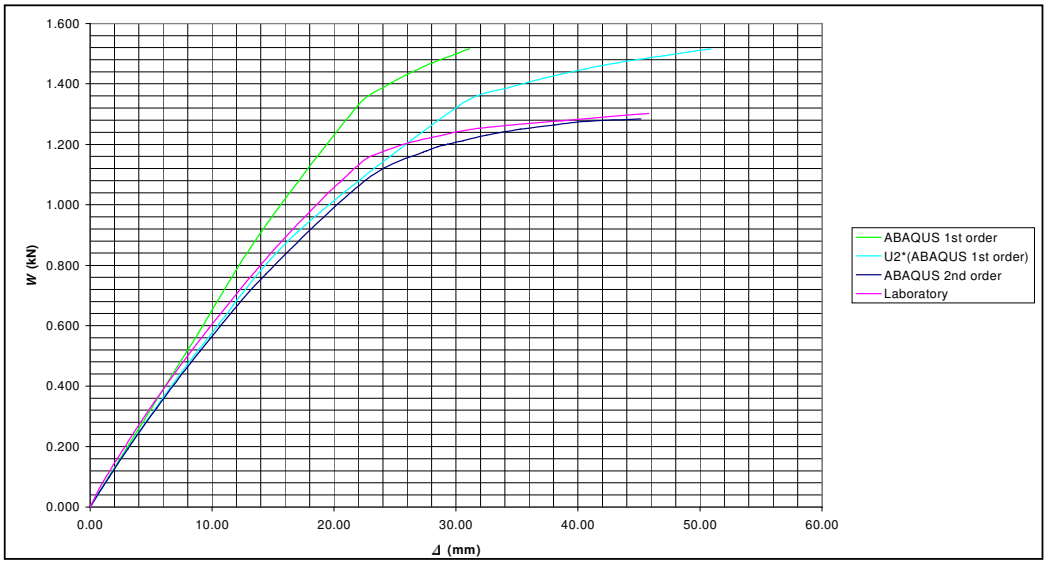


Fig. [5.2] *W*-Δ graph of 0.6span frame

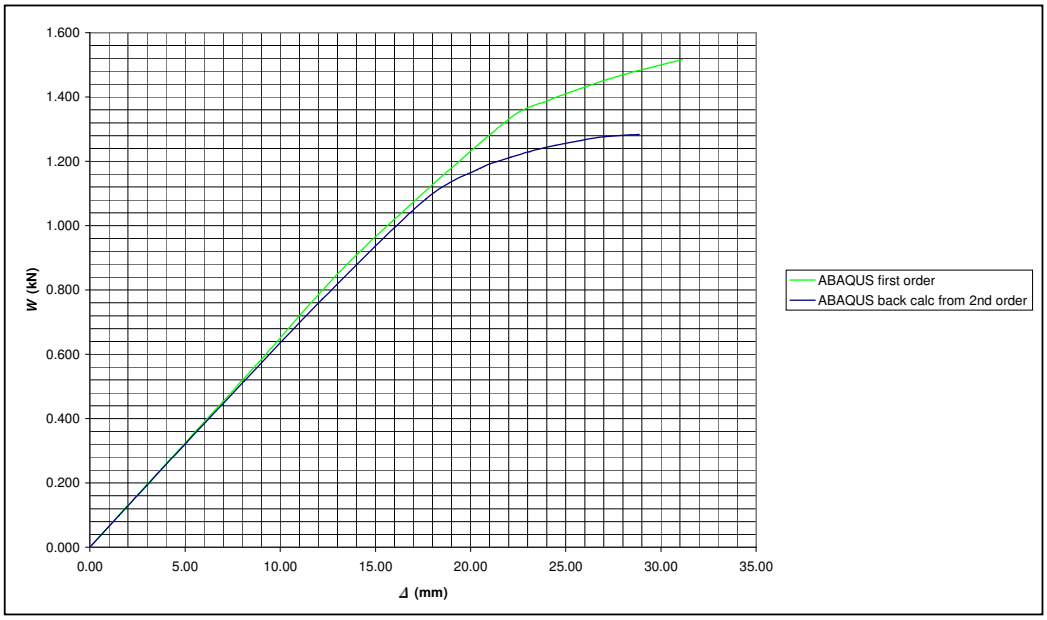


Fig. [5.3] First order *W-Δ* graph of 0.6span frame

Sway measurements taken in the laboratory and from the second order ABAQUS analyses were converted to equivalent first order deflections by using Eqn. (3.9). This equation was derived using Kemp's expression for the amplification factor, which has been shown here to underestimate second order effects. As a result, the deflections so calculated were correspondingly larger than actual first order deflections. This is illustrated in Fig. [5.3] where the back-calculated deflections of Eqn. (3.9) are graphed with deflections obtained from a first order ABAQUS analysis.

$$\Delta_I = \frac{\Delta}{1+(C\Delta)/(VL)} \tag{3.9}$$

It follows that a load-*X* graph constructed using actual first order deflections would have differed similarly to the results of a graph using back-calculated deflections. Figure [5.4] compares both versions of the load-*X* graphs for the 0.6span frame. It can be seen that the bilinear graph approximated the back-calculated curve more closely than it did the curve based on first order deflections. This figure also demonstrated that the results of applying the failure criterion to a load-*X* curve composed of first order deflections would be an inaccurate prediction of failure load. The 0.6span frame failed at a load of approximately 1.30kN, yet the purple load-*X* curve based on first order deflections shows the frame to be elastic at this load. Applying the failure criterion of Eqn. (4.30) to this curve yields a failure load prediction of 1.52kN. For the longer span frames, where the critical first order mechanisms were member mechanisms, the results would be more unpredictable still.

$$U_2 W_f = W_s \tag{4.30}$$

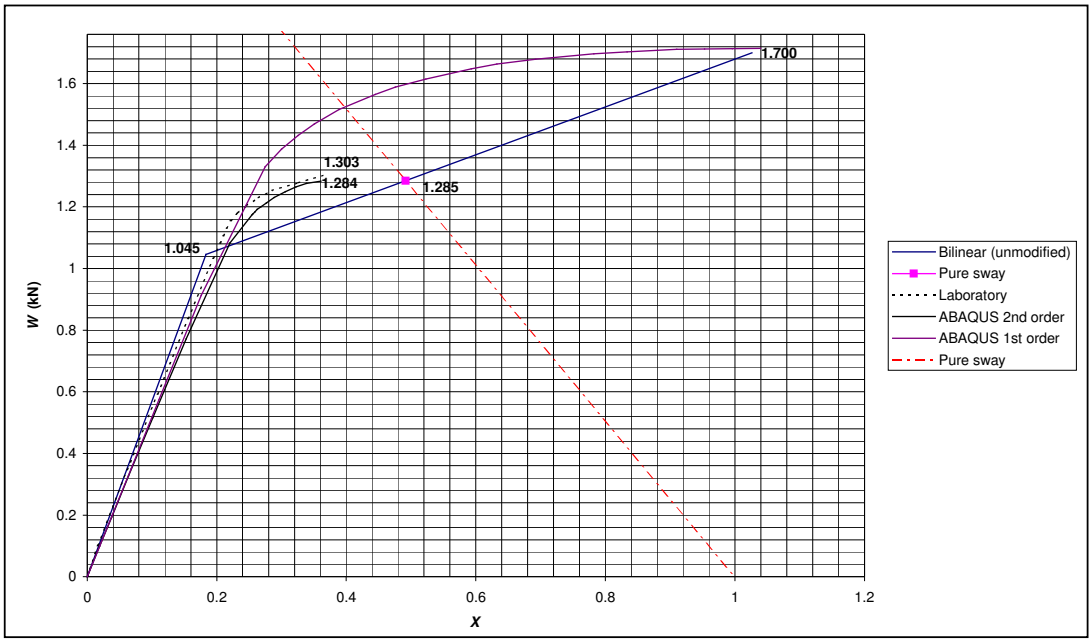


Fig. [5.4] Bilinear *W-X* graph of 0.6span frame

5.3 Application of the Amplification Factor and Failure Criterion

The amplification factor of Kennedy et al was derived such that it could be applied to stresses, deflections or loads. An example of the amplification of deflections and load factor is illustrated in the load-Δ graphs of Fig. [5.5]. The two curves therein represent the first and second order analyses of the 0.6span frame before the onset of plasticity. At a load of 0.56kN, the first order sway deflection is 8.6mm. When multiplied by an amplification factor of 1.16, the product is the corresponding total deflection of 10mm. Alternatively, one may amplify the 0.56kN load by the same factor of 1.16. The resulting load of 0.65kN also produces a 10mm deflection in a first order analysis. The ability to amplify a load and obtain the same deflection effect using that load in a first order analysis is due in part to the constant sway stiffness of an elastic rectangular frame. This allows proportionality to be used between load and deflection. It is also a result of the fact that vertical or gravitational loads do not induce first order sway deflections in perfectly vertical columns. Since real columns will always deviate from the vertical, designers compensate by adding notional horizontal loads at each floor level equal to 0.5% of total vertical load at that floor. This induces the same sway moment as the first iteration of second order moment caused by columns that are 0.5% out of plumb. When calculating total bending moments, it is only the horizontal translational load effects that are amplified. At a given load, this is equivalent to adding the amplified translational moments to the unamplified gravitational moments as per Eqn. (2.50).

$$M = U_2 M_{It} + M_g \qquad (2.50)$$

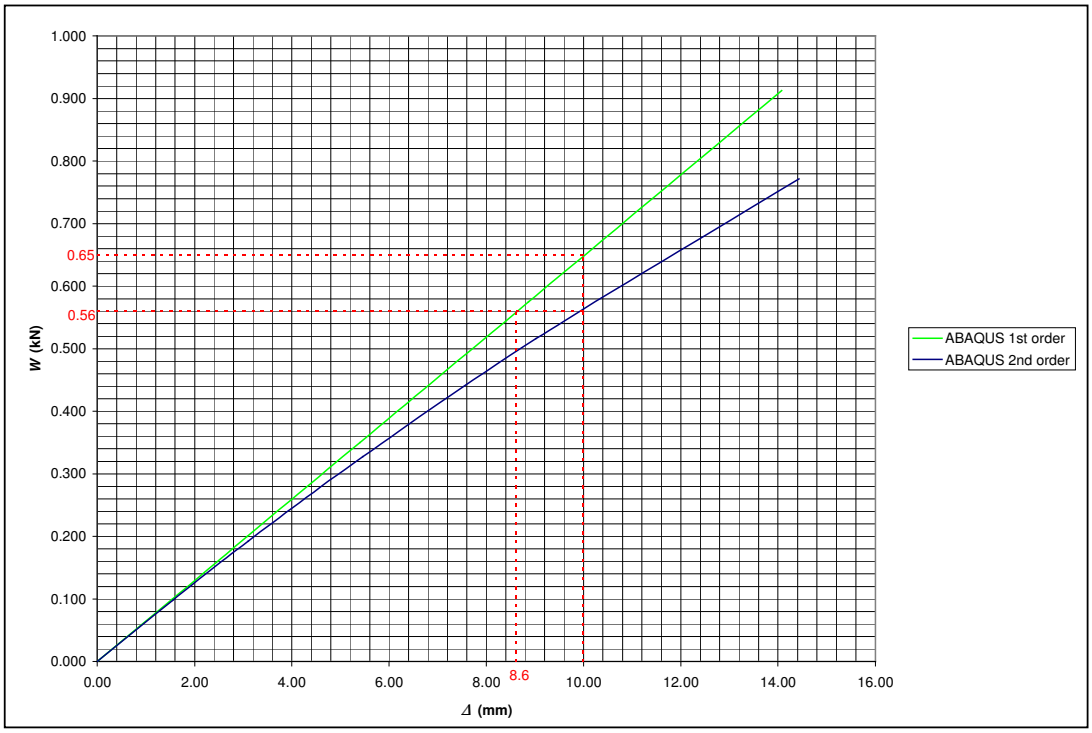


Fig. [5.5] Partial elastic *W-Δ* graph of 0.6span frame

Kemp's amplification factor has been derived such that it can be applied in the general case to a sum of virtual work, not to individual moments or deflections, or to a load factor. It would clearly be meaningless to amplify a stress or moment that has reached its maximum plastic limit. Nevertheless, the incremental amplification factor X is proportional to the first order sway deflection Δ_I of a rectangular frame for all loads. This means that the sway deflections measured in the laboratory could be used to calculate the values of U_2, regardless of the fact that the amplification factor was not intended for application to individual deflections. The loading state of most interest to the designer is usually the one that causes structural instability. It was thus at the collapse load that the application of Kemp's amplification factor, and the formulation of the failure criterion was investigated.

In Chapter 4.3, it was noted that Kemp's bilinear method produced excellent predictions of failure loads for the laboratory frames, yet calculated comparatively excessive values of X. Since U_2 is dependant on the value of X, it seemed unlikely that his method could accurately calculate failure loads with significantly different amplification factors. That the failure criterion produced a failure load for the 0.6rigidspan frame that was greater than W_p (see Fig. [5.9]) was also cause for concern. It is probable that these outcomes result from Kemp's assumptions that there exists a single amplification factor per sway mode per structure, and that collapse will occur in a pure sway mode. These issues are discussed below in more detail.

It is possible that the amplification of the effects of a load, or load group, may differ to the amplification of other load effects on the same structure. This notion is supported by the method suggested by Kennedy et al to calculate the total bending moment at any point in a frame. As described in Eqn (2.50) above, only the

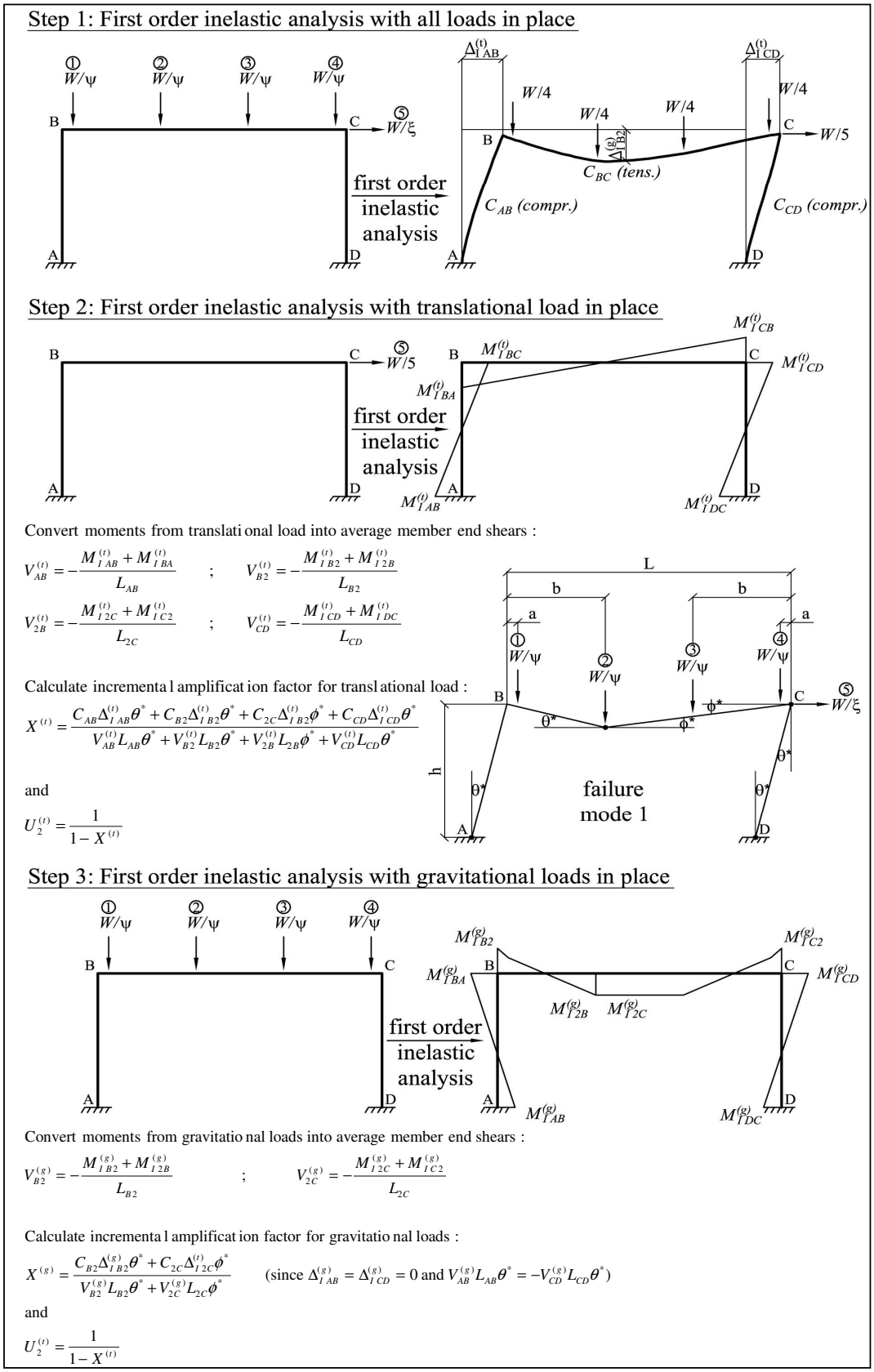


Fig. [5.6] Calculation of the modified amplification factors $U_2^{(t)}$ and $U_2^{(g)}$

translational moments are amplified, as the gravitational loads do not directly induce member sways. Since the second order moments and deflections are expressed as fractions of the first order sway moments and deflections, it follows that load effects should not be amplified if they arise from loads that do not induce sways. Multiple amplification factors allow proper account to be taken of the effects of various load groups in the failure criterion. Since Kemp's amplification factor has been derived for a virtual work sum, it is perhaps best to express the failure criterion in similar terms. By recognising that load factor is proportional to virtual work, the terms of Eqn. (4.30) can be swapped to create a virtual work equivalent of the failure criterion.

$$
\begin{aligned}
&U_2 W_f = W_s \\
&\text{but for a given mode } W \alpha \Sigma VL\phi^* \\
&\therefore U_2 (\Sigma VL\phi^*)_f = (\Sigma VL\phi^*)_s
\end{aligned}
\tag{5.1}
$$

This indicates that failure should occur when the amplified virtual work (either internal or external) of the first order inelastic analysis equals the unamplified virtual work of the first order plastic analysis of the frame in its pure sway mode. When adopting a pure sway mode of failure for the laboratory frames, it is not necessary to take account of the gravitational loads, as these load do not contribute to the virtual work. However, nearly every frame tested in the laboratory, and in ABAQUS, failed in the same combined mechanism mode. This type of failure was named 'mode 1', and it is illustrated in Fig [5.6]. When using this combined mode in the failure criterion, it becomes necessary to take into account the virtual work exerted by the gravitational loads as well as to amplify this work appropriately. I do not advocate that Kemp's method be altered to allow for multiple amplification factors. There would be many difficulties involved in doing so, and even if possible to do so for the general case, the calculation of such factors would negate the simplicity of his method. It was desirable, however, to determine whether multiple amplification factors would enable a load-*X* graph and a failure criterion that would be comparable to those of the laboratory and ABAQUS tests. For this reason a method was developed for calculating two factors per test frame: one for the translational load, and one for the gravitational loads. The sequence of these operations, described graphically in Fig. [5.6], was as follows:

1. A first order inelastic analysis of the frame was performed in ABAQUS with all loads in place. The results of this analysis were used to calculate the axial loads in the members, as well as sway deflections.

2. The structure was then reanalysed with the translational load acting in isolation. This analysis provided the moments that were used to calculate the average shears in the members. Using the axial forces and first order sways from step 1, and the average shears from step 2, an incremental amplification factor was established for the translational load effects.

$$X^{(t)} = \frac{\Sigma C_{ij} \Delta_{I\,ij}^{(t)} \phi_{ij}^*}{\Sigma V_{ij}^{(t)} L_{ij} \phi_{ij}^*} \tag{5.2}$$

where $\Delta_{I\,ij}^{(t)}$ is the first order sway deflection of member ij resulting from the translational load.
$V_{ij}^{(t)}$ is the average shear in member ij resulting from a first order analysis with only translational loads in place.

$X^{(t)}$ was then used in the normal manner to calculate the factor $U_2^{(t)}$ for application to the virtual work resulting from translational load effects.

$$U_2^{(t)} = \frac{1}{1 - X^{(t)}} \tag{5.3}$$

3. The structure was analysed with the gravitational loads acting in isolation. A similar procedure was followed to calculate the amplification factor $U_2^{(g)}$ applicable to the virtual work arising from gravitational loads.

$$X^{(g)} = \frac{\Sigma C_{ij} \Delta_{I\,ij}^{(g)} \phi_{ij}^*}{\Sigma V_{ij}^{(g)} L_{ij} \phi_{ij}^*} \tag{5.4}$$

where $\Delta_{I\,ij}^{(g)}$ is the first order sway deflection of member ij resulting from the gravitational load.
$V_{ij}^{(g)}$ is the average shear in member ij resulting from a first order analysis with only gravitational loads in place.

and

$$U_2^{(g)} = \frac{1}{1 - X^{(g)}} \tag{5.5}$$

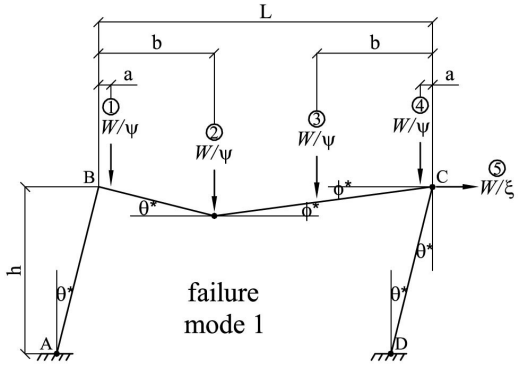
Ordinarily, the sway deflections caused by gravitational loads would have equalled zero. However, since failure in mode 1 was under consideration, the sag in the beams from the gravitational loads caused sways in members B2 and 2C. The tension in the beam resulted in negative values for $U_2^{(g)}$.

4. The sway equilibrium equation that accounted for second order effects could now be rewritten.

$$\Sigma V_{ij} L_{ij} \phi_{ij}^* = -\Sigma (M_{ij} + M_{ji}) \phi_{ij}^* - U_2^{(t)} \Sigma C_{ij} \Delta_{I\,ij}^{(t)} \phi_{ij}^* - U_2^{(g)} \Sigma C_{ij} \Delta_{I\,ij}^{(g)} \phi_{ij}^* \tag{5.6}$$

Initially, steps 2 and 3 were to be used, each in turn, to calculate the sway deflections arising from the load groups acting in isolation. It was found, however, that the spread of plasticity caused by all the loads acting simultaneously greatly increased the actual first order deflections. Consequently the step 1 analysis was used to calculate member sways since any weakening effects attributed to both load groups acting together would result from material nonlinearity. The accounting of material nonlinearity in the amplification factor is, by definition, dealt with directly in the first order sways used to calculate X. The simple nature of the test frames allowed the assumption that sway deflections in the columns were still due mostly to translational loads, while transverse deflections in the beam were due mostly to gravitational loads.

The analysis of step 2 was, however, used to calculate the sway deflection $\Delta_{IB2}^{(t)}$ of member B2 due to translational loads only. In a complex structure, it would be far more challenging to determine which proportions of sways could be attributed to which loads were all loads to act together.



Modified failure criterion :

unamplified virtual work at plastic collapse = amplified virtual work from first order inelastic analysis

$$\Sigma((W_p/\psi)_i\partial_i^*)+\Sigma((W_p/\xi)_i\partial_i^*)=U_2^{(t)}\Sigma((W_f/\psi)_i\partial_i^*)+U_2^{(g)}\Sigma((W_f/\xi)_i\partial_i^*) \quad (5.7)$$

Considering each half of the equation separately :

unamplified external virtual work at first order plastic collapse in mode 1

$$=(W_p/\psi)(a\theta^*+b\theta^*+b\phi^*+a\phi^*)+(W_p/\xi)h\theta^*$$

$$=(W_p/\psi)(a(L-b)\phi^*/b+b(L-b)\phi^*/b+b\phi^*+a\phi^*)+(W_p/\xi)h(L-b)\phi^*/b \quad (\text{since } \theta^*=(L-b)\phi^*/b)$$

$$=(W_p)[(1/\psi)(aL+bL)/b+(1/\xi)(hL-hb)/b](\phi^*) \quad (A)$$

amplified external virtual work at collapse load W_f :

$$U_2^{(g)}(W_f/\psi)(a\theta^*+b\theta^*+b\phi^*+a\phi^*)+U_2^{(t)}(W_f/\xi)h\theta^*$$

$$=U_2^{(g)}(W_f/\psi)(a(L-b)\phi^*/b+b(L-b)\phi^*/b+b\phi^*+a\phi^*)+U_2^{(t)}(W_f/\xi)h(L-b)\phi^*/b$$

$$=(W_f)[(U_2^{(g)}/\psi)(aL+bL)/b+(U_2^{(t)}/\xi)(hL-hb)/b](\phi^*) \quad (B)$$

Set (A) = (B) and solve for W_f :

$$W_f=\frac{(W_p)[(1/\psi)(aL+bL)/b+(1/\xi)(hL-hb)/b]}{[(U_2^{(g)}/\psi)(aL+bL)/b+(U_2^{(t)}/\xi)(hL-hb)/b]} \quad (5.8)$$

$\psi = 4$ for all tested frames

$\xi = 3$ for the 0.33sway frame

$\xi = 5$ for the remaining frames

Fig. [5.7] Derivation of the modified failure criterion

The modified incremental amplification factors $X^{(t)}$ returned by Eqn. (5.2) were nearly identical to the values of Kemp's X that were calculated from the first order ABAQUS analyses of the frames. This is illustrated in the load-X graph of the kempsp1 frame in Fig. [5.8] where the $X^{(t)}$ values are represented by the light blue line. The negative $X^{(g)}$ figures were relatively small as a result of the low amounts of the tension in the beam. For real structures, the presence of multiple amplification factors would introduce the additional complication of multiple load-X relationships. For the test

frames, however, $U_2^{(t)}$ was regarded as the principal amplification factor, and $U_2^{(g)}$ needed to be calculated only at the point of collapse for the purposes of the failure criterion. It was decided that the structure would become unstable when the appropriately amplified virtual work of the first order inelastic analysis equalled the unamplified virtual work at first order plastic collapse in combined mode 1. This condition defined the modified failure criterion of Eqn. (5.7) for the test frames.

$$\Sigma((W_p/\psi)_i\partial_i^*)+\Sigma((W_p/\xi)_i\partial_i^*)=U_2^{(t)}\Sigma((W_f/\psi)_i\partial_i^*)+U_2^{(g)}\Sigma((W_f/\xi)_i\partial_i^*) \quad (5.7)$$

where ∂^* = Virtual displacement of load $(W)_i$ in the line of action of the load

The simplification of this formula is given in Fig. [5.7], resulting in the isolation of the failure load as per Eqn. (5.8).

$$W_f=\frac{(W_p)[(1/\psi)(aL+bL)/b+(1/\xi)(hL-hb)/b]}{[(U_2^{(g)}/\psi)(aL+bL)/b+(U_2^{(t)}/\xi)(hL-hb)/b]} \quad (5.8)$$

Since the amplification factors $U_2^{(t)}$ and $U_2^{(g)}$ can be written in terms of their respective incremental amplification factors $X^{(t)}$ and $X^{(g)}$, Eqn. (5.8) describes a failure surface in the load-$X^{(t)}$-$X^{(g)}$ space. Instead of regarding $X^{(g)}$ as a further variable, its value was calculated at the actual failure load of the structure, and treated it as a constant. This reduced the failure surface of Eqn. (5.8) to a two dimensional failure line that could be drawn on the load-$X^{(t)}$ graph for each frame. The modified failure lines for selected span variation frames are shown in the load-X graphs of figures [5.8] to [5.11]. In each case the failure line passes very closely to the failure point of the back-calculated ABAQUS curve. Such favourable comparisons of failure loads and values of X for a variety of frames seem to support strongly the validity of differential amplification of loads. This is especially so when one considers that the modified failure criterion succeeded for the 0.6rigidspan frame where the original amplification factor theory failed.

The process of calculating multiple amplification factors and a modified failure criterion was laborious and complicated even for the simple test frames of this project. Clearly, such a process would need much simplification and validation were it to be used for practical structures and conditions. If it is true that loads are subject to differential amplification, then Kemp's method is empirical not only in its bilinear approximation of the load-X graph, but also in the derivation of a single amplification factor and the failure criterion. This would imply that modifications to his theory would also be at least semi-empirical in nature, and would therefore be subject to certain specific conditions. The modifications proposed in this report seek to maintain the accuracy and ease with which failure loads have been predicted, while adding a mechanism to allow for different types of instability in different structures. The attempts at doing so are discussed in the following section.

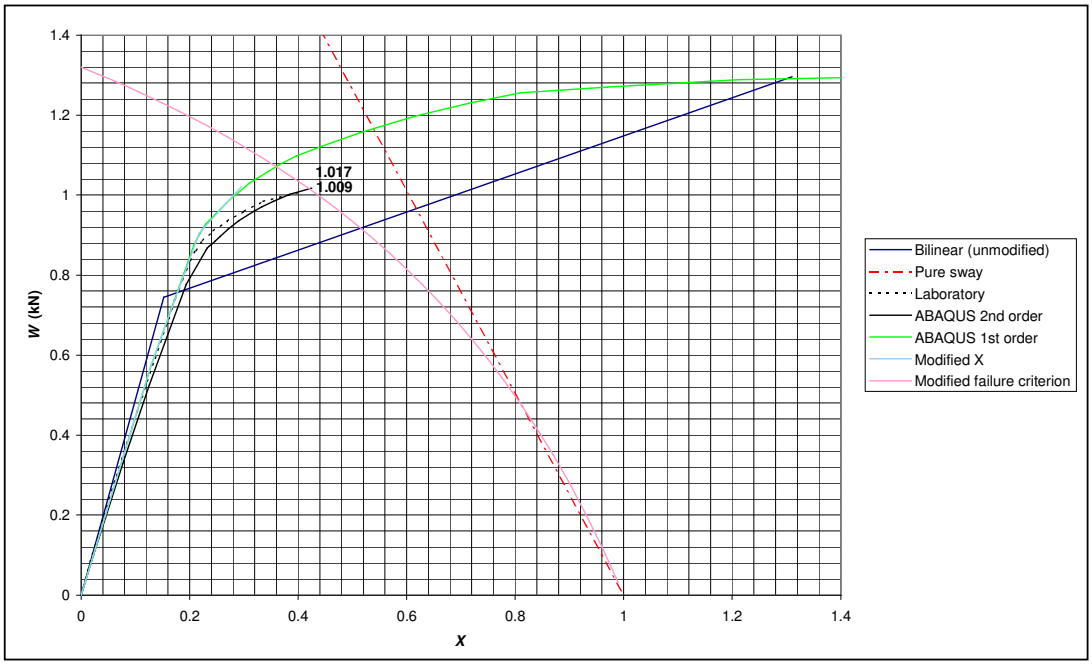


Fig. [5.8] *W-X* graph of kempsp1 frame with modified failure criterion.

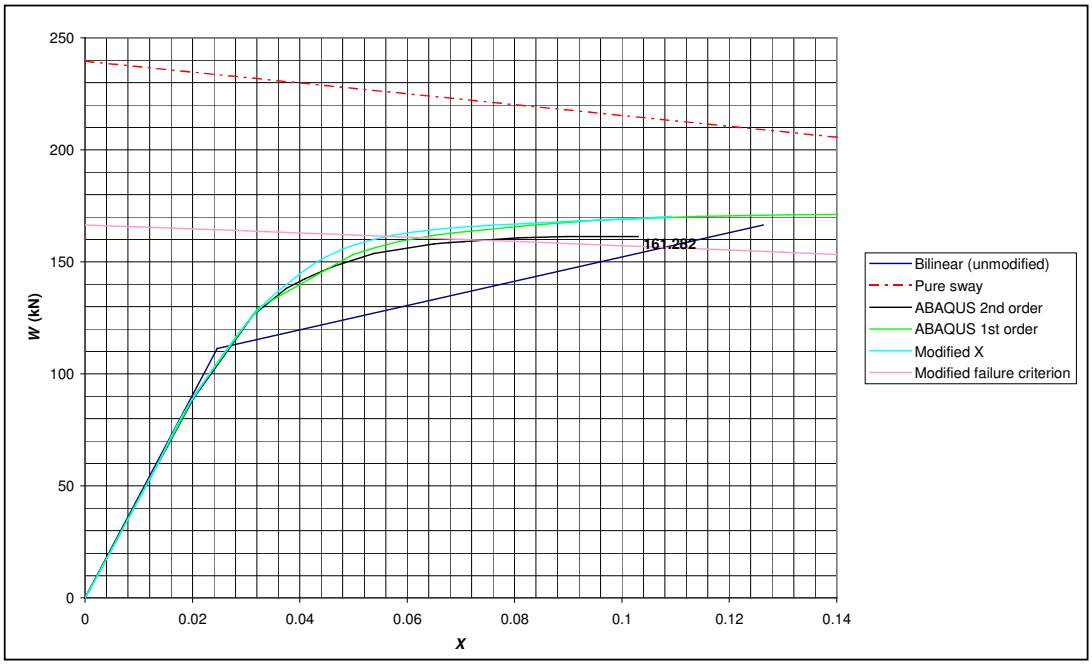


Fig. [5.9] *W-X* graph of 0.6rigidspan frame with modified failure criterion

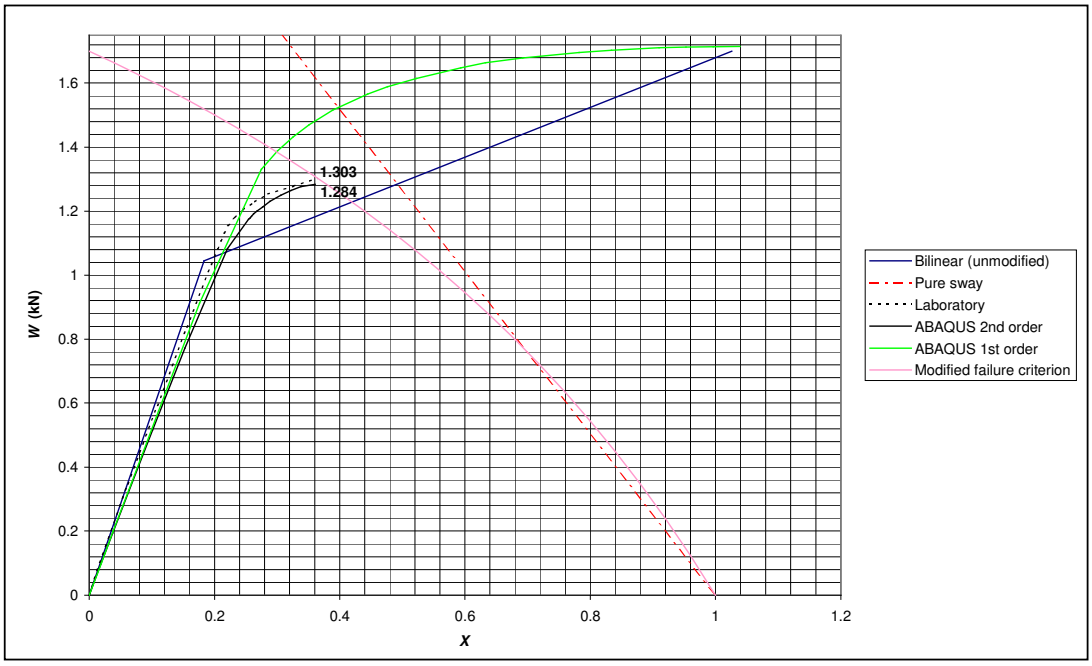


Fig. [5.10] *W-X* graph of 0.6span frame with modified failure criterion

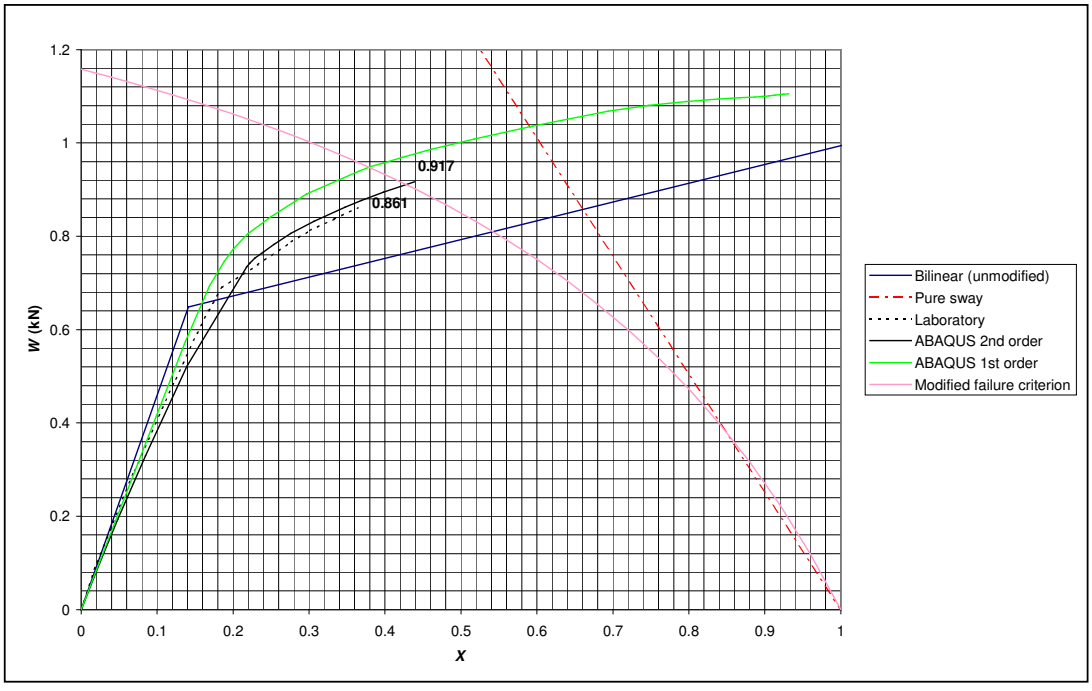


Fig. [5.11] *W-X* graph of 1.2span frame with modified failure criterion

5.4 Usefulness of Test Frame Results

The appraisal of Kemp's theory has identified various assumptions and simplifications that adversely affect its ability to model nonlinear behaviour. These theoretical findings were substantiated by the results of the laboratory tests and the ABAQUS analyses. The shortcomings of the bilinear method appeared to be significant for the test frames, yet it was clear that the frames differed in many respects to most practical structures. It was therefore necessary to investigate the impact of these differences on the usefulness of the test results. This subject is dealt with below in a discussion of the pertinent scale effects of the model analyses. Following this are the recommended modifications to Kemp's amplification factor method.

All scale models are subject to varying degrees of distortion in their representation of the prototype. A researcher, whilst trying to minimise distortion, is limited by the available resources, and guided by the intended function of the model analysis. It is seldom necessary to construct a model that enforces conditions of similitude for all physical properties that affect the behaviour of a structure. Such highly accurate 'strength' or 'realistic' models are required when the consequences of failure are dire or extremely costly, and the available theoretical models are unreliable or incomplete. Strength models are expensive, technically difficult and time consuming to construct and test. Consequently, they are mostly reserved for large building projects that fall beyond the scope of conventional design. For the purposes of research, models are commonly designed to adhere only to those conditions of similitude that are thought to affect the relevant structural behaviour. This simplifies the modelling process, but jeopardises the results if the researcher misjudges the importance of one or more physical aspects of the model.

It was decided at the outset of this research project not to attempt a validation of Kemp's amplification factor method for any particular structure. Since Kemp has proposed that his method is applicable to all shapes of unbraced sway frames, the choice of a specific structural configuration seemed arbitrary. A more useful approach was to investigate the derivation of the method and thereby to assess the impact of any assumptions and simplifications on the general validity of the theory. Simple scale models were devised to test the findings and to assess the trends that resulted from basic variations of spans and load positions. Since the models were not used to refine empiricisms for a particular application, the need to conform to stringent conditions of similitude was relaxed. Consequently, the design of the models was chosen to aid the fabrication and testing processes, rather than to simulate the physical attributes of practical structures. The rectangular test frames eliminated potential errors in the incremental amplification factor arising from the sway deflections of inclined members. Concentrated loads, fixed bases and full-strength joints were convenient to model, and also helped to identify the possible failure modes of the frames. The most significant distortions of similitude were considered to be the shape of the flat bar section, and the slenderness of the members. These aspects were investigated in their capacity to invalidate the test results and the subsequent proposed modifications to Kemp's amplification factor method.

5.4.1 Section shape

The 25x5mm mild steel flat bar was a practical and effective choice of section for the test frames. The material was readily available, and its solid rectangular shape simplified the fabrication process. Out-of-plane behaviour was conveniently excluded by orientating the section appropriately, and the ductility ensured large deflections that were easy to measure and resulted in significant second order effects. For these reasons, the section had already been used in similar frames by Kemp to illustrate his method in post-graduate design courses, and by Scholz (1981) in his thesis on the plastic design of partially braced and unbraced frames.

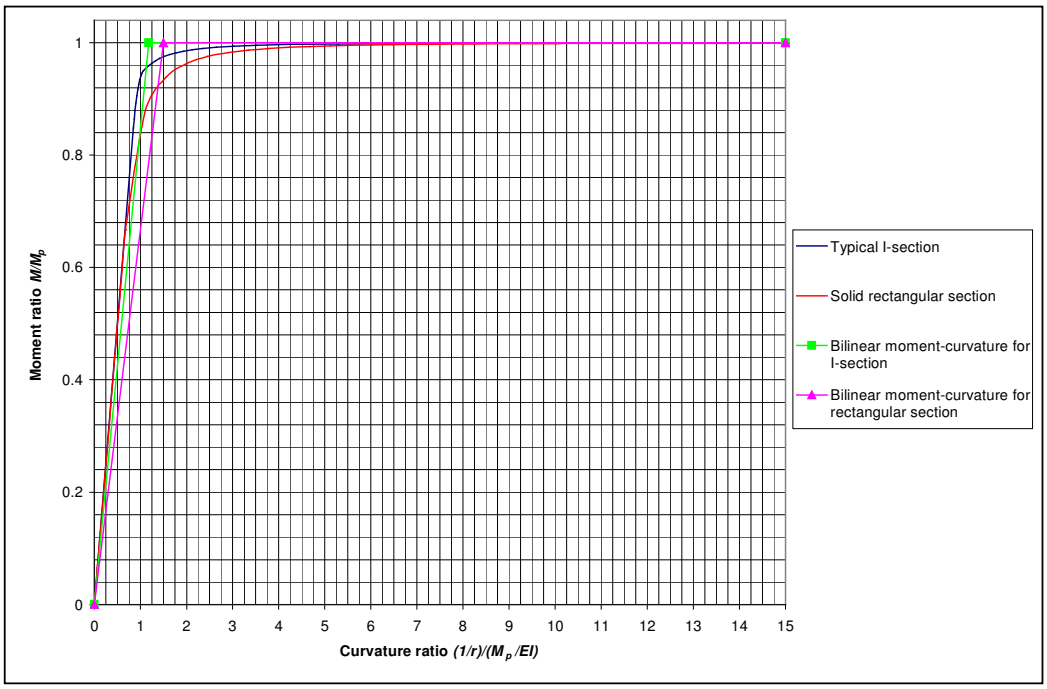


Fig. [5.12] Moment-curvature graphs of a typical I-section and solid rectangular section

A disadvantage of using the flat bar arose from the unusual moment-curvature relationship of such a section. Figure [5.12] compares the moment-curvature graph of a typical structural I-section to that of a solid rectangular shape bending about a principal axis. Both sections begin to lose flexural rigidity at their respective yield moments M_y. For the rectangular section, this moment represents a relatively lower proportion of the fully plastic moment M_p than it does for the I-section. Simple bending theory shows that the shape of the inelastic moment-curvature relationship is closely related to the ratio between the fully plastic moment and the yield moment of a section. This ratio, or 'shape factor' f, commonly equals 1.15 for structural I-sections, and always equals 1.5 for a solid rectangular section bending about a principal axis. The high shape factor of the rectangular section indicates a member that will lose flexural rigidity under relatively low load intensities. In contrast, the I-section maintains its rigidity, then undergoes a more abrupt spread of plasticity once the yield moment has been attained at high load intensities. These characteristics affect the load-deflection relationships of members, and hence the structures to which they belong.

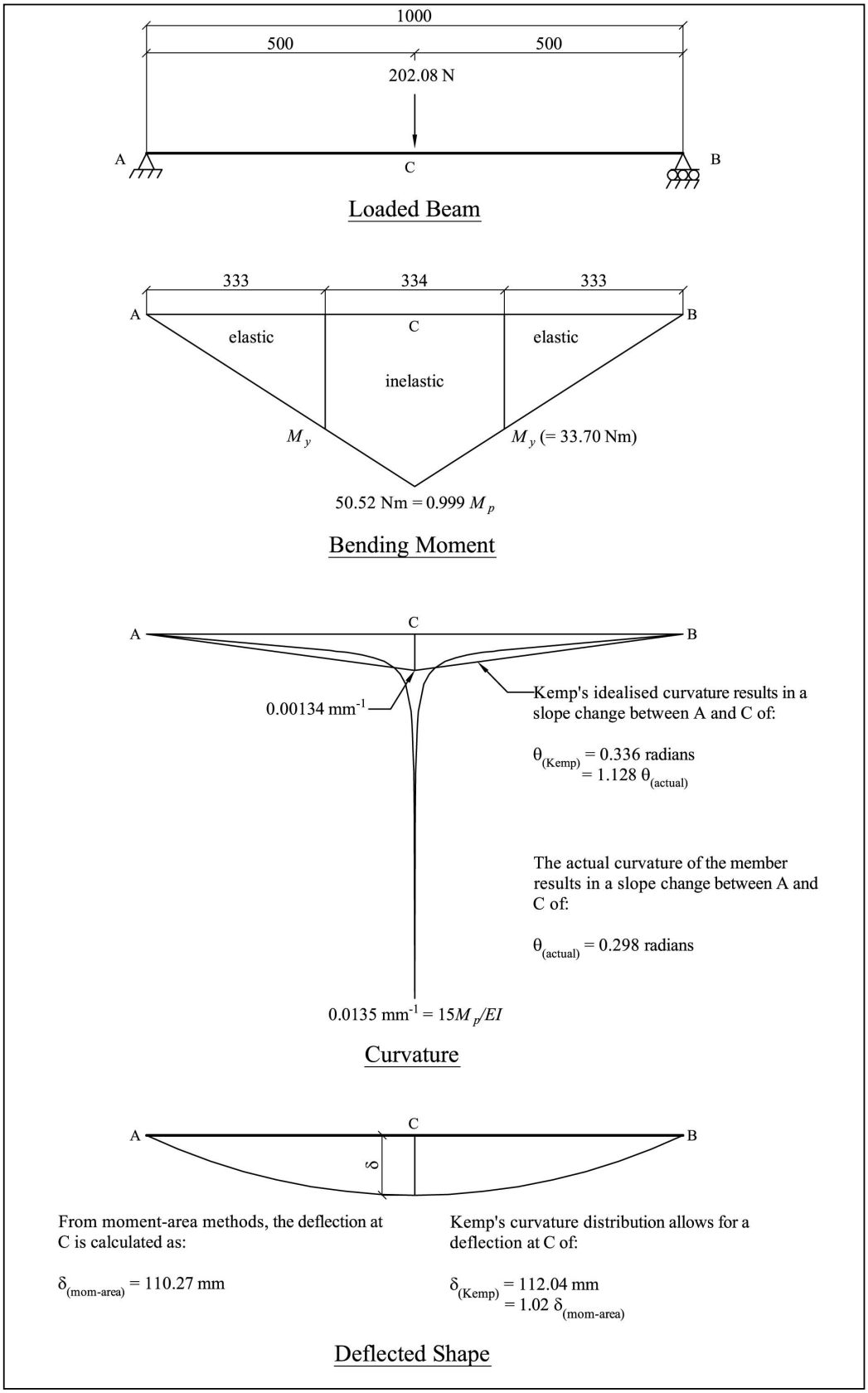


Fig. [5.13] Inelastic deflection of a simply supported beam

The bilinear load-X graph requires the calculation of the first order sway deflection Δ_p at collapse of the frame in the critical combined mechanism. This deflection is used to define the value X_p for the limit (X_p, W_p) in the bilinear load-X graph. Kemp's method for calculating this deflection uses his empirically derived Eqn. (2.65) to account for the loss of flexural rigidity in members containing plastic hinges. This equation simplifies the moment-curvature relationship of a section into a bilinear elastic-perfectly plastic graph with a reduced elastic flexural rigidity EI', and a reduced plastic moment M'_p. The bilinear approximation is such that a member subjected to a bending moment that varies linearly from zero to M'_p will rotate by the same amount at a maximum curvature of $15M_p/EI$. This graph is illustrated in Fig. [5.12] for the typical I-section and the solid rectangular section. The effects of reductions in plastic moment have been ignored in these examples due to the low axial loads in the test frames.

Kemp had developed Eqn. (2.65) for use with conventional structural sections, hence there was uncertainty regarding the suitability of the formula for flat bar sections. As a test of its accuracy for such use, an analysis was performed on the simply supported beam illustrated in Fig. [5.13]. Using the moment-curvature relationship of the 25x5mm flat bar, it was established that a centrally placed concentrated load of 202.08N would induce a curvature at midspan of $15M_p/EI$. The change in slope of the beam between the support and the load was calculated using the conjugate beam method and was found to equal 0.298 radians. Had this test been performed physically, the conjugate beam method would have been invalid as it applies to small deflection theory only. However, the effects of large deflections in the slender beam were irrelevant as the loads, spans and section properties were arbitrary in this example. Kemp's method was then used to recalculate the deflection for the same scenario. Using the reduced flexural rigidity from Eqn. (2.65) for the length of beam between the support and midspan, the change in slope was found to be 0.336 radians. This rotation, being only 12.8 percent greater than the theoretical counterpart, was a favourable display of Eqn. (2.65)'s ability to model slope change for the rectangular section. Furthermore, Kemp's method calculated a central deflection of 112mm, which was only two percent greater than the 110mm deflection determined using the moment area method. Despite these results, it was necessary to determine how this would translate to the calculation of deflections for the test frames. The simplest and most effective means of establishing this was to compare the predictions of Kemp's method to the results of the first order ABAQUS analyses. These highly comparable results have been discussed and illustrated in section 4.3 for those frames whose critical first order failure mechanisms were sway-related. Mathematical proof of the suitability of Eqn. (2.65) for a rectangular section was not sought due to the empirical nature of the equation, and the hypothetical nature of the first order deflection at load W_p. Nonetheless, it appeared from the comparisons that the rectangular section had not adversely affected the calculation of the point (X_p, W_p) for the test frames. As explained in section 5.4.2, however, it became apparent that the ductility of the flat bar section might have improved the accuracy with which the failure criterion calculated the failure load W_f.

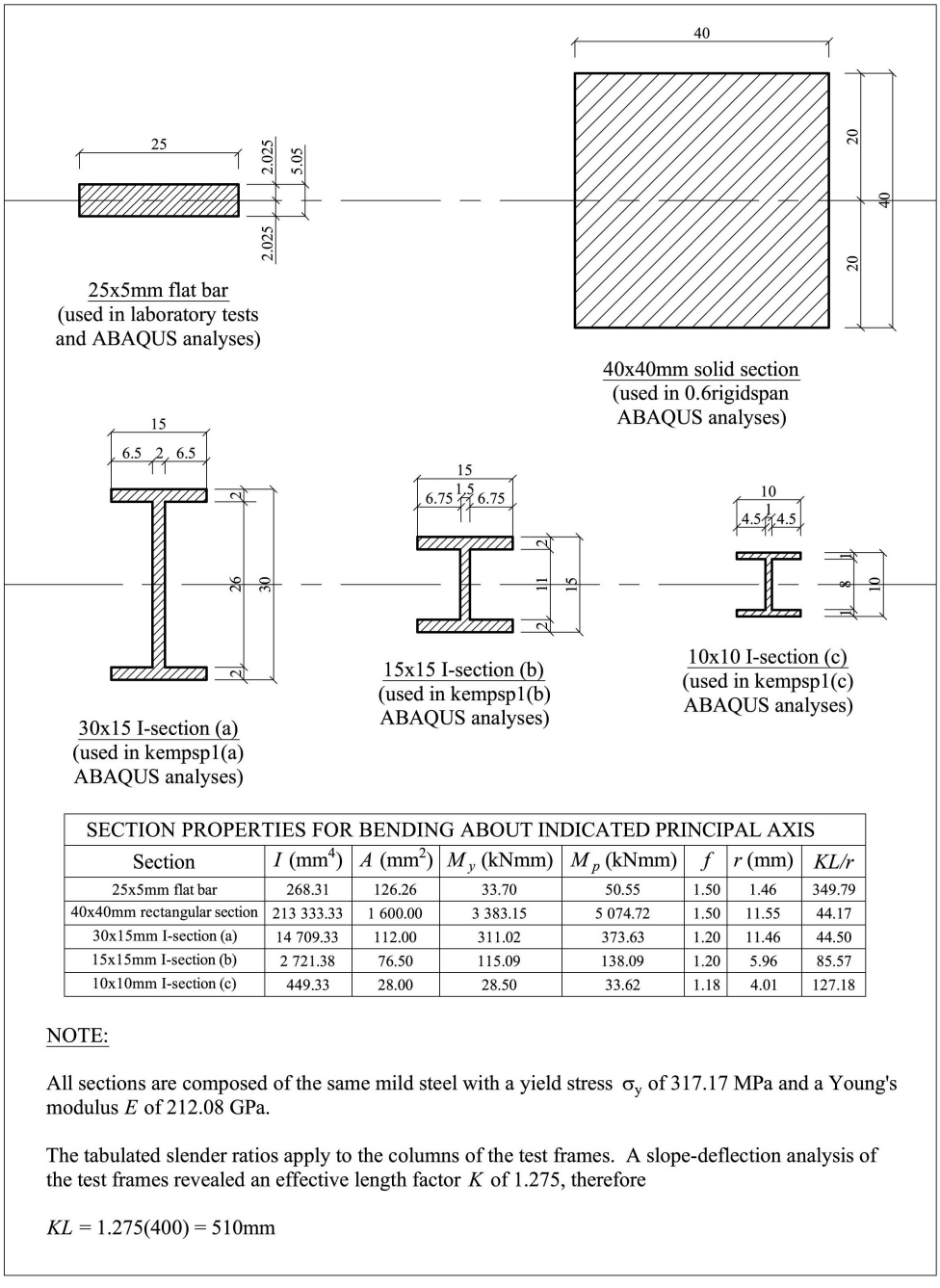
5.4.2 Member slenderness

Conventional beam theory assumes that transverse loads are transmitted to beam supports entirely by means of shear, flexural and torsional forces within the member. This assumption is accurate when the ends of the beam are unrestrained against lateral translation, or when the transverse deflections are small. Translational restraint of the member ends allows the beam to develop significant axial, or membrane, forces as it deflects under load. These forces posses a vertical component by virtue of the beam's deflection, and can therefore transmit a portion of the load to the supports. As the deflections increase, the growing tensile forces may greatly enhance the load carrying capacity of a member. This phenomenon is illustrated by the example of an initially unstressed steel cable spanning horizontally between two supports. Under conventional beam analysis, the addition of a vertical load within the length of the cable would cause instability due to the negligible flexural rigidity of the cable. In reality, the sag of the cable and its tensile strength may allow it to support the load. In a framed structure, the restraint of a beam's ends is derived from the rigidity of the joints and the adjoining members. Any membrane forces will be transmitted through the joints to be resisted by the remainder of the structure. While these forces may strengthen the beam itself, they can have unpredictable consequences on the stability of the structure in its entirety. In extreme cases, membrane effects may invalidate a conventional first order analysis, and even change the failure mode of a frame.

It is generally considered that membrane effects become significant after the transverse deflection of a member has exceeded ten percent of its section depth. The deflections of most unbraced sway frames would exceed this value prior to achieving their ultimate limit states. Consequently, such structures will be subjected to significant membrane forces should they approach collapse. For the test frames, the unusually flexible members predisposed the frames to correspondingly severe deflections. The beam of the 0.6span frame had a slenderness ratio of approximately 300, which equalled the limiting slenderness for tension members as per SANS 10162-1:2004. The maximum deflection of this member at collapse exceeded four times the section depth, or forty times the limit at which consideration of membrane effects was warranted. Such deflections may have altered the manner in which the frames resisted load, and thereby compromised the usefulness of the test results. This was apparent in 0.4ll and the 1.4span frames where tensile beam forces resulted in unusual failure mechanisms with widespread plasticity in the columns. Since Kemp's method was developed for use with practical structures, it may have been inappropriate to assess it with test results in which deflections were so pronounced. Consideration, therefore, was to be given to the manner in which membrane effects might have influenced the test results.

An attempt at directly quantifying the membrane effects in the test frames seemed to be a pointless exercise. Second order analyses of the frames required the presence of axial forces within the beams in order to maintain equilibrium. Axial forces could have been prevented only through the use of sections with zero axial stiffness. However, such beams would lengthen and fail immediately upon deflection under transverse loads. A possible method of eliminating the membrane effects on the columns would have been to apply compensating loads at the column tops to oppose

the beams' axial forces. The vertical loads may also have required modification in order to counteract the increased load carrying capacities of the beams. Such modifications would have been counter-productive by further affecting the performance of the frames and complicating the interpretation of results. It was decided rather to analyse similar yet stiffer frames that were less susceptible to deflections. In this way, the results from the new stiffer frames could be compared to those of the original frames to establish whether membrane effects had played a significant role.



SECTION PROPERTIES FOR BENDING ABOUT INDICATED PRINCIPAL AXIS							
Section	I (mm^4)	A (mm^2)	M_y (kNmm)	M_p (kNmm)	f	r (mm)	KL/r
25x5mm flat bar	268.31	126.26	33.70	50.55	1.50	1.46	349.79
40x40mm rectangular section	213 333.33	1 600.00	3 383.15	5 074.72	1.50	11.55	44.17
30x15mm I-section (a)	14 709.33	112.00	311.02	373.63	1.20	11.46	44.50
15x15mm I-section (b)	2 721.38	76.50	115.09	138.09	1.20	5.96	85.57
10x10mm I-section (c)	449.33	28.00	28.50	33.62	1.18	4.01	127.18

NOTE:

All sections are composed of the same mild steel with a yield stress σ_y of 317.17 MPa and a Young's modulus E of 212.08 GPa.

The tabulated slender ratios apply to the columns of the test frames. A slope-deflection analysis of the test frames revealed an effective length factor K of 1.275, therefore

$KL = 1.275(400) = 510$mm

Fig. [5.14] Test frame sections and properties

One such structure had already been analysed in the form of the 0.6rigidspan frame. The 40x40mm solid square section used in this frame produced a low slenderness ratio for the columns of 44.17. ABAQUS calculated that the maximum beam deflection at the point of failure equalled 5.3mm, or just over one tenth of the 40mm section depth. It appeared that membrane effects could safely be ignored in this case. Kemp's method calculated a failure load W_f that exceeded the first order critical plastic collapse load W_p. This is evident in Fig. [5.9] where the graphed failure criterion passes beyond the bilinear load-X graph. With an invalid failure load prediction, the opportunity to assess effects of membrane forces was lost. Attention was therefore turned towards the cause of the miscalculation of W_f. It was thought to have resulted either from an inaccurate (X_p, W_p) limit, an invalid failure criterion, or a combination of these two factors. The likelihood of an inaccurate (X_p, W_p) limit was small given that Kemp's Eqn. (2.65) had been shown to account favourably for the moment-curvature relationship of the flat bar rectangular section. Since all solid rectangular sections that bend about a principal axis have the same shape factor, the 40x40mm section should have permitted an equally accurate calculation of (X_p, W_p). This argument was supported by the first order inelastic ABAQUS analysis, which can be seen passing in close proximity to the (X_p, W_p) limit in Fig. [5.9]. It was more probable therefore, that the poor W_f value arose from an invalid failure criterion. To investigate this possibility further, additional ABAQUS analyses were performed on three new variations of the kempsp1 frame. Each new frame used a unique yet more conventional I-section designed to allow varying slenderness ratios. The intention was to exclude the possibility of invalid W_f values arising due to unconventional section shapes and unrealistic member stiffnesses. Figure [5.14] provides the properties of the new I-sections, and of the sections used in the original frames for comparative purposes. The results of the new frame analyses are presented in the load-X graphs of figures [5.15] to [5.17], each frame being named after its respective section.

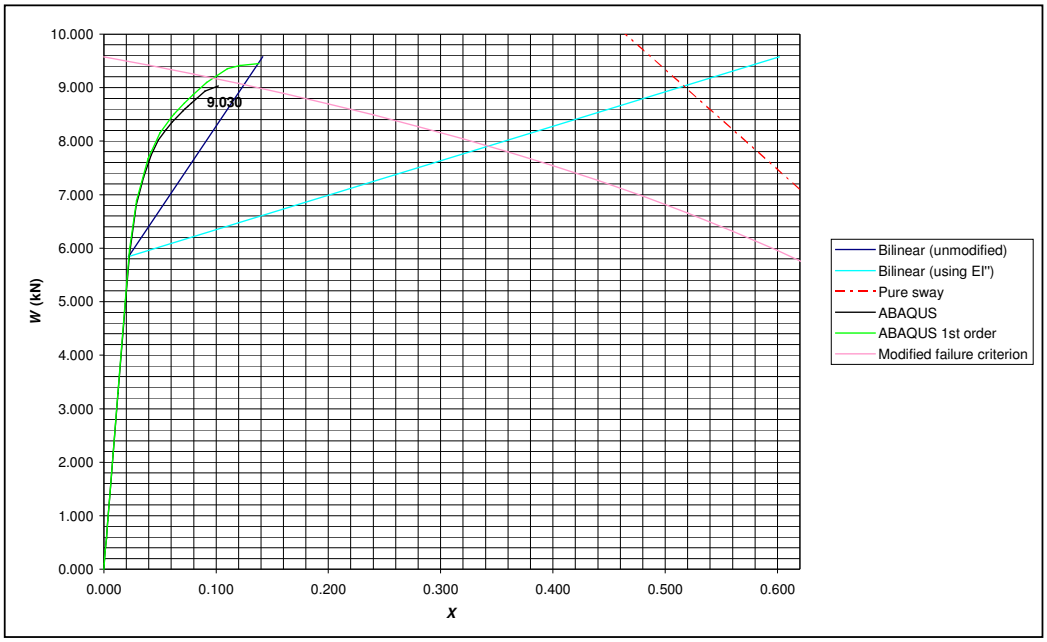


Fig. [5.15] *W-X* graph of kempsp1(a) frame with modified failure criterion

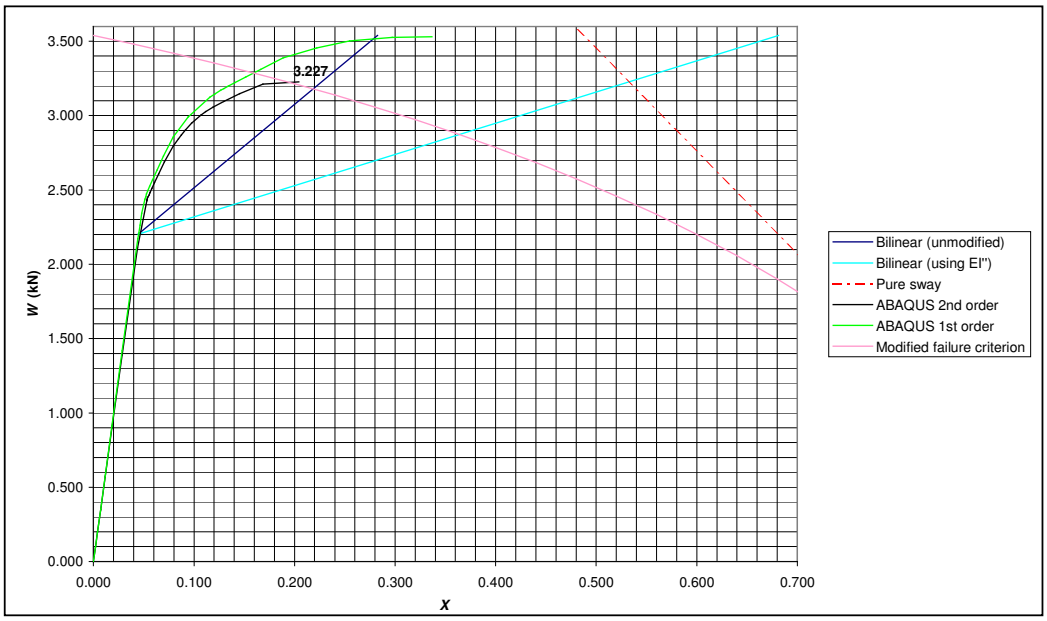


Fig. [5.16] *W-X* graph of kempsp1(b) frame with modified failure criterion

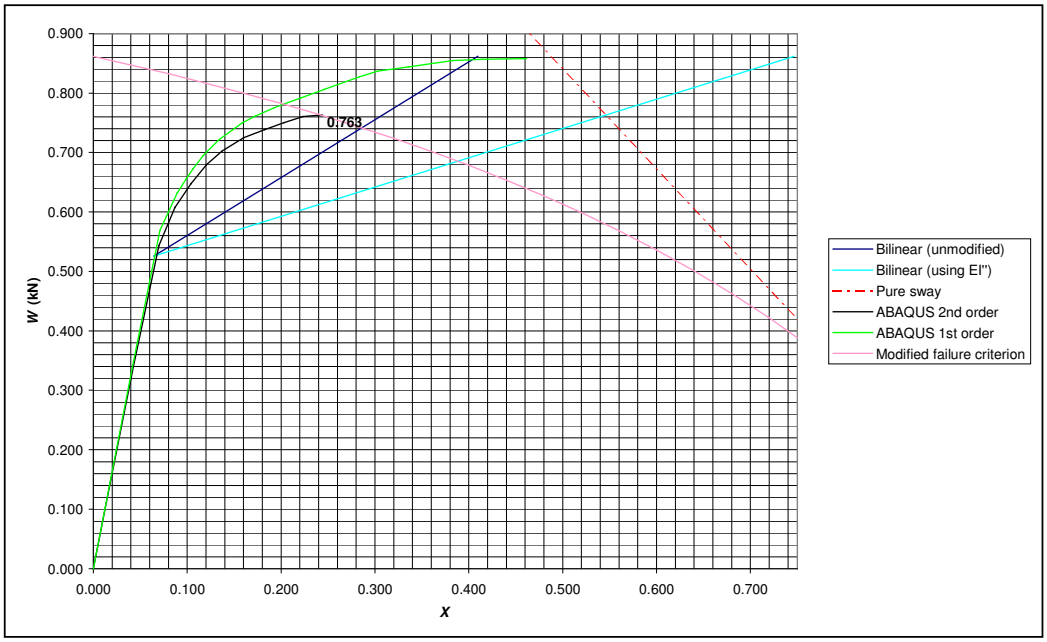


Fig. [5.17] *W-X* graph of kempsp1(c) frame with modified failure criterion

The failure criterion's predictions were again found to exceed the respective W_p loads of all three frames. It was recognised that the failure criterion may have intersected the bilinear graphs had smaller values of reduced flexural rigidity *EI'* allowed for larger values of X_p. The remote possibility that incorrect values of *EI'* were responsible for the miscalculations of W_f was subsequently considered.

The new I-sections had similar shape factors and could thus be expected to lose similar proportions of flexural rigidity due to the spread of plasticity. By extension, if the assumed values of *EI'* were responsible for the miscalculations of W_f, then the correct predictions of W_f would have required similarly reduced flexural rigidities for all three frames. The values of *EI''* that were required to force the correct failure loads were calculated and are listed in Table [5.1]. The resulting load-*X* graphs were plotted as the light blue lines in figures [5.15] to [5.17]. Table [5.1] reveals that the ratio *EI/EI''* varied considerably between the three frames. This implied that each section would had to have lost different proportions of flexural rigidity in order to produce the correct failure load predictions. Given the similar natures of the sections, this was an unlikely requirement. Furthermore, by forcing the correct failure loads with *EI''*, the resulting values of X_f were greatly in excess of the ABAQUS counterparts. It was clear that the section shapes and member slenderness ratios were not the cause of the miscalculations of W_f.

	EI'' ($kNmm^2$)	EI ($kNmm^2$)	EI/EI''
kempsp1(a)	610795	3119555	5.11
kempsp1(b)	199288	577149	2.90
kempsp1(c)	44287	95295	2.15

Table [5.1] Reduced flexural rigidities *EI''* required to force correct failure load predictions from Kemp's method

It is suspected that the poor failure load predictions resulted from Kemp's failure criterion of Eqn. (4.30). For the original test frames, the accuracy of the failure loads despite Kemp's assumption of a pure sway failure mode was probably a enabled by the ductility of the flat bar. The 25x5mm section allowed extensive inelastic deflections and hence large values of X_p. Consequently, Eqn. (4.30) was certain to intersect the load-*X* graph regardless of the actual failure mode. The ductility of the flat bar section appeared to have aided the predictions of a flawed failure criterion. For the newer test frames, the first order deflections at failure were considerably smaller, as were the corresponding values of X_p. The failure criterion therefore passed outside of the (X_p, W_p) limit. An accurate formulation of the failure criterion was required to ensure a valid prediction of failure load. This requirement was met by the modified failure criterion of Eqn. (5.8). For each new test frame, Eqn. (5.8) passed in close proximity to the failure point of the back-calculated ABAQUS load-*X* graph. The modified criterion also provided information on the extent of membrane effects in the test frames. The maximum vertical deflection of the beam in the kempsp1(c) frame was 33mm, or 330 percent of the section depth at failure. It was clear that membrane effects were present in this frame, yet the miscalculations of W_f by Kemp's Eqn. (4.30) obscured the assessment of these effects. By contrast, the modified failure criterion provided consistently accurate curves regardless of section shape, size or rigidity. Since the modified criterion neglected membrane forces, its accuracy would have been compromised had the membrane forces significantly affected instability. The 0.4ll frame was the only structure for which the modified criterion significantly overestimated the failure load. This frame's beam had the most severe deflection/span ratio of 1/4.85 and was observed to fail in an unconventional mode in both the laboratory and the ABAQUS analyses. Similar inaccuracy was expected of

Eqn. (5.8) for the 1.4span frame owing to the equally unusual failure mode and severe deflections recorded in the tests. However, it was found that Eqn. (5.8) accurately predicted failure for the 1.4span frame, thus membrane effects on its instability were thought to be insignificant. It was concluded that with the exception of the 0.4ll frame, membrane forces had little effect on the instability of the test frames. It was furthermore apparent that the inaccuracies introduced by Kemp's failure criterion were significantly greater than those arising from both section shape and member slenderness.

5.4.3 Support and joint behaviour

An additional variable that was considered beyond the scope of this project was the effect of real support and joint behaviour on stability. The supports of the test frames offered full fixity, and the welded joints were at least as rigid and strong as the parent members. In practical design, the bending moment restraint of a column at its base is usually assumed to be either fully fixed or perfectly pinned. Joints are often treated as having the same moment-curvature relationships as the parent members, and pins are assumed not to transmit any moment. In reality, moment restraint and transfer will always be partial to some degree, and the rigidity of joints will depend upon the method of fastening and the quality of fabrication. These aspects affect the overall rigidity of the structure, and therefore its susceptibility to geometric nonlinearity. In the application of Kemp's method, the nature of the support and joint behaviour may have an effect on the quality of the failure load prediction. If full fixity is incorrectly assumed, then the displacements allowed by semi-rigid joints and supports will cause an early onset of nonlinear behaviour. Effectively, the amplification of first order effects will be larger than anticipated, thus resulting in a possible over estimation of the failure load. Conversely, the assumption of perfectly pinned bases may result in an underestimation of the failure load. The impact of real support and joint behaviour on stability is probably unique to each structure and therefore to each application of Kemp's method. However, the assumption of ideal support and joint behaviour has long been considered acceptably accurate for most practical design methods. It is therefore unlikely that a simplified empirical method will require or justify an allowance for the same. Furthermore, the effect of small miscalculations of fixity and joint rigidity should be insignificant when compared to the errors introduced by a bilinear load-X graph and the empirical failure criterion.

5.4.4 Overall impact of scale effects

It is likely that the accuracy of the failure load predictions was particular to the idealised structural shapes, loading configurations and support conditions of the test frames. This was partially due to the manner in which these properties were measured and contrived, but chiefly a consequence of the unique interaction between the properties themselves. All structures are affected differently by the interactions of their own physical characteristics. The effects thereof on the nonlinear behaviour may be quantified either through advanced theoretical analysis or scale model testing. Kemp's simplification of the load-X relationship into a bilinear graph discards a great deal of information concerning the structural behaviour. In so doing it prohibits a theoretical evaluation of the effects of variations in structural characteristics. The

empirical bilinear graph and failure criterion may be well suited to certain structures, but there is no reliable method of assessing its accuracy without knowing the actual failure load. In order to refine Kemp's method for a specific practical application, one would require scaleable test data from a representative model. The test frames were clearly unrepresentative of practical frames and consequently were unsuitable for use in fine-tuning the empirical aspects of the method. However, as has been argued above, it is believed that the scale effects present in the test frames were not sufficient to invalidate the results that were recorded. Importantly, the test frame results supported the independently derived theoretical evaluations and modifications of Kemp's method. This agreement between practice and theory suggested the usefulness and quality of the test data overall, and the validity of the method evaluation. The proposed modifications of the following section are based largely upon the theoretical appraisal of Kemp's method. The modifications have been adapted to suit the test frame results, yet there is a mechanism included that allows for an adjustment of the proposed failure criterion. It is believed that the ability to adjust the failure criterion will extend the applicability of the proposed modifications to more practical structures, should further research be conducted in this regard.

5.5 Modifications to Kemp's Amplification Factor Theory

The choice of a bilinear representation of the load-X graph seems to be both a logical and practical simplification of the 'actual' relationship. Since the instability of most sway frames occurs after the spread of plasticity, the amplification factor must be able to be modelled for inelastic stress. It is impossible to represent the entire load-X relationship with acceptable accuracy by means of a single straight line. Curves involving higher powers of X would offer better accuracy, but would increase the work involved in constructing the curve and calculating the failure load. This would also be true of a trilinear graph, with the added difficulty of choosing a meaningful and generally applicable condition at which to segment the bilinear graph into three parts. In contrast, the two conditions (X_i, W_i) and (X_p, W_p) chosen by Kemp to describe the bilinear graph are relevant to most sway frames and are relatively easily calculated. These two conditions also lend themselves readily to adjustment. As the main purpose of Kemp's theory is to assess inelastic instability, it follows that the most important elements of his theory with respect to modifications are the definitions of the failure criteria, and the positioning of the inelastic portion of the bilinear load-X graph. The chosen approach was to adjust these elements so as to bring the failure prediction closer to that of the back-calculated laboratory and ABAQUS curves.

While it is unfeasible for a simplified method to predict the exact manner of instability for the general case of sway frame, it should be possible to use simple and repeatable steps to determine the upper and lower limits of failure load. The first upper bound load that is calculated in Kemp's method is the load that defines the end of the bilinear graph, W_p. Being that W_p is obtained from a first order analysis, the actual structure should fail at a lower load due to the weakening effects of second order stresses. A further possible upper limit to the failure load is provided by Kemp's failure criterion. Though it takes into account the second order effects, it assumes failure in the non-critical pure sway mode and ignores the work done by the gravitational loads. The modified failure criterion will always calculate a lower

failure load as it applies a similar amount of amplification to the translational load effect, but equates the amplified virtual work sum to that of the critical failure mode (as opposed to the pure sway mode in Kemp's criterion). A lower bound load may be calculated using Eqn. (5.9) below.

$$U_2 W = W_p \tag{5.9}$$

This equation calculates a load factor that, when multiplied by the corresponding amplification factor, equals W_p. Graphically, this relationship is represented by a straight line that intersects the X axis at 1 and the load axis at W_p. When converted to an equivalent virtual work equation, it becomes similar to Eqn. (5.7) above except that the same 'principal' amplification factor is applied to both translational and gravitational loads.

$$\Sigma((W_p / \psi)_i \partial_i^*) + \Sigma((W_p / \xi)_i \partial_i^*) = U_2 \Sigma((W / \psi)_i \partial_i^*) + U_2 \Sigma((W / \xi)_i \partial_i^*) \tag{5.10}$$

As a result, the second order effects due to the gravitational loads are over estimated, and the load so calculated should be lower than the actual failure load. These lower bound failure lines are shown as the dotted red lines on the load-X graphs of figures [5.18] to [5.29] at the end of this chapter. They consistently intersect the load-X relationships at loads lower than actual failure. The triangular area bounded by the lesser of the two upper bound failure loads and Eqn. (5.9) defines a zone in which a load multiplied by its corresponding amplification factor might equal the actual failure load. The feasible area of this zone is limited to the portion of bilinear graph that falls between the limits. It became apparent that for a typical test frame the second order ABAQUS failure usually fell near to the midpoint of the feasible bilinear graph. This midpoint may be described as falling on the intersection of the bilinear graph and the failure criterion of Eqn. (5.11) below.

$$U_2 W = (W_{f(L)} + W_{f(U)}) / (\eta - X_{f(L)} + X_{f(U)}) \tag{5.11}$$

where $W_{f(L)}$ is the load where the lower bound failure line intersects the W-X graph
$W_{f(U)}$ is the load where the upper bound failure line intersects the W-X graph
$X_{f(L)}$ and $X_{f(U)}$ are the corresponding values of X
η is a constant that defines the proximity of the line to the upper and lower boundary conditions (= 2 to bisect the triangle). The value of c is subject to the following limits:

$$\frac{(W_{f(L)} + W_{f(U)} + W_p(X_{f(L)} - X_{f(U)})}{W_p} \le \eta \le \frac{(W_{f(L)} + W_{f(U)} + W_s(X_{f(L)} - X_{f(U)})}{W_s}$$

Instead of using Eqn. (5.11), it is much simpler to draw the upper and lower boundaries, and then find the midpoint of the bilinear graph between these two limits. The limits on η are to keep the failure line of Eqn. (5.11) between the upper and lower bound failure lines. The actual value of η will be dependent on the degree of amplification at failure, as well as the mode of instability. These factors will in turn be a function of the structural geometry and loading conditions, relative member and joint stiffnesses, member slenderness and ductility. Such characteristics are unique to

different structures, and thus a value of η can only be relied upon if it has already been checked for similar conditions by experimentation. Equation (5.11) is the proposed form of the failure criterion, and altering the value of η is a means of empirically adjusting the accuracy for various structures and conditions. For all of the test frames, a value of '$\eta = 2.0$' provided very favourable results.

The inelastic portion of the bilinear *W-X* graph is repositioned by modifying the limits (X_i, W_i) and (X_p, W_p). The point (X_i, W_i) represents a structure's 'limit of elastic behaviour' and is found by satisfying the interaction equation of Eqn. (4.2) below by means of a first order elastic analysis. This equation determines the load at the formation of the first fully plastic section. The point (X_p, W_p) represents the limit of plastic behaviour of a structure. This is regarded as being the collapse in the critical combined mechanism as determined from a first order plastic analysis. In section 4.3, Kemp's method was noted for the impressive accuracy with which it calculated the point (X_p, W_p). For frames with sway-related critical collapse mechanisms, Kemp's values of first order sway deflections at failure correlated very closely with those taken from first order inelastic ABAQUS analyses. To enable such accuracy, it was necessary for validity both in his virtual work method of calculating first order deflection, as well as his empirical expression for reduced flexural rigidity. Since both of these requirements appeared to have been met for the test frames, and considering that (X_p, W_p) represents an actual limit that is broadly applicable to sway frames, this research does not justify modification of this limit.

$$\frac{C}{C_y} + \frac{U_2 M_1}{M_p} + \frac{0.5\sigma_{res}}{\sigma_y} = 1.0 \qquad (4.2)$$

The theoretical limit of elastic behaviour is a limit that is open to interpretation. It may be taken as the point at which the first outer fibres of a flexural member achieve plastic strain. Alternatively, as in Eqn. (4.2), it may be regarded as the load at which the first fully plastic section occurs. If the point (X_i, W_i) is to be calculated with a first order elastic analysis, then any condition involving inelastic stress, and hence material nonlinearity, cannot be properly represented. This means that using such an analysis to calculate the load at the first fully plastic section is not theoretically correct. Furthermore, it has been mentioned in this chapter that the use of the amplification factor is not intended for the stresses or deflections at any single location in a structure. Consequently, Eqn. (4.2) makes incorrect use of the amplification factor and provides an empirical elastic limit. Considering the degree of accuracy that is lost in approximating a load-*X* curve with two straight lines, it is evident that (X_i, W_i) need not fall upon the actual curve. It is more important that the choice of elastic limit allows the bilinear graph to approximate the actual curve near failure than that it represents a true condition under load. For the test frames, the inelastic portion of the bilinear *W-X* graph needed to be raised if the proposed failure criterion was to provide realistic failure loads. The first attempt at raising the graph was to apply the amplification factor in Eqn. (4.2) only to the moments arising from translational loads. This was done in accordance with Kennedy et al's Eqn. (2.50) for determining the total moment at a given location in a structure. The purple graph in Fig. [5.18] for the kempsp1 frame shows the results of amplifying the translational moments alone. The (X_i, W_i) point was clearly raised relative to Kemp's original method, and the accuracy of the proposed failure criterion was improved. The problems inherent to

Kennedy et al's method are that it is only valid for rectangular frames, elastic stresses and clearly definable gravitational and translational loads. An alternative means of raising the turning point of the bilinear graph was to ignore amplification altogether as per Eqn. (5.12).

$$\frac{C}{C_y}+\frac{M_1}{M_p}+\frac{0.5\sigma_{res}}{\sigma_y}=1.0 \tag{5.12}$$

This formula provides a simpler means of calculating (X_i, W_i), and further raises W_i along the elastic slope of the graph. The results of applying the proposed failure criterion to the modified bilinear graph are illustrated in figures (5.18) to (5.29) for all of the test frames. The proposed failure line in each case is pink, and the modified bilinear graph is light blue. For comparison, Kemp's original bilinear graph is shown in dark blue and the red chain-dashed line represents his failure criterion. The modifications to Kemp's amplification theory resulted in maintained levels of accuracy for failure load prediction. When compared to ABAQUS failure loads, Kemp's margin of error ranged from –6.5% to +4.9% for the laboratory frames, with invalid calculations of (X_f, W_f) for the 0.6rigidspan and kempsp1 I-section variation frames. The proposed method gave an error range for the failure loads of –7% to +4.4% for all of the frames. The more visible effect of the modifications was to improve significantly the values of X_f. Kemp's valid X_f values exceeded the ABAQUS equivalents by +36% to +66%, while the new discrepancies for all of the frames ranged from –2% to +26%. These failure loads were calculated using a default value of 2 for the variable η. The proposed modifications to the amplification factor theory resulted in a method that displayed the following effects and benefits:

- The calculation of point (X_i, W_i) was simplified due to the exclusion of the amplification factor in Eqn. (5.12). Given that the original limit of elastic behaviour is semi-empirical, such a modification should be allowed if it can be shown to suit a broad range of structural applications.

- The new elastic limit brought the inelastic portion of the bilinear graph closer to the load-X curves of the laboratory tests and ABAQUS analyses. This was particularly evident near failure loads.

- Three important upper and lower bound failure conditions were recognised and represented graphically on the load-X axes. These boundary conditions involved the loads W_s and W_p that would normally have been calculated in Kemp's original method. Consequently, the representation of these boundaries was a simple task that did not require further calculation beyond what was performed for the original method.

- The proposed failure criterion could also be expressed graphically on the load-X axes with ease. With η equal to 2, the new failure criterion realised vastly improved amplification factor values at failure, while maintaining the accuracy of failure load prediction.

- The empirical variable η provided a means of adjusting the failure criterion to suit different structural applications. Even with a default value of 2, it allowed

improved values of W_p and X_f for all of the test frames, including the 0.6rigidspan and kempsp1 I-section variation frames.

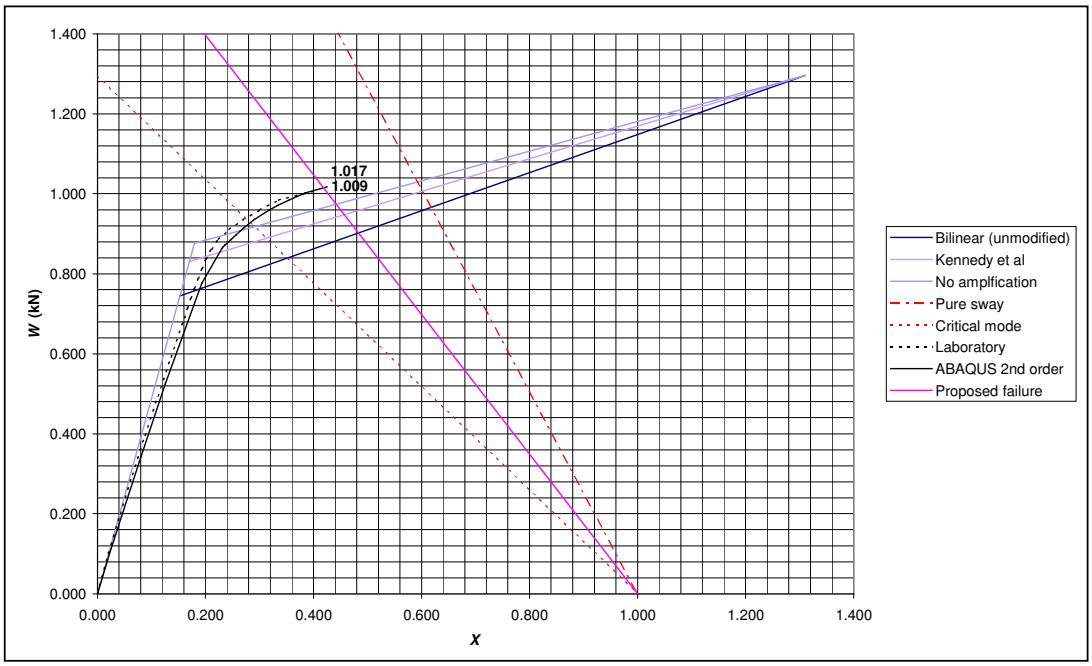


Fig. [5.18] *W-X* graph of kempsp1 frame with proposed failure criterion

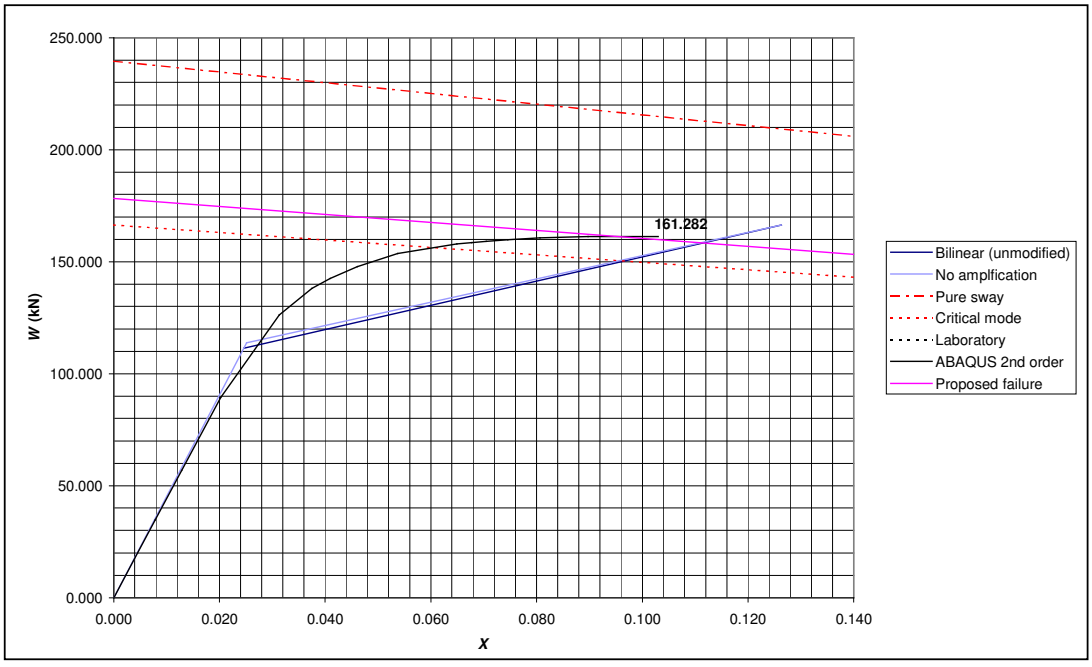


Fig. [5.19] *W-X* graph of 0.6rigidspan frame with proposed failure criterion

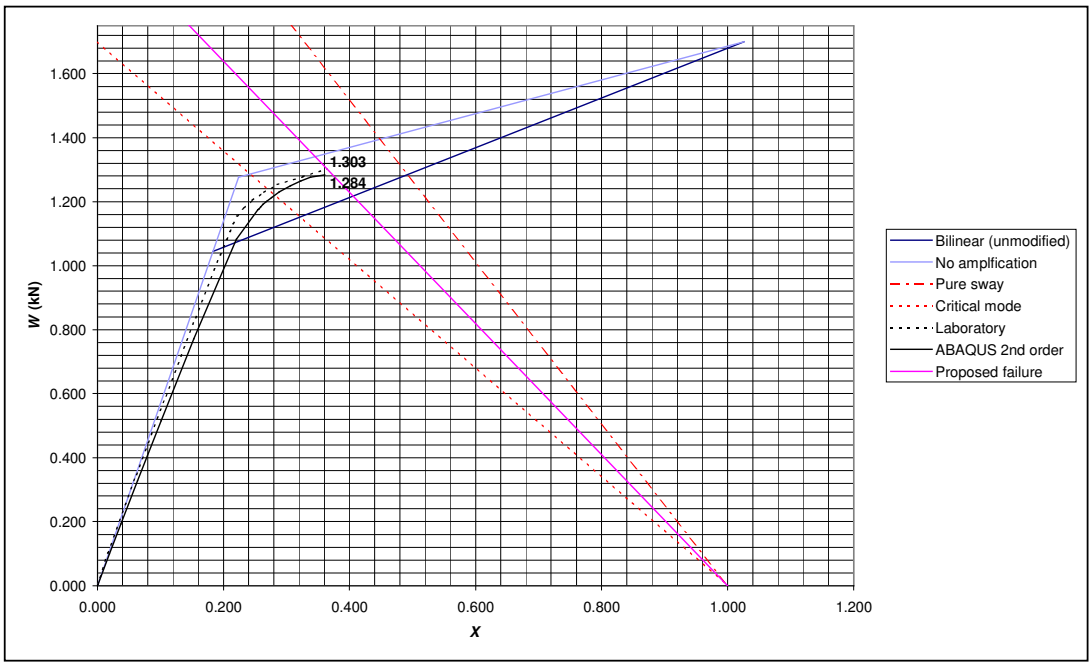


Fig. [5.20] *W-X* graph of 0.6span frame with proposed failure criterion

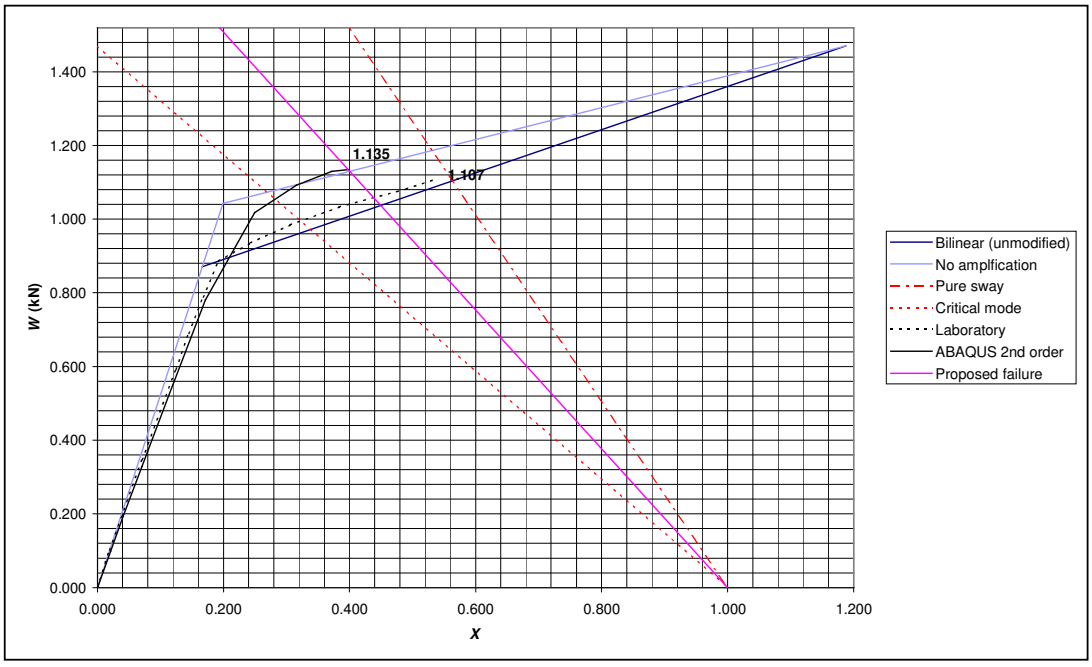


Fig. [5.21] *W-X* graph of 0.8span frame with proposed failure criterion

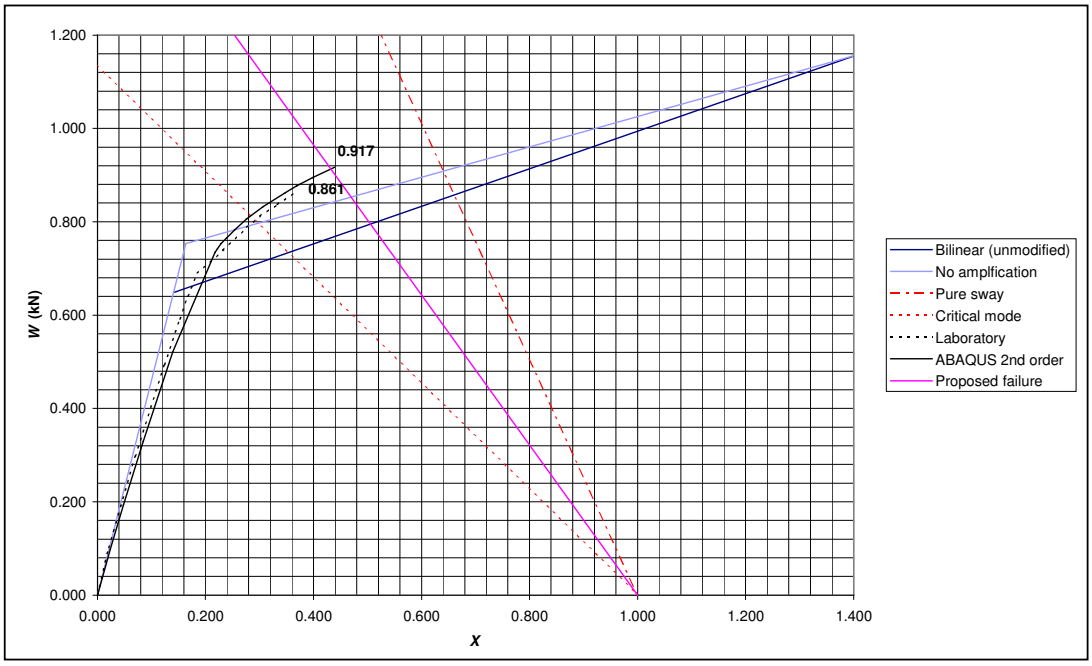


Fig. [5.22] *W-X* graph of 1.2span frame with proposed failure criterion

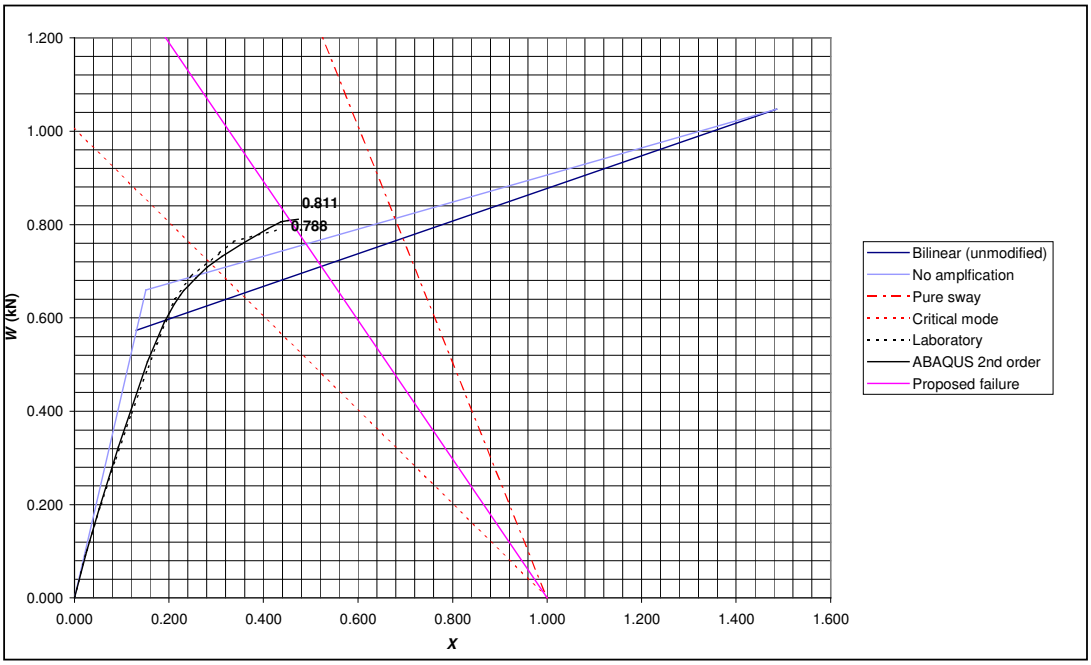


Fig. [5.23] *W-X* graph of 1.4span frame with proposed failure criterion

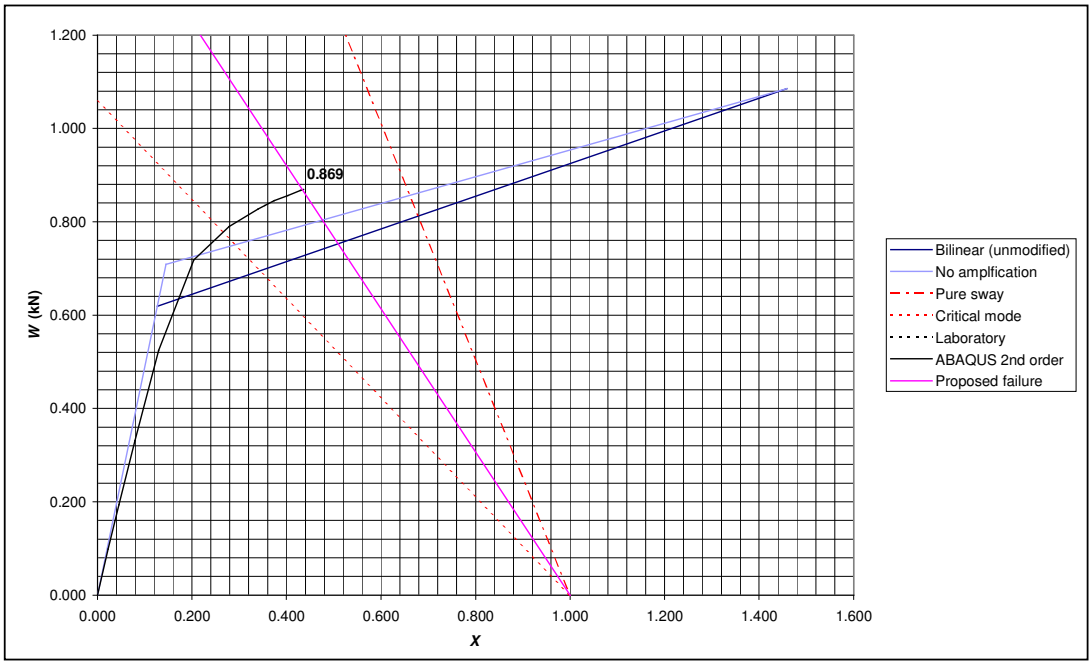


Fig. [5.24] *W-X* graph of 0.8ll frame with proposed failure criterion

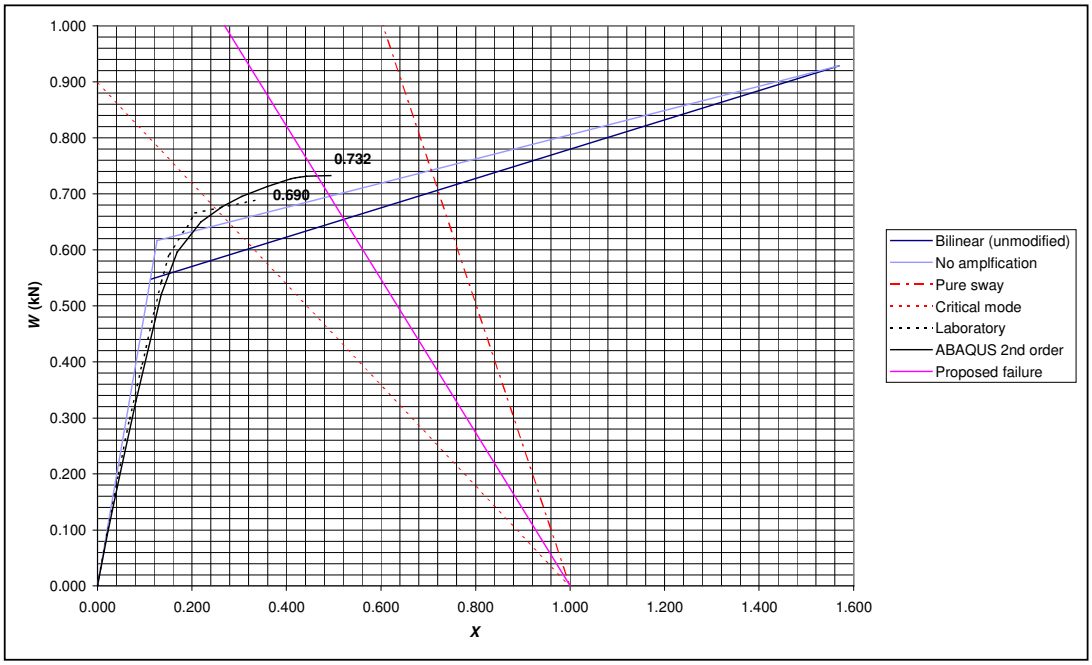


Fig. [5.25] *W-X* graph of 0.6ll frame with proposed failure criterion

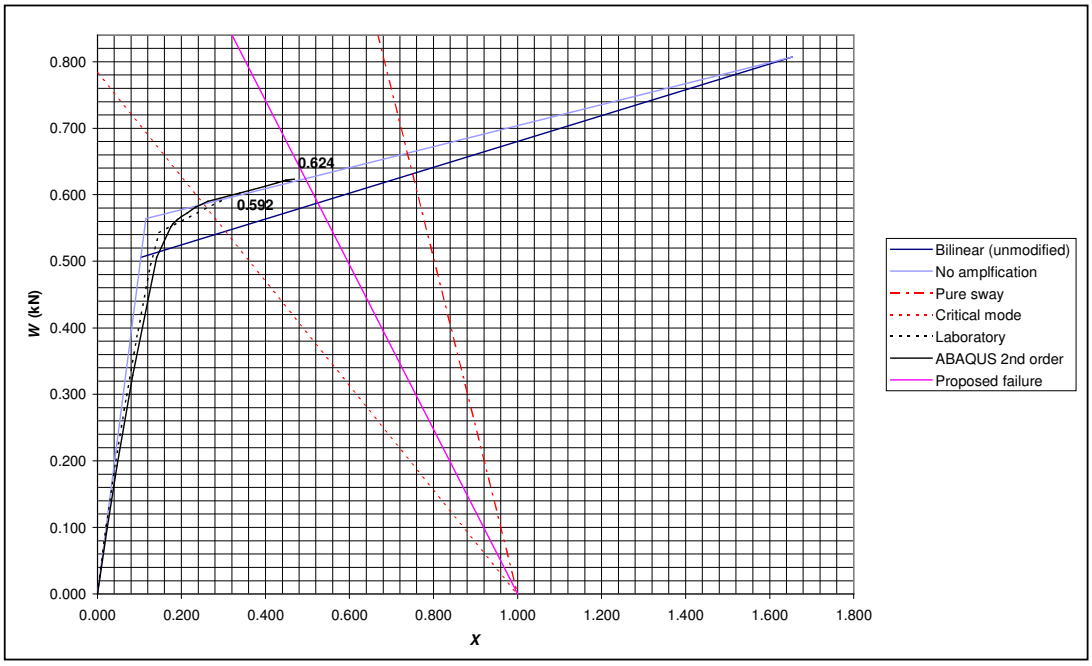


Fig. [5.26] W-X graph of 0.4ll frame with proposed failure criterion

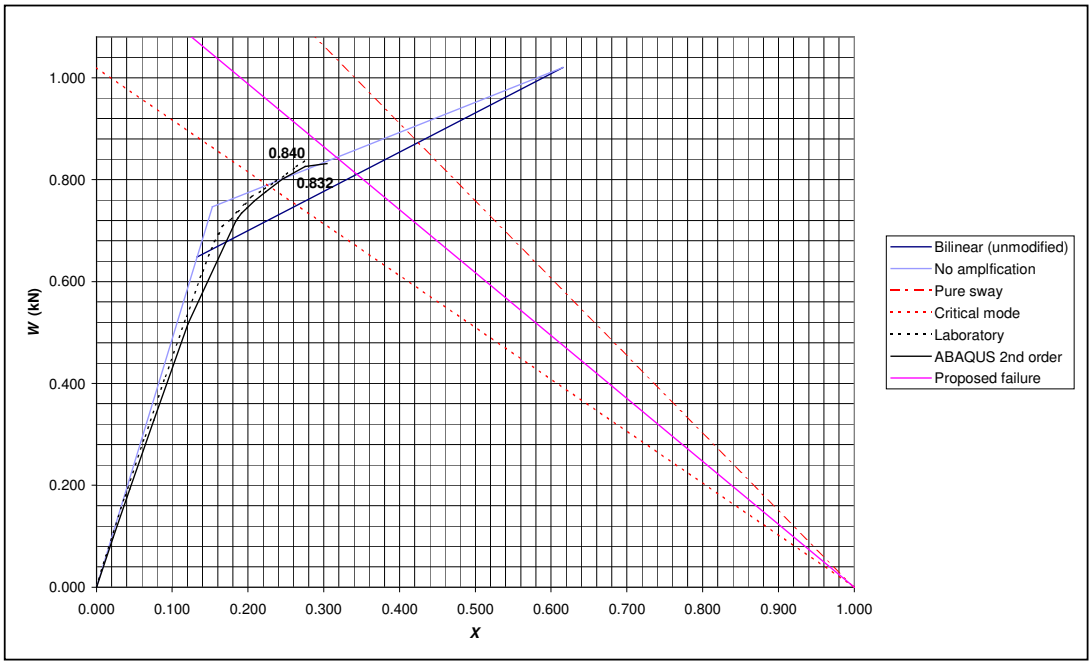


Fig. [5.27] W-X graph of 0.33sway frame with proposed failure criterion

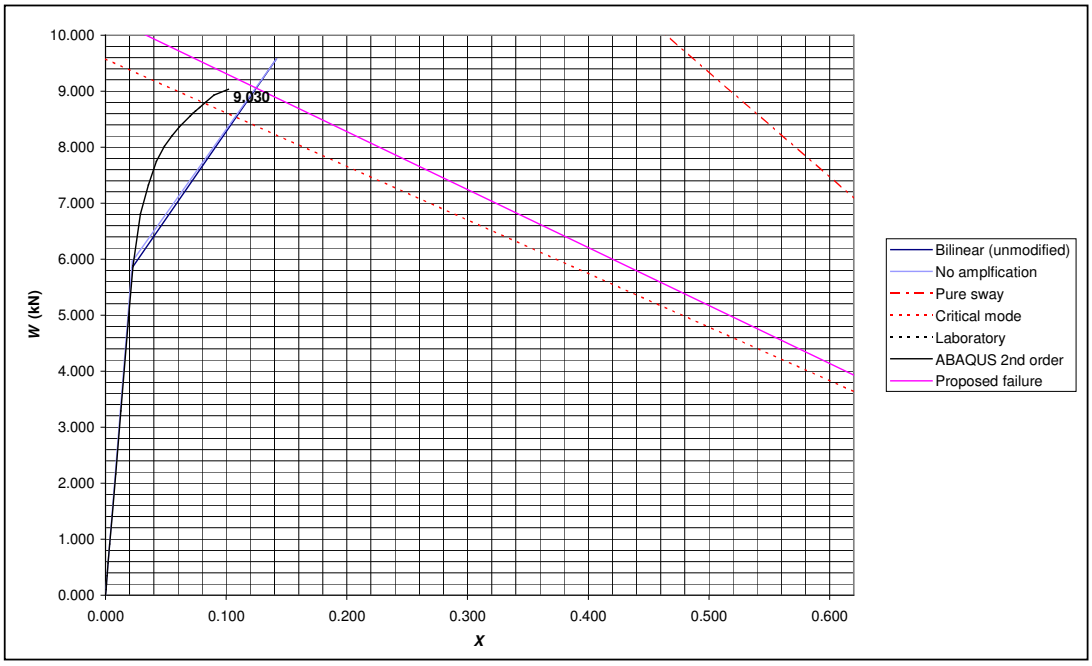


Fig. [5.28] W-X graph of kempsp1(a) frame with proposed failure criterion

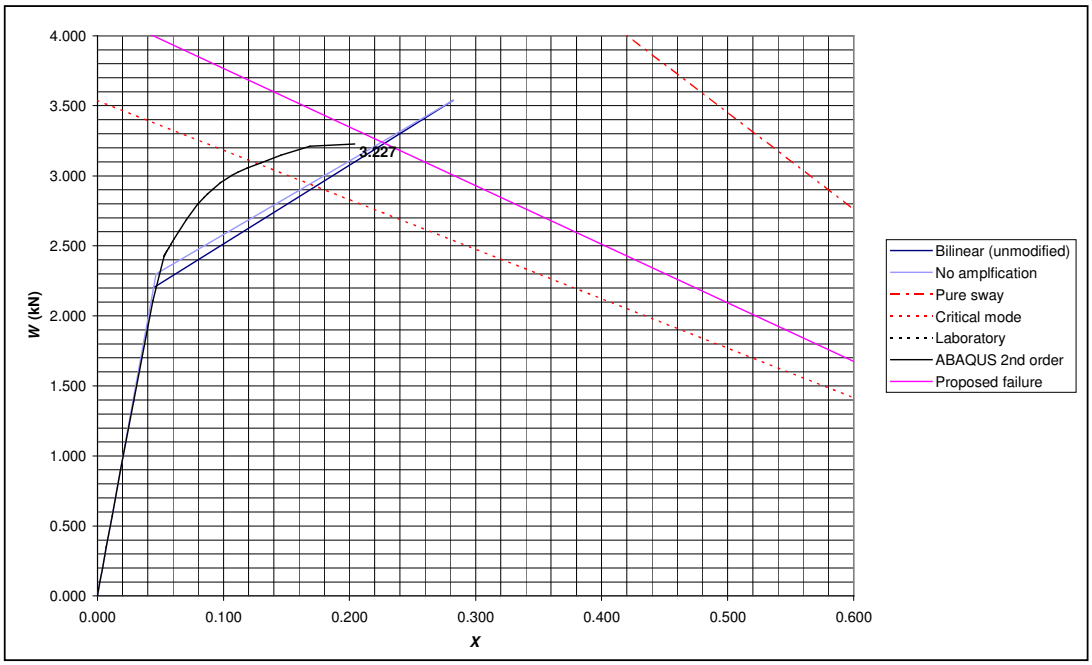


Fig. [5.29] W-X graph of kempsp1(b) frame with proposed failure criterion

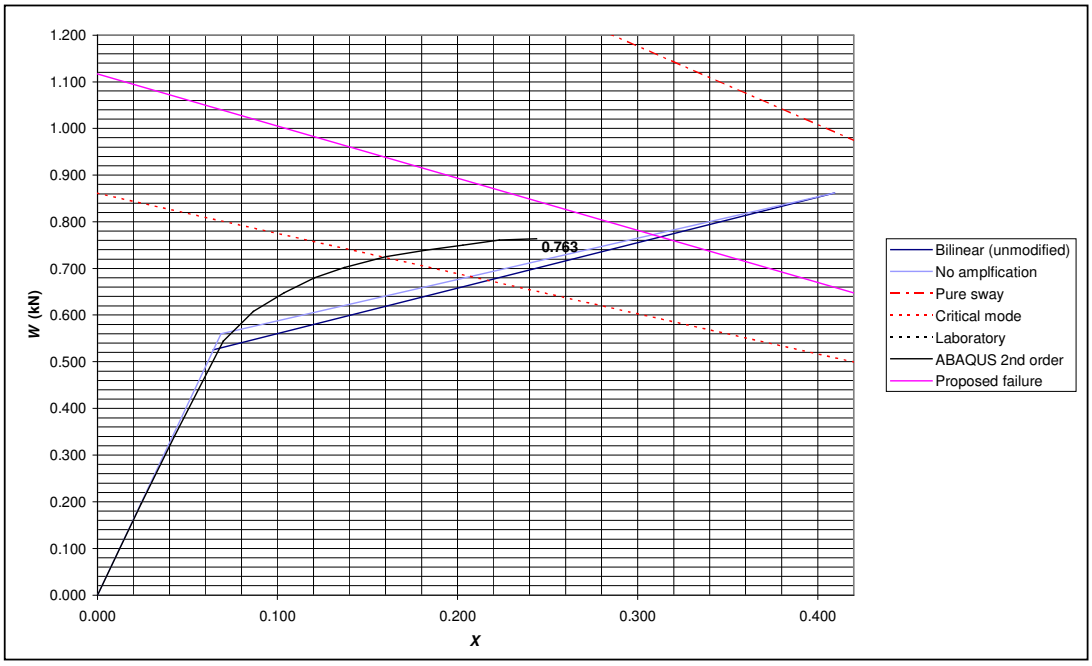


Fig. [5.30] W-X graph of kempsp1(c) frame with proposed failure criterion

6 CONCLUSIONS AND RECOMMENDATIONS

This chapter summarises the observations, findings and conclusions with reference to the objectives of the research project. Thereafter, modifications are recommended for Kemp's amplification factor theory, and issues that require further investigation are highlighted. A summary of the objectives is repeated here for the reader's convenience:

1. To establish how the chosen variations in column to beam span ratios, and positions of gravitational loads affected the accuracy of Kemp's method of failure load prediction.

2. To determine the accuracy with which the bilinear relationship approximated the actual load-*X* relationship of the test frames.

3. To perform a parametric study of the variables used in the amplification factor theory to enable modifications and improvements.

Having tested the frames in the laboratory and with ABAQUS, the results were compared to Kemp's predictions to address the first two objectives. These comparisons were then used to substantiate the appraisal and modification of Kemp's theory in achieving the third objective.

6.1 Failure Load Prediction

The ABAQUS and the laboratory results were very closely matched, rendering them almost interchangeable for the purposes of comparison to Kemp's results. The ABAQUS results were used primarily as the data recordings were taken at smaller load intervals, allowing smoother and more data-rich curves. The ABAQUS analyses also eliminated the various errors associated with laboratory testing (as discussed in chapter 3). Comparisons to Kemp's results yielded the following pertinent observations and deductions:

- There was an excellent degree of correlation between the failure loads of all test methods for the laboratory frames. The discrepancies between Kemp's loads and the ABAQUS equivalents ranged from –6.5 percent to +4.9 percent of the ABAQUS loads. A similar amount of variation was observed in the comparison of the ABAQUS and the laboratory test results. Kemp's accurate predictions of failure load were probably aided by the ductility of the flat bar section that was used in the test frames.

- There appeared to be a trend of diverging failure loads between Kemp's theory and the ABAQUS analyses as the spans changed. Kemp's failure loads were progressively lower than the ABAQUS counterparts for increasing spans. This trend was absent between the ABAQUS and laboratory results. It was

therefore likely that the divergence of the failure loads resulted from Kemp's theory. The progressive under-estimation of the strength of increasing spans by Kemp's method were probably due to the neglect of the effects of moment redistribution. The ABAQUS tests revealed that as the spans increased, the loss of stiffness and strength after the formation of the first fully plastic section became more gradual. This retention of strength was enabled by moment redistribution as the frames became more flexible. The bilinear load-X graph does not allow for the manner in which moment redistribution affects the shape of the actual load-X curve after plastic stresses are encountered.

- A similar trend was noted between the failure loads of ABAQUS and Kemp's method for the loading length variation frames. Kemp's failure load for the kempsp1 frame was lower than the ABAQUS counterpart, yet the discrepancies between loads reduced as the loading lengths shortened. Given that the loading length variation frames shared similar geometries, it was unlikely that this trend was due to changes in the ability of the frames to redistribute moment. Rather, it was more plausibly from the effect of the loading lengths on the sequence of plastic hinge formation in the frames. As the loading lengths reduced, the vertical loads caused increasingly severe moments at the column tops and at the centre of the beam. Plastic moment hinges occurred in these locations in quick succession, resulting in a rapid loss of stiffness and strength after the formation of the first hinge. This caused failure to occur in the actual test frames at progressively lower loads as the loading lengths shortened.

- Kemp's failure criterion suggests that failure will occur in a pure sway mode. The laboratory and ABAQUS tests showed that actual failure occurred in combined member and sway modes for all of the frames. Kemp's assumption of pure sway failure caused invalid calculations of failure load for the 0.6rigidspan frame and the I-section variations of kempsp1 frame. In these frames, the first order plastic sway deflections at collapse Δ_p were not large enough to ensure intersection of Eqn. (4.30) and the inelastic bilinear load-X graphs. This indicated that Kemp's amplification factor method would not necessarily be more applicable to conventionally shaped sections and realistically slender members.

- If failure were to occur in a pure sway mode, as per Kemp's assumption, then one might assume that the positions of the vertical loads on the beam would be irrelevant to the actual failure load. The positions of the loads, however, play a role in determining the critical first order plastic load of the frame. In doing so, they affect the position of the point (X_p, λ_p), and hence the shape of the load-X graph. Consequently, the positioning of the loads affects Kemp's prediction of failure load, even if failure does occur in a pure sway mode.

6.2 Load-X Curve Approximation

It is self evident that a bilinear graph cannot model a highly nonlinear curve accurately at all locations. Since the primary objective of Kemp's theory is to predict collapse loads, it is important that his bilinear load-X graph is near the actual curve at failure. It is also desirable that the bilinear graph follows the same general shape as the actual curve. The similar shape is an indication that the development of geometric and material nonlinearity is occurring as anticipated, and that appropriate limits have been chosen for the bilinear graph. Kemp's load-X graphs compared to the ABAQUS and laboratory counterparts in the following manner:

- Typically, the position of the elastic limit (X_i, λ_i) provided the correct slope for the elastic portion of the graph. Accurate calculations of sway stiffness required reliable section property values from the coupons tests. The quality of the ABAQUS frame analyses were also dependent on the section values, thus the agreement of the frame test results from three different methods further confirmed the accuracy of the test results overall.

- As anticipated, the frames exhibited nonlinear behaviour at loads below Kemp's λ_i. The load λ_i represented the condition of the formation of the first fully plastic section in the structure. Prior to this condition, the stiffness of the frame had been reducing due to the spread of plasticity. The loss of section stiffness, combined with the second order effects present in the flexible test frames, resulted in the divergence of the load-X curves at relatively low loads.

- The plastic portions of the bilinear load-X graphs passed consistently beneath the failure points of the ABAQUS curves. The differences in load between the bilinear and ABAQUS graphs at actual failure were dependant on the spans and load positions. These discrepancies increased with longer spans and greater loading lengths. Once more, this was conceivably due to moment redistribution in the longer spans, and rapid loss of stiffness where loads were concentrated near the centres of the beams.

- The calculation of the point (X_p, λ_p) required the first order sway deflection $\triangle_{Ip}$ of the frame at the point of collapse in the critical mode. Kemp had devised a method of calculating this deflection by using the virtual work principle and an empirical expression for reduced flexural rigidity. The expression for reduced rigidity was to allow for the effects of plasticity on members containing fully plastic sections. The ability of Kemp's method to calculate first order deflections at collapse was supported by favourable comparisons of Kemp's deflections to those obtained from first order ABAQUS. These validations of the deflections coupled with the relatively simple calculations of load λ_p provided a good basis for the limit of plastic behaviour (X_p, λ_p) on the bilinear graph.

- The incremental amplification factor values X_f of Kemp's method at failure were substantially larger than those of the other two methods. The values of X_f resulted in amplification factors for the laboratory tested frames that ranged from 126 percent to 212 percent of the ABAQUS U_2 values. The best-

matched U_2 values were of the 0.33sway frame, followed by the increasing spans of the span variation frames, and then by the decreasing loading length variations. These discrepancies implied that the amplified failure loads of the ABAQUS and laboratory tests were correspondingly lower than the respective first order pure sway collapse loads.

- The load-Δ curves that were extrapolated from the bilinear load-X graphs were unlike the ABAQUS or laboratory counterparts. The extrapolated load-Δ curves resembled bilinear graphs possessing slight curvatures that indicated nonlinear geometric effects. At loads below λ_i, the amplification factor method produced deflections that underestimated the actual deflections by twenty to thirty percent. The correlation of results was more favourable for the frames with shorter spans and greater loading lengths. At loads above λ_i, the validity of the load-Δ relationship was lost in all cases.

6.3 Appraisal of Kemp's Theory

The results of the frame tests revealed that Kemp's amplification factor theory should be improved both in the shape of the bilinear load-X graph, and in the conditions of the failure criterion. Initially, the intention was to perform a parametric study and thereby identify variables that could be adjusted to improve the method. It was soon apparent that the empirical factors used in the calculations had either provided favourable results, or had been ignored with no adverse effects. Modifications would need to be made to the theory itself, and this required a careful reassessment of Kemp's assumptions and workings. It was during the appraisal of Kemp's theory that conclusions were drawn about the efficacy and the validity of his method. Below is a summary of the findings as detailed in chapter 5:

- During Kemp's incremental consideration of second order effects, he assumes a proportional relationship between the second order virtual works of successive iterations for an arbitrarily shaped sway frame. Since the virtual deflections remain unchanged, the actual second order deflections must readjust at each increment in order that the total second order virtual work can be achieved. It is thus required that these actual deflection changes occur such that the conditions of moment equilibrium, compatibility and the value of X are simultaneously maintained at each iteration. If so, then it is possible that the problems associated with using an incremental moment equilibrium approach are reintroduced for nonrectangular structures and inelastic stress conditions.

- The value of the incremental amplification factor X for a given structure is dependent on the load-Δ_I relationships of the individual members. At any given load, Kemp's formula for calculating X considers the total forces in the members in relation to their total first order deflections. Consequently X relies on the effective sway stiffnesses of the members, rather than their tangent moduli. In the presence of plasticity, the effective sway stiffness of a member will always be greater than its tangent modulus. Using effective sway

stiffnesses in the calculation of X thus results in an overestimate of the rigidity of the structure. As the stresses becomes increasingly plastic, the tangential and effective stiffness values diverge, resulting in the progressive underestimation of second order effects. Furthermore, the geometric sum for U_2 cannot allow for the loss of stiffness due to second order strains albeit that these losses will probably become significant near failure loads only.

- Sway measurements taken in the laboratory and from the second order ABAQUS analyses were converted to equivalent first order deflections Δ_1 using Kemp's amplification factor. When plastic stresses were present in the frames, the back-calculated first order deflections were larger than their proper counterparts due to the underestimation of second order effects by U_2. Correspondingly, the load-X graphs that used back-calculated deflections showed greater losses of stiffness than the graphs using proper first order deflections (as taken from first order ABAQUS analyses). The 'proper' load-X graphs often indicated elastic stresses at loads above actual failure. This illustrated that the bilinear approximation should not model a load-X graph based on proper first order deflections.

- Kemp's amplification factor has been derived such that it can be applied in the general case to a sum of virtual work, not to individual moments or deflections, or to a load factor. Once stresses have reached their maximum values, it is meaningless to amplify them further. Member sway deflections may increase at different rates to each other within the same structure and therefore be subject to varying amounts of amplification. Fortunately, the incremental amplification factor X was at all times proportional to the first order sway deflection Δ_1 of the rectangular test frames. This allowed the use of the sway deflections measured in the laboratory to calculate the values of U_2.

- It is possible that the amplification of the effects of a load, or load group, differ to the amplification of other load effects on the same structure. This notion is supported by Kennedy et al's method in which only the effects of the sway-inducing lateral loads are amplified. If the concept of multiple amplification factors is valid, then U_2 for a particular load will be dependent on that load's ability to induce member end sways. The more these sways correlate to the virtual deflections of the chosen sway mode, the greater U_2 will be for the given load. As per usual, the magnitude of the amplification will also be dependent on the axial loads and the sway stiffnesses of the members.

- Given that the amplification factor has been derived in terms of virtual work, the failure criterion should be expressed in similar terms. Kemp's criterion is analogous to a virtual work equation if one assumes that there is a single amplification factor for a given structure. This assumption allows simple proportionality between the overall load factor and the virtual work sum. In the event of multiple amplification factors, the contribution of each load group would need to be weighted and appropriately amplified. In such a scenario,

the failure criterion could not simply be expressed in terms of a load factor but would need to be written in terms of virtual work.

- Separate amplification factors for the translational and gravitational loads on the test frames allowed proper account to be taken of the relative virtual work contributions. Actual failure of the frames occurred not in the pure sway mode, but in a combined sway and member mechanism. This combined mode involved vertical movement of the gravitational loads, thus allowing them to contribute to the virtual work sum. It was decided that the structure would become unstable when the appropriately amplified virtual work of the first order inelastic analysis equalled the unamplified virtual work at first order plastic collapse in the combined mode. The resulting modified failure lines were plotted on the load-X graphs and were found to pass very closely to the actual failure points. This seemed to be compelling support for the differential amplification of load effects

The most important discovery is the possibility that the nonlinear behaviour of a sway frame may be incorrectly modelled through the use of a single amplification factor. If differential amplification of load effects is necessary, then Kemp's method is empirical not only in the shape of the bilinear load-X graph, but also in the derivation of the amplification factor itself. In addition, the opportunity to write a non-empirical failure criterion may be lost if the correct amplification of the load effects is not applied. That Kemp's amplification factor and his failure criterion may be semi-empirical does not imply that his method needs correction in this regard. Amplification factors are intended to provide the designer with a simplified means of allowing for nonlinear behaviour. The calculation of two factors for a simple test frame was laborious, and that of the modified failure line was even more so. Even if it were possible to perform such calculations for practical structures, the work involved in doing so would negate the point of using a simplified method. In contrast, Kemp's relatively simple method has been shown to make good predictions of collapse loads for a variety of different structural shapes. The concerns regarding Kemp's derivation of U_2 and its tendency to underestimate geometric nonlinearity in the presence of plasticity are not problematic if one accepts the empirical nature of the method. Any modifications to Kemp's method, therefore, cannot be entirely theoretical and will need to be checked by experimentation for different types of structures.

6.4 Recommendations

It is my opinion that Kemp's formula for calculating U_2 and his bilinear representation of the load-X relationship should be retained. I have been unable to suggest alternative methods of calculating these variables that are as simple or as widely applicable. The recommendations involve the following changes to the limits of the bilinear load-X graph, and to the manner in which the collapse load is determined:

- When calculating the elastic limit (X_i, λ_i), the effect of the amplification factor is ignored in the interaction equation.

- Upper and lower bound failure lines are constructed in the load-X space, delineating a portion of the bilinear graph in which failure might occur. The actual failure point defaults to the centre of the delineated graph, but may be adjusted to suit the results of further experimentation.

These modifications can best be illustrated by comparing the sequence of operations required of Kemp's original method to those that are recommended here. Below are the steps that one would normally take to carry out Kemp's method:

1. Identify the most likely mode of pure sway failure of the frame, and calculate the corresponding first order plastic collapse load λ_s. This mode will be used to calculate the virtual deflections required by the amplification factor.

2. Identify the location in which the first fully plastic section of the frame will occur. This location will be the subject of the interaction Eqn. (4.1-1) below.

$$\frac{C}{C_y} + \frac{U_2 M_1}{M_p} + \frac{0.5\sigma_{res}}{\sigma_y} = 1.0 \qquad (4.1\text{-}1)$$

3. Perform a first order elastic analysis of the frame, and calculate the amplification factor U_2 for the frame using the following equations:

$$X = \frac{\Sigma C_{ij} \Delta_{1\,ij} \phi^*_{ij}}{\Sigma V_{ij} L_{ij} \phi^*_{ij}} \qquad (2.4\text{-}8)$$

$$U_2 = \frac{1}{1 - X} \qquad (2.4\text{-}11)$$

   Substitute the relevant terms from the analysis into Eqn. (4.1-1), and iterate the analysis until the left hand side of the interaction equation equals 1.0. At this point, the incremental amplification factor and the load factor represent the elastic limit (X_i, λ_i).

4. Identify the critical combined mechanism for first order plastic collapse of the frame, and calculate the corresponding load λ_p.

5. Calculate the first order sway deflections of the compression members at the point of plastic collapse in the critical combined mechanism. This is performed using Kemp's virtual work method, and his expression for reduced flexural rigidity in members containing fully plastic sections.

$$EI' = EI((1/f) - (1.1C/C_y)) \qquad (4.2\text{-}1)$$

6. Use Eqn. (2.4-8) to calculate X_p, and therefore the plastic limit (X_i, λ_i).

7. Plot the bilinear load-X graph (this step is optional).

8. Solve the failure criterion of Eqn. (2.5-5) simultaneously with the inelastic portion of the bilinear load-*X* graph (represented by Eqn. (2.5-2)) to calculate the failure load λ_f.

$$U_2\lambda_f = \lambda_s \tag{2.5-5}$$

$$\lambda_i < \lambda < \lambda_p \quad : \quad X = X_i + \left(\frac{(X_p - X_i)(\lambda - \lambda_i)}{\lambda_p - \lambda_i} \right) \tag{2.5-2}$$

The calculations performed in the modified method are for the most part identical to those listed above. Only those steps in which changes have been suggested are repeated below:

2. Identify the location in which the first fully plastic section of the frame will occur. This location will be the subject of the proposed interaction Eqn. (5.4-4) below.

$$\frac{C}{C_y} + \frac{M_I}{M_p} + \frac{0.5\sigma_{res}}{\sigma_y} = 1.0 \quad \text{(Note the exclusion of } U_2\text{)} \tag{5.4-4}$$

7. Plot the bilinear load-*X* graph (this step is no longer optional).

8. In the load-*X* space, plot the upper and lower bound failure lines represented respectively by Kemp's original failure criterion and by Eqn. (5.4-1).

   Upper bound failure line: $U_2\lambda = \lambda_s$ (2.5-5)

   Lower bound failure line: $U_2\lambda = \lambda_p$ (5.4-1)

   The portion of bilinear graph that passes between these two boundaries is the feasible failure zone. Bisect this line to find the default failure load λ_f of the frame.

The modified amplification factor method appears to have the following benefits and effects when applied to the test frames:

- The calculation of the elastic limit is simplified due to the exclusion of the amplification factor in Eqn. (5.4-4).

- The new elastic limit brings the inelastic portions of the bilinear graphs closer to the load-*X* curves of the ABAQUS analyses. This is particularly evident near failure loads.

- Two important upper and lower bound failure conditions are recognised and represented graphically in the load-*X* space. These boundary conditions involve the loads λ_s and λ_p that are normally calculated in Kemp's original

method. Consequently, the representation of these boundaries is a simple task that does not increase the amount of calculations required of the method.

- The proposed method of calculating λ_f realises vastly improved amplification factor values at failure for the test frames, while maintaining the accuracy of failure load prediction.

- The position of the failure point on the bilinear graph can be fine-tuned through experimentation to suit a variety of unbraced frames. However, even when using the default method of bisecting the feasible failure zone, the new method produces improved or comparable results for all the test frames.

These recommendations have been developed such that they maintain the simplicity and the broad applicability of Kemp's original method. Even so, the modifications of the bilinear load-*X* graph, and the position thereupon of the failure point have been chosen to provide favourable results for the test frames. This renders the recommendations at least semi-empirical in their nature. Given the numerous and substantial differences between the test frames and practical sway frames, the validity and accuracy of any modifications will need to be checked before they are used in practice. This may prove problematic for nonrectangular frames owing to the difficulties involved in converting several measured deflections for a single load state into first order equivalents. The absence of first order deflections will prevent the construction of the load-*X* curves, which will in turn prevent effective reshaping of the bilinear graph. In this case, the researcher will instead be limited to checking the failure load alone. Should Kemp's amplification factor method be investigated further, I suggest that the researcher checks its accuracy on full-scale models with realistic loading scenarios. The results should allow modifications that have immediate practical significance. Additionally, I propose an investigation of the validity of differential amplification of load effects and, if possible, a simplified method of calculating and applying such factors. If successful, such a theory may reduce the empirical component of the method and with it the need to check results by experimentation.

APPENDIX A LABORATORY COUPON TEST DATA

COUPON 1b				L (mm)	A (mm^2)	C (kN)	ΔL (mm)	σ (MPa)	ε	E (GPa)	σ_y (MPa)
				203	75.63	0	0	0	0	216.7	320
						2	0.025	26.443	0.000123		
	Breadth (mm)	Thickness (mm)	A (mm^2)			4	0.05	52.887	0.000246		
						6	0.075	79.330	0.000369		
End 1	15.07	5	75.35			8	0.1	105.773	0.000493		
						10	0.125	132.217	0.000616		
	Breadth (mm)	Thickness (mm)	A (mm^2)			12	0.15	158.660	0.000739		
						14	0.175	185.104	0.000862		
Middle	15.23	5	76.15			16	0.2	211.547	0.000985		
						18	0.225	237.990	0.001108		
	Breadth (mm)	Thickness (mm)	A (mm^2)			20	0.25	264.434	0.001232		
						22	0.275	290.877	0.001355		
End 2	15.08	5	75.4			24	0.305	317.320	0.001502		
						24.44	0.335	323.138	0.001650		
						24.53	0.505	324.328	0.002488		
						24.17	1.005	319.568	0.004951		
						24.21	1.505	320.097	0.007414		
						24.55	2.005	324.592	0.009877		
						24.3	2.505	321.287	0.012340		
						24.11	3.005	318.775	0.014803		
						24.3	3.505	321.287	0.017266		
						24.33	4.005	321.684	0.019729		
						24.4	4.505	322.609	0.022192		
						24.54	5.005	324.460	0.024655		
						25.5	5.505	337.153	0.027118		
						26.2	6.005	346.408	0.029581		
						26.8	6.505	354.341	0.032044		
						27.31	7.005	361.084	0.034507		
						27.81	7.505	367.695	0.036970		
						28.23	8.005	373.248	0.039433		
						28.66	8.505	378.933	0.041897		
						29.03	9.005	383.825	0.044360		
						29.41	9.505	388.850	0.046823		

Where:

L = Gauge lengh
A = Cross-sectional area
C = Tensile load
ΔL = Extension
σ = Axial stress
ε = Axial strain
E = Young's modulus
σ_y = Yield stress

Table [A-T1] Tensile test data of Coupon 1b

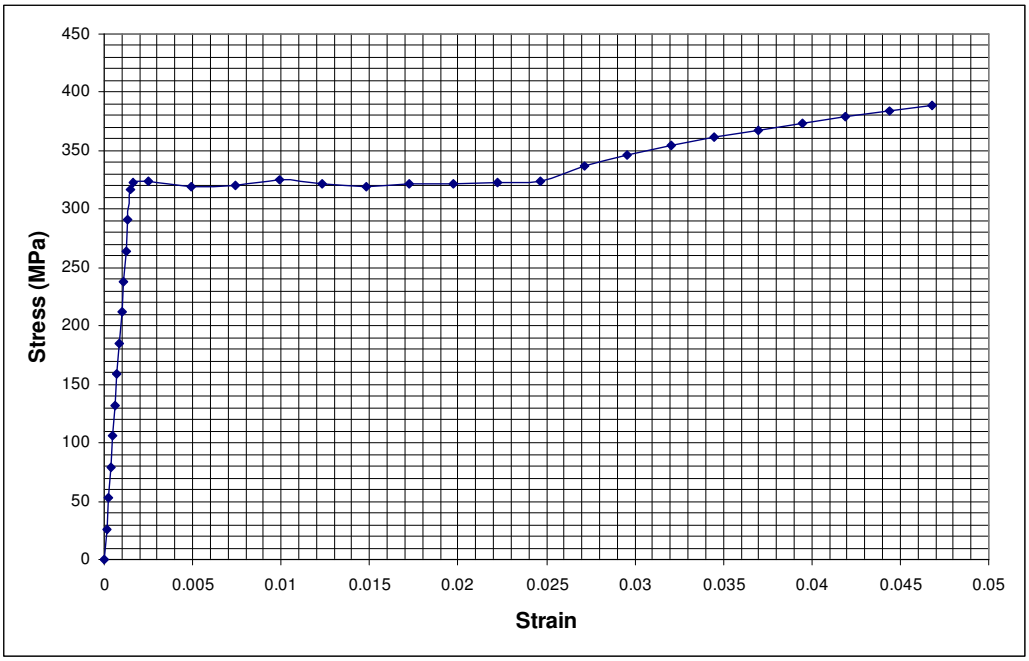


Fig. [A-F1] Coupon 1b stress-strain graph

APPENDIX A LABORATORY COUPON TEST DATA

COUPON 2a				L (mm)	A (mm^2)	C (kN)	ΔL (mm)	σ (MPa)	ε	E (GPa)	σ_y (MPa)
				203	75.25	0	0	0.000	0.000000	216.7	320
						2	0.025	26.579	0.000123		
	Width (mm)	Thickness (mm)	A (mm^2)			4	0.05	53.159	0.000246		
End 1	15.14	4.9	74.186			6	0.075	79.738	0.000369		
						8	0.1	106.318	0.000493		
						10	0.125	132.897	0.000616		
	Width (mm)	Thickness (mm)	A (mm^2)			12	0.15	159.476	0.000739		
Middle	15.15	5.01	75.9015			14	0.175	186.056	0.000862		
						16	0.205	212.635	0.001010		
						18	0.23	239.214	0.001133		
	Width (mm)	Thickness (mm)	A (mm^2)			20	0.255	265.794	0.001256		
End 2	15.07	5.02	75.6514			22	0.28	292.373	0.001379		
						24	0.31	318.953	0.001527		
						24.34	0.35	323.471	0.001724		
						24.87	0.85	330.515	0.004187		
						24.89	1.35	330.780	0.006650		
						25.07	1.85	333.173	0.009113		
						24.82	2.35	329.850	0.011576		
						24.78	2.85	329.319	0.014039		
						24.79	3.35	329.451	0.016502		
						25.2	3.85	334.900	0.018966		
						25.55	4.35	339.552	0.021429		
						25.57	4.85	339.817	0.023892		
						25	5.35	332.242	0.026355		
						26.72	5.85	355.101	0.028818		
						27.35	6.35	363.473	0.031281		
						27.88	6.85	370.517	0.033744		
						28.38	7.35	377.161	0.036207		
						28.85	7.85	383.408	0.038670		
						29.26	8.35	388.856	0.041133		
						29.64	8.85	393.906	0.043596		
						30	9.35	398.691	0.046059		

Where:

L = Gauge lengh
A = Cross-sectional area
C = Tensile load
ΔL = Extension
σ = Axial stress
ε = Axial strain
E = Young's modulus
σ_y = Yield stress

Table [A-T2] Tensile test data of Coupon 2a

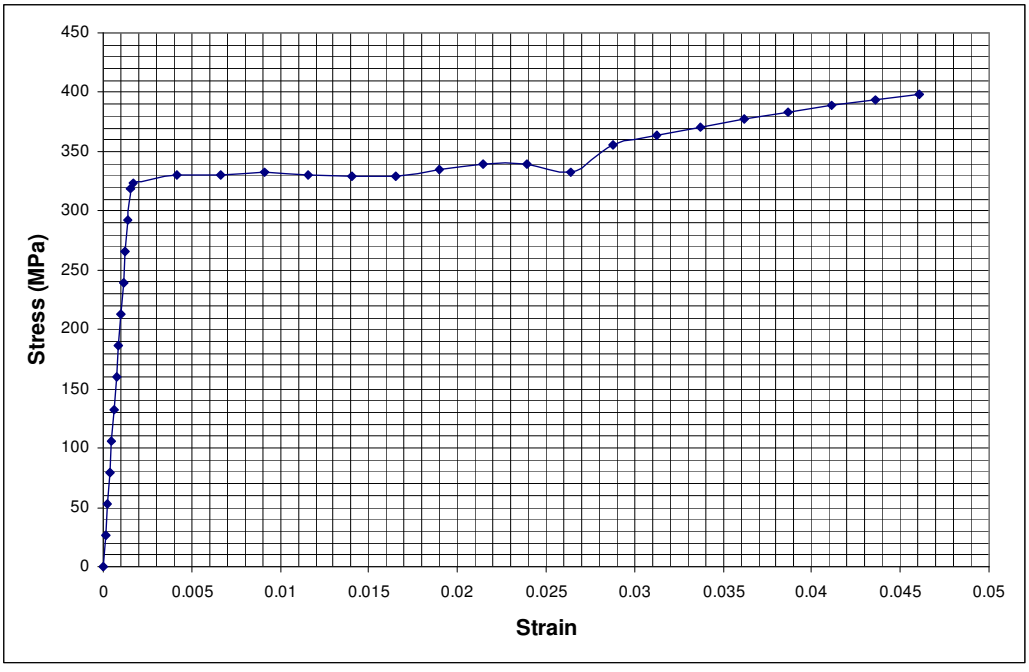


Fig. [A-F2] Coupon 2a stress-strain graph

APPENDIX A LABORATORY COUPON TEST DATA

COUPON 2b				L (mm)	A (mm^2)	C (kN)	ΔL (mm)	σ (MPa)	ε	E (GPa)	σ_y (MPa)
				203	77.730667	0	0	0.000	0.000000	207.1	315
						2	0.02	25.730	0.000099		
	Width (mm)	Thickness (mm)	A (mm^2)			4	0.055	51.460	0.000271		
End 1	15.05	5.15	77.5075			6	0.075	77.190	0.000369		
						8	0.105	102.919	0.000517		
						10	0.13	128.649	0.000640		
	Width (mm)	Thickness (mm)	A (mm^2)			12	0.155	154.379	0.000764		
Middle	15.13	5.15	77.9195			14	0.18	180.109	0.000887		
						16	0.205	205.839	0.001010		
						18	0.23	231.569	0.001133		
	Width (mm)	Thickness (mm)	A (mm^2)			20	0.255	257.299	0.001256		
End 2	15.1	5.15	77.765			22	0.285	283.029	0.001404		
						24	0.315	308.758	0.001552		
						24.85	0.49	319.694	0.002414		
						25.12	0.99	323.167	0.004877		
						24.58	1.49	316.220	0.007340		
						25.02	1.99	321.881	0.009803		
						25.17	2.49	323.810	0.012266		
						25.19	2.99	324.068	0.014729		
						25.22	3.49	324.454	0.017192		
						24.88	3.99	320.080	0.019655		
						25.46	4.49	327.541	0.022118		
						25.25	4.99	324.840	0.024581		
						25.5	5.49	328.056	0.027044		
						26.6	5.99	342.207	0.029507		
						27.29	6.49	351.084	0.031970		
						27.85	6.99	358.288	0.034433		
						28.35	7.49	364.721	0.036897		
						28.78	7.99	370.253	0.039360		
						29.19	8.49	375.527	0.041823		
						29.57	8.99	380.416	0.044286		
						29.94	9.49	385.176	0.046749		
						30.33	9.99	390.193	0.049212		

Where:

L = Gauge lengh
A = Cross-sectional area
C = Tensile load
ΔL = Extension
σ = Axial stress
ε = Axial strain
E = Young's modulus
σ_y = Yield stress

Table [A-T3] Tensile test data of Coupon 2b

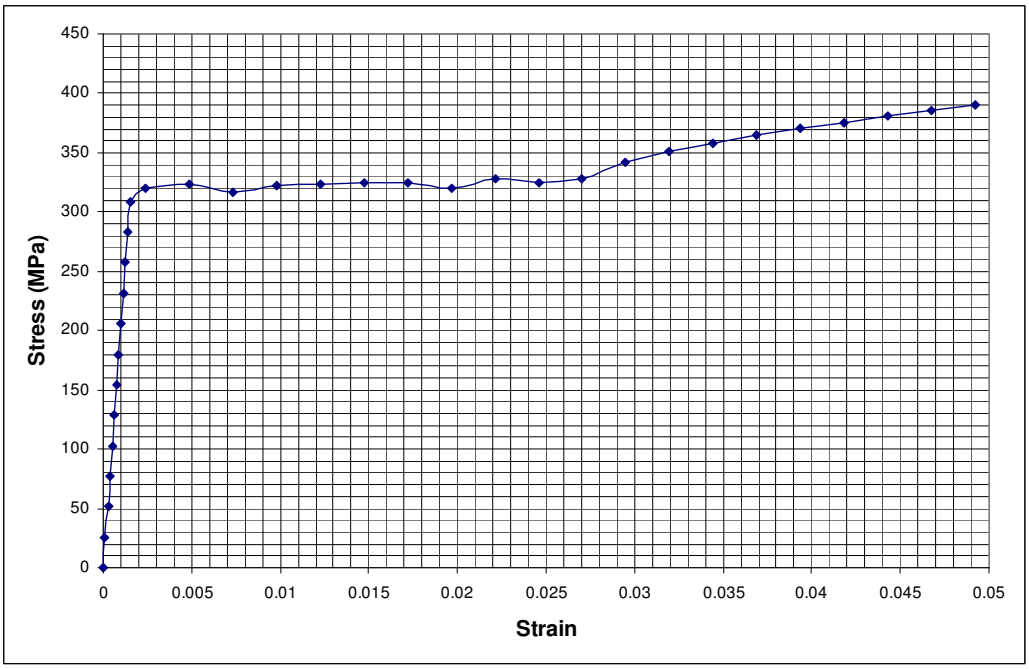


Fig. [A-F3] Coupon 2b stress-strain graph

APPENDIX A LABORATORY COUPON TEST DATA

COUPON 3a				L (mm)	A (mm^2)	C (kN)	ΔL (mm)	σ (MPa)	ε	E (GPa)	σ_y (MPa)
				203	76.38	0	0	0.000	0.000000	207.1	318
						2	0.025	26.186	0.000123		
	Width (mm)	Thickness (mm)	A (mm^2)			4	0.055	52.372	0.000271		
End 1	15.04	4.98	74.8992			6	0.08	78.559	0.000394		
						8	0.105	104.745	0.000517		
	Width (mm)	Thickness (mm)	A (mm^2)			10	0.13	130.931	0.000640		
						12	0.155	157.117	0.000764		
Middle	15.24	5.07	77.2668			14	0.18	183.303	0.000887		
						16	0.21	209.489	0.001034		
	Width (mm)	Thickness (mm)	A (mm^2)			18	0.235	235.676	0.001158		
						20	0.26	261.862	0.001281		
End 2	15.18	5.07	76.9626			22	0.285	288.048	0.001404		
						24	0.315	314.234	0.001552		
						24.53	0.57	321.173	0.002808		
						24.67	1.07	323.006	0.005271		
						24.98	1.57	327.065	0.007734		
						25.16	2.07	329.422	0.010197		
						24.88	2.57	325.756	0.012660		
						24.63	3.07	322.483	0.015123		
						25.01	3.57	327.458	0.017586		
						25.14	4.07	329.160	0.020049		
						25.05	4.57	327.982	0.022512		
						25.25	5.07	330.600	0.024975		
						24.86	5.57	325.494	0.027438		
						26.55	6.07	347.621	0.029901		
						27.19	6.57	356.001	0.032365		
						27.76	7.07	363.464	0.034828		
						28.27	7.57	370.141	0.037291		
						28.71	8.07	375.902	0.039754		
						29.14	8.57	381.532	0.042217		
						29.51	9.07	386.377	0.044680		
						29.86	9.57	390.959	0.047143		

Where:

L = Gauge lengh
A = Cross-sectional area
C = Tensile load
ΔL = Extension
σ = Axial stress
ε = Axial strain
E = Young's modulus
σ_y = Yield stress

Table [A-T4] Tensile test data of Coupon 3a

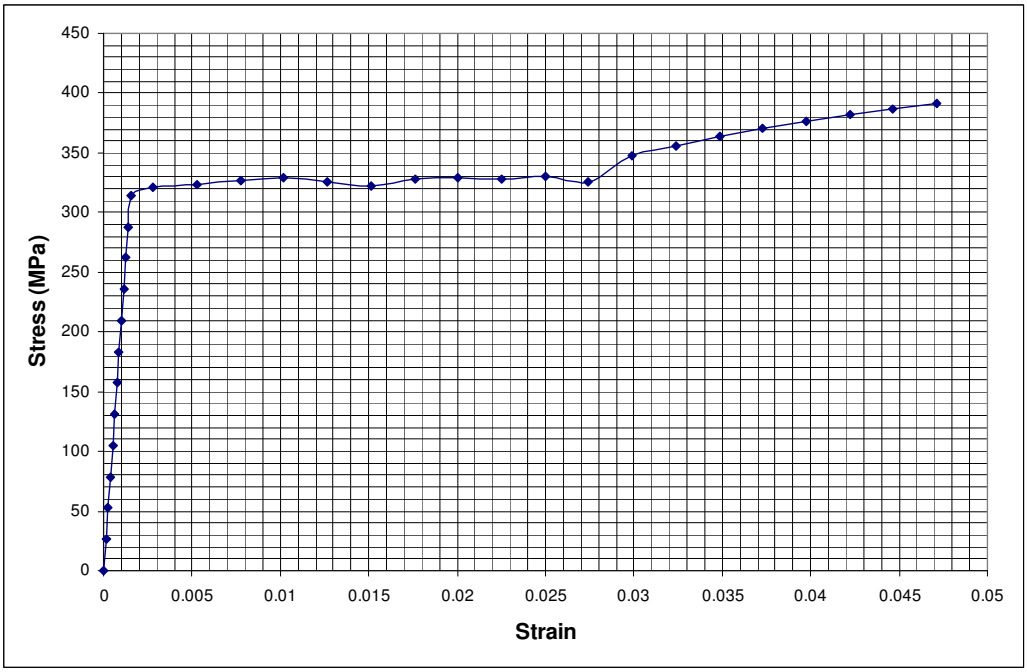


Fig. [A-F4] Coupon 3a stress-strain

APPENDIX A LABORATORY COUPON TEST DATA

COUPON 3b				L (mm)	A (mm^2)	C (kN)	ΔL (mm)	σ (MPa)	ε	E (GPa)	σ_y (MPa)
				203	77.27	0	0	0.000	0.000000	218.8	315
						2	0.03	25.884	0.000148		
	Width (mm)	Thickness (mm)	A (mm^2)			4	0.055	51.769	0.000271		
						6	0.08	77.653	0.000394		
End 1	15.2	5.07	77.064			8	0.1	103.537	0.000493		
						10	0.125	129.422	0.000616		
	Width (mm)	Thickness (mm)	A (mm^2)			12	0.15	155.306	0.000739		
						14	0.175	181.190	0.000862		
Middle	15.3	5.07	77.571			16	0.2	207.075	0.000985		
						18	0.225	232.959	0.001108		
	Width (mm)	Thickness (mm)	A (mm^2)			20	0.25	258.843	0.001232		
						22	0.275	284.728	0.001355		
End 2	15.22	5.07	77.1654			24	0.3	310.612	0.001478		
						24.41	0.5	315.918	0.002463		
						24.55	1	317.730	0.004926		
						24.81	1.5	321.095	0.007389		
						24.63	2	318.766	0.009852		
						24.7	2.5	319.672	0.012315		
						24.73	3	320.060	0.014778		
						24.76	3.5	320.448	0.017241		
						24.53	4	317.471	0.019704		
						25.31	4.5	327.566	0.022167		
						25.51	5	330.155	0.024631		
						25.09	5.5	324.719	0.027094		
						26.46	6	342.450	0.029557		
						27.09	6.5	350.603	0.032020		
						27.64	7	357.722	0.034483		
						28.12	7.5	363.934	0.036946		
						28.55	8	369.499	0.039409		
						28.97	8.5	374.935	0.041872		
						29.36	9	379.982	0.044335		
						29.71	9.5	384.512	0.046798		
						30.05	10	388.912	0.049261		

Where:

L = Gauge lengh
A = Cross-sectional area
C = Tensile load
ΔL = Extension
σ = Axial stress
ε = Axial strain
E = Young's modulus
σ_y = Yield stress

Table [A-T5] Tensile test data of Coupon 3b

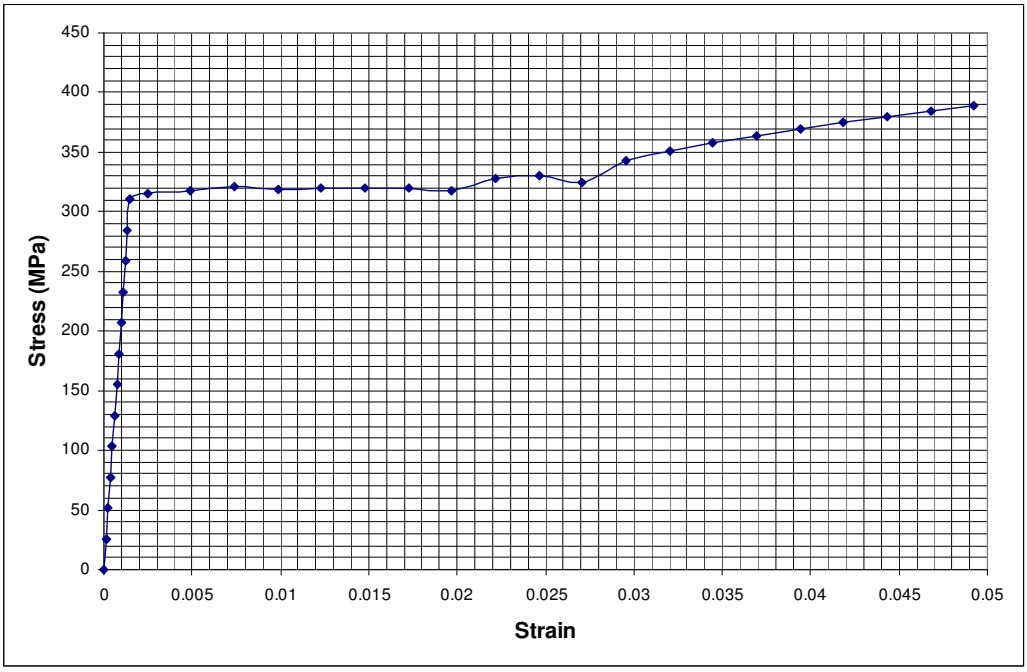
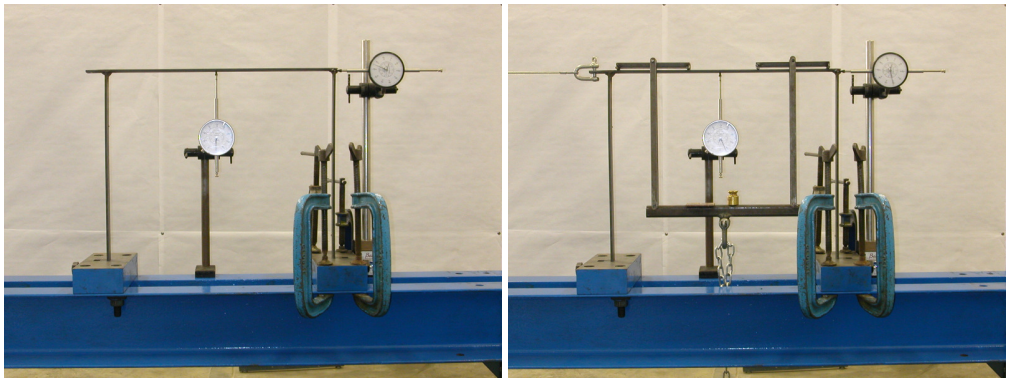


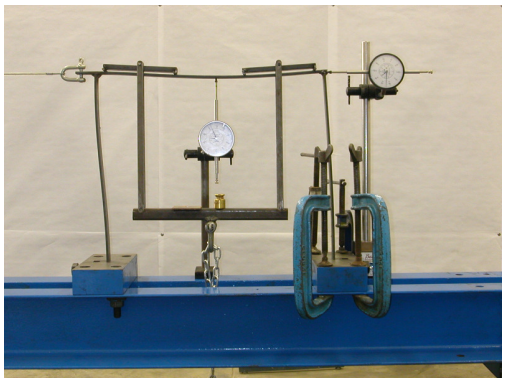
Fig. [A-F5] Coupon 3b stress-strain

APPENDIX B TEST FRAME PHOTOGRAPHS

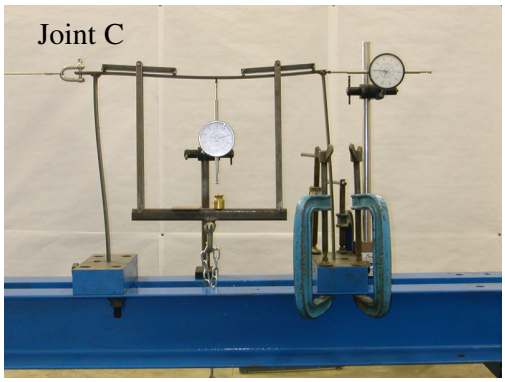


i) W=0

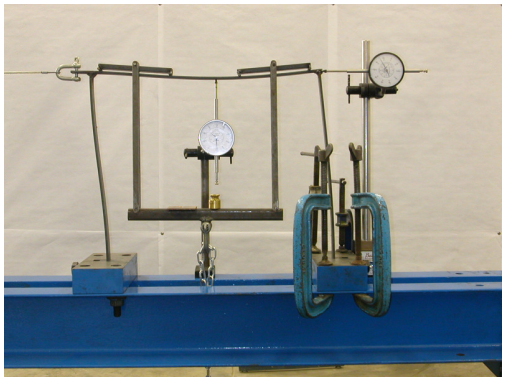
ii) W=0.102kN (=0.08W_f)



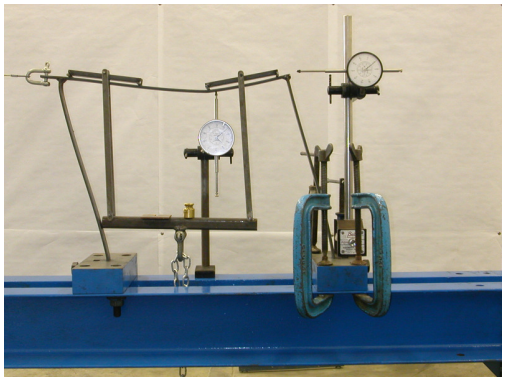
iii) W=1.107kN (=0.85W_f)



iv) W=1.180kN (=0.91W_f)
First hinge occurs at joint C



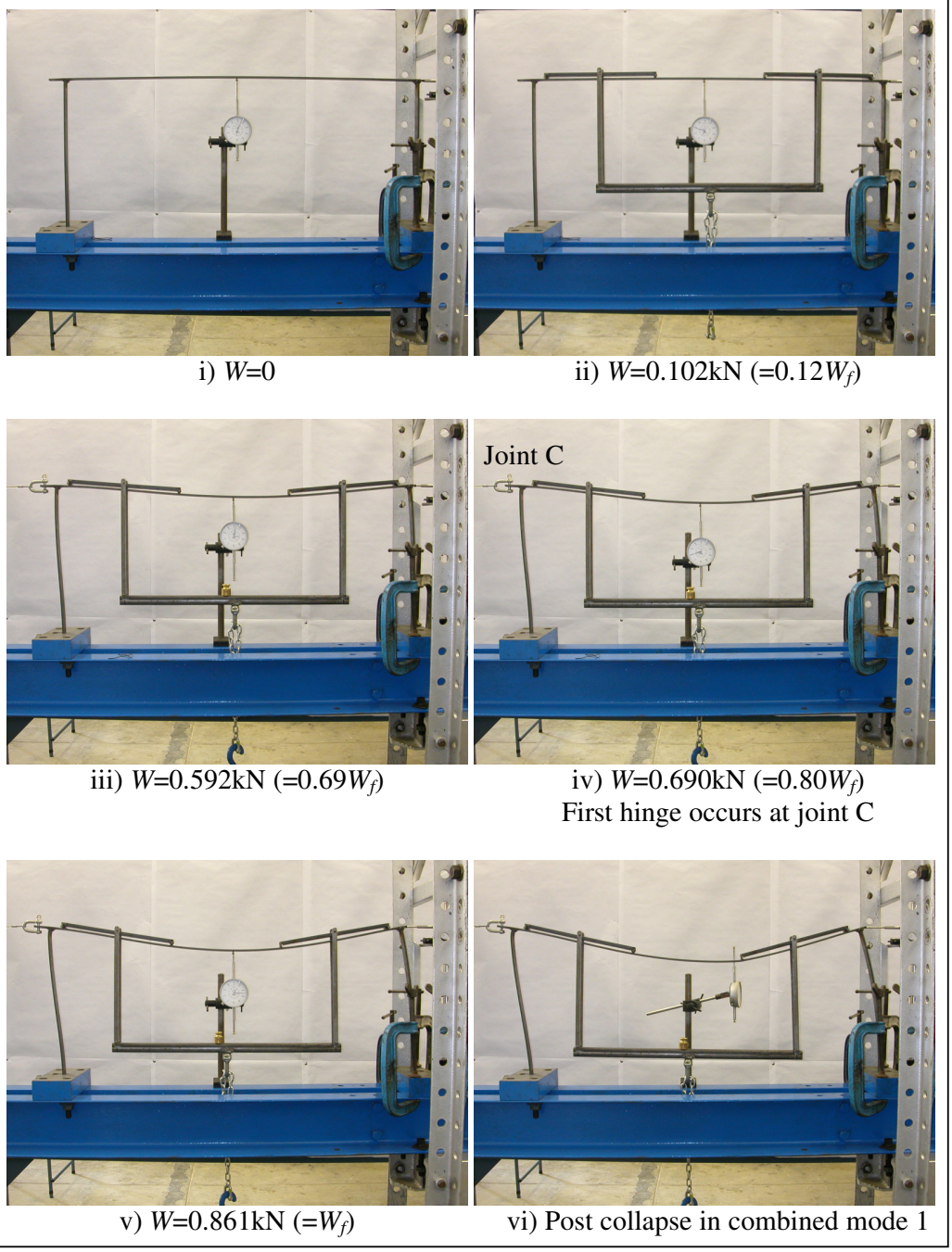
v) W=1.254kN (=0.96W_f)



vi) Post collapse in combined mode 1

Fig. [B-F1] Laboratory testing of the 0.6span frame

APPENDIX B TEST FRAME PHOTOGRAPHS



i) W=0

ii) W=0.102kN (=0.12W_f)

iii) W=0.592kN (=0.69W_f)

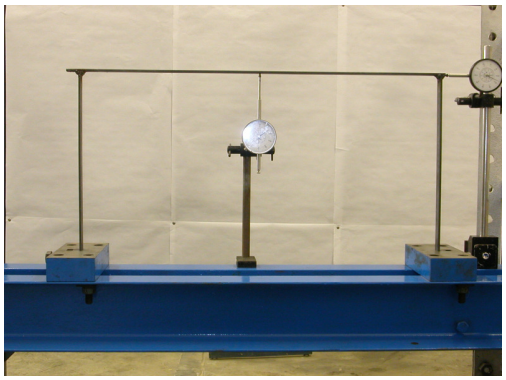
iv) W=0.690kN (=0.80W_f)
First hinge occurs at joint C

v) W=0.861kN (=W_f)

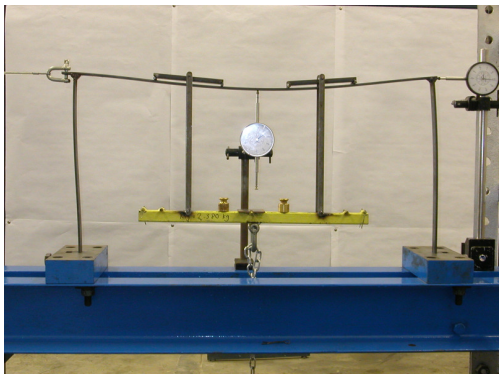
vi) Post collapse in combined mode 1

Fig. [B-F2] Laboratory testing of the 1.2span frame

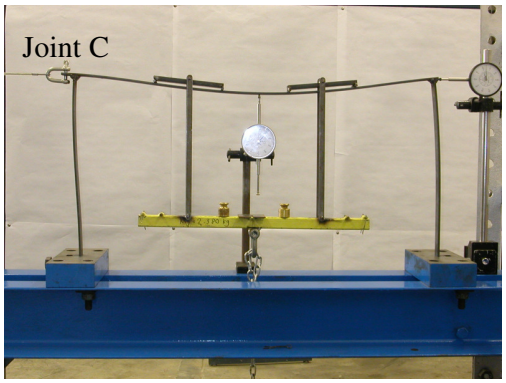
APPENDIX B TEST FRAME PHOTOGRAPHS



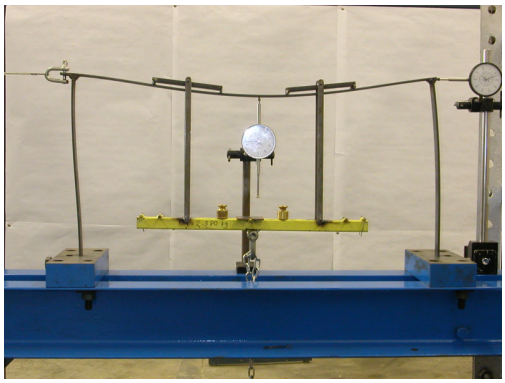
i) W=0



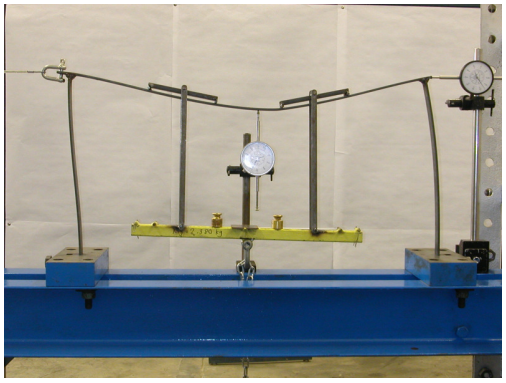
ii) W=0.494kN (=0.72W_f)



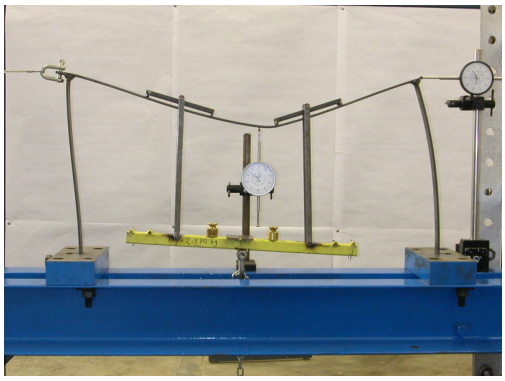
iii) W=0.592kN (=0.86W_f)
First hinge occurs at joint C



iv) W=0.641kN (=0.93W_f)



v) W=0.666kN (=0.97W_f)



vi) Post collapse in combined mode 1

Fig. [B-F3] Laboratory testing of the 0.6ll frame

APPENDIX C LABORATORY FRAME TEST DATA

KEMPSP1 LAB	*L* (mm)	Span (mm)	Loading Length (mm)	*W* (kN)	Δ (mm)	Δ_I (mm)	*X*	U_2
	400	800	740	0.000	0.00	0.00	0.000	1.000
				0.102	1.70	1.66	0.021	1.021
				0.200	3.54	3.39	0.042	1.044
				0.298	5.56	5.20	0.065	1.070
				0.396	7.75	7.07	0.088	1.097
				0.494	10.10	8.97	0.112	1.126
				0.592	12.64	10.92	0.136	1.158
				0.690	15.40	12.91	0.161	1.193
				0.715	16.02	13.35	0.167	1.200
				0.739	16.75	13.85	0.173	1.209
				0.764	17.53	14.38	0.180	1.219
				0.788	18.39	14.95	0.187	1.230
				0.813	19.25	15.52	0.194	1.241
				0.837	20.13	16.08	0.201	1.252
				0.862	21.41	16.89	0.211	1.268
				0.886	23.11	17.93	0.224	1.289
				0.911	25.81	19.51	0.244	1.323
				0.935	29.51	21.56	0.269	1.369
				0.960	34.39	24.05	0.301	1.430
				0.984	40.43	26.86	0.336	1.505
				1.009	54.83	32.53	0.407	1.685

Where:

L = Column length
W = Load factor (= λ)
Δ = Total sway deflection
Δ_I = First order sway deflection
= $\Delta/(1+W\Delta/VL)$
V = Horizontal sway load
= W/5
X = Incremental amplification factor
= $W\Delta_I/VL$
U_2 = Amplification factor
= 1/(1-X)

Table [C-T1] Laboratory test of kempsp1 frame

0.6SPAN LAB	*L* (mm)	Span (mm)	Loading Length (mm)	*W* (kN)	Δ (mm)	Δ_I (mm)	*X*	U_2
	400	480	444	0.000	0.00	0.00	0.000	1.000
				0.102	1.35	1.33	0.017	1.017
				0.347	5.27	4.94	0.062	1.066
				0.592	9.77	8.71	0.109	1.122
				0.837	14.76	12.46	0.156	1.185
				1.033	19.36	15.59	0.195	1.242
				1.082	20.68	16.43	0.205	1.259
				1.107	21.32	16.83	0.210	1.267
				1.131	21.98	17.24	0.216	1.275
				1.156	22.78	17.73	0.222	1.285
				1.180	24.30	18.64	0.233	1.304
				1.205	26.08	19.67	0.246	1.326
				1.229	28.76	21.15	0.264	1.360
				1.254	31.96	22.84	0.285	1.400
				1.278	38.70	26.08	0.326	1.484
				1.303	45.77	29.11	0.364	1.572

Where:

L = Column length
W = Load factor (= λ)
Δ = Total sway deflection
Δ_I = First order sway deflection
= $\Delta/(1+W\Delta/VL)$
V = Horizontal sway load
= W/5
X = Incremental amplification factor
= $W\Delta_I/VL$
U_2 = Amplification factor
= 1/(1-X)

Table [C-T2] Laboratory test of 0.6span frame

APPENDIX C LABORATORY FRAME TEST DATA

0.8SPAN LAB	*L* (mm)	Span (mm)	Loading Length (mm)	*W* (kN)	Δ (mm)	Δ_1 (mm)	*X*	U_2
	400	640	592	0.000	0.00	0.00	0.000	1.000
				0.102	1.57	1.54	0.019	1.020
				0.347	6.10	5.67	0.071	1.076
				0.592	11.37	9.96	0.124	1.142
				0.690	13.54	11.58	0.145	1.169
				0.788	16.12	13.42	0.168	1.202
				0.886	19.04	15.38	0.192	1.238
				0.935	25.63	19.41	0.243	1.320
				0.984	35.24	24.46	0.306	1.441
				1.033	49.79	30.69	0.384	1.622
				1.082	76.93	39.22	0.490	1.962
				1.107	91.36	42.65	0.533	2.142

Where:

L = Column length
W = Load factor (= λ)
Δ = Total sway deflection
Δ_1 = First order sway deflection
$= \Delta/(1+W\Delta/VL)$
V = Horizontal sway load
= W/5
X = Incremental amplification factor
$= W\Delta_1/VL$
U_2 = Amplification factor
= 1/(1-X)

Table [C-T3] Laboratory test of 0.8span frame

1.2SPAN LAB	*L* (mm)	Span (mm)	Loading Length (mm)	*W* (kN)	Δ (mm)	Δ_1 (mm)	*X*	U_2
	400	960	888	0.000	0.00	0.00	0.000	1.000
				0.102	1.72	1.68	0.021	1.022
				0.298	6.04	5.62	0.070	1.076
				0.494	11.37	9.96	0.124	1.142
				0.592	14.43	12.22	0.153	1.180
				0.641	16.11	13.41	0.168	1.201
				0.690	18.21	14.83	0.185	1.228
				0.739	24.24	18.60	0.233	1.303
				0.788	30.62	22.14	0.277	1.383
				0.812	34.47	24.09	0.301	1.431
				0.837	39.97	26.65	0.333	1.500
				0.861	45.82	29.13	0.364	1.573

Where:

L = Column length
W = Load factor (= λ)
Δ = Total sway deflection
Δ_1 = First order sway deflection
$= \Delta/(1+W\Delta/VL)$
V = Horizontal sway load
= W/5
X = Incremental amplification factor
$= W\Delta_1/VL$
U_2 = Amplification factor
= 1/(1-X)

Table [C-T4] Laboratory test of 1.2span frame

APPENDIX C LABORATORY FRAME TEST DATA

1.4SPAN LAB	L (mm)	Span (mm)	Loading Length (mm)	W (kN)	Δ (mm)	Δ_1 (mm)	X	U_2
	400	640	592	0.000	0.00	0.00	0.000	1.000
				0.102	2.17	2.11	0.026	1.027
				0.200	4.76	4.49	0.056	1.060
				0.298	7.68	7.01	0.088	1.096
				0.396	11.01	9.68	0.121	1.138
				0.494	14.80	12.49	0.156	1.185
				0.543	16.87	13.93	0.174	1.211
				0.592	19.24	15.51	0.194	1.241
				0.641	21.58	17.00	0.212	1.270
				0.690	26.35	19.82	0.248	1.329
				0.739	35.43	24.56	0.307	1.443
				0.764	40.65	26.95	0.337	1.508
				0.788	59.89	34.25	0.428	1.749

Where:

L = Column length
W = Load factor (= λ)
Δ = Total sway deflection
Δ_1 = First order sway deflection
= $\Delta/(1+W\Delta/VL)$
V = Horizontal sway load
= W/5
X = Incremental amplification factor
= $W\Delta_1/VL$
U_2 = Amplification factor
= 1/(1-X)

Table [C-T5] Laboratory test of 1.4span frame

0.6LL LAB	L (mm)	Span (mm)	Loading Length (mm)	W (kN)	Δ (mm)	Δ_1 (mm)	X	U_2
	400	800	444	0.000	0.00	0.00	0.000	1.000
				0.102	1.83	1.79	0.022	1.023
				0.200	3.74	3.57	0.045	1.047
				0.298	5.87	5.47	0.068	1.073
				0.396	8.38	7.59	0.095	1.105
				0.494	11.05	9.71	0.121	1.138
				0.543	12.50	10.81	0.135	1.156
				0.592	14.33	12.15	0.152	1.179
				0.641	18.67	15.14	0.189	1.233
				0.666	20.87	16.55	0.207	1.261
				0.690	41.47	27.31	0.341	1.518

Where:

L = Column length
W = Load factor (= λ)
Δ = Total sway deflection
Δ_1 = First order sway deflection
= $\Delta/(1+W\Delta/VL)$
V = Horizontal sway load
= W/5
X = Incremental amplification factor
= $W\Delta_1/VL$
U_2 = Amplification factor
= 1/(1-X)

Table [C-T6] Laboratory test of 0.6ll frame

APPENDIX C LABORATORY FRAME TEST DATA

0.4LL LAB	L (mm)	Span (mm)	Loading Length (mm)	W (kN)	Δ (mm)	Δ_I (mm)	X	U_2
	400	800	296	0.000	0.00	0.00	0.000	1.000
				0.102	1.72	1.68	0.021	1.022
				0.200	3.67	3.51	0.044	1.046
				0.298	5.99	5.57	0.070	1.075
				0.396	8.59	7.76	0.097	1.107
				0.494	11.54	10.09	0.126	1.144
				0.543	13.83	11.79	0.147	1.173
				0.592	33.70	23.71	0.296	1.421

Where:

L = Column length
W = Load factor (= λ)
Δ = Total sway deflection
Δ_I = First order sway deflection
$= \Delta/(1+W\Delta/VL)$
V = Horizontal sway load
= W/5
X = Incremental amplification factor
$= W\Delta_I/VL$
U_2 = Amplification factor
= 1/(1-X)

Table [C-T7] Laboratory test of 0.4ll frame

0.33SWAY LAB	L (mm)	Span (mm)	Loading Length (mm)	W (kN)	Δ (mm)	Δ_I (mm)	X	U_2
	400	800	740	0.000	0.00	0.00	0.000	1.000
				0.061	1.64	1.62	0.012	1.012
				0.179	5.23	5.03	0.038	1.039
				0.296	9.14	8.55	0.064	1.069
				0.414	13.35	12.13	0.091	1.100
				0.532	18.00	15.86	0.119	1.135
				0.620	21.73	18.68	0.140	1.163
				0.664	23.85	20.23	0.152	1.179
				0.679	24.57	20.75	0.156	1.184
				0.693	25.61	21.48	0.161	1.192
				0.708	26.63	22.20	0.166	1.200
				0.723	28.67	23.60	0.177	1.215
				0.737	30.57	24.87	0.187	1.229
				0.752	32.47	26.11	0.196	1.244
				0.767	34.44	27.37	0.205	1.258
				0.781	37.97	29.55	0.222	1.285
				0.796	41.22	31.49	0.236	1.309
				0.811	44.67	33.46	0.251	1.335
				0.826	47.77	35.17	0.264	1.358
				0.840	51.32	37.06	0.278	1.385

Where:

L = Column length
W = Load factor (= λ)
Δ = Total sway deflection
Δ_I = First order sway deflection
$= \Delta/(1+W\Delta/VL)$
V = Horizontal sway load
= W/3
X = Incremental amplification factor
$= W\Delta_I/VL$
U_2 = Amplification factor
= 1/(1-X)

Table [C-T8] Laboratory test of 0.33sway frame

APPENDIX D ABAQUS FRAME TEST DATA

KEMPSP1 ABAQUS	W (kN)	Δ_B (mm)	Δ_{BI} (mm)	X_B	Δ_C (mm)	Δ_{CI} (mm)	X_C	X_{ave}		W (kN)	Δ_I (mm)	X
	0.000	0.00	0.00	0.000	0.00	0.00	0.000	0.000		0.000	0.00	0.000
SECOND ORDER	0.098	1.84	1.80	0.022	1.80	1.76	0.022	0.022	FIRST ORDER	0.100	1.80	0.022
INELASTIC	0.194	3.74	3.57	0.045	3.58	3.43	0.043	0.044	INELASTIC	0.200	3.60	0.045
ANALYSIS	0.331	6.74	6.22	0.078	6.27	5.82	0.073	0.075	ANALYSIS	0.350	6.30	0.079
	0.525	11.49	10.05	0.126	10.28	9.11	0.114	0.120		0.575	10.35	0.129
	0.776	19.20	15.48	0.194	16.36	13.59	0.170	0.182		0.877	16.68	0.208
(1st hinge at C)	0.864	24.02	18.47	0.231	20.17	16.11	0.201	0.216		0.888	17.04	0.213
	0.868	24.28	18.63	0.233	20.38	16.24	0.203	0.218		0.905	17.58	0.220
	0.871	24.68	18.86	0.236	20.70	16.45	0.206	0.221		0.929	18.43	0.230
	0.877	25.28	19.21	0.240	21.19	16.75	0.209	0.225		0.952	19.76	0.247
	0.885	26.19	19.73	0.247	21.92	17.21	0.215	0.231		0.986	21.78	0.272
	0.897	27.56	20.50	0.256	23.02	17.88	0.223	0.240		1.030	24.83	0.310
	0.914	29.62	21.62	0.270	24.69	18.87	0.236	0.253		1.077	29.29	0.366
	0.936	32.73	23.23	0.290	27.16	20.28	0.253	0.272		1.098	31.76	0.397
	0.960	37.39	25.48	0.319	30.77	22.22	0.278	0.298		1.122	35.48	0.443
	0.971	40.03	26.68	0.334	32.77	23.25	0.291	0.312		1.155	40.96	0.512
	0.984	44.01	28.39	0.355	35.77	24.72	0.309	0.332		1.197	49.02	0.613
	1.002	49.98	30.76	0.385	40.06	26.69	0.334	0.359		1.229	57.13	0.714
	1.017	59.10	33.99	0.425	46.72	29.50	0.369	0.397		1.256	64.73	0.809
										1.270	77.64	0.970
										1.288	96.82	1.210
										1.298	125.58	1.570
										1.303	141.17	1.765

Table [D-T1] ABAQUS test of kempsp1 frame

0.6SPAN ABAQUS	W (kN)	Δ_B (mm)	Δ_{BI} (mm)	X_B	Δ_C (mm)	Δ_{CI} (mm)	X_C	X_{ave}		W (kN)	Δ_I (mm)	X
	0.000	0.00	0.00	0.000	0.00	0.00	0.000	0.000		0.000	0.00	0.000
SECOND ORDER	0.098	1.55	1.52	0.019	1.54	1.51	0.019	0.019	FIRST ORDER	0.100	1.54	0.019
INELASTIC	0.192	3.11	2.99	0.037	3.09	2.97	0.037	0.037	INELASTIC	0.200	3.09	0.039
ANALYSIS	0.327	5.46	5.11	0.064	5.41	5.06	0.063	0.064	ANALYSIS	0.350	5.40	0.067
	0.516	9.02	8.11	0.101	8.89	8.00	0.100	0.101		0.575	8.87	0.111
	0.772	14.43	12.22	0.153	14.12	12.00	0.150	0.151		0.913	14.08	0.176
	1.083	22.65	17.65	0.221	22.02	17.27	0.216	0.218		1.330	21.99	0.275
(1st hinges at C	1.176	27.32	20.36	0.255	26.49	19.90	0.249	0.252		1.388	24.02	0.300
and D)	1.178	27.56	20.50	0.256	26.73	20.03	0.250	0.253		1.432	26.05	0.326
	1.184	27.93	20.70	0.259	27.08	20.23	0.253	0.256		1.470	28.07	0.351
	1.192	28.49	21.01	0.263	27.61	20.53	0.257	0.260		1.516	31.09	0.389
	1.200	29.32	21.46	0.268	28.41	20.97	0.262	0.265		1.565	35.57	0.445
	1.213	30.58	22.12	0.277	29.62	21.62	0.270	0.273		1.589	38.08	0.476
	1.230	32.47	23.10	0.289	31.42	22.56	0.282	0.285		1.614	41.82	0.523
	1.250	35.28	24.48	0.306	34.10	23.91	0.299	0.302		1.648	47.43	0.593
	1.264	38.09	25.81	0.323	36.77	25.19	0.315	0.319		1.663	50.59	0.632
	1.277	40.91	27.07	0.338	39.42	26.41	0.330	0.334		1.679	55.38	0.692
	1.284	45.12	28.85	0.361	43.41	28.14	0.352	0.356		1.696	62.61	0.783
										1.703	66.68	0.834
										1.711	72.80	0.910
										1.713	76.25	0.953
										1.714	79.70	0.996
										1.715	83.14	1.039

Table [D-T2] ABAQUS test of 0.6span frame

APPENDIX D ABAQUS FRAME TEST DATA

0.8SPAN ABAQUS	W (kN)	Δ_B (mm)	Δ_{BI} (mm)	X_B	Δ_C (mm)	Δ_{CI} (mm)	X_C	X_{ave}		W (kN)	Δ_I (mm)	X
	0.000	0.00	0.00	0.000	0.00	0.00	0.000	0.000		0.000	0.00	0.000
SECOND ORDER	0.098	1.69	1.66	0.021	1.68	1.64	0.021	0.021	FIRST ORDER	0.100	1.68	0.021
INELASTIC	0.193	3.42	3.28	0.041	3.36	3.23	0.040	0.041	INELASTIC	0.200	3.36	0.042
ANALYSIS	0.329	6.08	5.65	0.071	5.90	5.49	0.069	0.070	ANALYSIS	0.350	5.87	0.073
	0.521	10.17	9.02	0.113	9.72	8.67	0.108	0.111		0.575	9.65	0.121
	0.781	16.54	13.70	0.171	15.49	12.98	0.162	0.167		0.910	15.32	0.191
(1st hinge at C)	1.017	26.61	19.97	0.250	24.52	18.77	0.235	0.242		1.053	18.64	0.233
	1.092	37.01	25.30	0.316	33.82	23.77	0.297	0.307		1.111	20.58	0.257
	1.130	47.36	29.75	0.372	42.78	27.87	0.348	0.360		1.171	23.55	0.294
	1.135	53.27	31.98	0.400	47.94	29.98	0.375	0.387		1.236	27.98	0.350
										1.284	32.34	0.404
										1.318	36.66	0.458
										1.336	39.07	0.488
										1.359	42.65	0.533
										1.377	46.25	0.578
										1.394	49.85	0.623
										1.420	55.24	0.690
										1.447	63.59	0.795
										1.467	76.62	0.958
										1.473	84.04	1.051
										1.481	95.19	1.190

Table [D-T3] ABAQUS test of 0.8span frame

1.2SPAN ABAQUS	W (kN)	Δ_B (mm)	Δ_{BI} (mm)	X_B	Δ_C (mm)	Δ_{CI} (mm)	X_C	X_{ave}		W (kN)	Δ_I (mm)	X
	0.000	0.00	0.00	0.000	0.00	0.00	0.000	0.000		0.000	0.00	0.000
SECOND ORDER	0.098	1.97	1.92	0.024	1.88	1.84	0.023	0.024	FIRST ORDER	0.100	1.91	0.024
INELASTIC	0.193	4.07	3.87	0.048	3.72	3.56	0.044	0.046	INELASTIC	0.200	3.82	0.048
ANALYSIS	0.329	7.43	6.80	0.085	6.39	5.92	0.074	0.079	ANALYSIS	0.350	6.68	0.084
	0.521	12.94	11.14	0.139	10.20	9.05	0.113	0.126		0.575	10.98	0.137
(1st hinge at C)	0.734	22.28	17.43	0.218	16.02	13.34	0.167	0.192		0.693	13.51	0.169
	0.743	22.86	17.78	0.222	16.38	13.60	0.170	0.196		0.747	15.10	0.189
	0.753	23.75	18.32	0.229	16.95	13.99	0.175	0.202		0.773	16.04	0.200
	0.765	25.14	19.13	0.239	17.88	14.61	0.183	0.211		0.805	17.55	0.219
	0.783	27.26	20.33	0.254	19.29	15.54	0.194	0.224		0.842	19.98	0.250
	0.806	30.50	22.08	0.276	21.42	16.90	0.211	0.244		0.891	23.74	0.297
	0.832	35.37	24.53	0.307	24.41	18.70	0.234	0.270		0.939	29.21	0.365
	0.863	42.67	27.83	0.348	28.43	20.98	0.262	0.305		0.949	30.51	0.381
	0.877	46.77	29.52	0.369	30.44	22.05	0.276	0.322		0.957	31.85	0.398
	0.895	52.98	31.87	0.398	33.25	23.49	0.294	0.346		0.969	33.87	0.423
	0.917	62.50	35.09	0.439	37.37	25.47	0.318	0.379		0.986	36.91	0.461
										1.009	41.42	0.518
										1.036	47.54	0.594
										1.068	55.50	0.694
										1.080	59.77	0.747
										1.088	63.75	0.797
										1.094	67.19	0.840
										1.097	69.35	0.867
										1.098	70.93	0.887
										1.099	71.79	0.897
										1.100	72.06	0.901
										1.101	72.47	0.906
										1.102	73.08	0.913
										1.104	74.00	0.925
										1.105	74.52	0.931

Table [D-T4] ABAQUS test of 1.2span frame

APPENDIX D ABAQUS FRAME TEST DATA

1.4SPAN ABAQUS	W (kN)	Δ_B (mm)	Δ_{BI} (mm)	X_B	Δ_C (mm)	Δ_{CI} (mm)	X_C	X_{ave}		W (kN)	Δ_I (mm)	X
	0.000	0.00	0.00	0.000	0.00	0.00	0.000	0.000		0.000	0.00	0.000
SECOND ORDER	0.098	2.11	2.05	0.026	1.94	1.89	0.024	0.025	FIRST ORDER	0.100	2.01	0.025
INELASTIC	0.191	4.40	4.17	0.052	3.73	3.56	0.045	0.048	INELASTIC	0.200	4.02	0.050
ANALYSIS	0.323	8.20	7.44	0.093	6.15	5.72	0.071	0.082	ANALYSIS	0.350	7.04	0.088
	0.506	14.63	12.37	0.155	9.19	8.25	0.103	0.129		0.573	11.59	0.145
	0.591	18.81	15.23	0.190	10.87	9.57	0.120	0.155		0.771	21.57	0.270
(1st hinge at C)	0.629	21.51	16.95	0.212	12.02	10.45	0.131	0.171		0.800	24.45	0.306
	0.649	23.11	17.93	0.224	12.70	10.96	0.137	0.181		0.821	27.22	0.340
	0.658	24.04	18.48	0.231	13.10	11.26	0.141	0.186		0.846	30.98	0.387
	0.669	25.52	19.35	0.242	13.81	11.78	0.147	0.195		0.875	36.66	0.458
	0.686	27.76	20.61	0.258	14.86	12.53	0.157	0.207		0.906	43.86	0.548
	0.708	31.20	22.45	0.281	16.40	13.61	0.170	0.225		0.918	47.07	0.588
	0.731	36.33	24.98	0.312	18.23	14.85	0.186	0.249		0.933	50.61	0.633
	0.759	43.92	28.35	0.354	20.03	16.02	0.200	0.277		0.941	52.52	0.656
	0.792	55.61	32.81	0.410	20.90	16.57	0.207	0.309		0.942	52.99	0.662
	0.806	62.01	34.93	0.437	20.53	16.34	0.204	0.320		0.943	53.15	0.664
	0.808	65.89	36.13	0.452	20.53	16.34	0.204	0.328		0.943	53.30	0.666
	0.811	72.00	37.89	0.474	20.79	16.50	0.206	0.340		0.943	53.53	0.669
										0.944	53.86	0.673
										0.945	54.37	0.680
										0.946	55.13	0.689
										0.948	56.28	0.703

Table [D-T5] ABAQUS test of 1.4span frame

0.8LL ABAQUS	W (kN)	Δ_B (mm)	Δ_{BI} (mm)	X_B	Δ_C (mm)	Δ_{CI} (mm)	X_C	X_{ave}		W (kN)	Δ_I (mm)	X
	0.000	0.00	0.00	0.000	0.00	0.00	0.000	0.000		0.000	0.00	0.000
SECOND ORDER	0.098	1.85	1.81	0.023	1.78	1.74	0.022	0.022	FIRST ORDER	0.100	1.80	0.022
INELASTIC	0.194	3.80	3.63	0.045	3.53	3.38	0.042	0.044	INELASTIC	0.200	3.60	0.045
ANALYSIS	0.331	6.90	6.35	0.079	6.10	5.67	0.071	0.075	ANALYSIS	0.350	6.30	0.079
	0.525	11.93	10.38	0.130	9.84	8.76	0.109	0.120		0.575	10.35	0.129
(1st hinge at C)	0.718	20.50	16.32	0.204	15.90	13.26	0.166	0.185		0.683	12.87	0.161
	0.790	30.86	22.27	0.278	23.11	17.93	0.224	0.251		0.784	17.37	0.217
	0.827	41.27	27.22	0.340	29.23	21.41	0.268	0.304		0.821	20.07	0.251
	0.835	43.87	28.33	0.354	30.58	22.12	0.277	0.315		0.858	23.89	0.299
	0.845	47.82	29.93	0.374	32.55	23.14	0.289	0.332		0.900	29.57	0.370
	0.857	53.97	32.23	0.403	35.48	24.58	0.307	0.355		0.917	32.83	0.410
	0.867	60.20	34.35	0.429	38.05	25.78	0.322	0.376		0.938	37.58	0.470
	0.869	61.78	34.86	0.436	38.70	26.08	0.326	0.381		0.965	44.12	0.552
										0.988	52.40	0.655
										0.992	54.15	0.677
										0.995	55.67	0.696
										0.997	56.69	0.709
										0.999	57.82	0.723
										1.000	58.75	0.734
										1.001	59.10	0.739
										1.003	59.63	0.745
										1.005	60.42	0.755
										1.005	60.46	0.756

Table [D-T6] ABAQUS test of 0.8ll frame

APPENDIX D ABAQUS FRAME TEST DATA

0.6LL ABAQUS	W (kN)	Δ_B (mm)	Δ_{BI} (mm)	X_B	Δ_C (mm)	Δ_{CI} (mm)	X_C	X_{ave}		W (kN)	Δ_I (mm)	X
	0.000	0.00	0.00	0.000	0.00	0.00	0.000	0.000		0.000	0.00	0.000
SECOND ORDER	0.098	1.87	1.82	0.023	1.76	1.72	0.022	0.022	FIRST ORDER	0.100	1.80	0.022
INELASTIC	0.193	3.87	3.69	0.046	3.45	3.31	0.041	0.044	INELASTIC	0.200	3.60	0.045
ANALYSIS	0.330	7.11	6.53	0.082	5.85	5.45	0.068	0.075	ANALYSIS	0.350	6.30	0.079
	0.520	12.50	10.81	0.135	9.20	8.25	0.103	0.119		0.567	10.52	0.131
(1st hinge at C)	0.596	16.26	13.51	0.169	11.56	10.10	0.126	0.148		0.652	13.59	0.170
	0.650	22.44	17.52	0.219	15.24	12.80	0.160	0.190		0.655	13.77	0.172
	0.677	28.79	21.17	0.265	18.50	15.02	0.188	0.226		0.659	14.04	0.175
	0.695	35.20	24.44	0.306	21.13	16.71	0.209	0.257		0.664	14.44	0.181
	0.713	44.97	28.79	0.360	23.97	18.44	0.231	0.295		0.671	15.04	0.188
	0.727	55.32	32.71	0.409	25.19	19.16	0.239	0.324		0.681	15.91	0.199
	0.729	57.62	33.49	0.419	24.79	18.93	0.237	0.328		0.693	17.19	0.215
	0.730	59.94	34.27	0.428	24.35	18.67	0.233	0.331		0.712	19.13	0.239
	0.731	63.52	35.41	0.443	23.75	18.31	0.229	0.336		0.734	22.08	0.276
	0.732	69.15	37.09	0.464	23.06	17.90	0.224	0.344		0.758	26.27	0.328
	0.732	78.15	39.53	0.494	22.44	17.52	0.219	0.357		0.785	32.12	0.402
										0.797	37.21	0.465
										0.799	38.25	0.478
										0.801	39.20	0.490
										0.803	40.03	0.500
										0.805	40.87	0.511
										0.805	41.07	0.513
										0.806	41.38	0.517
										0.808	41.84	0.523
										0.809	42.10	0.526

Table [D-T7] ABAQUS test of 0.6ll frame

0.4LL ABAQUS	W (kN)	Δ_B (mm)	Δ_{BI} (mm)	X_B	Δ_C (mm)	Δ_{CI} (mm)	X_C	X_{ave}		W (kN)	Δ_I (mm)	X
	0.000	0.00	0.00	0.000	0.00	0.00	0.000	0.000		0.000	0.00	0.000
SECOND ORDER	0.098	1.88	1.84	0.023	1.74	1.70	0.021	0.022	FIRST ORDER	0.100	1.80	0.022
INELASTIC	0.193	3.94	3.75	0.047	3.36	3.23	0.040	0.044	INELASTIC	0.200	3.60	0.045
ANALYSIS	0.328	7.33	6.71	0.084	5.58	5.21	0.065	0.075	ANALYSIS	0.350	6.30	0.079
	0.506	13.15	11.30	0.141	8.61	7.77	0.097	0.119		0.550	10.77	0.135
(1st hinges at B	0.552	16.99	14.02	0.175	10.29	9.11	0.114	0.145		0.556	11.03	0.138
and under load 2)	0.554	17.21	14.16	0.177	10.38	9.18	0.115	0.146		0.564	11.43	0.143
	0.556	17.53	14.38	0.180	10.51	9.29	0.116	0.148		0.575	12.03	0.150
	0.559	18.04	14.72	0.184	10.74	9.47	0.118	0.151		0.589	13.04	0.163
	0.563	18.82	15.24	0.190	11.10	9.75	0.122	0.156		0.603	14.67	0.183
	0.567	20.01	16.00	0.200	11.62	10.15	0.127	0.163		0.620	16.98	0.212
	0.573	21.78	17.12	0.214	12.35	10.70	0.134	0.174		0.629	18.30	0.229
	0.581	24.45	18.73	0.234	13.31	11.41	0.143	0.188		0.640	20.24	0.253
	0.590	28.55	21.04	0.263	14.56	12.32	0.154	0.208		0.646	21.28	0.266
	0.595	32.72	23.22	0.290	15.43	12.94	0.162	0.226		0.651	22.76	0.284
	0.599	36.94	25.27	0.316	15.95	13.30	0.166	0.241		0.658	24.85	0.311
	0.603	41.14	27.17	0.340	15.87	13.24	0.166	0.253		0.666	27.39	0.342
	0.608	47.24	29.70	0.371	14.58	12.34	0.154	0.263		0.669	28.59	0.357
	0.613	53.23	31.96	0.400	12.56	10.85	0.136	0.268		0.671	29.53	0.369
	0.618	59.40	34.09	0.426	10.27	9.10	0.114	0.270		0.673	30.15	0.377
	0.620	63.20	35.31	0.441	8.97	8.07	0.101	0.271		0.674	30.40	0.380
	0.621	63.40	35.37	0.442	8.91	8.01	0.100	0.271		0.674	30.51	0.381
	0.621	63.72	35.47	0.443	8.81	7.93	0.099	0.271		0.675	30.62	0.383
	0.621	64.19	35.62	0.445	8.66	7.81	0.098	0.271		0.676	30.79	0.385
	0.622	64.91	35.84	0.448	8.43	7.63	0.095	0.272		0.676	30.89	0.386
	0.622	65.33	35.96	0.450	8.31	7.53	0.094	0.272		0.676	30.95	0.387
	0.622	65.96	36.15	0.452	8.14	7.38	0.092	0.272		0.676	30.98	0.387
	0.622	66.93	36.44	0.456	7.87	7.17	0.090	0.273		0.677	30.99	0.387
	0.623	68.38	36.87	0.461	7.48	6.84	0.086	0.273				
	0.624	70.59	37.50	0.469	6.90	6.35	0.079	0.274				

Table [D-T8] ABAQUS test of 0.4ll frame

APPENDIX D ABAQUS FRAME TEST DATA

0.33SWAY ABAQUS	W (kN)	Δ_B (mm)	Δ_{BI} (mm)	X_B	Δ_C (mm)	Δ_{CI} (mm)	X_C	X_{ave}		W (kN)	Δ_I (mm)	X
	0.000	0.00	0.00	0.000	0.00	0.00	0.000	0.000		0.000	0.00	0.000
SECOND ORDER	0.098	3.04	2.97	0.022	3.00	2.93	0.022	0.022	FIRST ORDER	0.100	3.00	0.022
INELASTIC	0.193	6.15	5.88	0.044	5.99	5.73	0.043	0.044	INELASTIC	0.200	6.00	0.045
ANALYSIS	0.328	10.94	10.11	0.076	10.46	9.70	0.073	0.074	ANALYSIS	0.350	10.50	0.079
	0.517	18.37	16.15	0.121	17.16	15.21	0.114	0.118		0.575	17.24	0.129
	0.719	30.03	24.51	0.184	27.37	22.71	0.170	0.177		0.691	21.07	0.158
	0.725	30.66	24.93	0.187	27.92	23.09	0.173	0.180		0.799	27.06	0.203
	0.734	31.61	25.55	0.192	28.75	23.65	0.177	0.185		0.861	33.20	0.249
	0.744	33.04	26.48	0.199	30.00	24.49	0.184	0.191		0.911	39.38	0.295
	0.758	35.18	27.84	0.209	31.86	25.71	0.193	0.201		0.969	48.34	0.363
	0.776	38.42	29.83	0.224	34.69	27.53	0.206	0.215		0.992	53.37	0.400
	0.800	43.30	32.69	0.245	38.93	30.13	0.226	0.236		1.014	61.19	0.459
	0.826	50.73	36.75	0.276	45.42	33.88	0.254	0.265		1.024	69.18	0.519
	0.832	58.24	40.54	0.304	52.17	37.50	0.281	0.293		1.029	77.32	0.580
										1.031	85.59	0.642

Table [D-T9] ABAQUS test of 0.33sway frame

0.6RIGIDSPAN ABAQUS	W (kN)	Δ_B (mm)	Δ_{BI} (mm)	X_B	Δ_C (mm)	Δ_{CI} (mm)	X_C	X_{ave}		W (kN)	Δ_I (mm)	X
	0.000	0.00	0.00	0.000	0.00	0.00	0.000	0.000		0.000	0.00	0.000
SECOND ORDER	9.978	0.18	0.18	0.002	0.18	0.18	0.002	0.002	FIRST ORDER	10.000	0.18	0.002
INELASTIC	19.911	0.36	0.36	0.004	0.36	0.36	0.004	0.004	INELASTIC	20.000	0.36	0.005
ANALYSIS	34.729	0.63	0.63	0.008	0.63	0.63	0.008	0.008	ANALYSIS	35.000	0.63	0.008
	56.771	1.04	1.03	0.013	1.04	1.03	0.013	0.013		57.500	1.04	0.013
	89.375	1.65	1.62	0.020	1.65	1.62	0.020	0.020		91.152	1.65	0.021
(1st hinge at C)	126.197	2.58	2.50	0.031	2.58	2.50	0.031	0.031		129.262	2.57	0.032
	138.081	3.12	3.00	0.037	3.10	2.99	0.037	0.037		153.087	3.98	0.050
	142.460	3.42	3.28	0.041	3.40	3.26	0.041	0.041		156.453	4.33	0.054
	147.831	3.87	3.69	0.046	3.85	3.67	0.046	0.046		159.125	4.68	0.059
	153.694	4.54	4.30	0.054	4.52	4.27	0.053	0.054		161.846	5.21	0.065
	157.980	5.56	5.20	0.065	5.51	5.16	0.064	0.065		162.981	5.50	0.069
	158.569	5.81	5.42	0.068	5.76	5.38	0.067	0.067		164.335	5.95	0.074
	159.069	6.07	5.64	0.070	6.01	5.59	0.070	0.070		166.217	6.62	0.083
	159.778	6.45	5.97	0.075	6.39	5.91	0.074	0.074		168.510	7.63	0.095
	160.706	7.02	6.46	0.081	6.95	6.39	0.080	0.080		170.315	9.15	0.114
	161.275	7.89	7.18	0.090	7.80	7.10	0.089	0.089		170.784	10.01	0.125
	161.282	9.19	8.24	0.103	9.07	8.15	0.102	0.102		170.993	10.49	0.131
										171.045	11.21	0.140
										171.123	12.29	0.154
										171.240	13.92	0.174
										171.368	16.35	0.204
										171.431	20.01	0.250

Table [D-T10] ABAQUS test of 0.6rigidspan frame

KEMPSP1(A) ABAQUS	W (kN)	Δ_B (mm)	Δ_{BI} (mm)	X_B	Δ_C (mm)	Δ_{CI} (mm)	X_C	X_{ave}		W (kN)	Δ_I (mm)	X
	0.000	0.00	0.00	0.000	0.00	0.00	0.000	0.000		0.000	0.00	0.000
SECOND ORDER	0.100	0.03	0.03	0.000	0.03	0.03	0.000	0.000	FIRST ORDER	0.100	0.03	0.000
INELASTIC	0.200	0.06	0.06	0.001	0.06	0.06	0.001	0.001	INELASTIC	0.200	0.06	0.001
ANALYSIS	0.350	0.11	0.11	0.001	0.11	0.11	0.001	0.001	ANALYSIS	0.350	0.11	0.001
	0.574	0.18	0.18	0.002	0.17	0.17	0.002	0.002		0.575	0.18	0.002
	0.910	0.28	0.28	0.003	0.28	0.28	0.003	0.003		0.913	0.28	0.003
	1.414	0.44	0.43	0.005	0.43	0.43	0.005	0.005		1.419	0.43	0.005
	2.166	0.67	0.66	0.008	0.66	0.65	0.008	0.008		2.178	0.66	0.008
	3.289	1.02	1.01	0.013	1.01	0.99	0.012	0.013		3.317	1.01	0.013
	4.961	1.56	1.53	0.019	1.52	1.49	0.019	0.019		5.026	1.53	0.019
(1st hinge at C)	5.883	1.87	1.82	0.023	1.81	1.77	0.022	0.022		5.972	1.83	0.023
	6.801	2.38	2.31	0.029	2.31	2.25	0.028	0.029		6.888	2.33	0.029
	7.326	2.94	2.84	0.035	2.85	2.76	0.034	0.035		7.670	3.16	0.039
	7.747	3.52	3.37	0.042	3.41	3.27	0.041	0.042		8.153	3.99	0.050
	8.017	4.10	3.90	0.049	3.96	3.77	0.047	0.048		8.439	4.80	0.060
	8.202	4.66	4.40	0.055	4.50	4.26	0.053	0.054		8.500	4.99	0.062
	8.361	5.21	4.89	0.061	5.02	4.72	0.059	0.060		8.585	5.29	0.066
	8.558	6.04	5.61	0.070	5.78	5.39	0.067	0.069		8.705	5.72	0.072
	8.604	6.24	5.79	0.072	5.97	5.56	0.069	0.071		8.868	6.37	0.080
	8.646	6.45	5.97	0.075	6.16	5.72	0.072	0.073		9.095	7.34	0.092
	8.708	6.76	6.23	0.078	6.45	5.97	0.075	0.076		9.351	8.79	0.110
	8.799	7.22	6.62	0.083	6.87	6.33	0.079	0.081		9.415	9.69	0.121
	8.932	7.92	7.20	0.090	7.50	6.86	0.086	0.088		9.444	11.04	0.138
	9.030	9.06	8.14	0.102	8.55	7.73	0.097	0.099		9.486	13.05	0.163

Table [D-T11] ABAQUS test of kempsp1(a) frame

APPENDIX D ABAQUS FRAME TEST DATA

KEMPSP1(B) ABAQUS	W (kN)	Δ_B (mm)	Δ_{BI} (mm)	X_B	Δ_C (mm)	Δ_{CI} (mm)	X_C	X_{ave}		W (kN)	Δ_I (mm)	X
	0.000	0.00	0.00	0.000	0.00	0.00	0.000	0.000		0.000	0.00	0.000
SECOND ORDER	0.100	0.16	0.16	0.002	0.16	0.16	0.002	0.002	FIRST ORDER	0.100	0.16	0.002
INELASTIC	0.199	0.33	0.32	0.004	0.32	0.32	0.004	0.004	INELASTIC	0.200	0.32	0.004
ANALYSIS	0.348	0.57	0.57	0.007	0.57	0.56	0.007	0.007	ANALYSIS	0.350	0.57	0.007
	0.570	0.94	0.93	0.012	0.93	0.92	0.011	0.012		0.575	0.93	0.012
	0.901	1.50	1.48	0.018	1.48	1.45	0.018	0.018		0.913	1.48	0.018
	1.391	2.36	2.29	0.029	2.29	2.23	0.028	0.028		1.419	2.30	0.029
	2.109	3.68	3.51	0.044	3.52	3.37	0.042	0.043		2.171	3.53	0.044
	2.426	4.48	4.24	0.053	4.26	4.05	0.051	0.052		2.208	3.60	0.045
	2.429	4.49	4.25	0.053	4.27	4.06	0.051	0.052		2.262	3.70	0.046
	2.433	4.50	4.26	0.053	4.29	4.07	0.051	0.052		2.342	3.85	0.048
	2.437	4.52	4.28	0.054	4.31	4.09	0.051	0.052		2.436	4.10	0.051
	2.445	4.55	4.31	0.054	4.33	4.11	0.051	0.053		2.455	4.16	0.052
	2.453	4.60	4.35	0.054	4.38	4.15	0.052	0.053		2.474	4.22	0.053
(1st hinge at C)	2.465	4.67	4.41	0.055	4.44	4.21	0.053	0.054		2.496	4.32	0.054
	2.483	4.78	4.51	0.056	4.54	4.30	0.054	0.055		2.525	4.47	0.056
	2.509	4.94	4.65	0.058	4.69	4.43	0.055	0.057		2.569	4.70	0.059
	2.548	5.18	4.86	0.061	4.92	4.63	0.058	0.059		2.633	5.04	0.063
	2.606	5.54	5.18	0.065	5.26	4.93	0.062	0.063		2.727	5.56	0.069
	2.689	6.09	5.66	0.071	5.77	5.38	0.067	0.069		2.854	6.34	0.079
	2.796	6.92	6.37	0.080	6.54	6.04	0.076	0.078		2.990	7.52	0.094
	2.845	7.39	6.77	0.085	6.97	6.41	0.080	0.082		3.124	9.28	0.116
	2.870	7.66	6.99	0.087	7.22	6.62	0.083	0.085		3.148	9.71	0.121
	2.903	8.06	7.32	0.092	7.59	6.94	0.087	0.089		3.171	10.13	0.127
	2.950	8.66	7.82	0.098	8.15	7.39	0.092	0.095		3.183	10.38	0.130
	3.003	9.56	8.54	0.107	8.96	8.06	0.101	0.104		3.199	10.74	0.134
	3.026	10.05	8.93	0.112	9.40	8.41	0.105	0.108		3.224	11.28	0.141
	3.057	10.80	9.51	0.119	10.06	8.94	0.112	0.115		3.259	12.10	0.151
	3.094	11.92	10.37	0.130	11.05	9.71	0.121	0.126		3.311	13.32	0.166
	3.147	13.61	11.63	0.145	12.52	10.83	0.135	0.140		3.387	15.11	0.189
	3.212	16.23	13.49	0.169	14.76	12.46	0.156	0.162		3.455	17.75	0.222
	3.227	20.51	16.32	0.204	18.52	15.04	0.188	0.196		3.503	20.37	0.255
										3.526	23.77	0.297
										3.531	26.93	0.337

Table [D-T12] ABAQUS test of kempsp1(b) frame

KEMPSP1(C) ABAQUS	W (kN)	Δ_B (mm)	Δ_{BI} (mm)	X_B	Δ_C (mm)	Δ_{CI} (mm)	X_C	X_{ave}		W (kN)	Δ_I (mm)	X
	0.000	0.00	0.00	0.000	0.00	0.00	0.000	0.000		0.000	0.00	0.000
SECOND ORDER	0.099	0.99	0.98	0.012	0.98	0.97	0.012	0.012	FIRST ORDER	0.100	0.98	0.012
INELASTIC	0.197	2.01	1.96	0.024	1.96	1.91	0.024	0.024	INELASTIC	0.200	1.96	0.025
ANALYSIS	0.340	3.57	3.42	0.043	3.42	3.28	0.041	0.042	ANALYSIS	0.350	3.43	0.043
	0.544	6.01	5.59	0.070	5.64	5.27	0.066	0.068		0.569	5.66	0.071
(1st hinge at C)	0.608	7.59	6.93	0.087	7.06	6.49	0.081	0.084		0.632	7.15	0.089
	0.648	9.26	8.30	0.104	8.57	7.74	0.097	0.100		0.644	7.53	0.094
	0.680	10.97	9.64	0.121	10.11	8.97	0.112	0.116		0.655	7.91	0.099
	0.702	12.70	10.96	0.137	11.66	10.18	0.127	0.132		0.672	8.49	0.106
	0.725	15.26	12.82	0.160	13.89	11.84	0.148	0.154		0.695	9.37	0.117
	0.738	17.81	14.57	0.182	16.03	13.36	0.167	0.175		0.722	10.70	0.134
	0.750	20.38	16.25	0.203	18.14	14.78	0.185	0.194		0.750	12.68	0.159
	0.761	23.00	17.87	0.223	20.24	16.15	0.202	0.213		0.761	13.77	0.172
	0.763	25.79	19.50	0.244	22.56	17.59	0.220	0.232		0.775	15.38	0.192
			0.00	0.000		0.00	0.000	0.000		0.782	16.29	0.204
			0.00	0.000		0.00	0.000	0.000		0.792	17.66	0.221
			0.00	0.000		0.00	0.000	0.000		0.806	19.70	0.246
			0.00	0.000		0.00	0.000	0.000		0.827	22.67	0.283
			0.00	0.000		0.00	0.000	0.000		0.837	24.25	0.303
			0.00	0.000		0.00	0.000	0.000		0.844	26.83	0.335
			0.00	0.000		0.00	0.000	0.000		0.854	30.63	0.383
			0.00	0.000		0.00	0.000	0.000		0.857	33.19	0.415
			0.00	0.000		0.00	0.000	0.000		0.858	36.90	0.461

Table [D-T13] ABAQUS test of kempsp1(c) frame

REFERENCES

1. Kemp AR. Inelastic instability of rectangular and non-rectangular frames. Canadian Journal of Civil Engineering 1999;26(3):282-92.
2. SANS. The structural use of steel. SANS 10162-1:2004, South African National Standard, Pretoria (2004).
3. Scholz HE. A new multi-curve interaction method for the plastic analysis and design of unbraced and partially braced frames. Thesis submitted in fulfilment of the Ph.D. degree, University of the Witwatersrand, Johannesburg, South Africa (1981).
4. Kennedy DJL, Picard A, Beaulieu D. New Canadian provisions for the design of steel beam-columns. Canadian Journal of Civil Engineering 1990;17:873-93.
5. Chen WF, Lui EM. Stability design of steel frames. CRC Press, Boca Raton (1991).
6. Essa HS, Kennedy DJL. Proposed provisions for the design of steel beam-columns in S16-2001. Canadian Journal of Civil Engineering 2000;27:610-619.
7. Rosenblueth E. Slenderness effects in buildings. Journal of the Structural Division ASCE 1965;91(ST2):229-252.
8. Coates RC. Coutie MG. Kong FK. Structural analysis, Third edition. Chapman & Hall, London (1997).
9. Kemp AR. A consistent mixed approach to computer analysis of frames. Civil Engineering in South Africa 1989;30(7):317-322.
10. Kemp AR. Quantifying limit-states of rotation-capacity in flexural members. Proceedings of the Institution of Civil Engineers 1990;89(9):387-406.
11. Kemp AR. Compatibility relationships in a mixed flexibility-based method of frame analysis. Engineering Structures 1997;19(3):267-275.
12. Kemp AR. Calculation of inelastic displacements in plastic analysis. SAICE Journal 1999;41(2):7-13